Vol. 49, No.2 / 2016

e: ISSN 2068 – 2239
p: ISSN 2068 – 4215

INMATEH - AGRICULTURAL ENGINEERING

MAY - AUGUST

Editorial

The National Institute of Research-Development for Machines and Installations designed to Agriculture and Food Industry - INMA Bucharest has the oldest and most prestigious research activity in the field of agricultural machinery and mechanizing technologies in Romania.

Short History

- *In 1927, the first research **Center for Agricultural Machinery** in Agricultural Research Institute of Romania - ICAR (Establishing Law was published in O.D. no. 97/05.05.1927) was established;*
- *In 1930, was founded **The Testing Department of Agricultural Machinery and Tools** by transforming Agricultural Research Centre of ICAR - that founded the science of methodologies and experimental techniques in the field (Decision no. 2000/1930 of ICAR Manager - GHEORGHE IONESCU ŞIŞEŞTI);*
- *In 1952, was established the Research Institute for Mechanization and Electrification of Agriculture - ICMA Băneasa, by transforming the Department of Agricultural Machines and Tools Testing;*
- *In 1979, the Research Institute of Scientific and Technological Engineering for Agricultural Machinery and Tools – ICSITMUA was founded - subordinated to Ministry of Machine Building Industry - MICM, by unifying ICMA subordinated to MAA with ICPMA subordinated to MICM;*
- *In 1996 the National Institute of Research-Development for Machines and Installations designed to Agriculture and Food Industry – INMA was founded – according to G.D. no.1308/25.11.1996, by reorganizing ICSITMUA, G.D no. 1308/1996 coordinated by the Ministry of Education and Research G.D. no. 823/2004;*
- *In 2008 INMA has been accredited to carry out research and developing activities financed from public funds under G.D. no. 551/2007, Decision of the National Authority for Scientific Research - ANCSno. 9634/2008.*

*As a result of widening the spectrum of communication, dissemination and implementation of scientific research results, in 2000 was founded the institute magazine, issued under the name of SCIENTIFIC PAPERS **(INMATEH)**, ISSN 1583 – 1019.*

*Starting with volume 30, no. 1/2010, the magazine changed its name to **INMATEH - Agricultural Engineering**, appearing both in print format (ISSN 2068 - 4215), and online (ISSN online: 2068 - 2239). The magazine is bilingual, being published in Romanian and English, with a rhythm of three issues / year: January-April, May-August, September-December and is recognized by CNCSIS – with B^+ category. Published articles are from the field of AGRICULTURAL ENGINEERING: technologies and technical equipment for agriculture and food industry, ecological agriculture, renewable energy, machinery testing, environment, transport in agriculture etc. and are evaluated by specialists inside the country and abroad, in mentioned domains.*

*Technical level and performance processes, technology and machinery for agriculture and food industry increasing, according to national requirements and European and international regulations , as well as exploitation of renewable resources in terms of efficiency, life, health and environment protection represent referential elements for the magazine „**INMATEH - Agricultural Engineering**".*

We are thankful to all readers, publishers and assessors.

Editor in chief,
Ph.D. Eng. Pirnă Ion

In the present, *INMATEH - Agricultural Engineering* journalis indexed in the next international databases:
ULRICHSWeb: Global Serials Directory, CABI, SCIPIO, ELSEVIER /SciVerse SCOPUS, Index COPERNICUS International, EBSCO Publishing, Elektronische Zeitschriftenbibliothek

INMATEH - Agricultural Engineering
vol. 49, no.2/ 2016
NATIONAL INSTITUTE OF RESEARCH-DEVELOPMENT FOR MACHINES AND INSTALLATIONS DESIGNED TO AGRICULTURE AND FOOD INDUSTRY - INMA Bucharest

6 Ion Ionescu de la Brad Blvd., sector 1, Bucharest

Three issues per year,
e ISSN: 2068 – 2239
p ISSN: 2068 – 4215

Edited by: INMA Bucharest

CONTENT

STUDY ON THE SCOOP ANGLE CHARCTERISTICS OF A HANDHELD TILLER'S ROTARY BLADE
/
微耕机用旋耕弯刀正切刃背角特性研究

Ms. Stud. Eng. Zhang Y.H.[1)], As. Ph.D. Eng. Yang L.[1)], Ms. Stud. Eng. Niu P. Ms. Stud. Eng. Li S.T.[1)], Prof. Ph.D. Eng. Xie S.Y.[1)], Prof. Eng. Chen X.B.*[2)], Prof. Ph.D. Eng. Yang M.J.*[1)]
[1)] Southwest University, College of Engineering and Technology / P. R. China;
[2)] Key Laboratory of Modern Agricultural Equipment, Ministry of Agriculture / P. R. China
Tel: 8613883002509; E-mail: chxibi@126.com; ymingjin@swu.edu.cn

Keywords: *handheld tiller, rotary blade, scoop angle, plane conversion*

ABSTRACT
A mathematical model of scoop angle of the sidelong edge of a handheld tiller's rotary blade was established by plane conversion and angle change. The effects of cornerite of the sidelong edge and bending angle of the blade on scoop angle were studied as well. The results showed that: with increase of the cornerite, scoop angle linearly increases at large; for sidelong edge of cornerite from 30.5 to 45.4°, the corresponding scoop angle increases from 66.6 to 76.6°; for a position, of same cornerite (other parameters remain constant), on the sidelong edge, scoop angle increases with increase of bending angle.

摘要
通过平面转换和角度改变，建立微耕机用刀盘式湿地弯刀正切刃背角的数学模型，研究了正切刃包角和弯折角对正切刃背角的影响。结果表明：随着正切刃包角的增大，正切刃背角逐渐增大，呈近似线性关系；当正切刃包角取值范围为 30.5-45.4° 时，对应的正切刃背角为 66.6-76.6°；在其他参数不变的情况下，对于正切刃同一包角位置，正切刃背角随着弯折角的增大而增大。

INTRODUCTION
Handheld tillers are mainly used for such cultivating works as paddy field tillage, upland field tillage, pastoral management and protected agriculture tillage, etc. The rotating tilling parts, namely the rotavators, are directly driven by the drive shaft of a tiller *(Peng, et al, 2014)*. The interaction of rotavator and soil while soil-tilling functions as both "hands" and "feet": the "hands" function includes soil cutting, pulverization, soil turning, soil throwing and soil levelling, etc., and the "feet" function pushes the tiller forward by the soil reacting force from the soil-tilling. The rotavator consists of some rotary blades and a shaft, with rotary blades mounted on the shaft according to a certain arrangement. The sidelong section and lengthwise section of the rotary blade undertake the soil-tilling task, and the geometric parameters of the blade directly affect the performance of a rotavator and the corresponding handheld tiller *(Niu, et al, 2015; Yang, et al, 2015)*. The sidelong section of the blade takes the main responsibility for the soil-tilling and has an important influence on the spraying performance, soil turning and soil throwing. The scoop angle and clearance angle of the sidelong section of a blade are complementary. The scoop angle is one of the main parameters of the sidelong section and has an important influence on the soil-cutting resistance and soil throwing *(Peng, 2014)*. At the present, many scholars made some extensive investigations on scoop angle or clearance angle of the rotary blade. Sakai et al experimentally studied the effects of scoop angle on soil cutting process, and obtained the reasonable range of scoop angle of the rotary blade under different soil conditions *(Sakai, et al, 1984; Sakurai, et al, 1989)*. Ding et al studied the effects of blade edge sharpening way and soil cutting mode on the clearance angle of the rotary blade, and obtained the minimum value of clearance angle of wide-type rotary blade with inside-edged and double-edged curves *(Ding, et al, 1997)*. Matin et al studied the variation of blade clearance angle for a conventional blade with the rotary speed of rotavator from 125 rpm to 500 rpm, analysed the furrowing performance of a straight blade with clearance angle 15° at the position of edge curve tip, and pointed out that the inside-edged blade could enhance furrow backfill to improve seed bed, thereby to improve the germination percentage and seeding vigour after sowing *(Matin, et al, 2015; Matin et al, 2016)*.

In this study, taking the handheld tiller's rotary blade as a case study, the mathematical model of the scoop angle of the sidelong edge of the rotary blade was established by means of plane conversion and angle change. The changing rule of scoop angle with changing of positions of the sidelong edge and the effects of bending angle on the scoop angle characteristics were studied as well. As a result, the study can provide references to the design calculation, force and vibration reduction, and performance optimization for a handheld tiller's rotary blade.

MATERIAL AND METHOD

The rotary blade, adaptable for wetland sticky paddy field tillage, consists of holding section, neck, sidelong section and lengthwise section. It was designed according to Chinese National Standard GB/T 5669-2008 "Rotary tiller-rotary blades and blade holders", Chongqing Standard DB50/T 277-2008 "Blades of micro-cultivator", and Japanese National Standard JIS B 9210-1988 (2008 confirmed) "Blades for tillers". The main design contents of a rotary blade include edge curve, back edge curve, rotation radius R, maximum cornerite of the lengthwise edge curve θ_{max}, cutting angle α, bending angle β, bending radius r and tilling width B, etc., as shown in fig. 1.

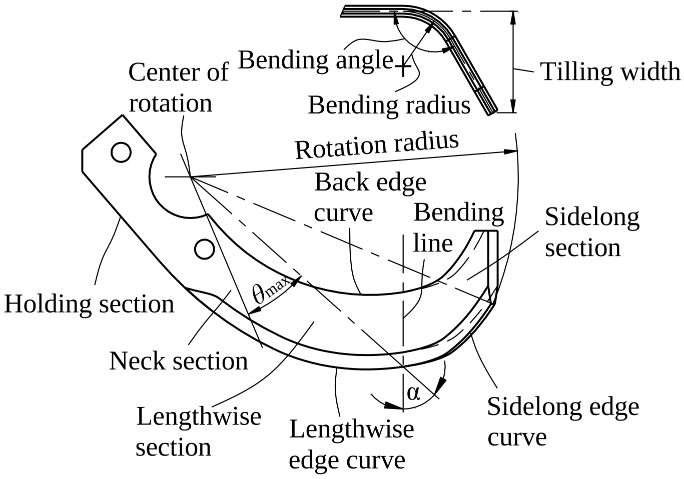

Fig.1 - The structure of a rotary blade

Considering that the rotation radius of the handheld tiller's rotary blade is small, a circular shape back edge curve was adopted. A spiral of Archimedes was adopted for the edge curve, and its equation is as follows:

$$R_n = a_1 R + a_0 R\theta \text{, [mm]} \tag{1}$$

where: R_n is rotation radius at a selected point on the edge curve, [mm];
R – rotation radius of a rotary blade, [mm];
θ – cornerite of the edge curve, [degree];
a_0 and a_1 – constants.

The sidelong section takes the main responsibility for the soil-cutting, and geometric parameters directly affect the performance of a rotavator and the corresponding handheld tiller. While rotary tilling, the trajectory of any point on the sidelong edge is a trochoid. The cross section at any selected point on the sidelong edge was obtained through a section plane, at the selected point, that is perpendicular to the rotation axis of the rotary blade, as shown in fig. 2. β_1 is scoop angle, γ_0 is rake angle, i is sharpening angle, δ is clearance angle or relief angle.

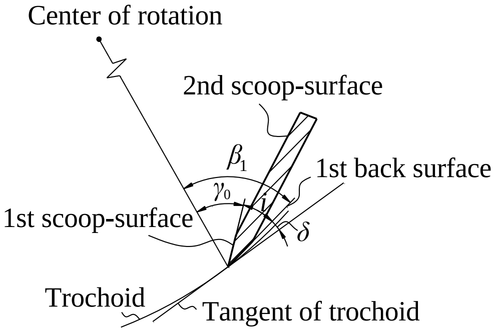

Fig.2 - The cross-section of sidelong section

Numerical method was adopted to analyze the characteristics of the sidelong edge scoop angle of a handheld tiller's rotary blade. A mathematical model of the scoop angle was established by means of plane conversion and angle change.

In order to provide convenience for the build-up of mathematical model of the scoop angle, three planes were defined as follows: plane P_0 is the plane that contains a selected point on the sidelong edge and is perpendicular to the sidelong edge or its tangent, plane P_1 is the plane that contains the selected point and is perpendicular to the plane of sidelong section and parallels to the bending line of the rotary blade, and plane P_2 is the plane that contains the selected point and is perpendicular to the rotation axis of the rotary blade, as shown in fig. 3 and fig. 4. Scoop angle β_1, sharpening angle i and clearance angle δ are measured in plane P_2.

By plane conversion, dimensions of blade thickness in these three planes are e_0, e_1 and e_2, respectively, and the dimensions of edge width, blade edge surface width, and blade edge surface height in these three planes are as follows correspondingly: c_0, c_1 and c_2; l_0, l_1 and l_2; and h_0, h_1 and h_2. And there are relations of $e_0=e_1$, $c_0=c_1$ and $h_1=h_2$.

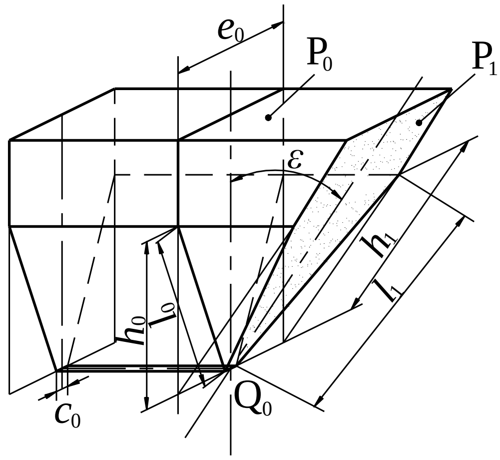

Fig.3 - Apparent section P_0 and actual section P_1 of lengthwise section

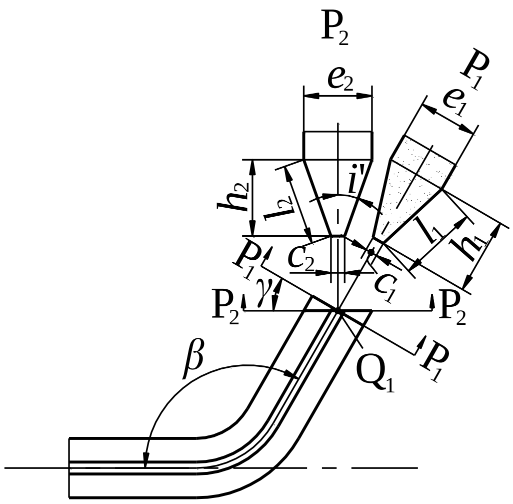

Fig.4 - Sections P_1 and P_2

The scoop angle in plane P_2 can be expressed as follows (see fig. 5):

$$\beta_1 = i' + \varphi \text{ , [degree]} \tag{2}$$

where:

β_1 is scoop angle, [degree];

i' – half-sharpening angle, and $i' = i/2$, [degree];

φ – the angle between rotation radius and bending line on the sidelong edge, [degree].

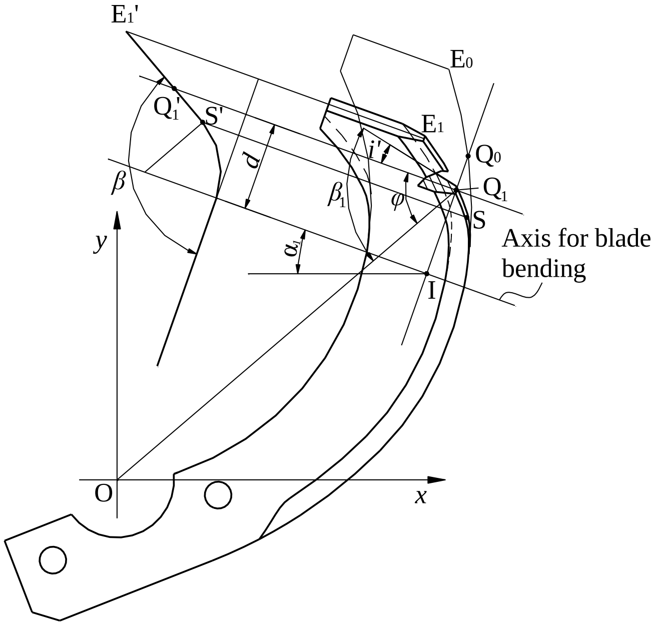

Fig.5 - Schematic paragraph of scoop angle

Half-sharpening angle could be calculated in the cross-section of the cutting edge in P$_2$, with expression as follows:

$$i' = \arctan\left(\frac{e_2 - c_2}{2h_2}\right), \text{ [degree]} \tag{3}$$

Because e_0=e_1, the thickness of blade e_2 can be expressed as (see Figure 4):

$$e_2 = \frac{e_0}{\cos\gamma}, \text{ [mm]} \tag{4}$$

where:

γ – the angle between plane P$_1$ and P$_2$, and $\gamma = \beta - \pi/2$, [degree]. β is bending angle, and it is generally set as 120^o.

Similarly, edge width c_2 can be expressed as:

$$c_2 = \frac{c_0}{\cos\gamma}, \text{ [mm]} \tag{5}$$

Since h_1=h_2, the height of the blade edge surface h_2 can be expressed as (see fig. 3):

$$h_2 = \frac{h_0}{\cos\varepsilon}, \text{ [mm]} \tag{6}$$

where:

ε – the angle between the plane P$_0$ and P$_1$, [degree];

h_0 – width of the blade edge surface, mm, and $h_0 = \sqrt{l_0^2 - \left(e_0 - c_0\right)^2/4}$, [mm].

By substituting equations (4), (5) and (6) into equation (3), the following expression is established:

$$i' = \arctan\left(\frac{(e_0 - c_0)\cos\varepsilon}{2\cos(\beta - \frac{\pi}{2})\sqrt{l_0^2 - \frac{(e_0 - c_0)^2}{4}}}\right), \text{ [degree]} \tag{7}$$

For calculating the angle between rotation radius and bending line at the selected point on sidelong edge, a Cartesian coordinate system of the edge curve was established, as shown in fig. 5. The selected point Q$_0$ on the sidelong edge becomes Q$_1$ by the bending deformation, and their coordinates are (x_0, y_0)

and (x, y), respectively, and (x, y) can be calculated according to the fact: the length of the edge curve keeps constant before and after the bending deformation. Then, the angle between rotation radius and bending line at any selected point on the sidelong section can be expressed as:

$$\varphi = \arctan(\frac{y}{x}) + \alpha_1, \text{ [degree]} \tag{8}$$

where:

α_1 – the angle between bending line and x-axis, [degree].

By substituting equations (7) and (8) into equation (2), the mathematical model of scoop angle of the sidelong edge can be obtained as:

$$\beta_1 = \arctan\left(\frac{(e_0 - c_0)\cos\varepsilon}{2\cos(\beta - \frac{\pi}{2})\sqrt{l_0^{\,2} - \frac{(e_0 - c_0)^2}{4}}} \right) + \arctan(\frac{y}{x}) + \alpha_1, \text{ [degree]} \tag{9}$$

RESULTS

Taking the handheld tiller's rotary blade as a case study, the characteristics of the scoop angle of the rotary blade's sidelong edge was studied in this work. The parameters of the rotary blade are defined as shown in table 1, and the edge curve equation of the sidelong section is $R_n = 0.58R + 0.128R\theta$.

Table 1

Parameters of the rotary blade

Parameter	Value	Parameter	Value
Rotation radius of the blade, R [mm]	180	**Blade thickness in plane P_0, e_0 [mm]**	6
Maximum cornerite of lengthwise edge curve, θ_{max} [degree]	22.2	**Edge width in plane P_0, c_0 [mm]**	2.5
Cutting angle at θ_{max}, α [degree]	45.2	**Edge surface width in plane P_0, l_0 [mm]**	8
Bending radius, r [mm]	30	**Cornerite at point S, θ_S [degree]**	30.5
Bending angle, β [degree]	120	**Cornerite at point E_1, θ_{E1} [degree]**	45.4
Start Radius of spiral of Archimedes, R_0 [mm]	104.4	**Angle between bending line and x-axis, α_1 [degree]**	23

According to the mathematical model of the scoop angle, scoop angle at positions, with different cornerites, on the sidelong edge of the defined rotary blade could be calculated. Curves of scoop angle, rake angle and sharpening angle of the sidelong edge with cornerite were shown in fig. 6. The sharpening angle is calculated by equation (7), and the rake angle γ_0 is the difference between scoop angle and sharpening angle.

Similarly, scoop angle at positions, with different cornerites, on the sidelong edge of the rotary blade with different bending angles can be obtained by changing bending angle from 115 to 125° and keeping other parameters unchanged as shown in table 1. The curves of scoop angle with bending angle were shown in fig. 7.

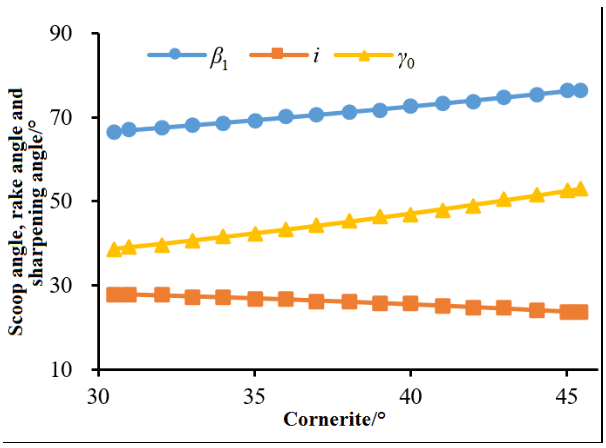

Fig.6 - Curves of scoop angle, rake angle and sharpening angle with cornerite

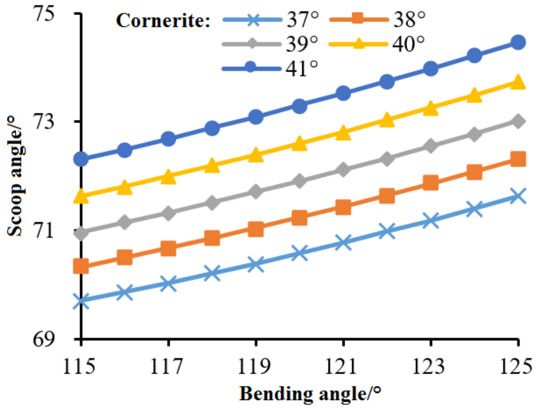

Fig.7 - Curves of scoop angle with bending angle

As can be seen from fig. 6, with the increase of cornerite of the sidelong edge, the scoop angle increases. For the rotary blade with parameters listed in Table 1, the cornerite of the sidelong edge of the linear section ranges from 30.5 to 45.4°, and the corresponding scoop angles linearly increase from 66.6 to 76.6° at large. Note: this linear section refers to section of sidelong edge starting from point S to E_1, namely, not including the bending part of the sidelong section.

According to literature *(Sakai, et al, 1984)*, with the increase of scoop angle, soil-cutting resistance decreases and the soil-throwing performance degrades, and it is recommended that the general scoop angle ranges as follows: 40-55° for soft soil such as sandy or muddy soil, 55-75° for normal soil such as sandy loam, loam or clay loam, 75-85° for hard soil such as heavy clay or dry soil. The scoop angle of the rotary blade with parameters listed in table 1 ranges within 66.6-76.6°, which indicates that the rotary blade is suitable for tilling in loam and clay loam, and is consistent with the application situation of such soil type as wet and sticky soil of the rotary blade studied.

In fact, the main reason for soil-cutting resistance decrease with the increase of scoop angle is as follows: the rake angle increases with the increase of sidelong edge's cornerite, and the larger rake angle, the shaper the edge, and as a result, the smaller the soil-cutting resistance. At the same time, the increase of rake angle leads to the decrease of deformation level of the soil out-flowing from the scoop surface, which results in the decrease of soil-cutting energy consumption. The deformation decrease leads to the degrading of performance of soil-throwing. However, the clearance angle decreases with the increase of scoop angle on the sidelong edge, which results in the increase of friction between back surface of the sidelong section and soil.

In addition, with the increase of cornerite of sidelong edge, the actual sharpening angle decreases, which makes the blade edge sharper and benefits the blade on the soil-cutting resistance reduction. However, the decrease of actual sharpening angle results in the easy worn-out of the sidelong edge, and the worn-out of edge close to the blade tip is more serious.

According to literature *(Ding, et al, 2004)*, 50-80% of energy consumption of tilling is consumed by soil-cutting of sidelong section of a rotary blade. As the main angle parameter of sidelong section, the scoop angle has crucial relations with rake angle and clearance angle of the sidelong edge while sharpening angle keeps constant. As a result, the scoop angle is an angle parameter that reflects the comprehensive effect of rake angle and clearance angle of the sidelong edge, and it has an important influence on the soil-cutting resistance and soil-throwing performance of the rotary blade.

As shown in fig. 7, for a position, with the same cornerite (while other parameters remains constant), on the sidelong edge, the scoop angle increases with the increase of the bending angle of the rotary blade. This is beneficial to the soil-cutting resistance reduction but it results in the soil-throwing performance degrading. The bending angle falls into range of 115-125º in this study.

At the same time, for rotary blades of different bending angle, the scoop angle increases with the increase of cornerite of the sidelong edge, which is consistent with the aforementioned effect of cornerite on characteristics of scoop angle.

In practical selection, the bending angle should be determined under comprehensive consideration, and the recommended value for the bending angle of a rotary blade is 120º by Chinese standard GB/T 5669-2008.

CONCLUSIONS

The sidelong section of a rotary blade takes the main responsibility for soil-cutting. The scoop angle is one of the main parameters of the sidelong section and has an important influence on the soil-cutting resistance and soil throwing. Taking the handheld tiller's rotary blade as a case study, the mathematical model of the scoop angle of the sidelong edge of the blade was established by means of plane conversion and angle change. The main conclusions are as follows:

(1) With increase of cornerite of the sidelong edge, scoop angle linearly increases at large. For sidelong edge of cornerite ranging from 30.5 to 45.4°, the corresponding scoop angle increases from 66.6 to 76.6°, which indicates that the rotary blade is suitable for tilling in loam and clay loam, and it is consistent with the application situation of the soil type of the rotary blade studied.

(2) For a position, with the same cornerite (other parameters remains constant), on the sidelong edge, scoop angle increases with increase of bending angle of the rotary blade. This is beneficial to the soil-cutting resistance reduction.

(3) The scoop angle is an angle parameter that reflects the comprehensive effect of rake angle and clearance angle of the sidelong edge. The scoop angle has crucial relations with rake angle and clearance angle of the sidelong edge while sharpening angle keeps constant, and it has an important influence on the soil-cutting resistance and soil-throwing performance of the rotary blade.

ACKNOWLEDGEMENT

The work has been funded by Fundamental Research Funds for the Central Universities of China (XDJK2014C033), Ph.D. Research Project of Southwest University (SWU115011), and Fund from Key Laboratory of Modern Agricultural Equipment, Ministry of Agriculture, P. R. China (2016-001).

REFERENCES

[1] Ding W., Peng S., (1997), Research on design of wide rotary blade (宽型旋耕弯刀的设计研究), *Transactions of the Chinese Society for Agricultural Machinery*, vol. 28, issue 3, pp. 144-148;

[2] Ding W., Wang Y., Peng S., (2004), Analysis on sidelong portion of an up-cut rotary blade (反转旋耕刀正切面分析及参数选择), *Transactions of the Chinese Society for Agricultural Machinery,* vol. 35, issue 4, pp. 40-43;

[3] Matin M.A., Desbiolles J.M.A., Fielke J.M., (2016), Strip-tillage using rotating straight blades: effect of cutting edge geometry on furrow parameters, *Soil & Tillage Research,* vol. 155, issue S, pp. 271-279;

[4] Matin M.A., Fielke J.M., Desbiolles J.M.A., (2015), Torque and energy characteristics for strip-tillage cultivation when cutting furrows using three designs of rotary blade, *Biosystems Engineering,* vol.129, pp.329-340;

[5] Niu P., Yang L., Zhang Y., Gao B., Li Y., Yang M., (2015), Finite element analysis of the rotary blade of a mini-tiller based on ANSYS Workbench (基于 ANSYS Workbench 的微耕机用旋耕弯刀有限元分析), *Journal of Southwest University (Natural Science Edition)*, vol. 37, Issue 12, pp. 162-147;

[6] Peng B., (2014), Modelling and simulation of soil-cutting dynamics of rotary roller of mini-tiller (微耕机刀辊切土动力学建模及仿真), M.S. thesis, Southwest University, Chongqing / P. R. China;

[7] Peng B., Yang L., Yang M., Guo M., Ye J., Chen J., (2014), On connotation analysis and development countermeasures of the mini-tiller standard system (微耕机标准体系的内涵分析及其发展对策), *Journal of Southwest Normal University (Natural Science Edition)*, vol. 39, issue 4, pp.141-146;

[8] Sakai J., Lam Van H., Iwasaki K., Shibata Y., (1984), Tillage resistance characteristics of Japanese rotary blades– distribution of tilling resistance to the tipless (straight) blade and bending tip portion of a rotary blade (ロータリ耕なたづめの耕うん抵抗特性-直刃部とわん曲部へのトルク分配), *Journal of the Japanese Society of Agricultural Machinery,* vol. 46, issue 1, pp. 593-598;

[9] Sakurai H., Sakai J., (1989), Study on the mathematical model of Japanese rotary blades for Computer Aided Design (CAD) - (part 1) blades-tip and edged curve portion (耕うん用なた刃 CAD 用数 理モデノレ研究 (第 1 報) -わん曲部および刃部), *Journal of the Japanese Society of Agricultural Machinery*. vol. 51, issue 1, pp. 29-35;

[10] Yang M., Niu P., Peng B., Yang L., Li Y., Chen X., Peng Z., (2015), Soil-cutting performance analysis of a handheld tiller's rotavator by Finite Element Method (FEM). *INMATEH-Agricultural Engineering Journal*, Vol. 47, issue 3, pp. 13-20;

[11] ***Ministry of Industry and Information Technology of the P. R. China, (2013), *Handheld tillers* JB/ T 10266-2013 (*微型耕耘机* JB/ T 10266-2013), China Machine Press, P. R. China;
[12] ***Chinese Standard Committee, (2008), Rotary tiller - rotary blades and blade holders, GB/T 5669-2008 (旋耕机械刀和刀座, GB/T 5669-2008), Chinese Standard Press, P. R. China;
[13] ***Chongqing Bureau of Quality and Technology Supervision, (2008), Blades of micro-cultivator, DB50/T 277-2008 (微耕机配套用旋耕刀, DB50/T 277-2008), Chongqing, P. R. China;
[14] ***Japanese Industrial Standards Committee, (2008), Blades for tillers, JIS B 9210-1988 (2008 confirmed)(耕うんづめ, JIS B 9210-1988(2008 確認)), Japanese Standards Association, Japan.

INTERRELATION BETWEEN INCIDENCE ANGLE AND ROLL ANGLE OF CONCAVE DISKS OF SOIL TILLAGE IMPLEMENTS
/
ВЗАЄМОЗВЯЗОК МІЖ КУТАМИ АТАКИ ТА КРЕНУ СФЕРИЧНИХ ДИСКІВ ГРУНТООБРОБНИХ ЗНАРЯДЬ

Lect. Ph.D. Eng. Klendii M.B., **Ph.D. Eng. Klendii O.M.**
Separated Subdivision of National University of Life and Environmental Sciences of Ukraine Berezhany Agrotechnical Institute / Ukraine
E-mail: alex_ks@mail.ru

Keywords: *concave disk, direction of unit motion, incidence angle and roll angle, back angle, cone of grinding*

ABSTRACT
A holistic analytical model of a concave disk, which is arranged in a three-dimensional coordinate system with a given direction of unit motion along OY-axis, has been developed. It includes the design parameters of a disk and the depth of soil tillage. An interrelation between an incidence angle and a roll angle of a disk under a set value of a back angle at field surface level has been determined.

РЕЗЮМЕ
Розроблено цілісну аналітичну модель сферичного диска, розташованого в просторовій системі координат із заданим напрямом руху агрегату вздовж осі OY. До неї входять конструктивні параметри диска та глибина обробітку ґрунту. Встановлено взаємозв'язок між кутами атаки і крену диска для заданого значення затильного кута на рівні поверхні поля.

INTRODUCTION
The design parameters of a disk and the angles of its installation influence the technological process of unit operation (turning and breaking up soil, cutting nutrient residues and their mixing up with soil, disk width etc.). Each parameter has its specific influence on the technological process flow. For example, an incidence angle increase results in the improvement of mixing up soil with nutrient residues and a disk width increase, however, angular velocity of rotation can be decreased due to disk drawing and, as a result, clogging of space between disks with soil and nutrient residues. If disks are installed upright, soil takes up mainly tearing and shearing strains, the height of its lift is small and as a result it does not mix well with nutrient residues. If there is a deflection in the upright direction of a disk blade through the so called roll angle, the moving is improved, but it is the case only to a certain increase in the value of this angle.

Main geometrical characteristics of a disk of specified dimensions and setting angles, which determine its operating capacity at a certain depth of tilling, are the following: a back angle and a slope angle of generators of a cone of grinding *(Zaika P.M., 2001)*. A back angle is changed according to the depth of soil tillage: it is a maximum at a furrow bottom and its value decreases as field surface is approached. At field surface level its value must range from 3^0 to 5^0, in some cases it may equal to zero *(Zaika P.M., 2001)*. In upper sections, that is above the field surface, this angle will decrease still further and its smallest value will be reached in diametric section, but all these sections are outside the soil and are inactive. Under a negative value of this angle in the operating area, a disk, leaning with its back on a furrow bottom, rolls out to the field surface, thus the depth of soil tillage decreases. Disk setting angles (incidence angle and roll angle) influence the value of a back angle. It is important to choose their correct combination in order to provide a specified value of a back angle at field surface level.

Designing of disk soil tillage implements has been considered in the paper *(Zaika P.M., 2001)* and other research works *(Sineokov G.N. and Panov I.M., 1977; Hevko R.B. et. al., 2012; Hevko R.B. and Klendiy O.M., 2014; Hevko R.B. et. al., 2014; Hevko R.B. et. al., 2015)*. There are scientific works fully devoted to this subject *(Strelbitskii V.F., 1978; Tsimmerman M.Z., 1978; Blednyx V.V., 2010; Posmetyev V.I. et. al.. 2013;* Demydenko A.I. et. al., 2009*)*. More specified works investigate different aspects of the improvement of the quality of soil tillage by means of such implements *(Hrynenko O. and Lebedev S., 2011; Haponenko O.I., 2012; Soxt K.A., 2014)*. Prospects of further improvement of disk and other soil tillage implements have been considered in the paper *(Heruk S.M. and Petrychenko E.A., 2014)*.

MATERIAL AND METHOD

A disk is characterized by the following design parameters (Fig.1, a): diameter *D*, radius of a sphere *R*, angle *σ* of slope of generators to a cone axis with its vertex in the middle of a sphere and which leans against the cutting edge of a disk, angle *δ* of slope of generators of a cone of grinding to cutting edge area and a cutting-point angle *i*. There are relations between them:

$$D = 2R\sin\sigma; \qquad \delta = i + \sigma. \tag{1}$$

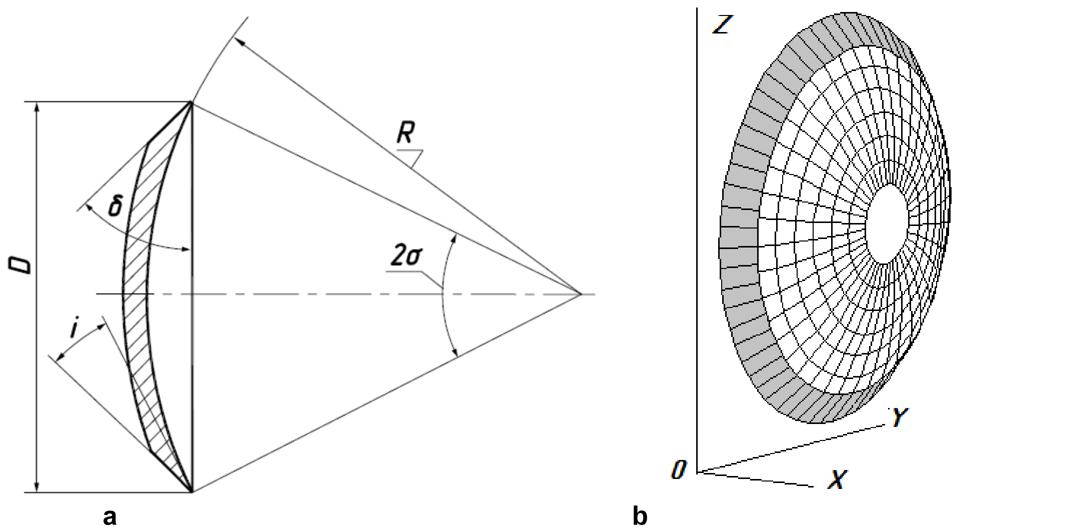

Fig.1 - Picture of a soil tillage disk: a) crosscut; b) axonometry

If *OY*-axis is taken as a direction of unit motion, taking into consideration an incidence angle *α* and a roll angle *β* in a three-dimensional coordinate system *OXYZ*, concave disk parametric equations can be written down as follows *(Pylypaka S.F. and Klendii M.B., 2016)*:

$$\begin{aligned} X &= R\left(\cos u\cos\alpha\cos\beta - \sin u\sin v\sin\alpha + \sin u\cos v\cos\alpha\sin\beta\right);\\ Y &= R\left(\cos u\sin\alpha\cos\beta + \sin u\sin v\cos\alpha + \sin u\cos v\sin\alpha\sin\beta\right);\\ Z &= R\left(-\cos u\sin\beta + \sin u\cos v\cos\beta\right), \end{aligned} \tag{2}$$

where *v* and *u* – independent variables of the surface; *v* being an angle of rotation of a variable point of a sphere about *OX*-axis along the parallel (*v=0…2π*); *u* being an angular coordinate of this point along the meridian, the reading of which begins at the cross point of *OX*-axis and the surface of a sphere (*u=0…σ*).

Analogically, the equations of the surface of a cone of grinding can be written down as follows *(Pylypaka S.F. and Klendii M.B., 2016)*:

$$\begin{aligned} X &= r\left[u\mathrm{tg}\delta\cos\alpha\cos\beta - (1-u)\sin v\sin\alpha + (1-u)\cos v\cos\alpha\sin\beta\right];\\ Y &= r\left[u\mathrm{tg}\delta\sin\alpha\cos\beta + (1-u)\sin v\cos\alpha + (1-u)\cos v\sin\alpha\sin\beta\right];\\ Z &= r\left[-u\mathrm{tg}\delta\sin\beta + (1-u)\cos v\cos\beta\right], \end{aligned} \tag{3}$$

where *v* and *u* – independent variables of the surface; *v* being an angle of rotation of a variable point of a cone about *OX*-axis (*v=0…2π*); *u* being a rectilinear coordinate of this point along the generator of a cone, the reading of which begins at its base; *r* -radius of the base of a cone.

Fig.1b shows the back surface of a concave disk, constructed from the equations (2), and the surface of a cone of grinding under *α=β=0*, constructed from the equations (3). In this case a cutting edge is in the plane of *ZOY*. For better visualization, the surface of a cone of grinding is darkened. If a disk is arranged in such a way, it does not perform its task when moving along *OY*-axis; it will only rotate and leave a mark in the soil. In order to make it cut and turn the soil, it is necessary to select an incidence angle by rotating the cutting edge plane about *OZ*-axis in such a way as to build the angle *α* between it and the plane of *ZOY*. This angle has its limits, because as it increases, there is a point at which the angular velocity of disk rotation can decrease due to its drawing. In order to have better visualization of disk installation, taking into consideration the back angle, a nonworking incidence angle is selected to be *α=90º*, such that the disk does not rotate.

If the cutting edge plane is positioned at a right angle to the direction of unit motion along *OY*-axis ($\alpha=90^o$, Fig. 2), soil undergoes deformation due to its simple shearing away from the direction of unit motion without disk rotation. In this case the back angle is invariable at a specified depth of soil tillage. In case of a disk that is deepened into the soil at the depth of the radius $r=D/2$, the back angle ε on the field surface will be equal to ($90^o-\delta$) on both sides of a disk (Fig.2, side view). It is built as a result of the section of a cone by the field surface plane, which in this case passes through the vertex of a cone. The back angle increases as the cutting plane approaches a furrow bottom. For example, at distance *a* from a furrow bottom it accounts for ε_a and is built by a tangent to a hyperbola – a correspondent horizontal plane section of a cone – with the direction of unit motion. Thus, if the depth of soil tillage is specified by *a*, the least value of the back angle from top to bottom of a furrow will be at field surface level and will account for ε_a. Difference with the angle $90^o-\delta$ will be $\Delta\varepsilon$ (Fig.2).

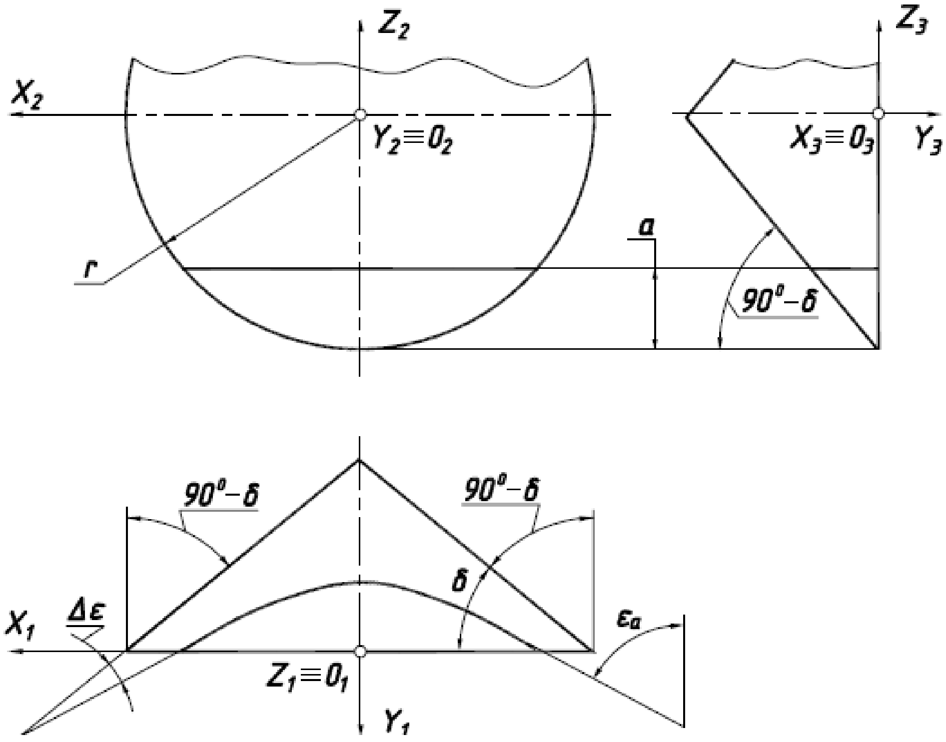

Fig.2 – Three projections of a cone of grinding under the nonworking incidence angle $\alpha=90^o$

Now, an operating incidence angle is selected to be equal to the angle of disk grinding: $\alpha=\delta$. In this case, the outside generator of a cone coincides with the direction of unit motion, which can be seen in the side view (Fig.3). If a disk is deepened to a half of its height, in other words if a field surface plane passes through its vertex, the back angle at field level will be equal to zero, that is to say there might be friction of soil against the surface of a cone of grinding. But if a disk tills the soil at a depth of *a* under the same incidence angle $\alpha=\delta$, the back angle at field surface level will be equal to $\Delta\varepsilon$ (Fig. 3).

It is necessary to determine the value of this angle, since the specified value of a back angle must be 3^0-5^0, otherwise as the back angle increases, the incidence angle α and the cutting angle γ ($\gamma=\varepsilon+i$) will increase as well. The determination of the angle $\Delta\varepsilon$ does not depend on the value of the incidence angle α. But in order to simplify analytical calculation, it is to the purpose to select $\alpha=90^0$, which corresponds to Fig. 2. Under the value of $\alpha=90^0$ and $\beta=0$ (roll angle is nonexistent), parametric equations of the surface of a cone of grinding (3) can be written down as follows:

$$\begin{aligned} X &= -r\left[(1-u)\sin v\right]; \\ Y &= ur\,\mathrm{tg}\delta; \\ Z &= r\left[(1-u)\cos v\right]\ , \end{aligned} \tag{4}$$

Where: $r=D/2=R\sin\sigma$ according to (1).

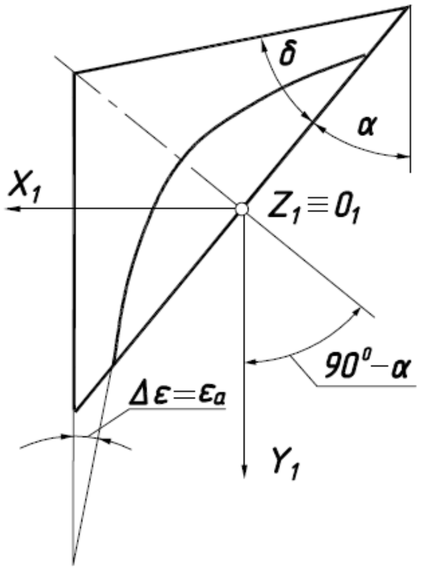

Fig.3 – Side view of a cone of grinding under roll angle *α=δ*

We shall find the curve of the surface section of a cone of grinding (4) by the horizontal plane of a field under the specified depth *a* of soil tillage. In this case a coordinate *Z* of a field surface level will be equal to *Z=-a+r – const*. We shall equate this value to the last equation (4) and we obtain:

$$r\left[(1-u)\cos v\right]=-r+a \qquad (5)$$

The equation (5) is an intrinsic equation of a hyperbola – a cone section, which establishes interdependence between variables *u* and *v* of the surface of a cone. It can be solved as *u=u(v)* or *v=v(u)*. Both variants are given below:

$$u=\frac{r\left(1+\cos v\right)-a}{r\cos v}; \qquad v=\operatorname{Arc}\cos\frac{a-r}{r\left(1-u\right)}. \qquad (6)$$

The substitution of one of the expressions (6) in the equation (4) gives parametric equations of hyperbola –section of a cone of grinding at a height of *a* from a furrow bottom. In order to build it, it is better to use the first expression (6), which gives two half-hyperbolas, whereas the second one gives one. But it is to the purpose to use the second one when determining the angle $\Delta\varepsilon$, which has one side that is tangent to a hyperbola at its tie point with a blade, that is to say under the value of u*=0,* whereas in the first expression the value of variable *v* for this point must have been determined. If we substitute the second expression (6) in the cone equation (4), we obtain the equation of its section by field level plane under the specified depth of tillage *a*:

$$x=\sqrt{r^2\left(1-u\right)^2-\left(a-r\right)^2}; \qquad y=ur\,\mathrm{tg}\delta. \qquad (7)$$

The direction of a tangent line can be determined by the differentiation of the expressions (7) in variable *u*:

$$x'=\frac{r^2\left(1-u\right)}{\sqrt{r^2\left(1-u\right)^2-\left(a-r\right)^2}}; \qquad y'=r\,\mathrm{tg}\delta. \qquad (8)$$

We determine the angle between *OY*-axis and the tangent (Fig. 2) from the expression:

$$\varepsilon_a=\operatorname{Arctg}\frac{x'}{y'}=\operatorname{Arctg}\frac{r\left(1-u\right)\mathrm{ctg}\delta}{\sqrt{r^2\left(1-u\right)^2-\left(a-r\right)^2}}. \qquad (9)$$

The expression (9) under *u=0* provides the value of the angle of the tangent to a hyperbola at its tie point with a blade. The angle $\Delta\varepsilon$ is determined as the difference between the angles (Fig. 2): $\Delta\varepsilon=\varepsilon_a-(90^0-\delta)$. Taking into consideration the above mentioned, we can write down the following:

$$\Delta\varepsilon = \varepsilon_a - \left(90^0 - \delta\right) = \mathrm{Arctg}\frac{r\,\mathrm{ctg}\,\delta}{\sqrt{r^2 - \left(a-r\right)^2}} - \left(\frac{\pi}{2} - \delta\right). \tag{10}$$

For example, we shall take a disk with the specified design parameters of a cone of grinding and the depth of soil tillage (taken from the scientific work *(Zaika P.M., 2001*): *δ=39,2⁰; r=225 mm; a=80 mm*. The substitution of these data into the expression (10) results in (the value of the angle *δ* must be substituted in radians): $\Delta\varepsilon = 0.13$ *rad* $= 7.2^0$. Thus, if a disk is arranged under the incidence angle *α=δ* (Fig. 3), the back angle at field surface level is $\varepsilon_a = \Delta\varepsilon = 7.2^0$. Accordingly, the incidence angle can be adjusted in such a way that the back angle obtains a specified value (for instance $\varepsilon_a = 3^0$). If we reduce the incident angle by Δε, the back angle ε_a at field surface level will be equal to zero. Thus, in order to obtain a specified value of the back angle, the incidence angle must be reduced by the value of $\Delta\varepsilon - \varepsilon_a$. In his case the incidence angle is obtained from the expression: $\delta - (\Delta\varepsilon - \varepsilon_a)$, since the initial incidence angle is *α=δ* according to Fig.3. In our case the incidence angle reaches $\alpha = \delta - \Delta\varepsilon + \varepsilon_a = 39.2^0 - 7.2^0 + 3^0 = 35^0$. The same result is given in the paper [1], but it has been obtained not on the basis of a holistic three-dimensional model, but on the basis of projections. The analyzed procedure of obtaining the incidence angle *a* under the specified parameters of a cone of grinding, the depth of soil tillage *a* and the back angle ε_a is demonstrative but long. It would be easier to obtain the angle between the tangent to a hyperbola – the section of a cone of grinding turned though the incidence angle by horizontal plane of field level – and the direction of unit motion. It should be obtained similarly to the analyzed case, in which we took $\alpha = 90^0$, $\beta = 0$ in the equations (3). Under the specified value of the angles *α* and *β=0* we obtain the equation that is similar to the equation (9), which includes the angle *α*, that is to say one can find the back angle ε_a under the specified *α*, or vice versa, one can find the incidence angle *α* at vertical mounting of a disk under the specified back angle ε_a.

The developed three-dimensional model gives the opportunity to determine not only the incidence angle *α*, but also the roll angle *β* of a disk, under which the availability of the specified back angle ε_a is provided, since if there is an additional vertical deviation of the blade plane of a disk through the angle *β*, the back angle ε_a will change. Thus, using the analogical approach, one can determine the dependence (9), which interrelates the angles *α*, *β* and ε_a (that is to say under *β≠0)*. This expression will certainly be more cumbersome than (9). Its closed form (at *u=0*) is the following:

$$\mathrm{tg}\varepsilon_a = -\frac{\sqrt{a\left(2r\cos\beta - a\right)}\cos\alpha\,\mathrm{tg}\delta - \sin\alpha\left[r\cos\beta\sec\delta\cos(\beta+\delta) + a\sin\beta\,\mathrm{tg}\delta\right]}{\sqrt{a\left(2r\cos\beta - a\right)}\sin\alpha\,\mathrm{tg}\delta + \cos\alpha\left[r\cos\beta\sec\delta\cos(\beta+\delta) + a\sin\beta\,\mathrm{tg}\delta\right]}. \tag{11}$$

RESULTS

The expression (11) determines a dependence of the design parameters of a cone of grinding (*r* and *δ*) and the angles *α*, *β* and ε_a at the specified depth of soil tillage *a*. On substituting the values of the disk angles $\alpha = 35^0$, $\beta = 0^0$, the parameters of a cone of grinding *r=225 mm*, $\delta = 39.2^0$ and the depth of soil tillage *a=80 mm* into it, we get the value of the back angle $\varepsilon_a \approx 3^0$, that is to say the result, which was previously obtained. By the expression (11) one can determine a dependence *α=α(β)* with the known design parameters and the specified back angle ε_a and the depth of tillage *a*. Fig.4 graphically illustrates such a dependence.

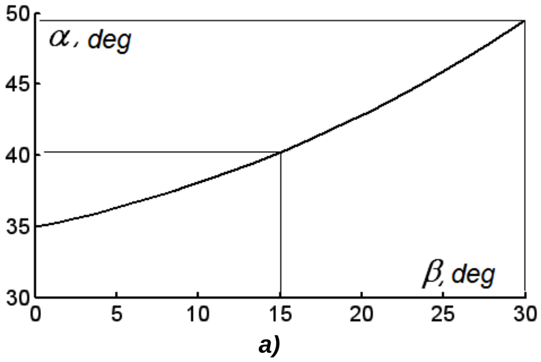

a)

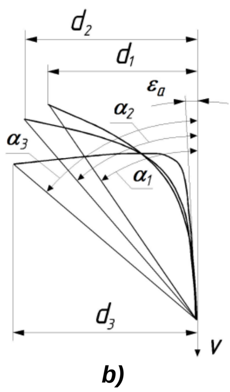

b)

Fig.4 – Graphic illustration of disk installation with design parameters *r=225 mm*, *δ=39.2⁰*, depth of soil tillage *a=80 mm* and specified back angle $\varepsilon_a = 3^0$:
a) graph α=α(β) of incidence angle versus roll angle;
b) horizontal plane section lines at field level under different disk angles

As the graph suggests, vertical deviation of a disk plane results in the increase of the incidence angle α. If the roll of a disk is nonexistent ($\beta=0^0$), the minimum value of the incidence angle, which provides the specified back angle $\varepsilon_a=3^0$, must be $\alpha=35^0$. If we set the roll angle of a disk $\beta=15^0$, the back angle must be increased by 5^0 (Fig. 4.a). We can determine the precise value of the incidence angle in this case - $\alpha=40.2^0$. Accordingly, if $\beta=30^0$, the incidence angle is $\alpha=49.4^0$. For better visualization horizontal plane sections of a cone of grinding at field level for all three cases have been prepared. Fig. 5 illustrates such a section for disk installation under angles $\beta=30^0$, $\alpha=49.4^0$.

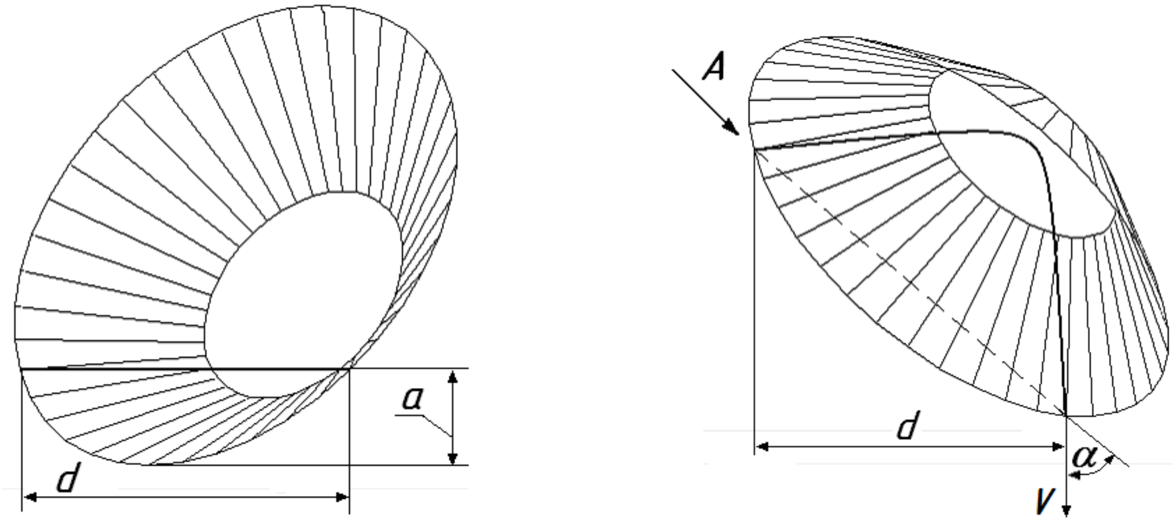

a)

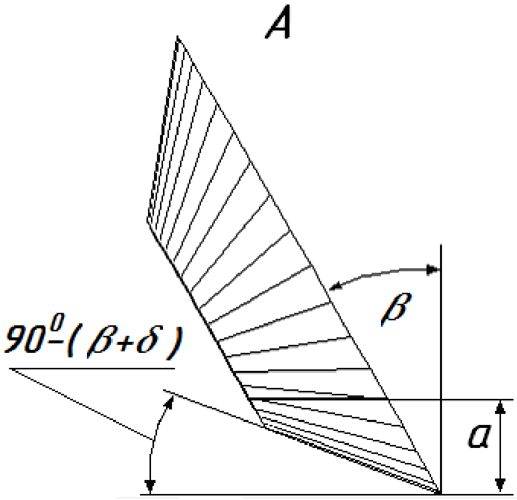

b)

Fig.5 – Rectangular projections of a cone of grinding:
a) front projection and side view;
b) additional view in direction A, when a blade plane is projected on a straight line

The symbols are the following: V – direction of speed motion of a unit, d –grip of a disk at field level (front projection of an intercept of soil entry points of a blade). If the incidence angle β is present, the angle between the lower generator of a cone and a furrow bottom decreases by its value. In our case it is equal to $90^0-(30^0+39.2^0)=20.8^0$. The back angle at the lower point of a disk depends on it.

Fig.4.b combines three sections of a cone of grinding for three values of the roll angle ($\beta=0^0$, $\beta=15^0$ and $\beta=30^0$) with the corresponding incidence angles and under the specified value of a back angle $\varepsilon_a=3^0$. It shows, that the distance d increases with the increase of the roll angle (and the correspondent increase of the incidence angle), which results in the increase in the grip of a disk. However, this is inferred based only on providing the value of the back angle, which does not prevent a disk from being deepened into the soil without taking into consideration the requirements for cutting and mixing crop residues with soil. Uncontrolled increase of the incidence angle under the increase of the roll angle may cause disk drawing.

CONCLUSIONS

Due to the developed holistic three-dimensional model of disk arrangement one can calculate all the necessary data of disk installation for soil tillage with the specified design parameters. It allows getting the values of an incidence angle and a roll angle under which a specified back angle is provided and vice versa, it allows determining the value of a back angle under specified values of an incidence angle and a roll angle. Besides, one can get the curves of horizontal plane section of a cone of grinding at any level of tillable soil. The indicated parameters are merely geometrical and are not connected with the technological process flow. In order to interrelate geometrical and technological parameters it is necessary to use the developed model when investigating the interaction between a disk and soil.

REFERENCES

[1] Blednyx V.V., (2010), Arrangement, design and engineering of soil tillage tools. Tutorial (Устройство, расчет и проектирование почвообрабатывающих орудий. Учебное пособие). CGAA, p.160, Chelyabinsk;

[2] Demydenko A.I., Snigerev D.S., Vaymer E.Y., (2009), On the development of the working body of the milling for cutting slits (К вопросу создания фрезерного рабочего органа для нарезки щелей). *Materials of the 63rd Scientific and Technical Conference "SibADI" GOU (Материалы 63-й научно-технической конференции ГОУ "СибАДИ")*, Book 1, pp. 240-243, Omsk;

[3] Haponenko O.I., (2012), Programming of the uniformity of tillage by disk operating elements with spring tines (Програмування рівномірності обробітку дисковими робочими органами на пружних стійках), *Collection of scientific papers of Vinnytsia National Agrarian University. Part: Technical Sciences (Збірник наукових праць Вінницького національного аграрного університету. Серія: Технічні науки.),* № 11, Vol. 2 (66), pp.135–141, Vinnitsa;

[4] Heruk S.M., Petrychenko E.A., (2014), Development trends in designing sowing units (Тенденції розвитку конструкцій посівних агрегатів)*, Technical Servicing of agroindustrial, forestry and transportation complexes (Технічний сервіс агропромислового, лісового та транспортного комплексів)*, № 1, pp.31-45, KIyiv;

[5] Hevko R.B., Dzyura V.O., Romanovsky R.M., (2014), Mathematical model of the pneumatic-screw conveyor screw mechanism operation, *INMATEH-Agricultural Engineering Journal*, vol.44, no.3, pp.103-110, Bucharest/Romania;

[6] Hevko R.B., Synii S.V., Osuhovskyi V.M., (2012), The new compact potato harvester (Новий малогабаритний комбайн для збирання картоплі), *Journal of Engineering Academy of Ukraine (Вісник інженерної академії України)*, № 3-4, pp.72-76, Kyiv;

[7] Hevko R.B., Klendiy O.M., (2014), The investigation of the process of a screw conveyer safety device actuation, *INMATEH-Agricultural Engineering Journal*, vol.42, no.1, pp.55-60, Bucharest;

[8] Hevko R.B., Zalutskyi S.Z., Tkachenko I.G., Klendiy O.M., (2015), Development and investigation of reciprocating screw with flexible helical surface*, INMATEH-Agricultural Engineering Journal*, vol.46, no.2, pp.133-138, Bucharest/Romania;

[9] Hrynenko O., Lebedev S., (2011), Investigation of the vibration of disk soil tillage equipment (Дослідження коливань дискових ґрунтообробних знарядь), *Technical and technological aspects of the development and testing of new machinery and technologies in agriculture of Ukraine: collection of scientific papers L. Pohorilyi UNDIPVT (Техніко-технологічні аспекти розвитку та випробування нової техніки і технологій для сільського господарства України: зб. наук. праць УкрНДІПВТ ім. Л.Погорілого)*, Investigative, Issue15 (29), pp.50–53;

[10] Pylypaka S.F., Klendii M.B., (2016), Analytical model of concave disk mounting for soil tillage for the determination of geometrical and technological characteristics (Аналітична модель установки грунтообробних сферичних дисків для визначення геометричних та технологічних характеристик)*, Scientific Bulletin of NULES of Ukraine. Part: Technology and Power Engineering in AIC (Науковий вісник НУБіП України: Серія "Техніка та енергетика АПК")*, Vol. 241, Part.1, (ISSN 2222 - 8594), pp.104-115, Kyiv;

[11] Posmetyev V.I., Zelikov V.A., Latysheva M.A., (2013), Condition and ways of solution of the problem zaglublyaemosti of the spherical disk working organs of tillers forest (Состояние и пути решения проблемы заглубляемости сферических дисковых рабочих органов лесных

почвообрабатывающих орудий), *Voronezh Scientific and Technical Gazette (Воронежский научно-технический вестник),* p.218, Voronezh;
[12] Sineokov G.N., Panov I.M., (1977), Theory and design of soil tillage machinery (Теория и расчет почвообрабатывающих машин), *Mechanical Engineering (Машиностроение)*, p.311, Moskow;
[13] Soxt K.A., (2014), Disk harrows and disk stubble ploughs. *Tutorial (Дисковые бороны и лущильники. Учебное пособие)*, KGAU, 2014, p.164, Krasnodar;
[14] Strelbitskii V.F., (1978), Disk soil tillage machinery (Дисковые почвообрабатывающие машины), *Mechanical Engineering (Машиностроение)*, p.218, Moskow;
[15] Tsimmerman M.Z., (1978), Operating elements of soil tillage machinery (Рабочие органы почвообрабатывающих машин). *Mechanical Engineering (Машиностроение)*, p. 162 pg. Moskow;
[16] Zaika P.M., (2001), Theory of agricultural machinery (Теорія сільськогосподарських машин), Vol. I (Part 1), *Machinery and tools for soil tillage (Машини та знаряддя для обробітку ґрунту)*, Oko, p.444, Kharkiv.

SELF-DRIVEN STUBBLE CLEANING AND LAND PREPARATION COMBINED MACHINE, CHINA
/
自驱动灭茬联合整地机的设计与试验研究

Ph.D. Hu Jun [1], Ph.D. LI Hailiang [1], B.S. Song Yujie [1], B.S. Zhang Haibo [1,2], B.S. Zhang Zhongxuan [1,2], Ph.D. Khokan Kumer Sarker[3]
[1]College of Engineering, Heilongjiang BA YI Agricultural University, Daqing/China; [2]Heilongjiang province Beian Authority, Jianshe farm / China; [3]Bangladesh Agricultural Research Institute, Dhaka/ Bangladesh
Tel: +86-130-69645265; E-mail: gxcylhl@163.com

Keywords: *stubble-breaking cultivating machine;self-driven;design;test*

ABSTRACT
In order to solve the problem consisting in the large amount of energy consuming of stubble-breaking cultivating machines, according to the current cultivation mode in the northeast China and the conservation tillage agriculture technical requirements, a self-driven stubble-breaking combined cultivating machine that can work with big-power tractors has been designed. Also, there were designed the transmission system, cutting stumbles device and self-driven wheel on the basis of calculating the size and analyzing the track of the moving parts; the speed range of stubble cutter shaft is 904~1365rad/min. Experiment results showed that the machine's cutting stubbles rate is 92.30%, mashing clods rate is 95.03%, saved fuel consumption is about 25.3~33.8%, function and technology meet the requirements of corn no-till seeding of ridge culture area in northeast China. The results of the study have a great significance in reducing the agricultural equipment energy consumption, providing reference for the study of the corresponding high efficiency and energy saving of equipment.

摘要
灭茬整地是耕作过程中的重要环节，其在工作过程中需要消耗大量的功耗，是影响农业生产成本的主要因素。为了减少整地的功耗，降低生产成本，提高农民收入，本文设计了一款可与大马力拖拉机配套使用的自驱动灭茬联合整地机。首先，根据东北地区的耕作模式和保护性耕作的技术特点，提出自驱联合整地机的设计要求。其次，通过理论分析与计算对传动系统、灭茬装置和自驱装置等主要结构进行了设计。最后，制作样机并进行田间试验，试验结果表明：自驱动灭茬联合整地机的灭茬率为 92.30%，碎土率为 95.03%，节省油耗约为 25.3～33.8%，工作效果显著，技术性能可靠，满足东北垄作区玉米免耕播种的要求。研究结果对降低农业机具的工作能耗具有重要的意义，为研究相应的高效节能机具提供了参考。

INTRODUCTION
Conservation tillage technology has matured and has been gradually recognized worldwide. This technology has been widely used in China *(LV R, et al., 2014)*, due to its advantages of environmental sustainability and increased grain production. A stubble cleaning and land preparation combined machine suitable for the specific national conditions of China is important to improve the domestic agricultural mechanization in the country *(Kassam A. H. W. Li, et al., 2006)*.

Stubble cleaning and land preparation are important links in tillage conservation and are characterized by heavy work and large working resistance. Stubble cleaning and land preparation combined machines are vital to agricultural production and have been studied extensively. Internationally, Mouazen A M used a finite element method to analyze and optimize sub-soiling shovels *(Mouazen A.M.; Neményi M. et al., 1999)*. W.C. Swick constructed a dynamic model of land tillage parts to predict the shear and friction stresses of working parts. Subrata Karmakar used the fluid dynamic (computational fluid dynamic) method to analyze stresses on land tillage parts during operation *(Karmakar S. and Kushwaha R.L., et al., 2006)*. Domestically, Jia Honglei designed a rotary stubble cleaning and land preparation combined machine that is suitable for cultivation tillage *(Swick W.C. et al., 1988; Jia H L. et al., 2007; Jia H L. et al., 2009)*. Tong Jin optimized the design of the rotary and stubble blades according to the theory of bionics *(Jin T. et al., 2015)*. Sun Rongrong designed a stubble breaking device to prevent large soil disturbances *(Sun R R , et al., 2008)*. Lin Jing designed the Archimedes spiral-type cap-cutting disc, which can effectively reduce stubble breaking resistance and improve ditching quality *(Lin J, et al., 2014)*. These studies focused on the design of deep-tillage parts and soil breaking parts, as well as the parameter optimization of stubble cutting and breaking devices. Consequently, the stubble breaking rate is improved. However, studies on energy conservation and consumption reduction methods to reduce the cost of agricultural production are scarce.

In this study, a self-driven stubble cleaning and land preparation combined machine (self-driven combined land preparation machine hereinafter) is presented. This machine can be used with a high-powered tractor. The rest of the paper is organized as follows. In the second part, the working principle of the proposed self-driven combined land preparation machine is clarified according to its technical requirements. The driving system, stubble cleaning device, and self-driven wheel designs are explained with theoretical analysis. In the third part, a prototype is produced and a field experiment is conducted to validate the design feasibility. The machine transforms the torque produced by friction between the self-driven wheels and the ground into the rotary driving force of the stubble cleaning blade axis. As a result, energy consumption is decreased effectively and the stubble cleaning and soil breaking rates are assured. Therefore, the machine achieves high performance efficiency and reduces cost.

MATERIAL AND METHOD

Overall design of the system

Stubble cleaning and land preparation combined machines can create good bed conditions for planting, improve the passing performance of the seeder, and ensure seeding quality. According to the working conditions and actual agronomic requirements, the technical requirements of the proposed stubble cleaning land preparation combined machine are as follows:

(1) This machine can reduce energy consumption during operation and reduce production cost effectively.

(2) This machine can complete root stubble crushing and soil breaking effectively. This machine can also meet the agronomic and conservation tillage technology requirements in the cold and ridge areas in Northeast China.

(3) This machine is mobile and has a complete machine structure with small vibration and consistent performance.

The entire structure of the self-driven combined land preparation machine is designed according to the basic parameters for completing stubble cleaning and proper land preparation. The main components of the machine are as follows: traction frame, walking wheels, stubble cleaning mechanism, transmission mechanism, gearboxes, and self-driven wheels (Fig.1). The transmission mechanism, stubble cleaning mechanism, and self-driven wheels are the main structures of the machine and are the main focus of this study.

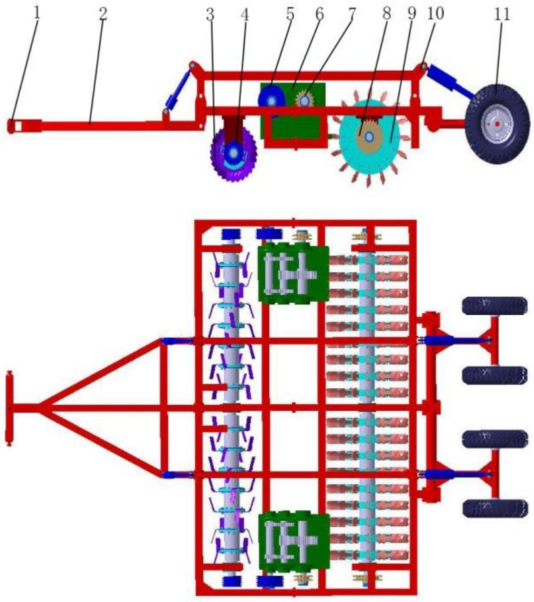

Fig.1 - Self-driven Combined Land Preparation Machine

1.Traction Beam; 2.Tripodal; 3.Stubble Cleaning Mechanism; 4.Small Pulley; 5.Large Pulley; 6.Gearbox; 7.Small Sprocket Wheel; 8.Large Sprocket Wheel; 9.Self-driven Wheel; 10.Frame; 11.Walking Wheel

The self-driven combined preparation machine works under the traction of the hydraulic suspension system of the tractor. During operation, the torque caused by friction between the self-driven wheels and the ground drives the self-driven axis to rotate, and the power is transmitted to the stubble cleaning device through the chain drive, gearbox, and belt drive. The stubble cleaning device thus accomplishes stubble cleaning and soil breaking. The driving pawl of the self-driven wheels is embedded into the ground, which can also accomplish some stubble cleaning work. The working depth can be adjusted by the depth-limited cylinder. The driving force needed by the self-driven combined land preparation machine is no longer provided by the tractor, but transformed from the torque generated by friction. This phenomenon reduces the power output of the tractor and energy consumption. The main performance indicators and technical parameters of the machine are shown in Table 1.

Table 1

Main Performance Indicators and Technical Parameters of the Self-driven Combined Land Preparation Machine

Item	**Parameter**	**Item**	**Parameter**
Size (L×W×H) / (mm×mm×mm)	8000×5570×1300	**Diameter of Stubble Cleaning Blade Axis** (mm)	500
Working Width (mm)	4400	**Rotation Speed of Stubble Cleaning Blade** (rad/min)	904~1365
Operation Speed (km/h)	8~12	**Stubble Cleaning Depth** (mm)	720
Traction Power (kW)	180~220	**Stubble Cleaning Rate** (%)	92.30
Diameter of Self-driven Wheel (mm)	1075	**Soil Breaking Rate** (%)	95.03

Design of the driving system

The tillage power of the self-driven combined land preparation machine is generated by the rotation of driving wheels. The rotation speed of these wheels is limited by the walking speed of the machine. A speed change device must be installed to satisfy the required rotation speed transmitted to the stubble cleaning shaft, thereby satisfying the agricultural technical requirements of straw returning.

The drive system design requires rational allocation at all levels to meet the rotation speed requirement and ensure the minimum size of the overall drive system. The design scheme is shown in Fig. 2. The machine has a biaxial structure. The self-driven wheels in the self-driven area rotate because of friction with the ground. The rotation speed increases through the chain drive, secondary gearbox, and belt drive, and then is transmitted to the stubble cleaning shaft in the stubble cleaning area where stubble cleaning work is accomplished. The two-gearbox structure can ensure the stability and reliability of power transmission.

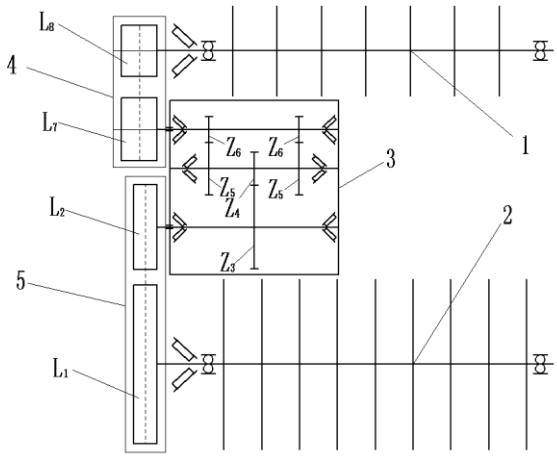

Fig.2 - Drive System Design Scheme

1. Stubble Cleaning Shaft; 2. Self-driven Shaft; 3. Gearbox; 4. Belt Drive; 5. Chain Drive

The feed speed of land preparation machines commonly used in the three provinces of Northeast China is 8 km/h to 12 km/h, and the common rotation speed of the stubble cleaning shaft ranges from 1000 r/min to 1500 r/min. The diameter of the self-driven wheel disc is Φ800 mm. Using Formulas (1) and (2), the range of the drive ratio *i* of the drive mechanism is 12.5≤i≤18.86.

$$n = \frac{V}{2\pi r} \tag{1}$$

$$i = \frac{V_M}{n} \tag{2}$$

Where *n* is the rotation speed of the self-driven pawl (r/min), *V* is the edge linear speed of the self-driven fixed pulley (m/min) ,V_M is the general rotation speed of the stubble cleaning shaft, 1000 (r/min), *i* is the drive ratio.

After the calculation, the drive ratio of chain drive $i_{12} = \frac{L_1}{L_2} = 1.58$

the primary drive ratio of the straight gear $i_{34} = \frac{Z_3}{Z_4} = 3$

the secondary drive ratio of the straight gear $i_{56} = \frac{Z_5}{Z_6} = 2$

the belt drive ratio $i_{78} = \frac{L_7}{L_8} = 1.8$

The teeth number of gears at different levels and diameters of the chain and belt wheels of the drive system can be determined by referring to the mechanical design manual in Table 2.

Table 2

Drive Ratio of the Drive System and Size Parameters of Driving Parts

	Drive Ratio *i*	**Teeth Number of Large/Small Gear**	**Reference Diameter of Large/Small Chain Wheel** (mm)	**Diameter of Large/Small Belt Wheel** (mm)
Chain Drive	1.58	27/17	-	-
Gearbox Tier 1	3	-	386/128	-
Gearbox Tier 2	2	-	244/122	-
Belt Drive	1.8	-	-	180/100

The rotation speeds of the stubble cleaning blade axis at two running speeds are calculated as:

$$n''_{min} = n_{min} \times (i_{12} \times i_{34} \times i_{56} \times i_{78}) \approx 904 r/min$$

$$n''_{max} = n_{max} \times (i_{12} \times i_{34} \times i_{56} \times i_{78}) \approx 1365 r/min$$

The calculations show that, when the proposed self-driven combined land preparation machine runs at the speed of 8~12 km/h, the rotation speed of the stubble blade axis ranges from 904 rad/min to 1365 rad/min. This range is in accordance with the requirement of a common speed range for combined land preparation machines. Thus, the drive mechanism design is reasonable. The drive system is shown in Fig.3.

Fig.3 - Drive System of the Self-driven Combined Land Preparation Machine

Design of the Stubble Cleaning Device

To reduce the soil damage caused by the tillage process, the seeding process is conducted on the surface of the earth covered by crop straw and stubble. The no-till seeding machinery in China is behind that in foreign countries in terms of anti-blocking technology, and the seeding process has high seedbed requirements. Specifically, stubble in the land must be cleaned before seeding. The stubble cleaning device is an important part of the proposed self-driven combined land preparation machine. This device can break the roots and clods in soil and improve the passing performance and seeding quality of the seeder. It can also loosen the soil, maintain moisture, and improve the soil aggregate structure.

According to the movement mechanism of the self-driven stubble cleaning device, the stubble blade can move in two ways: one is the running of the entire machine at a certain speed v_m, and the other is the circular rotary motion of the blade around the blade axis at a certain linear velocity v_0. Thus, the vector equation of absolute velocity is established as

$$\bar{v} = \bar{v}_m + \bar{v}_o$$

Using the center of the blade axis O as the origin point, a rectangular coordinate system is established with the forward direction of the machine as the positive half of the x-axis, and the upward direction perpendicular to the earth as the positive half of the y-axis (Fig.4). The motion trajectory equation of the blade endpoint N(x,y) is obtained by

$$\begin{cases} x = v_m t + R\cos\varpi t \\ y = R\sin\varpi t \end{cases}$$

where ω is the angle speed of the blade axis (rad/s), v_m is the forward speed of the machine, R is the radius of gyration of the stubble cleaning blade (m) .

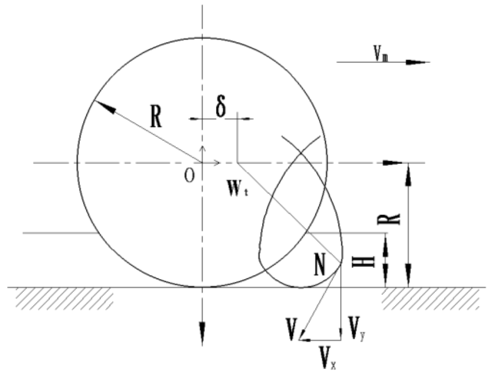

Fig.4 - Motion Trajectory Diagram of the Endpoint of the Blade

The ratio of the circular speed of the stubble cleaning blade to the moving speed of the machine is defined as the stubble cleaning ratio expressed by λ :

$$\lambda = \frac{v_0}{v_m} = \frac{R\varpi}{V_m} \tag{3}$$

The endpoint of the stubble cleaning blade is denoted as N. When $\lambda > 1$, the motion trajectory of N is trochoidal (Fig. 5). The trajectory in a period of motion is investigated. The maximum and minimum horizontal distances on the trajectory line are set as A, B, and C. When the blade moves to the BC section, the horizontal velocity of the absolute motion of the stubble cleaning blade endpoint is opposite the moving direction of the self-driven stubble cleaning device. In this case, the edge of the blade can cut the soil and stubble and throw them backward to achieve stubble cleaning and land preparation. To facilitate the rotary cutting function of the stubble cleaning blade and break the clods on the surface and the root stubble under the ground, $\lambda > 1$ in the design.

Fig.5 - Trochoidal Motion Trajectory of N

A straight blade is used as the stubble cleaning blade (Fig. 6). The size parameters of this blade are shown in Table 3. The straight blade is characterized by good soil cutting, breaking, and throwing properties. This blade is also widely used because of its simple manufacturing requirements. The stubble cleaning blade must have high wear resistance because it needs to contact the soil and reach into it. Accordingly, the stubble cleaning blade of 65 Mn is used in the design *(Zhang X Y et al., 2009)*.

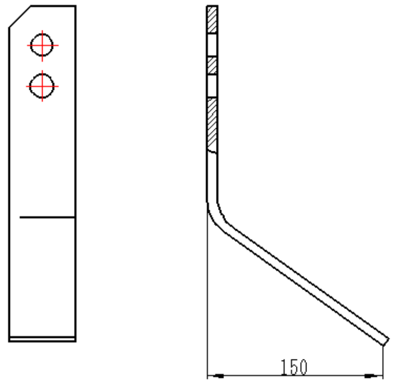

Fig. 6 - Straight Blade Stubble Cleaner

Table 1

Parameters of the Stubble Cleaning Blade

Item	Value	Item	Value
Indentation Angle	119°	**Bending Radius**	40 mm
Diameter of the Blade Axis	580 mm	**Blade Angle**	17°
Blade Thickness	1.5 mm	**Cutting Width**	150 mm

The structure of the stubble cleaning blade axis is determined on the basis of the motion analysis results and size of the stubble cleaning blade *(Shentu L F. et al., 2007)*. The main components of this blade axis are as follows: joint tray, stubble cleaning blade, blade disc, fastening device, blade axis, bearing, and belt wheel (Fig.7). A total of seven stubble cleaning blade discs are present on the blade axis. Each blade disc has a diameter of 350 mm and a rotation angle of 12.8°. Four straight blade stubble cleaners are fastened by bolts on each disc; two on the left and two on the right are fastened in alternating and symmetrical positions *(Jia H L. et al., 2011; Tu J P. et al., 2003)*. The width and depth of the stubble cleaning device are 4400 and 72 mm, respectively. The rotation speed of the stubble cleaning blade axis is 904 rad/min to 1365 rad/min. The stubble cleaning device is shown in Fig. 8.

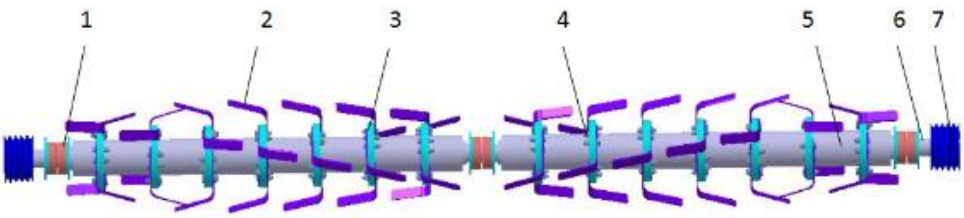

Fig.7 - Structure of the Stubble Cleaning Blade Axis

1.Joint Tray; 2.Stubble Cleaning Blade; 3.Stubble Cleaning Blade Disc; 4.Fastening Device; 5.Stubble Cleaning Blade Axis; 6.Bearing; 7.Belt Wheel

Fig.8 - Stubble Cleaning Device of the Self-driven Combined Land Preparation Machine

Design of Self-driven Wheels

During operation, the pawls on the self-driven wheels are embedded into the soil. The self-driven shaft rotates because of the soil resistance force, and the power generated is transmitted to the stubble cleaning assembly through the drive mechanism. Stubble cleaning and soil breaking are completed in the roll cutting operation.

The main components of the self-driven wheels are as follows: chain wheel, self-driven wheel pawl, self-driven wheel disc, self-driven shaft, fastening device, joint tray, and bearing (Fig. 9). Nine self-driven wheel discs alternate on the self-driven shaft, which can enhance the uniformity and stability of the device. The diameter of the self-driven wheel disc is set to 800 mm for the purpose of increasing the self-driven moment arm and improving the power conversion rate.

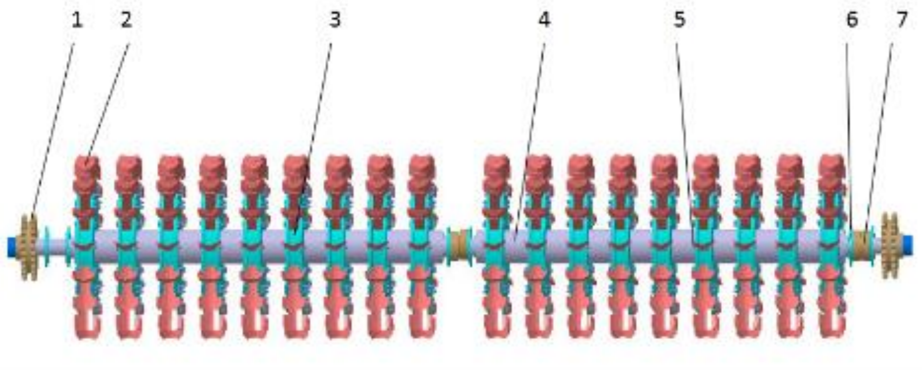

Fig.9 - Structure Display of the Self-driven Wheel

1.Chain Wheel; 2.Self-driven Wheel Pawl; 3.Self-driven Wheel Disc; 4.Self-driven Shaft; 5.Fastening Device; 6.Joint Tray; 7.Bearing

The self-driven wheels function as the power input part of the self-driven system, and the edge of each wheel is hollow. The fixed part of the self-driven pawl is embedded in the self-driven wheel and fastened through welding and fastening device to ensure the fastening strength. The parameters of the self-driven wheels are shown in Table 4, and the real object is shown in Fig. 10.

Table 4

Main Parameters of Self-driven Wheels

Item	Value	Item	Value
Size (mm)	1040×100	**Number of Pawls**	16
Wheel Disc Diameter (mm)	800	**Angle of Pawl** (°)	22.5
Space between Wheels (mm)	245	**Number of Wheels Discs**	9

Fig. 10 - Self-driven Wheels of the Self-driven Combined Land Preparation Machine

RESULTS

Field Experiment

The experiment was conducted in Team 2 corn stubble field of Jianshe Farm in Heilongjiang Province, during May 12 and May 26, 2013. No treatment was performed before the experiment. The experimental tools mainly included the proposed self-driven combined land preparation machine (Fig. 11), a Deer7820 tractor (equipped with GPS), a platform scale (accurate to 0.1 kg), a soil moisture measuring instrument, a soil density measuring instrument, a set of oil measuring devices, and two rulers. The physical parameters of the soil in the experimental field are shown in Table 5.

Fig. 11 - Self-driven Combined Land Preparation Machine

Table 5

Parameters of the Experimental Field

Item	Mean
Vegetation Amount (kg/m^3)	2.0
Soil Density (KPa)	36.5
Absolute Moisture Content in Soil (%)	19.8
Corn Stubble Height (cm)	15–36

Stubble Rate Measurement

In accordance with the industrial standards of the rotary tiller combined work machine (JB/T8401.2-2007), the measurement and calculation method of the stubble cleaning rate is as follows: select several points in the corn stubble field according to a specific schedule and write the number as n; mark a 1 m^2 area at each point to measure the root stubble in the scope; stubble shorter than or equal to 5 qualifies *(Ma H L, et al., 2007)*; substitute the data into Formula 4 to calculate the stubble cleaning rate:

$$P = \frac{M_h}{M_g} \times 100\% \tag{4}$$

where *P* is the stubble cleaning rate of the nth plot (%), M_h is the weight of the stubble shorter than 5 cm in the nth plot (Kg), M_g is the total weight of the stubble in the nth plot (Kg).

Soil Breaking Rate Measurement

The calibration method of the soil breaking rate is similar to that of the stubble cleaning rate. The measurement and calculation method is as follows: select several points in the corn stubble field according to a specific schedule and write the number as n; mark an area of 0.5 m×0.5 m at each point to measure the weight of clods with the longest edge of shorter than 4 cm and are within 10 cm under the ground and the total weight of all clods; substitute the data into Formula 5 to calculate the soil breaking rate:

$$E = \frac{M_a}{M_b} \times 100\% \tag{5}$$

where *E* is the soil breaking rate of the tillage layer within 10 cm under the ground in the nth plot (%), M_a is the total weight of the clods shorter than 4 cm within 10 cm under the ground in the nth plot (Kg), M_b is the total weight of the clods within 10 cm under the ground in the nth plot (Kg).

Oil Consumption Measurement

The starting and ending lines were marked before the experiment. A preparation area was set aside. The tractor pulled the self-driven combined land preparation machine to enter the detection area at a constant speed. When the front end of the machine touched the starting line, the oil measurement device was activated. When the back end of the machine touched the ending line, the measurement ended *(Guo Z J. et al., 2003)*. In the experiment, the speed, width, time, and working conditions were measured by the GPS on the tractor and the data were recorded. Oil consumption was calculated according to Formulas (6) and (7) *(Fang Z.H. et al., 2000)*.

$$K = \frac{G}{W} \tag{6}$$

$$W = 0.1BV \tag{7}$$

where K is the oil consumption amount (kg/hm^2), G is the oil consumption of the machine per hour (kg/h) , W is the productivity of the machine (hm^2/h), B is the working width (m), V is the operation speed of the machine (km/h).

Experimental Results

In the experiment, the tractor pulled the self-driven combined land preparation machine at a constant speed of 10 km/h for four land preparation cycles. Afterward, the parameters were measured and recorded and the means were calculated. The results are shown in Table 6.

Table 6

Operation Quality

Time	Stubble Cleaning Rate (%)	Soil Breaking Rate (%)	Oil Consumption (L·hm^{-2})
1	91.60	95.12	12.5
2	93.11	94.33	14.8
3	92.43	96.04	13.3
4	92.06	94.63	15.2
Mean	92.30	95.03	13.9

The results show the field environment has 36.5 KPa soil density, 19.8% moisture content, and 15~36 cm deep corn root stubble. The self-driven combined land preparation machine completes the stubble cleaning at 10 km/h and achieves a stubble cleaning rate of 92.30% and a soil breaking rate of 95.03%. The average oil consumption of the commonly used combined land preparation machines, such as Ecolo-Tiger 730C and John Deere 2700, is between 21.0L and 18.6L per hectare. Meanwhile, the oil conservation rate of the machine in this study is 25.3%~33.8%.

CONCLUSIONS

In this study, a self-driven combined land preparation machine is designed to overcome the large power consumption of the commonly used stubble cleaning and land preparation combined machines. The design of key parts of the proposed self-driven combined land preparation machine is discussed in detail. The main conclusions of this study are as follows. The alternating and symmetrical arrangement of the stubble cleaning blades improves the stubble cleaning effect and the stress of the stubble blade axis, and ensures the running stability of the machine. The increase in the diameter of the self-driven wheel disc increases the force provided to the self-driven arm, thereby obtaining superior driving effect. However, in terms of the counterweight of the entire machine, smaller diameter of self-driven wheel disc translates to better performance. The simulation analysis shows that a diameter of 800 mm provides optimal performance. With the increase in the running speed, the stubble cleaning blade axis rotates faster, thereby improving the rates of stubble cleaning and soil breaking. However, in high-speed operation, the load of the stubble cleaning blade increases and thus can result in its damage. Furthermore, overly high speeds may reduce the land preparation effect. The optimal speed for the combined land preparation machine is 10 m/s. These conclusions provide a reference for designing similar self-driven combined land preparation machine and shortening the development cycle. However, the practical production shows that, when the land humidity is high, the self-driven wheel pawls cannot be embedded in the soil firmly. As a result, the self-driven effect reduces and no effective driving force is provided. Therefore, the design of self-driven wheels must be optimized further, particularly the structure and arrangement of self-driven wheel pawls.

ACKNOWLEDGEMENT

This study was funded by the General Bureau of Heilongjiang Land Reclamation (HNKXIV-10-04a).

REFERENCES

[1] Fang Z.H., Zhou Z.L., Yang T.Z., (2000), Statistical properties of working load engine in ploughing *Journal of Transactions of the Chinese Society of Agricultural Engineering*, Vol.16, Issue 4, pp.85-87, Chinese Society of Agriculture Engineering/Peking;
[2] Guo Z.J., Zhou Z. Li, Xu D., et al., (2003), Experiment on high efficient and energy saving bionic sub soiling components. *Journal of Henan University of Science and Technology*, Natural Science, Vol.24, Issue 3, pp.1-3, Natural Science/ Luo Yang;
[3] Jia H.L, Huang D.Y, Liu X L. et al., (2011), Symmetrical multi-spiral arrangement of tillage blades on rotor. *Journal of Transactions of The Chinese Society of Agricultural Engineering*, Vol.27, Issue 4, pp.111-116, Chinese Society of Agriculture Engineering/Peking;
[4] Jia H.L, Ji W.F., Han W F. et al., (2009), Optimization experiment of structure parameters of rotating and stubble breaking universal blade. *Transaction of The Chinese Society of Agriculture Machinery,* Vol.40, Issue 7, pp.45-50, Chinese Society for Agriculture Machinery /Peking;
[5] Jia H.L., Ma C.G, Li G.Y, et al., (2007), Combined rototilling-stubble-breaking-planting machine. *Soil and Tillage Research,* Vol.96, Issue 1, pp.73-8, Elsevier Science BV/Netherlands;
[6] Jin T, Ji W.F, Jia H L et al., (2015), Design and Tests of Biomimetic Blades for Soil-rototilling and Stubble-breaking. *Journal of Bionic Engineering,* Vol.12, Issue 3, pp.495-503, Science Press/Changchun;
[7] Karmakar S, Kushwaha R.L., (2006) Dynamic modeling of soil-tool interaction: an overview from a fluid flow perspective. *Journal of Terra mechanics,* Vol.43, Issue 4, pp.411-425, Pergamon-Elsevier Science LTD/Netherlands;
[8] Kassam A.H.W.Li, H.W. Gao et al., (2006), Subsoiling effect and economic benefit under conservation tillage mode in Northern China. *Transactions of the Chinese Society of Agricultural Engineering,* Vol.10, pp.62-67, Chinese Society of Agriculture Engineering/Peking;
[9] Lin J, Li B., Li B.F., et al., (2014), Parameter Optimization and Experiment on Archimedes Spiral Type of Cap Cutting Disc. *Journal of Transaction of The Chinese Society of Agriculture Machinery*, Vol.45, Issue 6, pp.118-124, Chinese Society for Agriculture Machinery /Peking;
[10] Lv R, Xiong Y, Li Y. et al., (2014), Effect of Conservation Tillage on Soil Carbon Pool in Farmland. *Journal of Soil and Water Conservation*, Vol.4, institute of Soil and Water Conservation/Shanxi, pp.38;
[11] Ma H.L, Gao H.W, Li H.W. et al., (2007), Design and experiment of no-till planter with oblique driven disc. *Journal of Transaction of the Chinese Society for Agricultural Machinery*, Vol.38, Issue 5, pp.47-50, Chinese Society for Agriculture Machinery /Peking;
[12] Mouazen A M, Neményi M., (1999), Finite element analysis of subsoiler cutting in non-homogeneous sandy loam soil. *Soil and Tillage Research,* Vol.51, Issue 1, pp.1-15, Elsevier Science BV/Netherlands;
[13] Shentu L F, Shao P, (2007), Optimized design from rotor shaft of rotary tiller and stubble cutting machine. *Journal of Huaihai Institute of Technology*, Issue 6, pp.12-15, Journal of Huaihai Institute of Technology/Lianyungang;
[14] Sun R.R, Li W.Y., Li H.W., (2008), Design and Experiment on Power Driven Root-stalk Cutting Mechanism of Ridge-till and No-till Corn Planter. *Transaction of The Chinese Society of Agriculture Machinery*, Vol.08, pp.48-53, Chinese Society for Agriculture Machinery /Peking;
[15] Swick W.C, Perumpral J V., (1988) A model for predicting soil-tool interaction. *Journal of Terra mechanics,* Vol.25, Issue 1, pp.43-56, Pergamon-Elsevier Science LTD/Netherlands;
[16] Tu J.P, Xu X.H, Xia Z.Y, (2003), The study of the cutting-blade and optimum of the knife-array on field straw chopper. *Journal of Agricultural Mechanization Research,* Vol.4, pp.102-104, Mechanization Research/Harbin;
[17] Zhang X Y, Li L.H., Wang C. et al., (2009), Design and test of 1GSZ-350 stubble-breaking and rototilling combined cultivating machine. *Journal of Transactions of The Chinese Society of Agricultural Engineering*, Vol.25, Issue 5, pp.73-77, Chinese Society of Agricultural Engineering/Peking.

EFFECT OF PERMEABLE BOUNDARY OF WATER-CONDUCTING DEVICE ON WATER AND SALT TRANSPORT UNDER INDIRECT SUBSURFACE DRIP IRRIGATION

/

导水装置透水边界对间接地下滴灌水盐运移的影响

Assoc. Prof. QiaoXia An [1], Assoc. Prof. Ph.D. Stud. SanMin Sun [*1,2], M.S. Rong Xu [1], Stud. JingHao Zhao[1], Stud. KaiKai Gu [1] Stud. Hong Cai[1], Stud. JingYang Ma [1],

[1]College of Water Conservancy and Architecture Engineering, Tarim University, Alar / China
[2]College of Water Resources and Civil Engineering, China Agricultural University, Beijing/ China
Corresponding author： Sanmin Sun, Tel: +8609974680383; Email: ssmaqx@126.com

ABSTRACT

Indirect subsurface drip irrigation is an effective means for water-conservation irrigation. The diameter of water-conducting device and height of permeable boundary are two important design parameters for such irrigation. In this study, there were analyzed the effects of water-conducting device diameter and permeable stratum height on the characteristics of wetting front and water–salt distribution through a laboratory test. Results demonstrated that the two parameters have influenced the size and shape of the wetting, and they effected on water and salt transport in the wetting front. The suitable diameter of water-conducting device, height of permeable layer would be chosen to regulate of tree root growth, and to reduce effects of soil salinity on tree.

摘要

间接地下滴灌是一种节水高效的灌溉方式，其导水装置直径、透水边界是灌溉设计的重要参数，本文通过室内试验，分析导水装置直径、透水层高度对湿润体特征及湿润体内水盐运移的影响。结果表明：导水装置直径、透水层高度影响湿润体的大小和形状，同时也影响湿润体内水盐运移。选择适宜的导水装置直径，透水层高度，以调节作物根系的生长，同时减少土壤盐分对作物的影响。

INTRODUCTION

Drought and soil salinization coexist in South Xinjiang, China (*Wang et al, 2011; Hudan et al, 2012; Li et al, 2011).* However, red jujube, a characteristic forestry fruit with high economic value, develops rapidly with sufficient sunshine and is widely planted in South Xinjiang. This forestry fruit has brought remarkable economic, ecological, and environmental benefits to the area (*Hu et al 2016; Yao et al, 2011; Li et al, 2010*). Nevertheless, a serious secondary soil salinization exists, which is caused by the outdated irrigation technology, low water utilization, and unreasonable irrigation. Drought and soil salinization restrict further development of forest and fruit industries. Therefore, determining water-conservation and salinity-control irrigations for local red jujube deserves research attention.

Indirect subsurface drip irrigation, a novel and highly efficient water-conservation irrigation technology, is composed of a common drip irrigation system on the earth's surface and a water-conducting device in soils underneath the drip irrigation emitter. This water-conducting device consists of an upper impermeable boundary, a lower permeable boundary, and a permeable bottom (*Zhao et al, 2009*). The impermeable boundary generally uses polyvinyl chloride (PVC) tubes. Coarse sands are filled in these PVC tubes at certain depth below the bottom, hence forming a cylinder sand column below the tube bottom. The sand column and bottom surfaces are employed as the lower permeable boundary and permeable bottom layers, respectively. Water penetrates into surrounding soils through the permeable boundary and bottom layers. Indirect subsurface drip irrigation transports water directly into deep soils, where crop roots grow in, but holds the wetting front within the underground, thus reducing the evaporation of unavailable water on the soil surface, determining high water utilization, and saving water (*Meshkat et al, 2000*). This kind of irrigation is applicable to characteristic jujube in South Xinjiang. To obtain the optimum technological parameters and improve water utilization, the variation law of wetting front under different technical conditions and water–salt distributions in the wetting front after irrigation should be explored. Therefore, the current work studied the law of soil water–salt motion in indirect subsurface drip irrigation through a laboratory test. The variation law of wetting front features and water–salt distribution in the wetting front under different diameters of the water-conducting device and different heights of the permeable stratum was analyzed to provide theoretical supports for the use of Indirect subsurface drip irrigation in jujube plantation in South Xinjiang.

MATERIAL AND METHOD

Water-conducting device components

The water-conducting components are shown in Fig. 1 (*Sun et al, 2015; Sun et al, 2016*), including the drip irrigation pipe, small pipe, adjusting valve, water-conducting device, coarse sand filling inside the water-conducting device, impermeable boundary (PVC pipe), permeable boundary (coarse sand), and permeable bottom (coarse sand).

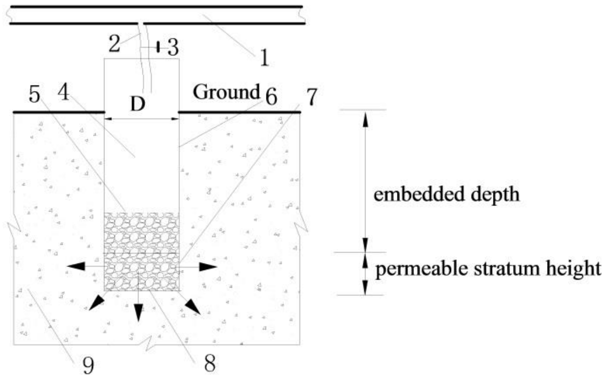

(a) schematic diagram

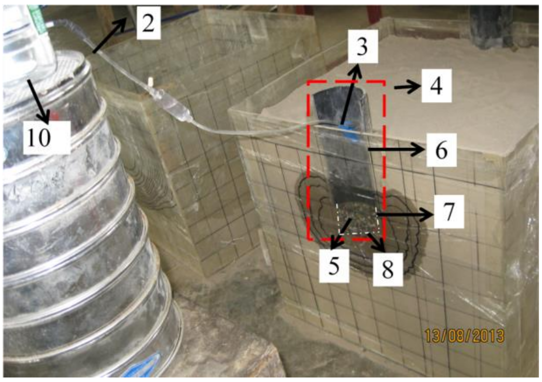

(b) real picture

Fig.1 - Diagram of indirect subsurface drip irrigation components and irrigation principles

1-drip irrigation pipe (for the field); 2-small pipe; 3-regulating valve; 4-water-conducting device; 5-coarse sand; 6-impermeable boundary of the water-conducting device; 7- permeable boundary of the water-conducting device; 8-permeable bottom; 9-root zone soil; 10- The bottle for water (for laboratory test)

Method and materials

The laboratory test was implemented in the irrigation test site of the College of Water Resources and Architectural Engineering of Tarim University from June to August 2013. Sample soils were collected in the jujube block in the test site from soil layers containing the main roots (20–40 cm deep). Soil bulk density and initial salinity were 1.40 g/cm3 and 0.68 g/kg, respectively. Soil samples were air-dried and screened by a 1 mm sieve to eliminate impurities.

The test system is composed of an organic glass test soil box and a water service. The soil box is a 500 mm (L) × 500 mm (W) × 500 mm (H) cube made of 8 mm-thick organic glasses. The length, width, and height of the soil box were scaled at 50 mm units. The water service was self-made, which connected a 2.5 L water bottle with a medical infusion tube. This system can provide stable water flow.

The water apparatus used a piece of cylinder of PVC tube. This PVC tube was divided symmetrically at the diameter of the bottom circle, placed into certain depth at the 1/2 inside wall of the soil box, and finally installed into the testing soils. Gravels screened by a 2–5 mm sieve were filled into the bottom of the PVC tube. When the sample soils remained static for 24 h, the PVC tube was uplifted to a certain height, finally forming a semi-cylindrical permeable boundary.

Stopwatch was used in irrigation. During the first hour of irrigation, the location of the wetting front was marked by a piece of black marking pen on the soil box every 5 min; subsequently, it was marked every 10 min until the end of irrigation. The upward, downward, and horizontal moving distance of the wetting front was measured by a steel ruler, and each corresponding time was recorded.

After 24 h irrigation, soil samples were collected from different profiles at 10, 20, and 30 cm (Profiles A, B, and C) away from the water-conducting device horizontally. The sampling depth of each profile was 40 cm, and every 5 cm depth was determined as one soil layer. A total of 24 soil samples were collected. Soil moisture content was measured by oven-drying method. The electrical conductivity of leach liquor was measured with the DDSJ-308A conductivity meter (INESA) by mixing 5 and 25 g of dried soil and water, respectively.

Testing program: The test designed two diameters for the water-conducting device (50 and 90 cm) and three heights for the permeable stratum (0, 5, and 10 cm). Water flow and irrigation amount were fixed at 2 L/h and 4 L, respectively. Further details about the testing program are shown in Table 1.

Table 1

Testing program

Test groups	Diameter of the water-conducting device	Height of the permeable stratum	Discharge	Irrigation amount
	[mm]	[mm]	[mm]	[L]
T1	50	0	2	4
T2	50	5	2	4
T3	50	10	2	4
T4	90	10	2	4

Data processing

The conversion between soil salinity content and soil conductivity is calculated as equation (1) (*Zhang et al, 2011*):

$$y = 3.63x + 0.108 \quad \text{[g/kg]} \qquad (1)$$

where: x - the 1:5 soil water extract conductivity [ms/cm]; y - soil salinity content .

Statistical method

Excel was used for the data processing and variance analyses.

RESULTS

Effect of water-conducting device diameter on soil wetting front

For convenient analysis of wetting front features, the wetting front at different time points was drawn by a piece of pen. The effect of permeable boundary size on the wetting front at different times is shown in Fig. 2. The wetting front under indirect subsurface drip irrigation is basically elliptical. The maximum horizontal wetting front mostly occurs at the bottom of the sand column, whereas the maximum vertical wetting front is located in the middle axle of the water-conducting device. Considering the maximum horizontal wetting front as the symmetry axis, the vertical upward and downward wetting fronts are basically equal. This conclusion agrees with the report of Zhao *et al* (2009). The above observations may be related to the characteristics of indirect subsurface drip irrigation. When irrigation water entered soil mass, some water parts will penetrate into soils and distribute evenly at different directions in homogeneous isotropic soils. Meanwhile, some parts will move downward because of gravity effect, and the remaining part will be pushed into soils by the water accumulated in the water-conducting device. Given that these two water parts cause mainly the same effect, the vertical downward wetting front and the downward wetting fronts are basically equal to each other.

Given the fixed height of the permeable stratum, the wetting front develops from a slim pattern to a flat shape with the diameter increase of the water-conducting device [see Figs. 2(c) and 2(d)].

Moreover, given the fixed diameter of the water-conducting device, the wetting front develops vertically but shrinks horizontally as the permeable stratum rises [see Figs. 2(a), 2(b), and 2(c)].

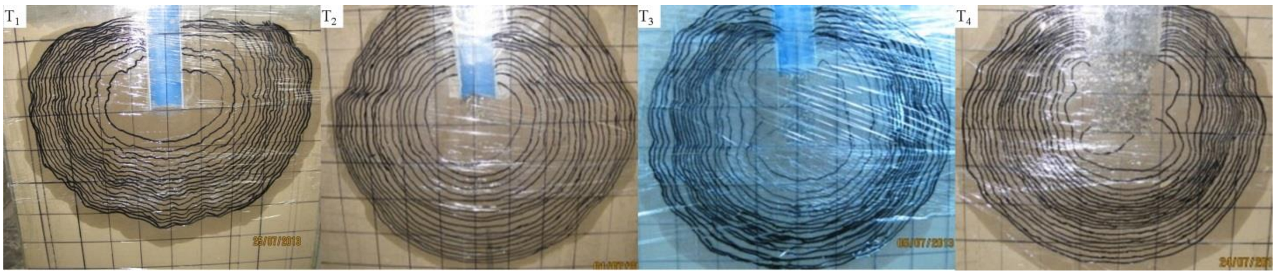

(a) (b) (c) (d)

Fig.2 - Effect of permeable boundary size on wetting front (real shot)

Effect of permeable boundary of the water-conducting device on soil water distribution

In this experiment, the water-conducting device was buried 20 cm deep into the soil. After irrigation, the highest soil moisture content was detected in 20–30 cm soil layers near the outlet. Soil moisture content decreased gradually as the layer moved farther from the outlet both vertically and horizontally (see Fig. 2).

Under the same conditions, with the diameter increase of the water-conducting device, the soil moisture content of Profiles A and B near the outlet decreases, whereas that of Profile C increases. Therefore, the increase in diameter of the water-conducting device can expand the wetting front horizontally and increase its volume, thus reducing the soil moisture content in the wetting front, which is in accordance with previous research (*Li et al, 2010*).

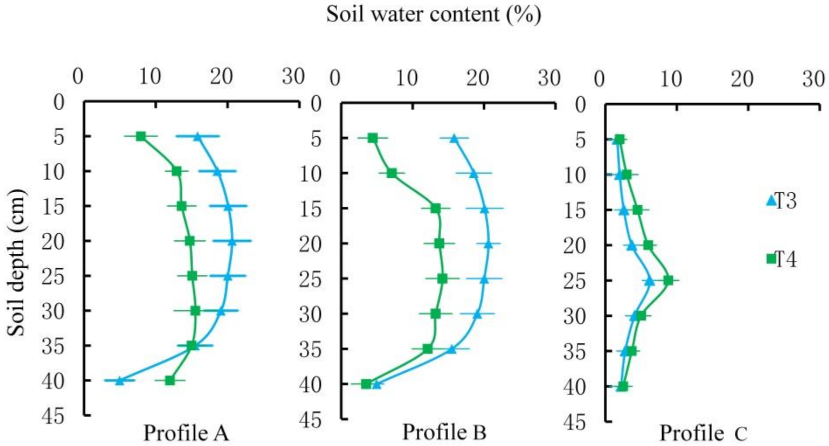

Fig.3 - Effect of water-conducting device diameter on soil water distribution

On Profiles A and B, T_1 is present significantly lower soil moisture content (30–40 cm) than the other test groups but higher soil moisture content (15–30 cm) on Profile C (see Fig. 4). The soil moisture content of T_3 on Profiles A and B changes more slightly than the other test groups, but that of T_3 on Profile C is higher than the other test groups. Therefore, increasing the permeable stratum can increase the vertical transport of water, whereas decreasing this parameter can increase the horizontal transport.

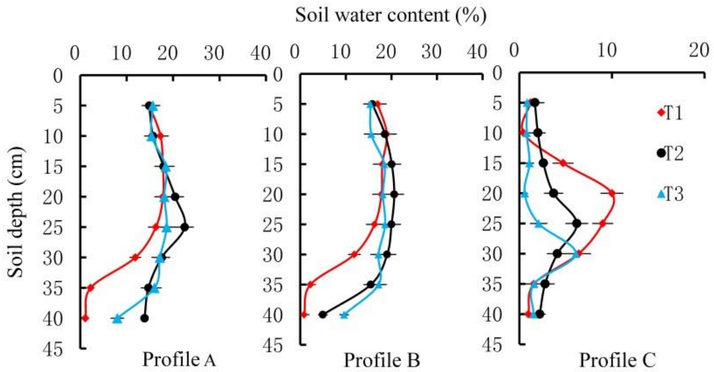

Fig.4 - Effect of permeable stratum height on soil water distribution

Effect of permeable boundary of the water-conducting device on soil salt distribution

When water entered the soil mass at the depth of 20–25 cm, the 20–30 cm-deep soil layers close to the outlet maintained high humidity, thus decreasing local soil salinity. As the water moves farther from the outlet vertically, water diffusion slows down gradually, and the leaching effect of water to soil salt weakens accordingly. This observation is manifested by the increasing soil salinity in upward and downward soil layers. As shown in Figs. 5 and 6, all the test groups showed decreased soil salinity at 20–30 cm depth but exhibited increased soil salinity at other vertical layers. Horizontally, the soil salinity of Profiles A and B is relatively lower, but that of Profile C is higher. The water-conducting device diameter and permeable stratum height can influence salt transport in the wetting front indirectly by affecting the wetting front size and water distribution. As shown in Fig. 5, when the diameter of the water-conducting device is small, the soil salinity of Profiles A and B is relatively lower, but that of Profile C is higher. This observation indicates that the small diameter of the water-conducting device can provide good leaching effect to soils near the outlet, but the leaching range is small. The larger diameter of the water-conducting device provides poorer salt-leaching effect near the outlet, but the leaching range expands.

Compared with other test groups, T_1 presents higher soil salinity at 30–40 cm soil layers on Profiles A and B but lower soil salinity at 20–30 cm soil layers on Profile C (Fig. 6). This result demonstrates that low permeable stratum will reduce downward salt leaching but increase horizontal salt leaching. By contrast, high permeable stratum will increase downward salt leaching but reduce horizontal salt leaching.

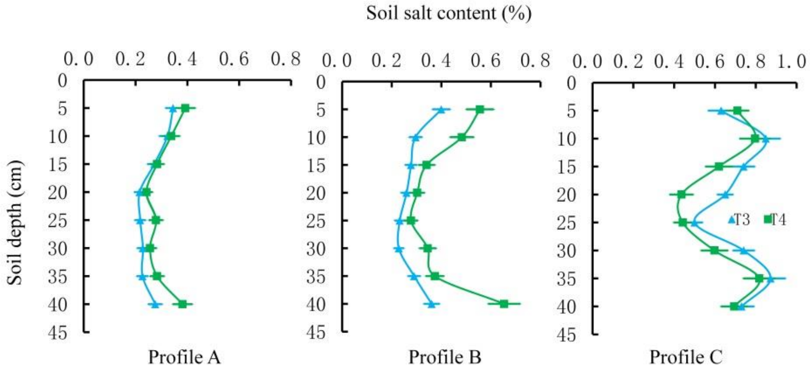

Fig.5 - Effect of water-conducting device diameter on soil salt distribution

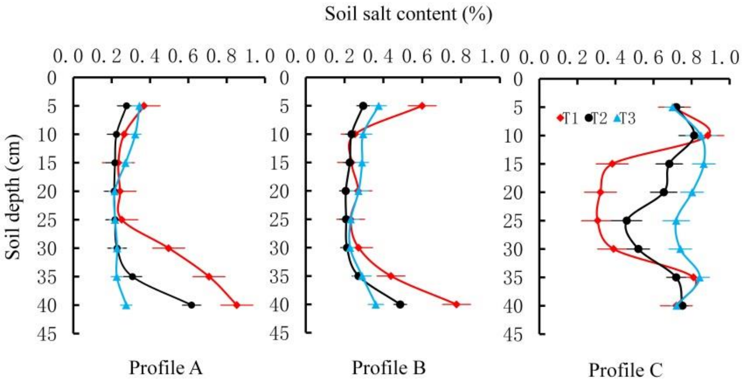

Fig.6 - Effect of permeable stratum height on soil salt distribution

CONCLUSIONS

(1) In indirect subsurface drip irrigation, the wetting front is basically elliptical. The maximum horizontal wetting front mainly occurs at the bottom of the sand column, whereas the maximum vertical wetting front is located in the middle axle of the water-conducting device. Considering the maximum horizontal wetting front as the symmetry axis, the vertical upward and downward wetting fronts are basically equal. Given the fixed height of the permeable stratus, the wetting front expands horizontally but narrows vertically with the increasing diameter of the water-conducting device. Moreover, given the fixed diameter of the water-conducting device, the wetting front develops vertically but shrinks horizontally as permeable stratum rises.

(2) After irrigation, the highest soil moisture content is detected in 20–30 cm soil layers near the outlet. Soil moisture content decreases gradually as the layer moves farther from the outlet both vertically and horizontally. With the increased diameter of the water-conducting device, the soil moisture content on Profile A and B close to the outlet decreases, whereas that on Profile C increases. Increasing the permeable stratum can increase the vertical water transport, whereas decreasing this parameter can increase the horizontal water transport.

(3) The lowest soil salinity is found in soil layers close to the outlet. Soil salinity increases gradually as the layer moves farther from the outlet. The small diameter of the water-conducting device can provide good leaching effect to soils near the outlet, but the leaching range is small. The larger diameter of the water-conducting device provides poorer salt-leaching effect near the outlet, but the leaching range expands. Furthermore, low permeable stratum will reduce downward salt leaching but increase horizontal salt leaching. By contrast, high permeable stratum will increase downward salt leaching but reduce horizontal salt leaching.

On the basis of the above results, high permeable stratum can induce downward growth of crop roots and relieve the influence of soil salinity on crop growth. Hence, this novel design should be used for the irrigation system of jujube tree. However, overly high permeable stratum will cause water penetration into deep soil layers and waste water resources. The diameter of the water-conducting device should be varied for the different growth stages of jujube tree: small diameter for young trees and large diameter for old trees. Nevertheless, this diameter design can produce an appropriate large wetting front for root to absorb water.

ACKNOWLEDGEMENT

This work was financially supported by the National Natural Science Foundation of China (Nos. 51069013 and 51369028), the College Students' Innovative Projects of China (No. 201410757004). The authors express their gratitude to Mr. HuanJie Cai, for his help in conducting this research.

REFERENCES

[1] BaoLin Yao, SanMin Sun, Ma J, et al., (2011), Influence of irrigation quota on distribution of soil water and salinity for the drip irrigation of red jujube, *China Rural Water and Hydropower*, Issue 4, pp.88-91, ISSN 1007-2284, Wuhan University, Wuhan/China;

[2] Hudan·T, Wu Zh G, Su L T, (2012), Numerical simulation of soil water-salt movement on drip irrigation cotton under film, *Soils*, vol.44, Issue 4, pp.665-670, ISSN 0253-9829, Institute of Soil Science, Chinese Academy of Sciences, Nanjing/China;

[3] JiaShuai Hu, ZhenHua Wang, XuRong Zheng, (2016), A study on effects of drip irrigation modes on perennial red jujube under the condition of changing flood irrigation into drip irrigation, *Water-Saving Irrigation*, Issue 6, pp.31-35, ISSN 1007-4929, Wuhan University, Wuhan/China;

[4] JingYe Li, Qiang Yuan, Hui Jiang, (2010), A discussion on development of featured forestry and fruit growing based on the regional adaptability, *Xinjiang Agricultural Sciences*, vol.47,Issue 4, pp.741-749, ISSN 1001-4330, Xinjiang Academy of Agricultural Sciences, Urumchi/China;

[5] LiChun Wang, JianChu Shi, Qiang Zuo, et al., (2011), Establishing and validating the root water uptake model of winter wheat under salt stress conditions, *Transactions of the Chinese Society of Agricultural Engineering*, vol.27, Issue 1, pp.112-117, ISSN 1002-6819, Chinese Society of Agricultural Engineering, Beijing/China;

[6] Tao Li, Jianfeng Zhang, Huijuan Cheng,et al., (2010), The wetting front distribution characteristic and the fitting model of single point free infiltration under deep pit irrigation in the field, *Agricultural Research in the Arid Areas*, vol.28,Issue 4, pp.36-39, ISSN 1000-7601, Northwest Sci-Tech University of Agriculture and Forestry, YangLin/China;

[7] Meshkat M R C, Warner R C, Workman S R, (2000),Evaporation reduction potential in an undisturbed soil irrigated with surface drip and sand tube irrigation, *Transactions of the ASAE*, vol.43,Issue 1, pp. 79-86, ISSN 0001-2351 , American Society of Agricultural and Biological Engineers / American;

[8] SanMin Sun, QiaoXia An, HuanJie Cai. et al., (2015), Research on salt movement law in jujube root zone under indirect subsurface drip irrigation, *Transactions of the Chinese Society for Agricultural Machinery*, vol.45,Issue 1, pp. 160-169, ISSN 1000-1298, Chinese Society for Agricultural Machinery, Beijing/China;

[9] Sun S. M., Yang P. L., An Q. X., et al., (2016), Investigation into surface and subsurface drip irrigation for jujube trees grown in saline soil under extremely arid climate, *European journal of horticultural science*, vol.81,Issue 3, pp. 165-174, ISSN1611-4426, International Society for Horticultural Science, Leuven/Belgium/China;

[10] WeiXia Zhao, ZhenHua Zhang, HuanJie Cai, et al., (2009), Parameter model of water-conducting device specification for indirect subsurface drip irrigation, *Journal of Hydraulic Engineering*, vol.40,Issue 3, pp. 355-363, ISSN 0559-9350, Chinese Hydraulic Engineering Society, Beijing/China;

[11] Yu, Zhang, LiHong, Wang, SanMin,Sun, et al., (2011), Indexes of salt tolerance of cotton in Akesu river irrigation district, *Scientia Agricultura Sinica*, vol.44, Issue 10, pp.2051-2059, ISSN 0578-1752, Chinese Academy of Agricultural Sciences, Beijing/China.

EFFECT OF PLASTIC MULCHING ON WATER BALANCE AND YIELD OF DRYLAND MAIZE IN THE LOESS PLATEAU

覆膜对黄土高原旱作玉米产量与农田水量平衡的影响

Ph.D. Stud. Zhou Shanshan [1], Prof. Liu Wenzhao [*1,2], Ph.D. Stud. Lin Wen [2]
[1]College of Natural Resources and Environment, Northwest A&F University, Yangling / Shaanxi / China; [2] State Key Laboratory of Soil Erosion and Dryland Farming on the Loess Plateau, Institute of Soil and Water Conservation, CAS & MWR, Yangling / Shaanxi / China
E-mail: wzliu@ms.iswc.ac.cn

Keywords: *plastic mulching, dryland maize, transpiration, evapotranspiration, water use efficiency*

ABSTRACT

Less and varied soil-water supply is the main limiting factor for crop production in the Loess Plateau of China. A field study on dryland spring maize was conducted to investigate the effects of plastic film mulching practice on maize growth, yield, water use efficiency (WUE), soil water storages (SWS) and the ratio of transpiration to evapotranspiration (T/ET) on the Changwu Tableland of the Loess Plateau in 2013. The T characteristics of maize were measured using the sap flow method. Results showed that plastic film mulching treatment had a seedling emergence rate of 98.1%, which was significantly higher than the 80.2% of the non-mulching treatment. Maize plants reached every growth stage earlier and the whole growth period was shortened by 14 days under plastic film mulching. Soil water storage was markedly higher in plastic mulching field than in non-mulching field before July. However, at reproductive stages soil water content within the 40-150 cm profile was lower under plastic film mulching because of relatively enhancement of root water absorption. The daily mean ET under plastic mulching was lower than that under non-mulching, whereas the daily mean T was the opposite. The T/ET of maize was 68.1% under non-mulching and 85.5% under plastic mulching from July to September. Under the same LAI, the T/ET of plastic mulcingh was greater than that under non-mulching conditions. The plastic mulching decreased ET but increased WUE by 89.8%. It was concluded that plastic mulching is beneficial for increasing available water and improving the yield of maize on the Loess Plateau.

摘要

基于黄土高原南部长武塬区旱作春玉米田间试验，就覆膜和露地（未覆膜）两种条件下玉米生长及蒸腾、蒸散过程进行监测与对比分析，探讨覆膜的作用与影响。蒸腾速率利用包裹式茎流计测定。结果表明：覆膜、露地处理玉米出苗率分别为98.1%和80.2%，其差异显著；覆膜提早玉米各生育阶段，缩短全生育期14 d。覆膜条件下，玉米在营养生长阶段土壤水分贮存量显著提升；然而40-150 cm土层的贮水量从7月初开始由于根系吸水相对增强而低于露地。覆膜条件下农田蒸散（ET）小于露地，而其蒸腾（T）却大于露地；7-9月露地与覆膜的T/ET分别为68.1%和85.5%；且在相同的LAI下覆膜的T/ET大于露地，土壤蒸发受到抑制。覆膜措施在降低农田耗水量的同时，随着蒸腾量的提升显著地提高了玉米产量和收获指数（P＜0.05），水分利用效率提高了89.8%。覆膜措施能增加黄土塬区旱作玉米的经济产量，并提高作物水分利用效率。

INTRODUCTION

The Loess Plateau is located in the upper and middle reaches of the Yellow River in China，and has an area of 640, 000 km2. In this region, precipitation is the major water resources for agriculture production, and less and varied soil water supply is the main limiting factor for crop yield (Kang et al., 2002; Liu W. Z., Zhang X. C., et al., 2010). Maize (Zea mays L.) is a major crop on the Loess Plateau. However, the low temperature in spring and drought stress normally resulted in poor grain yield of this crop *(Zhou et al., 2009)*.

Hence, management strategies to effectively use water and to sustain productivity are crucial for rainfed farming. In recent years, plastic film mulching with double ridges and furrows has been widely used in crop production in the Loess Plateau *(Li et al., 2013)*. The ridge directs the runoff to the furrow where the water infiltrates through capillaries to inside the ridge. Planting in the furrows ensures good water moisture in the soil near the plant *(Li et al., 2001)*. The surface film mulching favorably influences the soil moisture regime by controlling evaporation (E) from the soil surface *(Raeini-Sarjaz and Barthakur, 1997)*. This pattern increased yield and water use efficiency (WUE) significantly in this area *(Midega et al., 2013;*

Saidou et al., 2003; Sharma et al., 2011), due to increasing of soil temperature *(Anikwe et al., 2007; Hadrian et al., 2006)*, augmenting of available soil water *(Fisher,1995;Wang et al., 2009)*, and reducing soil E from evapotranspiration (ET) *(Li et al., 2013; Wang et al., 2011)*. ET, consisting of soil E and plant transpiration (T), is a major component of water balance in ecosystems *(Gentine et al, 2007)*. However, there are very few studies to investigate plant T and soil E and T/ET on rainfed dryland maize. Therefore, our field experiments were conducted with the following objectives: (1) to measure plant T characteristics of maize under dryland farming conditions in Loess Plateau using the sap flow method and analyze the effects of plastic film mulching on the T/ET; (2) to assess the effects of plastic film mulching on soil water content at various layers and dynamics of soil water storages (SWS) during the whole maize growing period; and (3) understand the relationship between yield and soil moisture under plastic film mulching.

MATERIAL AND METHOD

Site description

The field study was conducted in 2013 at the Changwu experimental station (35.28° N, 107.88° E, approximately 1200 m above sea level) located in a typical dryland farming area on the Loess Plateau in northwestern China. The average annual precipitation in the area was 584 mm, with 466.4 mm and 307.9 mm falling between April and September (i.e., maize growth season) and between July and September (maize silking usually occurs in the middle of July), respectively. The rainfall during the spring maize growing season amounted to 520.2 mm in 2013, accounting for 90.1% of the annual precipitation (Fig. 1). The annual average temperature is 9.7°C, and the annual frost-free period is 171 d. The ground water table is at a depth of more than 50 m, making groundwater unavailable for plant growth. The soil field capacity is 20% ± 2% by weight (g/g) and wilting coefficient is 6% ± 2% (g/g). The maize variety Pioneer 335, a very popular maize hybrid in this region, was used in this study.

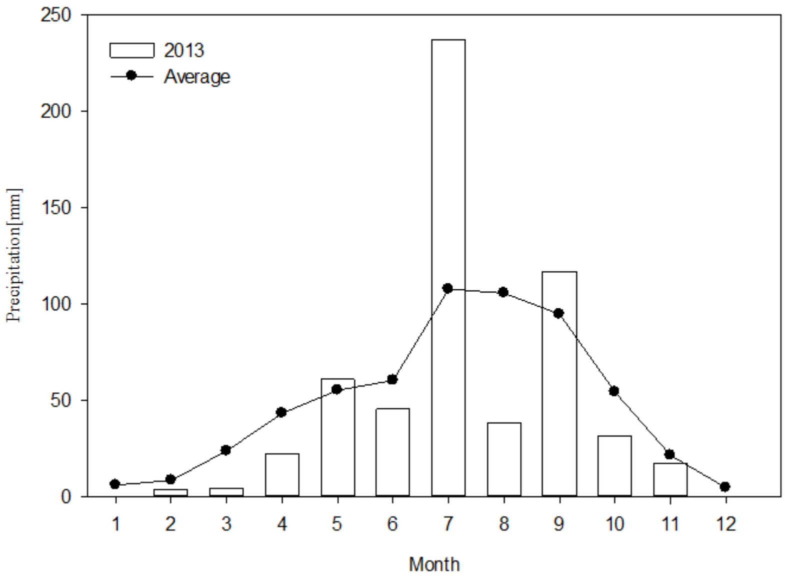

Fig.1 - Precipitation distribution during 2013 compared to the long-term means (1956-2005)

Experimental design and field management

In this experiment, two treatments—a control with non-mulching and treatment with plastic film mulching (Fig. 2) —were designed and applied. A planting pattern of double ridges and furrows was adopted in each treatment. The ridges were created in an alternating pattern consisting of large ridges (60 cm wide by 10 cm high) and small ridges (40 cm wide by 15 cm high). The plastic film mulching treatment involved mulching with pieces of white plastic film 120 cm wide and all ridges and furrows mulched with plastic film. In the bottom of the two ridges was the furrow where rainwater could be harvest. Each treatment was replicated three times and was applied to 40 m^2 (5 m × 8 m) plots arranged in randomized block design. Before ridging the treatment plots, chemical fertilizers were applied at rates of 225 kg of N ha^{-1} in the form of urea (46% N), 60 kg of P ha^{-1} in the form of calcium superphosphate (12% P_2O_5) and 30 kg of K ha^{-1} in the form of potassium sulfate (45% K_2O).

In each plot, the maize was planted in the furrows with a planting spacing of 30 cm and in all treatments at a density of 65,000 plants ha^{-1} to a depth of 5 cm using a hand-powered hole-drilling machine on April 23, 2013. During the maize growing season, the soil water supply was solely dependent on natural rainfall for all of the treatments. The non-mulching treatment and the plastic film mulching treatment were harvested on August 25 and September 8, 2013, respectively. The sap flow was measured by the stem flow gauge on three adult plants under each treatment after the 12-leaf stage.

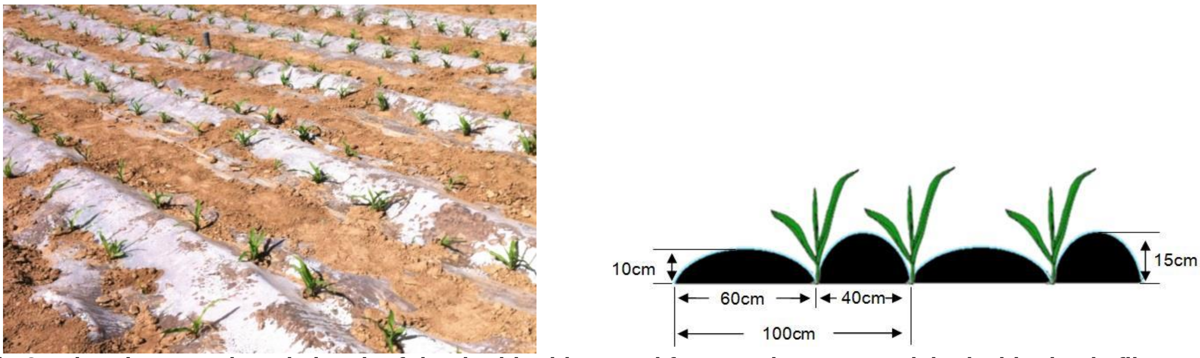

Fig.2 - The Photograph and sketch of the double ridges and furrows that were mulched with plastic film

Measurements and data calculation

(1) Leaf area indexes, yield and its components

The Seedling emergence rate and growth stages of the maize were recorded. Nine plants were marked randomly in each plot for measuring leaf area indexes (LAI), located at least 1 m from plot edges and 0.5 m from previous sampling sites.

Leaf area was calculated by multiplying their manually measured length and maximal width with a shape factor, k, empirically determined to be 0.75 for maize *(McKee, 1964)*. The LAI value for each plot was then calculated as the product of the leaf area value and the plant density (65,000 plants ha^{-1}), i.e., LAI = leaf area (m^2 $plant^{-1}$) × 65,000(plants ha^{-1})/10,000 (m^2 ha^{-1}). Shoot biomass was determined after oven drying, at 105°C for 30 min initially and then at 65-75°C for 48 h.

At maturity, the grain yield (kg ha^{-1}) was measured for all of the plants in a 16 m^2 area in each plot. Weight, length and rows of the ear, ear perimeter, Kernels per row/ear and 100-kernel weight were measured. The grain yield was determined based on the average of three plot replicates, and all of the samples were dried to a constant weight by natural air drying. The mass figures are expressed in terms of air dry weight. The harvest index (%) was calculated as the air dry grain yield divided by the total above ground air dry biomass at maturity.

A standardized maize development stage system was used to identify plant growth stages (Ritchie et al., 1992), and the date was recorded at which 50% or more of the maize plants in each plot reached the following vegetative and reproductive stages: planting time (PT), 4-leaf stage(V4), 6-leaf stage(V6), 8-leaf stage(V8), 12-leaf stage(V12), silking stage (R1), blister stage (R2), milk stage (R3), dent stage (R5) and physiological maturity stage (R6).

(2) Soil moisture content

The dynamic change in the gravitational soil moisture content (%) was determined using a neutron moisture meter (CNC503B). Before maize sowing, neutron probe tubes were installed in three replicated plots of each treatment, positioned in the middle of the plots. The water content in the soil profile was determined at 10cm depth intervals down to 100 cm and at 20 cm intervals from 100 to 300 cm. The measurements were conducted approximately every five days during the maize growing season.

(3) Sap flow

The sap flow (g h^{-1}) was measured by the sap flow gauge. The sap flow system used in this study was a commercially available Flow32-1K (Dynamax, Houston, USA), and the gauge signals were recorded using a CR1000 Datalogger, including PC400 data logger support software that was programmed to measure at 15 sec intervals and to store the average values over 1 h periods. And the sensor type is SGB25 in this study. The sensors were mounted on different plants every seven days to prevent plant desiccation resulting from the heating of the sensor. The sap flow gauge was installed to measure the sap flow of maize plants in the same period and under the same soil moisture conditions to identify differences among sensors; these differences were not significant. Therefore, the error in this study was caused by factors other than the sensors.

The scaling up T from single plant to whole plot requires an analysis of plant variability to correctly determine the mean plant value. This analysis was accomplished based on the variability of plant stem diameter *(Bethenod et al., 2000)*. The results showed a diameter classification in the range of 13 to 23 mm (Fig. 3).The crop was sufficiently homogeneous and plants with a diameter between 19 and 21 mm represented 76% of the total plants. We considered the plants belonging to this class to represent the "mean plant" in the field.

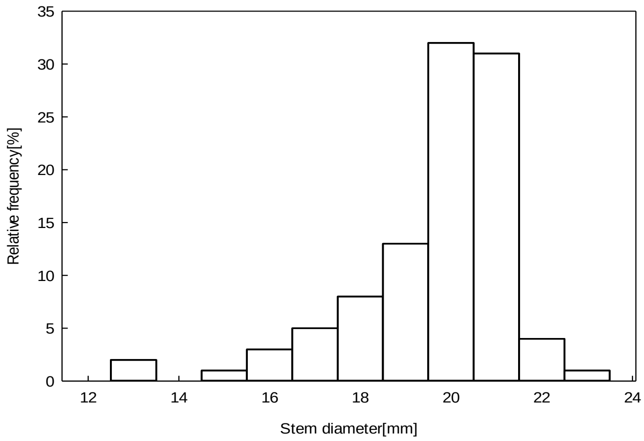

Fig.3 - Frequency distribution of the stem diameters of the maize plants that were sampled in the experimental plot (n =100)

(4) Evapotranspiration

The ET (mm) was determined by the following formula:

$$ET = \Delta W + P \quad (1)$$

Where ΔW is soil water depletion (mm) between planting and harvesting in 0-300 cm soil layer, P is the precipitation (mm) during the crop growing season. ET is the sum of soil E and crop T. Because the field plots were flat and each plot was surrounded by ridges, surface runoff is near zero and precipitation infiltration below 3 m is unlikely. Therefore, the surface runoff and deep drainage are neglected.

(5) Water use efficiency

WUE_T (kg ha^{-1} mm^{-1}) and WUE_{ET} (kg ha^{-1} mm^{-1}) were calculated by the formulas：

$$WUE_T = Y / T \quad (2)$$

$$WUE_{ET} = Y / ET \quad (3)$$

Where Y is grain yield (kg ha^{-1}), T is transpiration (mm), ET is evapotranspiration (mm).

(6) Meteorological data

The meteorological data during the year of experiment were measured at the Changwu automatic meteorological monitoring station situated within 50 m of the experimental field.

Statistical analyses

ANOVA from the SAS package was used to conduct analyses of variance.

RESULTS

Seedling emergence rate and growth stage

Seedlings (V4) emerged 6 d earlier in plastic film mulching treatment than in non-mulched plots (Fig. 4). Seedling emergence rates were 98.1% for film mulching and 80.2% for non-mulched plots, respectively. The time to the stage (V6), silking stage (R1), and maturity (R6) of maize in plastic film mulching treatment was 13 d, 9 d and 14 d shorter than in non-mulched treatment. One reason was that the plastic film mulching increased topsoil temperature during the early growth period *(Liu Y., Li S.Q., et al., 2010; Zhou et al., 2009)*, on the other hand, soil water content was significantly increased *(Zhang et al., 2014; Wang et al., 2011)*. Both of those reasons resulted in earlier germination and plant establishment, and enhancing the growth of maize. Similarly, each growth stage of spring maize under plastic film mulching treatment in the East of Loess Plateau emerged an average of 7 d in advance and the whole growth period shortened by 11 d as compared with non-mulching plots, the seedling emergence rates were 99.0 and 80.0%, respectively *(Wang et al., 2012)*. The whole growth period of maize from seedling emergence to physiological maturity was 15-17 d shorter in Loess Plateau *(Liu Y., Yang S. J., et al., 2010)*. Hence, plastic film mulching promoted maize germination and advanced growth stages.

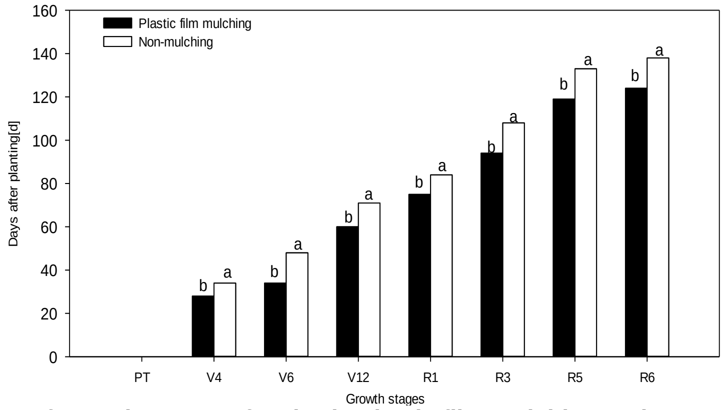

Fig.4 - Duration of growth stages of maize in plastic film mulching and non-mulching fields

PT, planting time; V4, 4-leaf stage; V6, 6-leaf stage; V12, 12-leaf stage; R1, the silking stage; R3, the milk stage; R5, the dent stage; R6, physiological maturity stage. Figures with different letters are significant at the 0.05 probability level.

Soil water

SWS (0-300 cm) increased slowly at the early growth stage though precipitation was low because maize consumed only a limited amount of water at this stage (Fig. 5). However, with increasing water use of maize to maintain active growth, SWS decreased from the middle of May to early July. Because of a large amount of rainfall in July, SWS raised greatly. In the middle of July, maize reached to the silking stage and plant T was the main way of water consumption.

SWS under plastic film mulching treatment was consistently higher than under non-mulching treatment during the whole vegetative growth, with a maximum difference of 66.2 mm. That is because those large amounts of soil moisture were lost in the non-mulching treatment through soil E; most of the soil surface was exposed to direct irradiation and a dry atmosphere. Hence, the plant growth was notably restricted by the ensuing water deficit, leading to reductions in LAI and shoot biomass *(Liu Y., Li S.Q., et al., 2010)*. However, at the reproductive stage, SWS under the non-mulching treatment was consistently higher than that in plastic film mulching plots due to that plant height and LAI under plastic film mulching reached the maximum values and significantly higher than that under non-mulching treatment, and the T of plastic film mulching was markedly higher which was the main reason of water deprivation at that stage in field *(Zhang et al., 2011)*. Hence plastic film mulching retains soil water in the early stage to promote maize development in the later stage.

The plastic film mulching treatment significantly increased the soil water content in the upper 150 cm soil layer, compared with the non-mulching treatments, while at other depths no significant differences were observed between treatments from V4 to V8 (Fig. 6). During this period, soil water depletion was in the 0-40 cm soil profile. At V12 stage, soil water depletion was in deeper soil layer (0-150cm). As precipitation increased, the topsoil water content restored, however, the deeper layer soil water was still depleted. From V12 to R3, the plastic film mulching plots had higher water content in the upper 40 cm soil layer but lower water content at depths from 40 cm to 150 cm compared with the non-mulching plots. The cause for this was that the better water-temperature conditions in mulching treatments made individual plant taller and more vigorous, it promoted the consumption of subsoil moisture *(Zhou et al., 2009)*. The plastic film mulching treatment used more water in the deeper soil than in the non-mulched treatment during this growth period. Soil water contents were almost similar at 150 cm for all treatments.

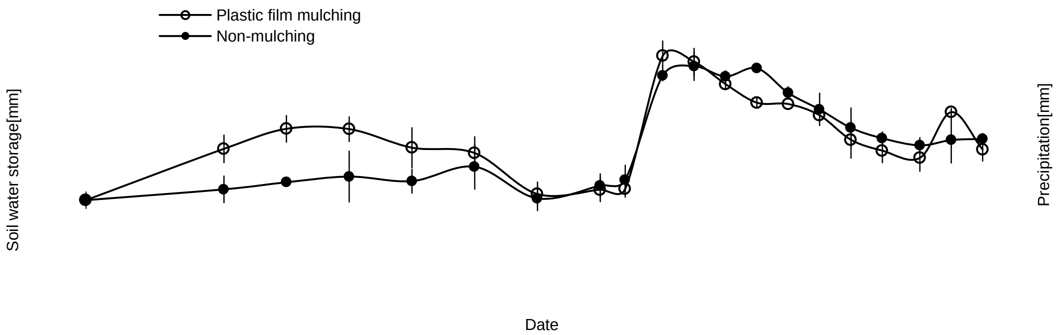

Fig.5 - Dynamics of soil water storage (SWS) in 0-300 cm layer during the maize growing period. Bars show standard errors

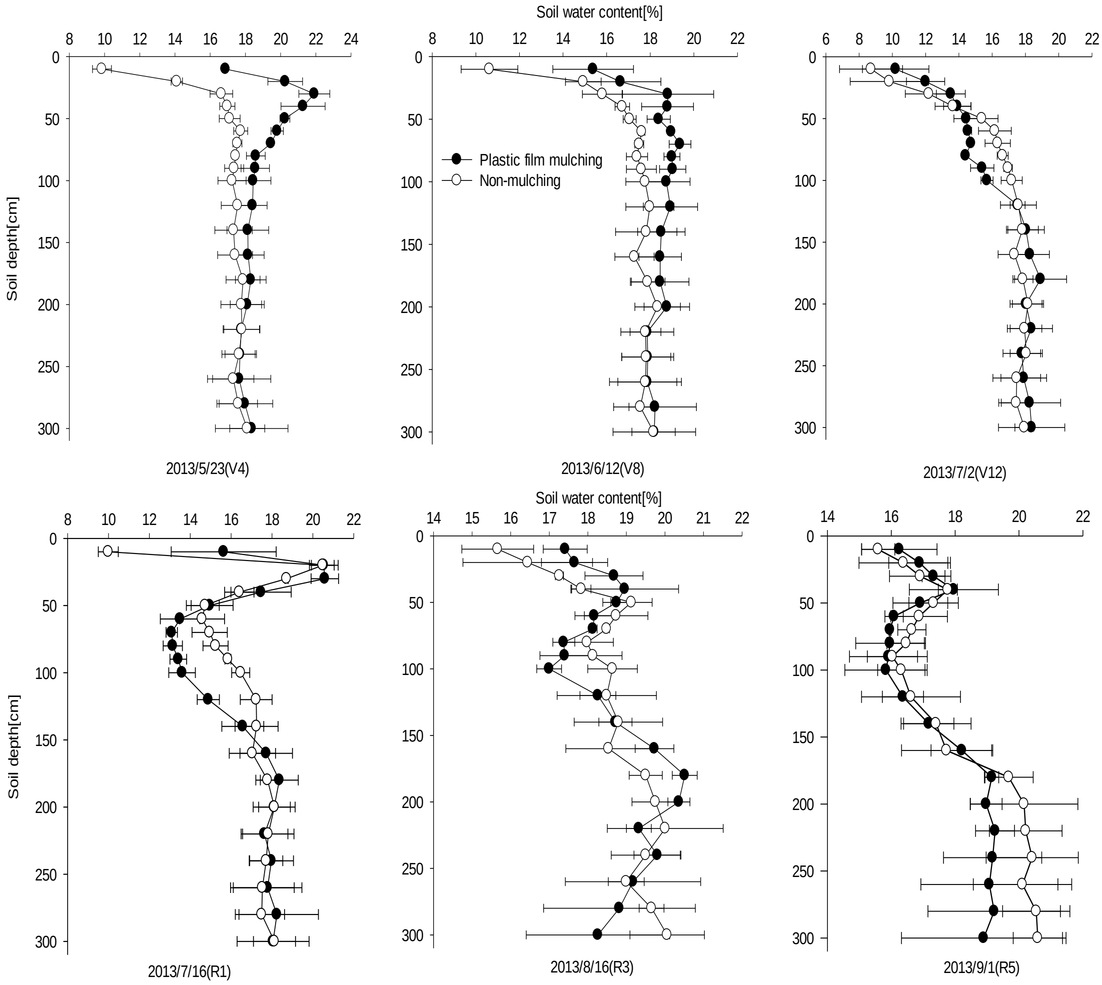

Fig.6 - soil water content in 0-300 cm layer along the soil profile in maize growing season

V4, 4-leaf stage; V8, 8-leaf stage; V12, 12-leaf stage; R1, the silking stage; R3, the milk stage; R5, the dent stage. Bars show standard errors.

Transpiration and evapotranspiration

The double mass curves of cumulative T versus cumulative ET in Fig. 7 shows the changes of T/ET with time. The T was calculated by multiplying the daily accumulated sap flow per plant by a density of 65,000 plants ha^{-1}. These curves showed that before August 21th T/ET was stable. And the mean T/ET was 89.1% under plastic film mulching, while it was 73.1% under non-mulching. The T/ET decreased under both treatments after August 21th.The daily mean ET under plastic film mulching was 4.9 mm and that under non-mulching treatment was 5.3 mm. Meanwhile, the daily mean T under plastic film mulching was 4.1 mm and that under non-mulching treatment was 3.6 mm.

The variation in T/ET is illustrated in Fig. 8 for the different treatments, T/ET decreased gradually from silking to maturity. From July to September the T/ET was 68.10% under non-mulching, while it was 85.50% under plastic film mulching. The values of T/ET were consistently higher in the plastic film mulching treatments than were those of the non-mulching treatment during the mid-late growth period. These results suggest that more water was used in plant T than soil surface E in the plastic film mulching treatments. Our results under non-mulching are within the range in studies in North China Plain. The T/ET of maize was 79.0% during the mid-late growth period using the sap flow gauge without mulching under dryland conditions *(Zhao et al. 2009)*. And the T/ET of maize was 66.4% during the same period using the same method in Khorchin sandy soil *(Tang et al., 2011)*. It was also observed that the T/ET was 61.7% to 67.7% by calculating T indirectly from measurements of micro-lysimeters *(Sun et al., 2005)*. Plastic film mulching treatment significantly enhances the T/ET ratio compared to that of the non-mulching treatment in the mid and later stage of maize. The increased T with little soil E promoted shoot biomass accumulation and accelerate plant development in plastic film mulching plots *(Liu Y., Yang S. J., et al., 2010)*. The T/ET of maize under both treatments decreased in the mid and later period of the growing season because of the senesces of lower leaves at late stage.

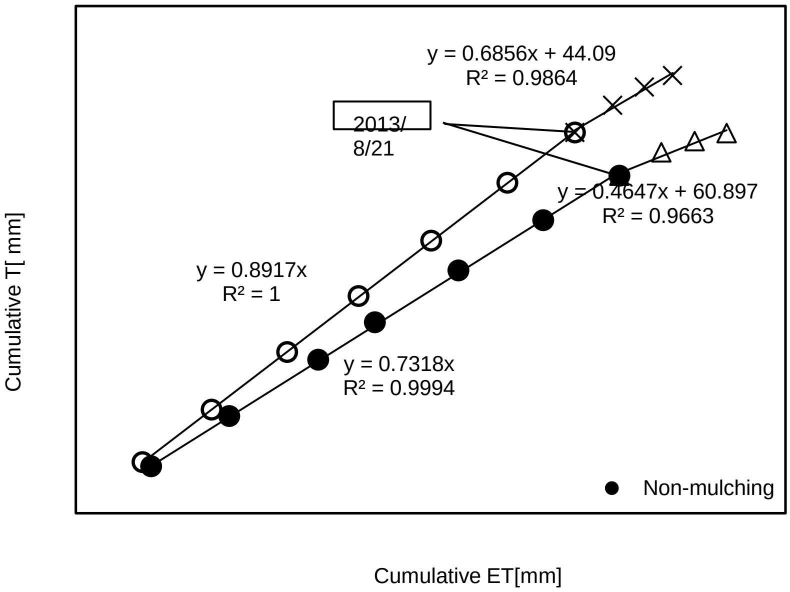

Fig.7 - Double mass curves of cumulative T versus cumulative ET of maize under two treatments during the mid-late growth period (7.16-9.8)

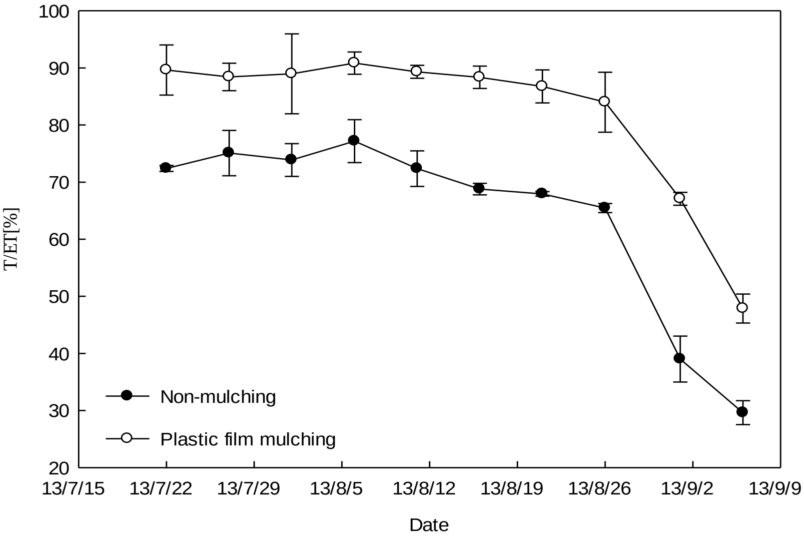

Fig.8 - Variation in the ratio of transpiration to evapotranspiration (T/ET) of maize during the mid-late growth period (7.16-9.8) for two treatments. Bars show standard errors

The relationship between the T/ET and LAI

From the perspective of Soil—Plant—Atmosphere Continuum (SPAC), the variations in T, ET are influenced by meteorological factors, soil (moisture) condition and vegetation factors. We compared the T/ET and LAI to analyze their relationships.

The T/ET and LAI showed a good relationship in a logarithmic function in Fig. 9. The T/ET increased logarithmically with an increasing LAI. The canopy shade conditions increased with the LAI, and the net radiation that was trapped by the canopy increased so that T and T/ET increased. When the LAI increased from 1 to 3.5, the T/ET under plastic film mulching rapidly increased from 47.9% to 84.1%, whereas that under the non-mulching treatment increased from 29.6% to 68.8%. However, with the increase in the LAI, the increasing rate of T/ET under both treatments became smaller. Under the same LAI, the T/ET of plastic film mulching was greater than that under non-mulching conditions.

Brission proposed that The T/ET and LAI showed a relationship in a logarithmic function, the equation is: T/ET=1- exp (-δ LAI), where δ is coefficient *(Brission, 1992)*. Most studies under irrigation demonstrated that E/ET and LAI was a logarithmic function. For instance, Sun et al. *(2005)* showed that $E/ET= 86.616e^{-0.2079LAI}$, $R^2= 0.93$; Wang et al. *(2007)* showed that $E/ET=0.9845e^{-0.345LAI}$, $R^2 = 0.93$. Our research directly studied the relationship of maize T and ET under dryland condition.

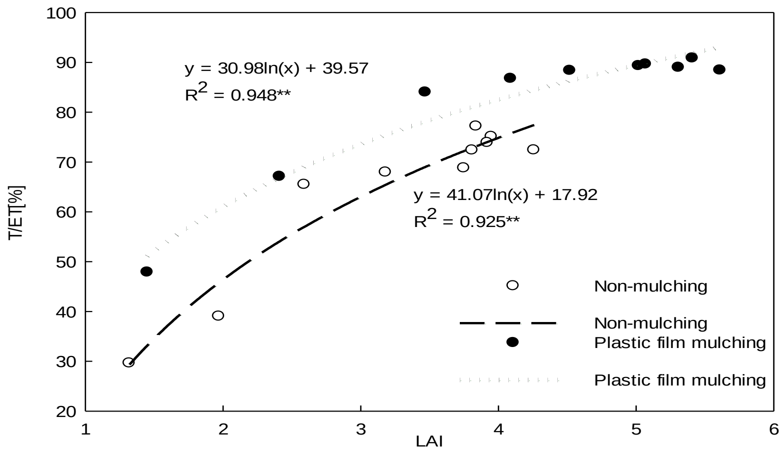

Fig.9 - Relationship between the variation in the ratio of transpiration and the evapotranspiration (T/ET) and leaf area index (LAI) during the measurement period; statistical significance level is at p< 0.01

Yield, yield components and WUE

Although no significant differences between two treatments were found in kernels per row, kernels per ear and 100-kernel weight of plastic film mulching plots were significantly higher than those of non-mulching plots (Table 1). The grain yields under plastic film mulching treatment were significantly greater than those under non-mulching treatment, with concomitant increases in shoot biomass production, total T and harvest index (Table 2).

The plant T component of ET is mainly used for plant growth, whereas the soil E component of ET does not contribute to plant growth. The T under plastic film mulching treatment was significantly greater than that under non-mulching treatment. Moreover, the plastic film mulching treatment significantly increased WUE. The WUE_T was 43.9 and 33.8 kg ha^{-1} mm^{-1} under plastic film mulching treatment and under non-mulching treatment, respectively. Meanwhile, the WUE_{ET} under plastic film mulching treatment was significantly greater than that under non-mulching treatment because of the restriction of water loss from E and the increase in plant T.

Plastic film mulching plots had higher yield and WUE because plastic film mulching improved soil water storage and water use dynamics *(Li et al., 2001; Zhou et al., 2009)*. Plastic film mulching improved soil water storage, decreased total ET but increased T/ET by reducing E and increasing T, and eventually enhanced maize development and increase grain yield and WUE *(Liu Y., Li S.Q., et al., 2010, Liu Y., Yang S. J., et al, 2010; Zhang et al., 2011)*. However, a few studies showed that plastic film decreased gain yield. Plastic film mulching did not significantly improve the soil water storage when soil moisture was extremely low, which may intensify drought stress and increase soil temperature *(Zhang et al., 2008)*. Therefore, plastic film mulching may be related to available soil water at planting and seasonal precipitation in different years.

Table 1

Maize yield components for two treatments

	Single ear weight [g]	Ear length [cm]	Ear perimeter [cm]	Fruit length [cm]	Ear rows	Kernels per row	Kernels per ear	100-kernel weight [g]
Plastic film mulching	346.96a	18.19a	22.19a	17.79a	17a	39a	659a	35.65a
Non-mulching	251.84b	17.93a	22.03b	17.07b	15b	39a	596b	30.12b

Note: Figures with different letters are significant at the 0.05 probability level

Table 2

Grain yield and crop water-use efficiency (WUE) for the two treatments

	Plastic film mulching	Non-mulching
Grain yield [kg ha^{-1}]	13,144±848a	7591±825b
Shoot biomass production [kg ha^{-1}]	22,106±1552a	15,780±1544b
Harvest index [%]	59.5±3.0a	48.1±2.2b
WUE_T [kg ha^{-1} mm^{-1}]	43.9±1.5a	33.8±1.2b
WUE_{ET}[kg ha^{-1} mm^{-1}]	35.5±1.8a	18.7±1.6b
T [mm]	299.1±7.2a	224.7±6.8b
ET [mm]	370.4±7.3a	406.5±14.6b

Note: Figures with different letters are significant at the 0.05 probability level

CONCLUSIONS

To investigate the effects of plastic film mulching on maize growth, yield, WUE, SWS and T/ET, the sap flow method was used in the dryland maize fields on the Loess Plateau, China. The conclusions were obtained as follows.

(1) Plastic film mulching promoted maize germination and advanced growth stages.

(2) Plastic film mulching retained soil water in the early stage to promote maize development in the later stage, and consumed more water in the deeper soil (40-150cm) during the reproductive stage.

(3) Plastic film mulching decreased the daily mean ET of maize, but increased the daily mean T, and significantly enhances the T/ET ratio compared to that of the non-mulching treatment in the mid and later growth stage. The T/ET is influenced greatly by the LAI and the T/ET increases logarithmically with increasing LAI. However, under the same LAI, the T/ET of plastic film mulching was greater than that under non-mulching conditions.

(4) Plastic film mulching enhanced grain yield, shoot biomass production, and harvest index. Plastic mulch also increased T, decreased ET, and with concomitant increased WUE_T and WUE_{ET}.

Plastic mulch is an effective way in the rainfed area of the Loess Plateau to increase water availability for higher crop yields and WUE. Whereas, it should be aware that plastic film mulching had a tendency of depleting soil water at deeper layers. Hence, further study is needed to investigate a better plastic mulch management way for maize to guarantee both high productions and system sustainability.

ACKNOWLEDGEMENT

This study was jointly supported by the National 863 Research Program of China (2013AA102904) and the National Natural Science Foundation of China (41171033).

REFERENCES

[1] Anikwe, M.A.N., Mbah, C.N., Ezeaku, P.I., Onyia, V.N., (2007), Tillage and plastic mulch effects on soil properties and growth and yield of cocoyam (Colocasia esculenta) in South-eastern Nigeria, *Soil & Tillage Research*, Vol.93, Issue 2, pp.264-272, Netherlands;

[2] Bethenod O., Katerji N., Goujet R., Bertolini J.M., Rana G., (2000), Determination and validation of corn crop transpiration by sap flow measurement under field conditions, *Theoretical and Applied Climatology*, Vol.67, Issue 3, pp.153-160, Germany;

[3] Brission, N., Seguin B., Bertuzzi P., (1992), Agro-meteorological soil water balance for crop simulation models, *Agricultural and Forest Meteorology*, Vol.59, Issue 3-4, pp. 267-278, Netherlands;

[4] Gentine P., Entekhabi D., Chehbouni A., Boulet G., Duchemin B., (2007), Analysis of evaporative fraction diurnal behaviour, *Agricultural and Forest Meteorology*, Vol.143, Issue 1-2, pp.13–29, Netherlands;

[5] Hadrian F. C., Gerardo S. B. V., Howard C. L. (2006), Mulch effects on rainfall interception, soil physical characteristics and temperature under Zea mays L, *Soil & Tillage Research, Netherlands*, Vol.91, Issue 1-2, pp. 227-235;

[6] Kang, S.Z., Zhang, L., Liang, Y.L., Cai H.J., (2002), Effects of limited irrigation on yield and water use efficiency of winter wheat in the Less Plateau of China, *Agricultural Water Management*, Vol.55, pp.203–216, Netherlands.

[7] Li R., Hou X. Q., Jia Z. K., Han Q.F., Ren X.L., Yang B.P., (2013), Effects on soil temperature, moisture, and maize yield of cultivation with ridge and furrow mulching in the rainfed area of the Loess Plateau, China, *Agricultural Water Management*, Vol.116, Issue 1, pp. 101-109, Netherlands;

[8] Li X.Y., Gong J.D., Gao Q.Z., Li F.R., (2001), Incorporation of Ridge and Furrow Method of Rainfall Harvesting with Mulching for Crop Production under Semiarid Conditions, *Agricultural Water Management*, Vol.50, Issue 3, pp.173-183, Netherlands;

[9] Liu W. Z., Zhang X. C., Dang T. H., Zhu O.Y., Wang J., Wang R., Gao C.P., (2010), Soil water dynamics and deep soil recharge in a record wet year in the southern Loess Plateau of China, *Agricultural Water Management*, Vol.97, Issue 8, pp.1133-1138, Netherlands;

[10] Liu Y., Li S.Q., Chen F., Yang S.J., Chen X.P., (2010), Soil Water Dynamics and Water Use Efficiency in Spring Maize (Zea Mays L.) Fields Subjected to Different Water Management Practices on the Loess Plateau, China, *Agricultural Water Management*, Vol.97, Issue 5, pp. 69-75, Netherlands;

[11] Liu Y., Yang S. J., Li S.Q., Chen X.P., Chen F., (2010), Growth and Development of Maize (Zea Mays L.) in Response to Different Field Water Management Practices: Resource Capture and Use Efficiency, *Agricultural and Forest Meteorology*, Vol.150, Issue 4, pp. 606-613, Netherlands;

[12] Midega C.A.O., Pittchar J., Salifu D., Pickett J.A., Khan Z.R., (2013), Effects of mulching, N-fertilization and intercropping with Desmodium uncinatum on Striga hermonthica infestation in maize, *Bioorganic & Medicinal Chemistry*, Vol.44, Issue 4, pp. 44-49, England;

[13] Raeini-Sarjaz M., Barthakur N.N. (1997), Water use efficiency and total dry matter production of bush bean under plastic covers, *Agricultural and Forest Meteorology*, Vol.87, Issue 1, pp.75-84, Netherlands;

[14] Ritchie, S.W., Hanway, J.J., Benson, G.O., (1992), How a maize plant develops, Special Report No.48, Iowa State University, Cooperative Extension Service, Ames, IA, http://maize. agron. iastate. Edu/maize grows.

[15] Saidou A., Janssen B.H., Temminghoff E. J. M., (2003), Effects of soil properties, mulch and NPK fertilizer on maize yields and nutrient budgets on ferralitic soils in southern Benin, *Agriculture, Ecosystems & Environment*, Vol.100, Issue 3, pp. 265-273, Netherlands;

[16] Sharma P., Abrol V., Sharmab R.K., (2011), Impact of tillage and mulch management on economics, energy requirement and crop performance in maize–wheat rotation in rainfed subhumid inceptisols, India, *European Journal of Agronomy*, Vol.34, Issue 1, pp. 46-51, France;

[17] Sun J.S., Kang S.Z., Wang J.L., Li X.D., Song N., (2005), Experiment on soil evaporation of summer maize under furrow irrigation condition (沟灌夏玉米棵间土壤蒸发规律的试验研究), *Transactions of the Chinese Society of Agricultural Engineering*, Vol.21, Issue 11, pp. 20-23, Beijing/China;

[18] Tang X., Cui J.Y., Zhao X.Y., Yun J.Y., Lian J., Wang X.Y., Li L.Q., (2011), Characteristics of maize transpiration and soil evaporation in Horqinsandland (科尔沁沙地玉米叶面蒸腾与棵间蒸发特性), *Pratacultural Science*, Vol.28, Issue 5, pp. 788-792, Lanzhou/China;

[19] Wang H.B., Gong D.Z., Mei X.R., Hao W.P. (2012), Dynamics comparison of rain-fed spring maize growth and evapotranspiration in plastic mulching and un-mulching fields (覆膜和露地旱作春玉米生长与蒸散动态比较), *Transactions of Chinese Society of Agricultural Engineering*, Vol.28, Issue 22, pp.88-94, Beijing/China;

[20] Wang J., Cai H. J., Kang Y. X., Chen F., (2007), Ratio of soil evaporation to the evapotranspiration for summer maize field (夏玉米棵间土面蒸发与蒸发蒸腾比例研究), *Transactions of Chinese Society of Agricultural Engineering*, Vol.23, Issue 4, pp.17-22, Beijing/China;

[21] Wang Y.J., Xie Z.K., Malhi S.S., Vera C.L., Zhang Y.B., Guo Z.H., (2011), Effects of Gravel–Sand Mulch, Plastic Mulch and Ridge and Furrow Rainfall Harvesting System Combinations on Water Use Efficiency, Soil Temperature and Watermelon Yield in a Semi-Arid Loess Plateau of Northwestern China, *Agricultural Water Management*, Vol.101, Issue 1, pp. 88-92;

[22] Zhang D.M., Chi B.L., Huang X.F., Liu E.K., Zhang J., (2008), Analysis of adverse effects on maize yield decrease resulted from plastic film mulching in dryland (地膜覆盖导致旱地玉米减产的负面影响), *Transactions of Chinese Society of Agricultural Engineering*, Beijing/China, Vol.24, Issue 4, pp.99-102;

[23] Zhang S.L., Li P.R., Yang X.Y., Wang Z.H., Chen X.P., (2011), Effects of tillage and plastic mulch on soil water, growth and yield of spring-sown maize, *Soil & Tillage Research*, Vol.112, Issue 1, pp.92-97, Netherlands;

[24] Zhang S.L., Victor S., Chen X.P., Zhang F.S., (2014), Water Use Efficiency of Dryland Maize in the Loess Plateau of China in Response to Crop Management, *Field Crops Research*, Vol.163, Issue 1, pp. 55-63, Netherlands;

[25] Zhao N.N., Liu Y., and Cai J.B. (2009), Experimental research on the ratio between evaporation and transpiration of maize (夏玉米生育期叶面蒸腾与棵间蒸发比例试验研究), *Journal of Irrigation and Drainage*, Vol.28, Issue 2, pp. 5-8, China;

[26] Zhou L.M., Li F.M., Jin S.L., Song Y.J., (2009), How Two Ridges and the Furrow Mulched with Plastic Film Affect Soil Water, Soil Temperature and Yield of Maize on the Semiarid Loess Plateau of China, *Field Crops Research*, Vol.113, Issue 1, pp. 41-47, Netherlands.

DEFINITION OF PERFORMANCES OF CONVEYOR POTATO-PLANTER APPARATUS WITH PINNING DEVICES
/
ВИЗНАЧЕННЯ ПОКАЗНИКІВ РОБОТИ КОНВЕЄРНИХ КАРТОПЛЕВИСАДЖУВАЛЬНИХ АПАРАТІВ З НАКОЛЮВАЛЬНИМИ ПРИСТРОЯМИ

Ph.D. Stud. Kozelko Y., Ph.D. Eng. Usenko M.
Lutsk National Technical University / Ukraine
Tel: +38(0332)74-61-32; Fax: +38(0332)74-61-03; E-mail: rector@lutsk-ntu.com.ua

Keywords: *conveyor, pinning device, ring, needle, potato, slope, moisture*

ABSTRACT
The advantages and disadvantages of different designs of potato-planter apparatus are analyzed. A new design of the conveyor potato-planter apparatus with pinning devices is presented. The performances of potato-planters with this apparatus are defined, namely deviation from straightness of planted rows and deviation from the specified row width depending on the angle of slope and soil moisture.

РЕЗЮМЕ
Проаналізовано переваги та недоліки різних конструкцій картоплевисаджувальних апаратів. Подані нові конструкції конвеєрних картоплевисаджувальних апаратів з наколювальними пристроями. Визначені показники роботи картоплевисаджувальних машин з даними апаратами, а саме відхилення від прямолінійності висаджених рядків та відхилення від заданої ширини міжрядь в залежності від кута схилу та вологості грунту.

INTRODUCTION
For agricultural operations in conditions of flat terrain a farm equipment that is designed for the working conditions of the plain is used. At the same time, many cultures around the world are grown in fields that are not characterized as flat. There are crops that are grown on the hills and slopes. In such conditions, equipment that is designed to work in the plain, cannot work efficiently. When working in such special conditions in all kinds of flat equipment appears a shortcoming that can be so significant that generally leads to the impossibility of its application. This includes tillage, sowing, planting, harvesting and other machinery. This also fully applies to such important operations like planting potatoes. On this operation the potato-planters which have different designs of potato-planter apparatus are used *(Emelin B.N., 2005; Misyan O.A, 1992; Sokolov V.A., 1993; Vatuhin A.P., 2005).*

Recently the conveyor potato-planter apparatus, which has many basic advantages, namely a small size, is distributed. This advantage allows to use such potato-planter apparatus and accordingly the potato-planters in the unit with small size tractors that worked well when working on slopes. A certain disadvantage of the given apparatus is a ring design, which does not provide reliable potatoes holding by the work of potato-planter in terms of uneven terrain, on the slopes, where there are vibrations and unit tilts. Logically, the main question is that of a reconstruction of rings that can provide reliable potatoes holding when using the unit in rough environment of slopes. The most perspective here can be applying of pinning device, such as a needle on the ring, which pins the potato and holds it firmly. In many scientific papers the work of potato-planters with conveyor type apparatus is described *(Kushnarev A. et al, 2007; Sysolin P.V., 2001; Zaligin O.G. et al, 1996).* But in these papers the improving of design of potato-planter apparatus has not been considered, any attention has not been paid to researches on basic agronomic performances of these potato-planters. These performances are important from point of view of potato-planter in terms of slopes and vibrations.

MATERIAL AND METHOD
For qualitative operation of potatoes planting we proposed two designs of conveyor potato-planter apparatus with pinning devices *(Usenko M.V. et al, 2010).* On the chain conveyor of apparatus, at regular intervals, the rings are placed. To each ring the needle on the bearer is attached. In one design a needle at the side of the ring is attached (Fig.1), and in the second design - from the rings bottom (Fig. 2).

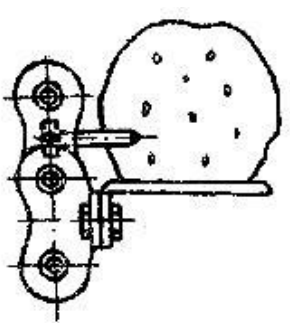

Fig.1 – Needle fixing at the side of the ring

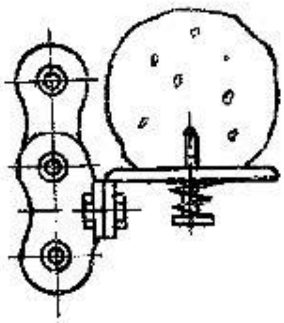

Fig.2 - Needle fixing from the rings bottom

Potato-planter apparatus with lateral needle on a flexible plate contains rings, fasteners, chain conveyor, sprocket, plate, needle, guard (Fig.1). On the chain conveyor at regular intervals the rings are attached. Above each ring considering in the course of the ascending branch of the conveyor chain, namely to the chain conveyors link located above this ring, the flexible plate is rigidly attached, to the center of which the needle is attached.

In this potato-planter apparatus the needle axis is located in a transverse direction to the movement of the conveyor chain and, accordingly, the needle pricks the potato from side. This allows to keep potato in the ring better, namely to counteract better to the weight of potato, under the influence of which it tries to fall out of the ring. This is because the force required to move the potato pinned on a needle in a transverse direction to the axis of the needle is greater than that required to move the potato along the axis of the needle. Thus, the potato pricked from the side by the needle is held better on that needle and a ring. Accordingly, a potato can be pricked at the smaller depth and the needles reverse movement from potato requires less power and takes less time.

But this design is more complicated from the constructive point of view than that in which the needle is attached from the rings bottom. We consider this design, which is relatively simple and can be more common.

Potato-planter apparatus with spring needle, which is attached from the rings bottom contains: bend *1*, ring-scoops *2*, fasteners *3*, chain conveyor *4*, sprocket *5*, guard *6*, needles *7*, bearers *8*, guides *9*, springs *10* (Fig. 3). Fig. 4 presents the tractor with potato-planter with apparatus with spring needle, which is attached from the rings bottom.

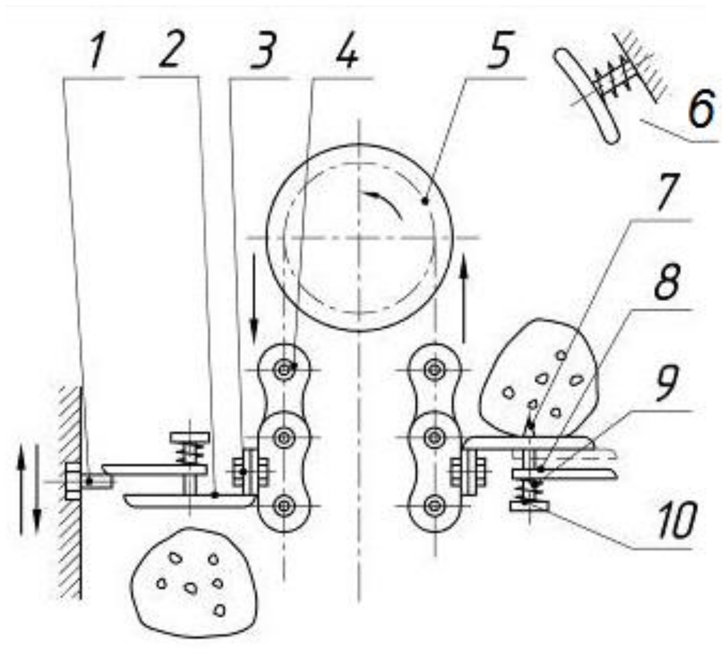

Fig.3 – Potato-planter apparatus with spring needle, which is attached from the rings bottom

1 – bend; 2 – ring-scoops ; 3 – fasteners; 4 – chain conveyor; 5 – sprocket; 6 – guard;
7 – needles; 8 – bearers; 9 – guides; 10 – springs

Fig.4 – Tractor with potato-planter with apparatus with spring needle

Chain conveyor *4* includes driven sprocket *5*. On the conveyor *4* at regular intervals the ring-scoops *2* by the fasteners *3* (bolt with nut) are fixed. To make this, fix the ring-scoop *2* and the relevant parts of the conveyor *4*. Each ring-scoop *2* is designed as a ring, to the bottom of which, considering in the course of the ascending branch of conveyor *4* (on Fig. 3 the ascending branch of the conveyor is located on the right of the sprocket *5*), diametrically opposite to each other the guides *9* are fixed rigidly, having removable stops (nuts with washers) at the ends. On the guides *9* through the holes made therein put on free the bearer *8* with the ledge on which the needle *7* is rigidly fixed so that it takes place in the centre of the ring. At the guides *9* in area between stops and bearer *8* the springs *10* are put on also. In the elliptical hole of casing the guard *6* is fixed by nut. It is a curved plate with threaded pins and notch for the ledge of the bearer *8*. On the threaded pins the springs of guard *6* are put on. In the elliptical hole of casing that covers the chain conveyor 4 is fixed by means of nut the bend *1*, which is a plate with threaded pin. Using the elliptical holes the bend *1* and guard *6* can be fixed in different positions.

Potato-planter apparatus works as follows. When moving potato-planter the bearing drive wheels are rotated and through transmission system set in motion the driven sprocket *5* and accordingly the conveyor *4* with ring-scoops. Ascending branch of the conveyor *4* moves in the bunker with root crops and catch those which are on the ring-scoops *2* way. The ledge of the bearer *8*, the end part of which is made round, is overhand a little from the ring toward the bunker with root crops. This allows, during the movement of the conveyor *4* to conduct a turning as of the total mass of potato, and, most importantly, directly at this ring-scoop *2* and thus help to direct potato to this ring-scoop *2*. The weight of potatoes presses on the ledge of the bearer *8*, under the action of which the bearer *8* is moved a little down, compressing the spring *10* partly and accordingly moving the needle *7* down, reducing its length in the upper area above the ring. This allows for getting into the ring-scoop *2* of potato virtually any size, with needle *7* prick only partially a root. As a result, the root that got the ring-scoop *2*, is located on the ring and additionally fixed in this position by the needle *7*, which pricked it and thus fixed it in the ring-scoop and hold from vibrations and possible displacement. Further, by upward movement the ring-scoop *2* with the root moves out of the zone where the mass of all roots is placed and the pressure on ledge of the bearer *8* disappears. Under the action of the spring *10* the bearing *8* is raised and the needle *7* pricks the root 7 at the deeper depth. The guard *6* presses root to the ring-scoop *2*, helping thus to prick it better on the needle *7*. In this position the root hold up in ring-spoon *2* firmly and cannot get away of it under its own weight, and it is important during the second phase of movement, when caught root goes gradually to conveyors *4* branch that moves down (located to the left of sprocket *5*), and in this position the root continues to be fixed in the ring-scoop *2* by the needle *7*, which holds it. When the bearer *8* by its ledge run into the bend *1*, then it starts to move away from the ring again, the force of the springs *10* and the needle *7* goes out of the root, releasing it. Released root under its own weight begins to drop and then gets into the coulter. The ledge of the bearer *8*, which is made of a flexible material, turns away gradually from the bend *1* and the springs *10* began to press again the bearer *8* to the ring, i.e. return the bearer *8* with the needle *7* in starting position.

RESULTS

Since the design of a needle that is attached to the rings bottom is more simple and widespread we define its basic agronomic performance. Experimentally it was researched deviation from straightness of planted potato rows for two machines: standard (without a pinning device) and experimental. Experimental design (described above) is improved, as has a potato-planter apparatus with needles in the rings bottom.

To determine the deviation from linearity we drew the straight line, starting from the first planted potatoes, then every 3 meters we measured the deviation in one or another side of it in cm.

Motion stability of potato-planter on slopes (even on slopes of 10-12º) is provided mainly by coulter, which is plunged in the soil to a depth of about 15 cm and therefore creates by its cheek the side reactions that prevents sliding unit.

So for motion stability on slopes it is enough to apply a simple coulter of standard design, unlike, for example, the seedling planter (here the coulter plunges to a depth of 10 cm) *(Ciuperca R. et al, 2012)*, and then to stabilize here the direction of motion we must apply except the coulter an additional stabilizing device.

The same small tractor for the standard and experimental potato-planters, was used. Operating speed was approximately 4 km/h. Two-section potato-planters with width between sections of 50 cm were used. So the productivity of both units was approximately 0.2 ha/h.

Fig. 5 presents a graph of dependence of potato rows straightness Π on the steepness of the slope α at different soil moisture W when using a standard potato-planter. This change comes in curvilinear dependence, that approximates the function of the form $\Pi = b\alpha^c$, where $c > 1$. Variation parameters: for W = 18 % - $\overline{\Pi}$ = 0.85 cm, σ = ± 0.03 cm, V = 3.5 %, m = ± 0.005 cm, P = 0.59 %; for W = 22 % - $\overline{\Pi}$ = 0.92 cm, σ = ± 0.035 cm, V = 3.8 %, m = ± 0.006 cm, P = 0.65 %; for W = 25 % - $\overline{\Pi}$ = 0.97 cm, σ = ± 0.04 cm, V = 4.1 %, m = ± 0.007 cm, P = 0.72 %.

Graphs analysis shows that increasing of the angle of slope has affected the deviation of potato rows straightness, because on a steep slope there is a breakdown of the unit course-keeping ability. Not quite perfect potato-planter apparatus cannot provide sufficiently accurate parameter value of the deviation of potato rows straightness, which is of $P \approx 2.6$ cm at soil moisture of W = 25%.

Fig.6 presents a graph of dependence of potato rows straightness Π on the steepness of the slope α at different soil moisture W when using an experimental potato-planter.

This change comes in curvilinear dependence, that approximates the function of the form $\Pi = b\alpha^c$, where $c > 1$. Variation parameters: for W = 18 % - $\overline{\Pi}$ = 0.7 cm, σ = ± 0.02 cm, V = 2.9 %, m = ± 0.004 cm, P = 0.57 %; for W = 22 % - $\overline{\Pi}$ = 0.75 cm, σ = ± 0.025 cm, V = 3.3 %, m = ± 0.005 cm, P = 0.67 %; for W = 25% - $\overline{\Pi}$ = 0.82 cm, σ = ± 0.03 cm, V = 3.7 %, m = ± 0.005 cm, P = 0.6 %.

Graphs analysis shows that increasing of the angle of slope has affected the deviation of potato rows straightness, because on a steep slope, as in the previous case, there is a breakdown of the unit course-keeping ability. In experimental potato-planter this deviation is maximum of 2.0 cm, which is less than in the previous case. This is due to the improved design of developed new machine, in which the use of new design of apparatus with pinning device helps to place potatoes accurately in the planned rows line.

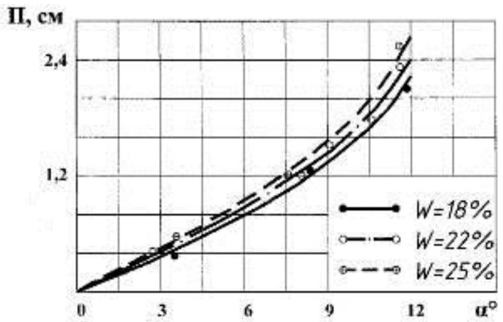

Fig.5 – Graph of dependence of potato rows straightness *П* on the steepness of the slope *α* at different soil moisture *W* by the work of standard potato-planter

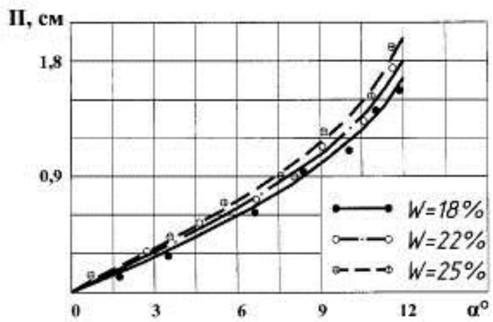

Fig.6 – Graph of dependence of potato rows straightness *П* on the steepness of the slope *α* at different soil moisture *W* by the work of experimental potato-planter

Also, we experimentally researched the deviation from the specified planted potato rows width for two machines: standard and experimental. We researched the deviation of width for guessing rows spacing because the deviation of major space between rows for all kinds of planting is not acceptable by agrotechnical requirements, i.e. ± 1.5 cm.

Fig.7 presents a graph of dependence of deviation from the rows width *B* on the steepness of the slope *α* at different soil moisture *W* when using a standard potato-planter. This change comes in curvilinear dependence, that approximates the function of the form $B = b\alpha^c$, where $c > 1$. Variation parameters: for W = 18% - $\overline{B}$ = 1.83 cm, σ = ± 0.63 cm, V = 34.4 %, m = ± 0.126 cm, P = 6.9 %; for W = 22% - $\overline{B}$ = 1.63 cm, σ = ± 0.58 cm, V = 35.6 %, m = ± 0.12 cm, P = 7.4 %; for W = 25% - $\overline{B}$ = 1.4 cm, σ = ± 0.49 cm, V = 35 %, m = ± 0.1 cm, P = 7.1 %.

Graphs analysis shows that increasing of the angle of slope affects the deviation from the rows width, because on a steep slope there is sliding process and there is a breakdown of the unit course-keeping ability. Not quite perfect potato-planter apparatus cannot provide an accurate rectilinear potatoes planting, which leads to maximum deviation from the rows width to 4 cm at soil moisture of *W* = 25%. By other values of the moisture and therefore more solid soil the motion of unit is more stable due to higher soil reactions on the coulter cheek and, therefore the deviation from the rows width will be lower.

Fig.8 presents a graph of dependence of deviation from the rows width *B* on the steepness of the slope *α* at different soil moisture *W* when using an experimental potato-planter. This change comes in curvilinear dependence, that approximates the function of the form $B = b\alpha^c$, where $c > 1$. Variation parameters: for W = 18% - $\overline{B}$ = 1.52 cm, σ = ± 0.52 cm, V = 34.2 %, m = ± 0.1 cm, P = 6.6 %; for W = 22% - $\overline{B}$ = 1.15 cm, σ = ± 0.38 cm, V = 33 %, m = ± 0.08 cm, P = 6.9 %; for W = 25% - $\overline{B}$ = 0.96 cm, σ = ± 0.35 cm, V = 36.5 %, m = ± 0.07 cm, P = 7.3 %.

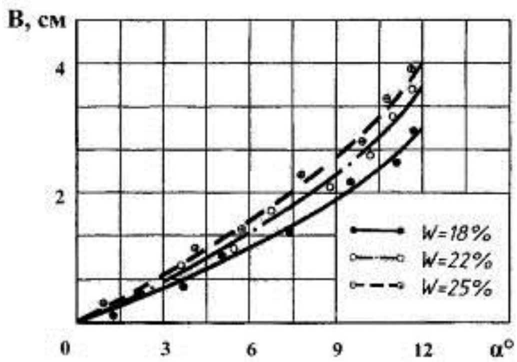

Fig.7 – Graph of dependence of deviation from the rows width *B* on the steepness of the slope *α* at different soil moisture *W* by the work of standard potato-planter

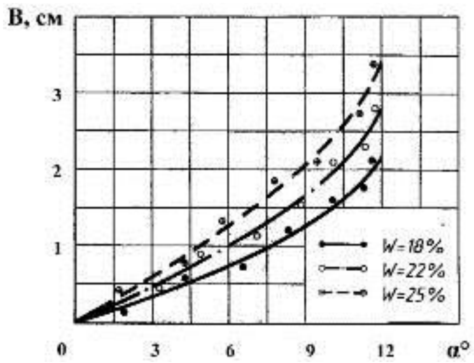

Fig.8 – Graph of dependence of deviation from the rows width *B* on the steepness of the slope *α* at different soil moisture *W* by the work of experimental potato-planter

Graphs analysis shows that increasing of the angle of slope has affected the deviation from the rows width, because on a steep slope there is the breakdown of the unit course-keeping ability. In experimental potato-planter this deviation is maximum of $B \approx 3.5$ cm at soil moisture of W = 25%, which is less than in the previous case and within the permissible range by agrotechnical requirements.

The improved design of developed new machine with new design of potato-planter apparatus with pinning device helps to place potatoes accurately in the planned rows line.

CONCLUSIONS

New designs of conveyor apparatus of potato-planter which are based on the pining devices are developed. In one design a needle at the side of the ring of potato-planter apparatus is attached, and in the second design - from the rings bottom.

It is established that the design of lateral needle is more complicated from the constructive point of view than that in which the needle is attached from the rings bottom, so the last design is relatively simple and can be more common.

We experimentally researched the deviation from straightness of planted rows *П* and deviation from the specified potatoes rows width *B* for two machines: standard (without pinning device) and experimental (with potato-planter apparatus with needles fixing from the rings bottom). In experimental potato-planter this deviation accordingly is maximum *П* = 2 cm and *B* ≈ 3.5 cm, which is less than in standard machine and within the permissible range according to agrotechnical requirements. The productivity of both units is about the same and is equal to 0.2 ha/h.

The experiments have confirmed the advantage of the experimental unit.

REFERENCES

[1] Ciuperca R., Popa L., Lazar G., et al., (2012), Comparative study on mechanized process of planting vegetable seedlings (Studiu comparativ asupra procesului mecanizat de plantat rasaduri de legume), *INMATEH-Agricultural Engineering Journal,* Vol.37, no.2, pp.61-68, Bucharest/Romania;

[2] Emelin B.N., (2005), To the substantiation of the geometric parameters of the dispenser-distributor of vermicompost (VC) to the potato-planter (К обоснованию геометрических параметров дозатора-распределителя вермикмпоста (ВК) к картофелепосадочной машине), *Scientific collection NAU,* Vol.92, pp.193-197, Kiev/Ukraine;

[3] Kushnarev A., Kushnarev S., (2007), The concept of science and technology policy to provide special equipment of small producers of vegetables and potatoes (Концепция научно-технической политики по обеспечению специальной техникой мелких производителей овощей и картофеля), *Engineering APK,* Vol.4-5, pp.33-36, Kiev/Ukraine;

[4] Misyan O.A., (1992), Potato-planter. USSR, Copyright certificate, No.1782403;

[5] Sokolov V.A., (1993), Potato-planter. USSR, Copyright certificate, No.1790843;

[6] Sysolin P.V., (2001), *Agricultural machines: theoretical foundations, design (Сільськогосподарські машини: теоретичні основи, конструкція, проектування),* Ed. Vintage, p.384, Kiev/Ukraine;

[7] Usenko M.V., Bulgakov V.M., Berezovy M.G., (2010), Rationale of the basic parameters of potato-planter apparatus with pining device (Обґрунтування основних параметрів картоплевисаджувального апарата з наколювальним пристроєм), *Scientific collection NUBiP,* Vol.144, no.4, pp.88-95, Kiev/Ukraine;

[8] Vatuhin A.P., (2005), Experimental potato-planter for simultaneous vermicomposts fertilization (Экспериментальная картофелепосадочная машина для одновременного внесения вермикомпостов), *Scientific collection NAU,* Vol.92, pp.197-200, Kiev/Ukraine;

[9] Zaligin O.G., Gusakov S.O., Zaborski V.P., et al., (1996), *Small mechanization in home and farm household (Малая механизация в приусадебном и фермерском хозяйствах),* Ed. Vintage, pp.368, Kiev/Ukraine.

DEVELOPMENT OF DESIGN AND INVESTIGATION OF OPERATION PROCESSES OF SMALL-SCLALE ROOT CROP AND POTATO HARVESTERS
/
РОЗРОБКА КОНСТРУКЦІЙ ТА ДОСЛІДЖЕННЯ ПРОЦЕСІВ РОБОТИ МАЛОГАБАРАТНИХ КОРЕНЕБУЛЬБОЗБИРАЛЬНИХ МАШИН

Prof. Ph.D. Eng Hevko R.B.[1)], Ph.D. Eng. Tkachenko I.G.[2)], Ph.D. Eng. Synii S.V.[3)], Ph.D. Eng. Flonts I.V.[4)]

[1)]Ternopil National Economic University / Ukraine; [2)]Ternopil Ivan Pul'uj National Technical University / Ukraine;
[3)]Lutsk National Technical University, / Ukraine; [4)] Separated Subdivision of National University of Life and Environmental Sciences of Ukraine Berezhany Agro-technical Institute / Ukraine
E-mail: alex_ks@mail.ru

Keywords: *root crop and potato harvesters, root cleaners, two-level cleaning system, conveyor*

ABSTRACT
Having analyzed the designs and the technological process performance of root crop and potato harvesting machines, new approaches to the designing of such types of machines, which allow to reduce their longitudinal clearance due to the use of a multilevel root crop and potato cleaning system and the decrease of the intensity of the effect of operating elements on root crops and potatoes as they move away from a digger, have been suggested. The article presents the developed designs of root crop and potato harvesters with alternating direction of conveyance and cleaning of root crops and potatoes and the results of their testing.

РЕЗЮМЕ
На основі аналізу конструкцій та показників якості виконання технологічних процесів малогабаритними корене- та картоплезбиральними машинами запропоновано нові підходи до проектування машин даного типу, які дозволяють зменшити їх повздовжні габаритні розміри за рахунок застосування багатоярусної системи очищення коренебульбоплодів та зниження інтенсивності дії робочих органів на коренебульбоплоди по мірі їх віддалення від копача. В статті представлено розроблені конструкції корене- та картоплезбиральних машин із знакозмінним напрямком транспортування та очищення коренебульбоплодів, а також наведено результати їх випробувань.

INTRODUCTION
A review of scientific and patent literature, technical and economic performance of machines, technologies of root crops and potato harvesting *(Kotsiuk V.V.et al., 2006; Bonchyk V.S., 2007; Hrushetskiy S.M., 2008; Heruk S.M. et. al., 2008; Klybanskyi O. P., 2010; Osukhovskyi V.M.and Saputskyi V.M., 2010; Kalverkamp Klemens, 2011; Dumych V. and Salo Ya., 2013)* with the help of mechanized complexes and machinery shows that they satisfy most of the requirements to a certain extent, but most of the machines have a great weight, material capacity and big overall dimensions. That is why, in order to satisfy the needs of the market, more attention should be paid to the development of small-scale equipment (one-, two- and three-row machines). In addition to that, it is necessary to eliminate technical contradiction between providing high quality performance of the technological process and optimum longitudinal and transverse size of the machines. Another important factor is the minimization of the material capacity of machines, which, on the one hand, allows to reduce specific pressure on the soil and, on the other hand, to decrease power inputs in order to move them on the field. Moreover, it is necessary to provide maximum possible limits for regulating design and kinematic parameters of operating elements as well as to provide fast replacement of technological units for the adjustment of the machines to specific soil and climatic conditions.

The aim of this research work was designing, constructing and testing trailing machines for harvesting sugar beets and potatoes with alternating and multilevel direction of conveyance and cleaning of root crops and potatoes and determining the effect of the design and kinematic parameters of operating elements on technological process performance.

MATERIAL AND METHOD

In order to provide minimum indices of damaging and satisfactory cleaning of root crops and potatoes with the help of harvesting machines and combines, a certain principle has been applied, which lies in the fact, that as moving away from the area of digging, the aggressive influence of the operating elements on root crops and potatoes must be reduced, since in the process of heap separation, the mass of soil stuck to root crops and potatoes decreases. At this point, there is an increased possibility of the direct contact of an operating element and a root crop, which leads to its damage.

In order to improve the process of separation of a heap of root crops, namely to reduce the degree of their damage at satisfactory separation of soil impurities and crop residues, a new system of cleaning has been suggested *(Fedirko P.P. et. al., 2014)*, the flow sheet of which is shown in Fig. 1. For performing this system of root crop cleaning, consecutive arrangement of the operating elements has been suggested: digging element 1, active shaking rod conveyer 2, beater shafts 3, and cleaning rolls 4.

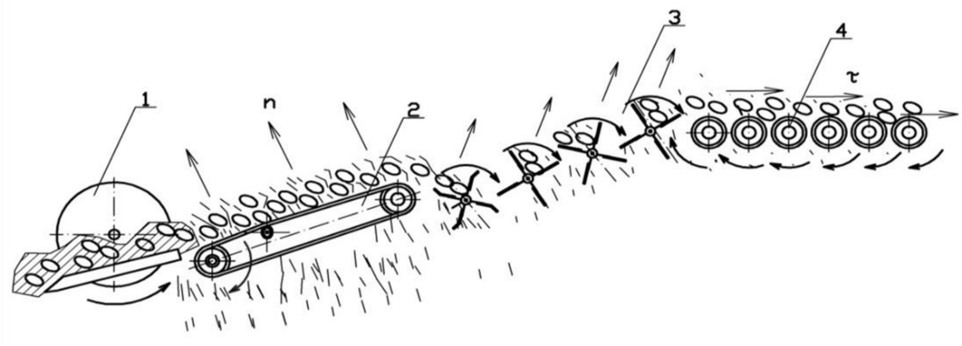

Fig.1 – Root crop and potato cleaning system

In the process of harvester operation, root crops and potatoes are dug with the help of a digger 1, after that the heap is conveyed to cleaning operating elements, namely to an active shaking rod conveyor, where it is scattered and partially cleaned up from soil and crop residues. Since at the first stage of cleaning there is a great amount of soil, that comes together with root crops and potatoes, the possibility of the direct hard contact of an operating element and the surface of a dug root crop is minor, that is why the intensity of the separation process must be at its peak level. Thus, the separation process of a root crop and potato heap at its first stage is carried out along a normal *n***,** which is perpendicularly to the surface of their body.

In the process of moving away from a digger, the amount of soil in the heap of root crops and potatoes decreases, that is why the intensity of the effect of an operating element on the product of cleaning must be reduced. Henceforward, the heap of root crops and potatoes is conveyed to beater shafts and cleaning rolls with smooth transition to the action of operating elements on root crops and potatoes along the tangent τ, (the tangential direction towards the body surface of root crops and potatoes).

The suggested system allows to improve the layout diagrams of small-scale harvesters and to improve the quality of cleaning of the heap of root crops and potatoes.

On the basis of this principle a potato harvesting machine *(Nalobina O.O. and Shymko A.V., 2015)* and a root crop harvester *(Hevko R.B. et. al., 2015)* have been developed; their design and process flow sheets being shown in Fig. 2 and 3. A frame 1 is attached to a tractor, it has 2 running wheels 2 and in the process of operation the right one can be placed closer or further apart according to the distance between the rows. In the process of operation a track roller 3 copies the surface of rakes and holds digging shares 5 at a given depth. Each flat cut off disk 4 is arranged on an axle with a slight spread and is rack-mounted to a frame. Two dissymmetric digging shares 5 are trapezoidal and are equipped with clapper valves in their rear parts. The valves improve the process of soil separation, prevent the rods of an intake conveyor 6 from becoming jammed and damaged because of hard clods and stones. Deepening of disks and shares into the soil can be regulated. When digging, vegetable soil is deformed by disks in horizontal and vertical directions and lifted by shares; that is why a clod, which comes for separation, has previously damaged bonds in its structure.

The main part of heap separation function, namely the separation of soil and the removal of crop residues, is done by an intake conveyor 6. As this takes place, a heap moves up to a receiving roll 8 and a transmission L-shaped conveyor. Rods 9, which are hinge mounted to a frame, are pressed to the canvas of an intake conveyor by their running ends and are used for removing the heap of crop residues. A receiving roll 8 (a hollow shaft), which turns towards the canvas of an intake conveyor, has several functions: it helps to tear tops off roots and to clean the rods 9; it shakes, turns over and presses heap components to the canvas of an intake conveyor and drops soil impurities, clods, stones and tops on the field; it reduces the impact force of roots and the canvas of a conveyor. The arrangement of a receiving roll relative to the conveyors can be regulated according to the conditions of harvesting.

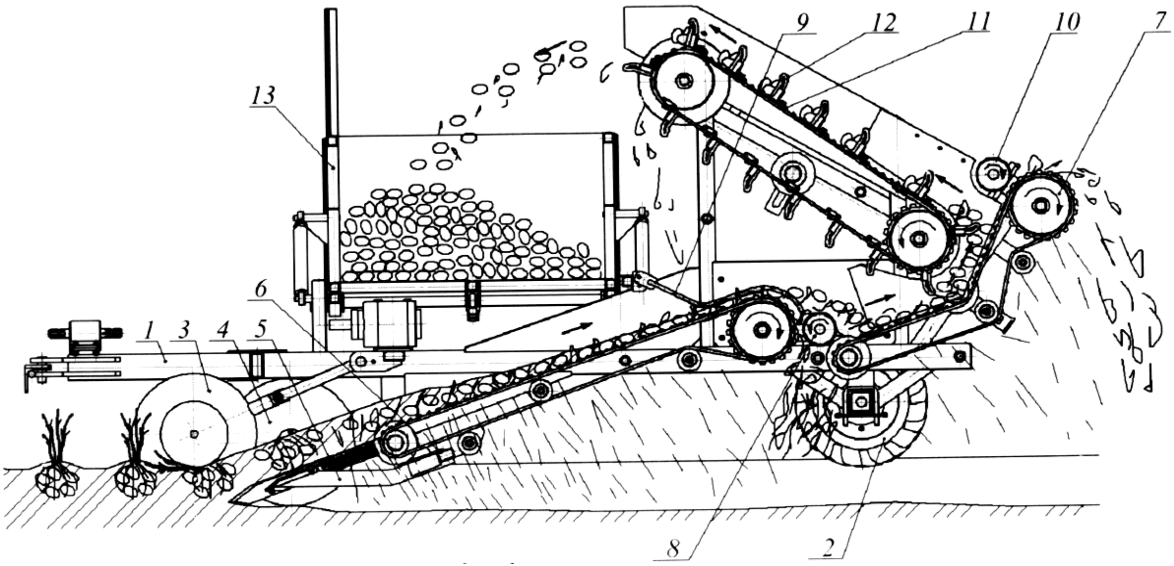

Fig.2 – Design and process flow sheet of a potato harvesting machine
1 – frame; 2 – running wheels; 3 – track roller; 4 – cut off disk; 5 – shares; 6 – intake conveyor; 7 – transmission L-shaped conveyer; 8 – receiving roll; 9 – top separator rods; 10 – beater roll; 11 – loader conveyor; 12 – scrapers; 13 – hopper

Transmission L-shaped conveyor 7 is used for intensive heap separation and conveying of potatoes with the remains of impurities to a scraping loader conveyor 11. The front part of a transmission conveyor 7 is inclined at an angle, which is close to the slope angle of the canvas of an intake conveyor 6 and intensively performs similar heap separation. A higher slope angle of the rear part of the canvas of an intake conveyor allows to remove crop residues in the process of heap separation on the principle of a finishing separator and to discharge them onto the field. In the process of separation, potatoes roll down into the L-shaped bend of a conveyor. In order to reduce damage in the process of potato conveying, the surface of rods is coated with an elastic material.

A beater roll 10 rotates in the same direction with the drive shaft of a transmission conveyor 7 and is used to prevent potatoes from being removed together with crop residues and discharged onto the field by this conveyor. The clearance (gap) between a roll and a conveyor can be regulated depending on the operating conditions.

A loader conveyor 11 traps a potato from the bend of a transmission conveyor 7 with the help of scrapers and conveys it to a hopper 13. A driven drum of a loader conveyor is mounted above the hopper with a clearance relative to it. Due to such arrangement, potatoes from a conveyor reach a hopper and crop residues get to a gap in front of a hopper and then to a conveyor 6 or to the harvested field.

A storage hopper 13 is made in the form of a box, the right panel of which is opened with the help of a hydraulic cylinder. The design of the machine provides side unloading of the gathered potatoes from the hopper on the principle of self-dumping truck operation – hydraulic cylinders open the right panel and tilt the bottom. The machine is equipped with a hopper of relatively little capacity (750kg) with a side panel, which provides: small overall dimensions of the machine (which means good mobility), little soil panning when operating, careful unloading of potatoes from a low height directing them onto a low surface. Overall view of the designed semi-trailing root crop harvested is shown in Fig.3. The machine is equipped with a special loading system and can be ganged up with type 14 kN or type 20 kN tractors. It has a frame *1*, a transmission *2*, digging wheels *3*, an intake of two-element separating conveyor *4*, an L-shaped loader conveyor *5*, a hopper *6*, which is made of two parts and a hydraulic system *7*.

An intake conveyor *4* consists of a frame *9*, lower and upper sections of which can be moved relative to the frame independently of one another; a power shaft, the driving drums *8* of which have the diameter of

240 mm and are made with slots for coupling the teeth of canvas; bottom rolls *10* with the diameter of 140 mm; and bearing rollers *11* with the diameter of 90 mm.

An operating surface of a conveyor is canvas *12*, which is made of two toothed rubber and cord belts, on which metal rods with the diameter of 12 mm are fixed with the spacing of 40 mm. The width of the canvas is 900 mm. Elastic scraper activators with the height of 40 mm are arranged on the rods with the possibility to change spacing according to certain soil and climatic conditions.

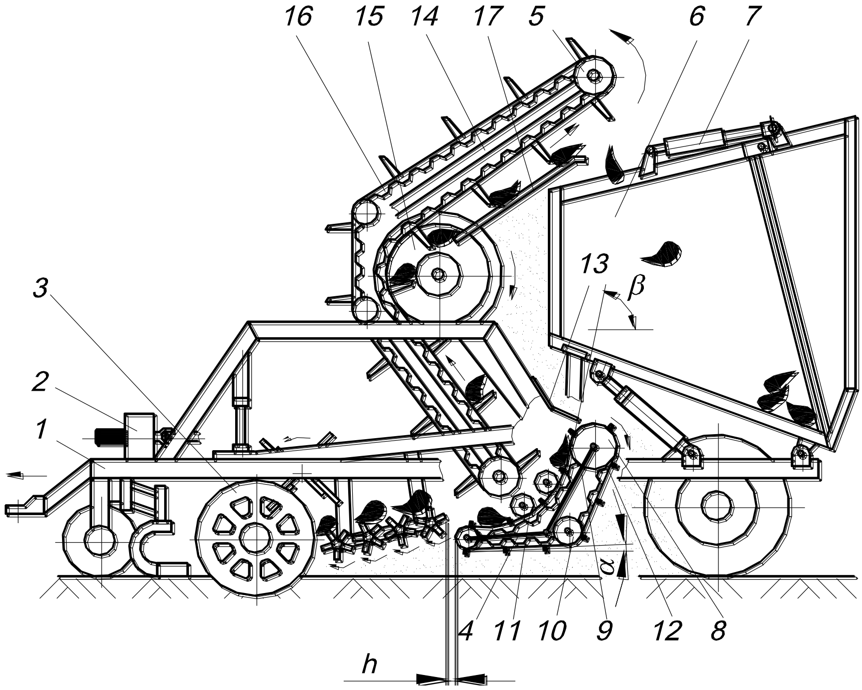

Fig.3 – Design and process flow sheet of a semi-trailing root crop harvester

1 – frame; 2 – transmission; 3 – digging wheels; 4 –intake two-element separating conveyor; 5 –loader conveyor; 6 – hopper; 7 – hydraulic system; 8 – driving drums; 9 – frame of intake conveyor; 10 – bottom rolls; 11 – bearing rollers; 12 – canvas; 13 – casing; 14 – frame of a loader conveyor; 15 – drum; 16 – canvas;17 – guide grid

A loader conveyor has a frame *14*, which is hard and the angle between its upper and lower parts is 90°. A drum *15* is used for smooth alteration of the conveying direction of root crops; it is stepped. The diameter of side discs, on which canvas bears, is 630 mm, and the diameter of a quill shaft, where root crops are conveyed, is 250 mm.

The canvas *16* of a loader conveyor is of similar design as that of an intake conveyor, but its width is 700 mm and it is equipped with scrapers, which have the height of 175 mm. In its bottom part, the conveyor canvas is cased, which prevents root crops from being removed by an intake conveyor and their loss. In the upper part, under the caring run of an intake conveyor canvas, there is a guide grid *17*, which is made of rods with the diameter of 16 mm, that are arranged with the clearance of 30 mm relative to each other.

In the process of its operation a digger digs up a root crop heap, partially cleans it from soil and crop residues and conveys it to an intake conveyor, which is arranged with a regulated clearance h. A conveyor canvas picks up root crops and conveys them with the growing angle from α to β. The degree of angle β is chosen in such a way, that root crops cannot hold on the canvas and roll down, and impurities are removed behind the machine. A casing *13* prevents root crops from being discharged onto the field.

After the main stage of separation, root crops are picked by a scraping canvas of a loader conveyor and move to a drum. Before being transferred to a discharging element of a conveyor, root crops move between the canvas and the drum. Due to powered side disks and a quill shaft, root crops are thrown on a rod guide grid. After that, with the help of the scrapers of a loader conveyor, root crops move along the grid, where they are entirely cleaned from soil and then enter a hopper. After the hopper is filled up, the unloading of root crops takes place with the help of hydraulic cylinders.

A two-element separating conveyor provides the removal of the lumps of soil and crop residues. The regulation of a slope angle of a discharging element of a separating conveyor allows to select rational parameters of an operating element for the machine performance under various natural and production conditions.

The overall view of a potato harvesting machine and a root crop harvester is shown in Fig.4 and Fig.5.

Fig.4 – Overall view of a potato harvesting machine

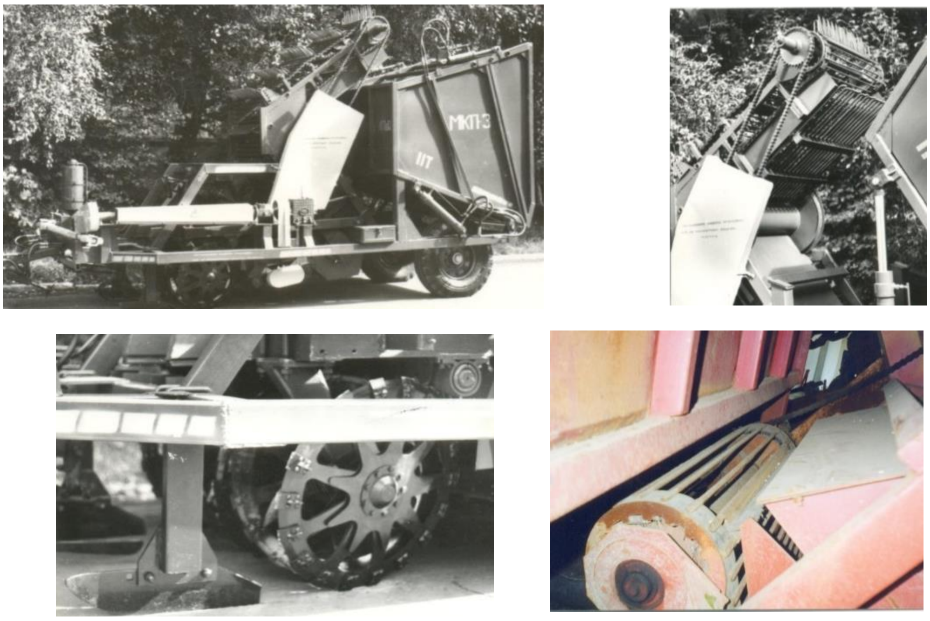

Fig.5 – Overall view of a root crop harvester and its operating elements

RESULTS

Main technical specifications of a potato harvesting machine (Fig.2) are the following: type – one-row trailing; unitizing 0.6 – 1.4 kN; overall dimensions: length – 4035 mm; width – 1875 mm; height – 1930 mm; weight – 1350 kg; hopper capacity – 0.75 t; distance between rows – 500-700 mm; operating rate 5.0 km/h; travelling speed 20 km/h; efficiency 0.2 ha/h; digging depth - 250 mm. On the basis of field experiments it has been determined that, the production process quality of this machine meets agro-technical requirements.

In the process of the experimental studies of a root crop harvester (Fig.3) the following parameters were variable: operating rate V_m = 0.79...1.85 m/s; running speed of an intake conveyor canvas V_c = 0.88...1.25 m/s; slope angle of an intake conveyor bottom section α = 10...25° and slope angle of an intake conveyor upper section β = 50...80°. After processing numerical values, regression equations, which define losses *L*, damage *D* and impurity *I* of root crops according to the change of the above mentioned parameters, have been obtained:

$$L = 1.59 + 0.06LnV_m + 0,06LnV_c + 0.04Ln\alpha - 0.08Ln\beta \quad (1)$$

$$D = 5.19 + 0.19LnV_m + 0,43LnV_c + 0.02Ln\alpha - 0.4Ln\beta \quad (2)$$

$$I = 3.99 + 0.4LnV_m + 0,77LnV_c + 0.06Ln\alpha - 0.93Ln\beta \quad (3)$$

Having analyzed regression equations (1) – (3) and the constructed response surfaces (Fig. 6, 7), it has been determined, that the losses L and the damage D of root crops do not exceed the acceptable ones, following agro-technical requirements, within the change of operative factors, that falls in the range of: L = 1.28…1.44 %, D = 3.2…3.8 %. As V_m and V_c increase, the loss L of root crops increases as well, which can be explained by the acceleration of per-second conveyance of a root crop heap; in the second case it can be explained by an increase in kinematic contact effect of operating elements on root crops.

The change in root crop damage D relative to a change in canvas running speed V_c and a slope angle of an intake conveyor upper section β has an inverse effect. As V_c increases from 0.9 to 1.3 m/s, the damage of root crop decreases from 3.6 % to 3.2 % respectively, and as β increases from 50° to 80°, the damage of root crop decreases from 3.6 % to 3.3 % respectively.

Minimum values of root crop losses L= 1.28…1.3 % have been obtained at operating rate of a machine V_m = 0.8…1.2 m/s, running speed of an intake conveyor canvas V_c = 0.9…1.2 m/s, angle α = 10...12° and angle β = 60...75° of an intake conveyor sections.

Minimum approximate function $D = f(V_m, V_c, \alpha, \beta)$, which defines the change in root crop damage and the values of which fall in the range of D = 3.2…3.3 %, has been obtained at the following change in operating factors: operating rate of a machine V_m= 0.8…1.3 m/s, running speed of an intake conveyor canvas V_c = 1.1…1.3 m/s, slope angle of its bottom section α = 15...20° and slope angle of its upper section β = 70...80°.

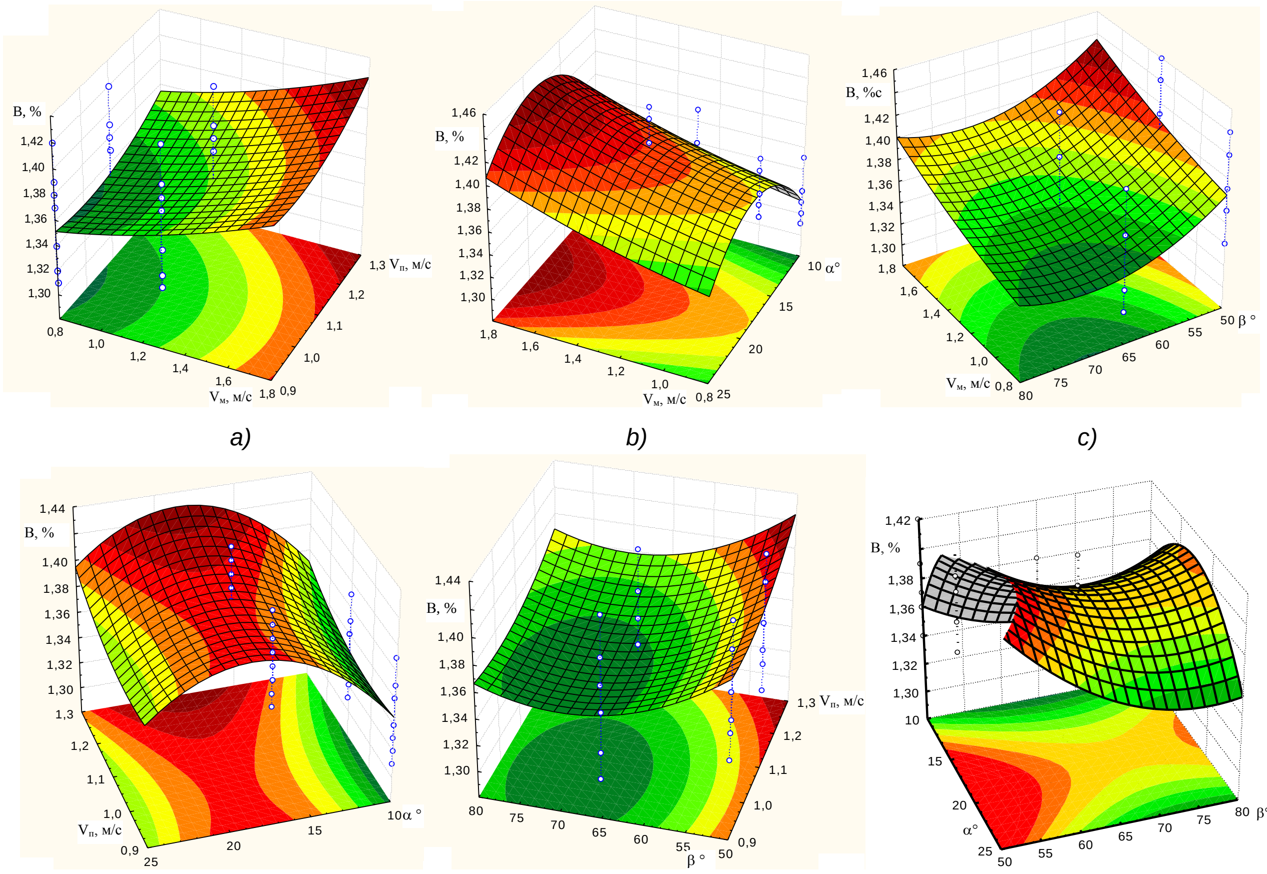

a) b) c) d) e) f)

Fig.6 – Response surfaces of losses L, % of root crops from

a): $L = f(V_m, V_c)$; b): $L = f(V_m, \alpha)$; c): $L = f(V_m, \beta)$; d): $L = f(V_c, \alpha)$; e): $L = f(V_c, \beta)$; f: $L = f(\alpha, \beta)$

If the value of machine operating rate V_m is more than 1.5 m/s, the value of the running speed of an intake conveyor canvas V_c is less than 1.2 m/s, the value of a slope angle of an intake conveyor bottom section α is more than 20° and the value of a slope angle of an intake conveyor upper section β is more than 70°, the overall amount of impurities I in a gathered root crop heap exceeds the standard limits for 8%

(Fig.8). Minimum I= 7.2%…7.6% has been obtained at the least values of V_m and β and the highest value of the running speed of an intake conveyor canvas V_c. Within the range of change in a slope angle of a conveyor bottom section α = 10...25°, the change in I is insignificant.

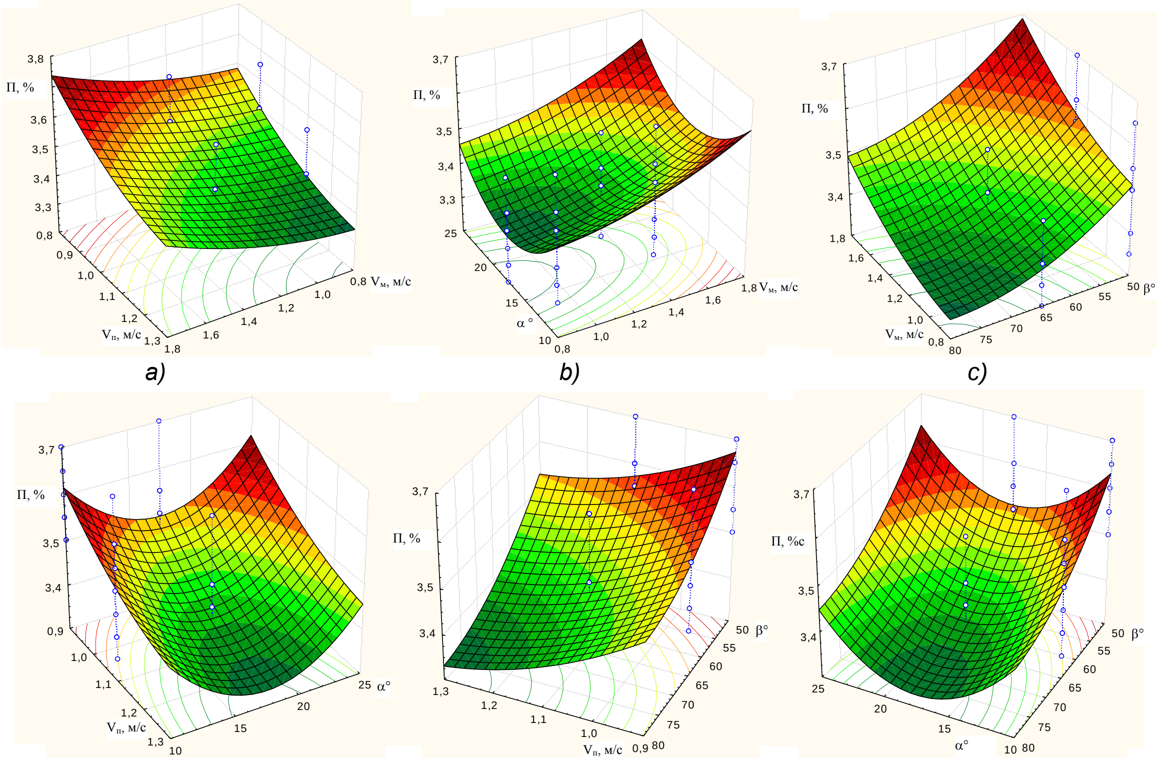

a) b) c)

d) e) f)

Fig.7 – Response surfaces of damage *D*, % of root crops from

a): D= f(Vc, Vc); b): D = f(α, Vm); c): D = f(β, Vm); d): D = f(α, Vc); e): D = f(β, Vc); f: D = f(α, β)

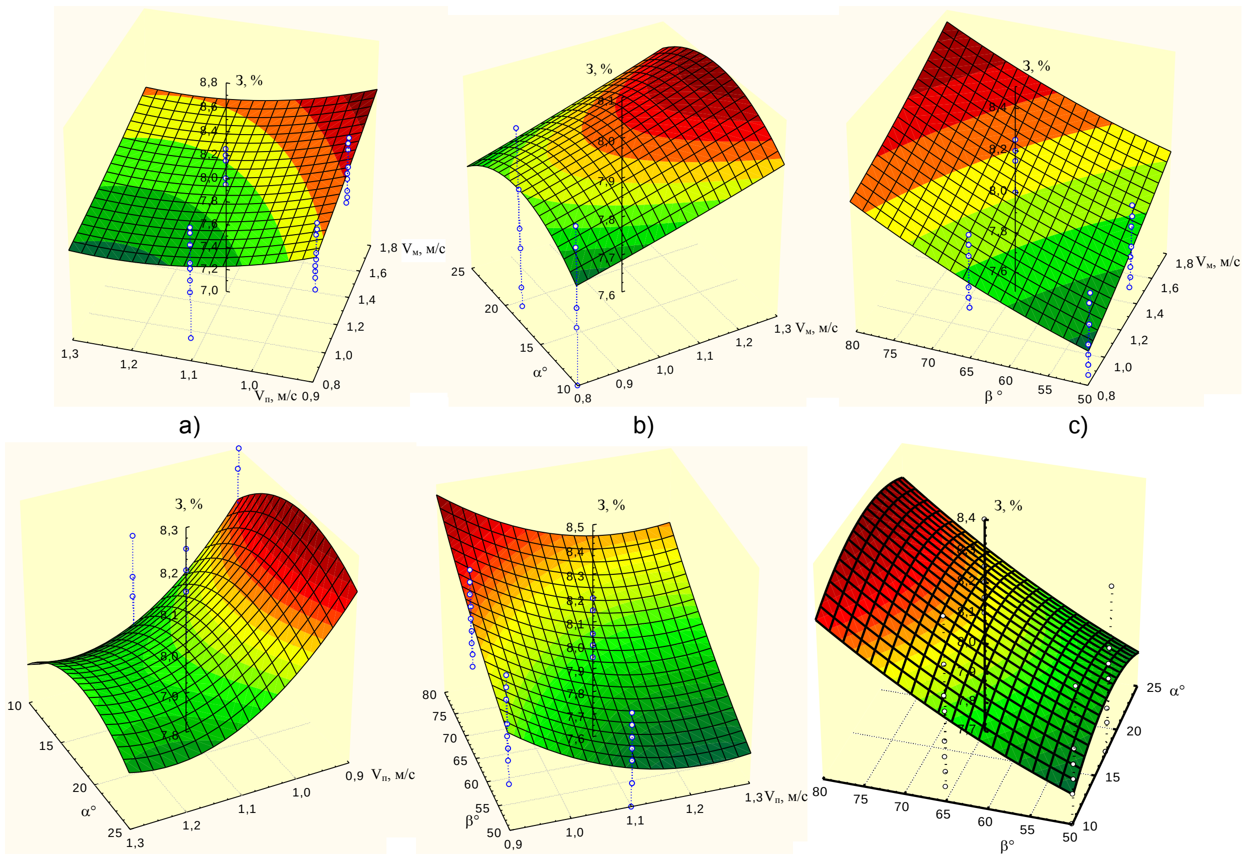

a) b) c)

d) e) f)

Fig.8 – Response surfaces of impurity *I*, % of root crops from

a): $I = f(V_c, V_m)$; b): $I = f(\alpha, V_m$; c): $I = f(\beta, V_m)$; d): $I = f(\alpha. V_c)$; e): $I = f(\beta, V_c)$; f): $I = f(\alpha, \beta)$

CONCLUSIONS

The analysis of present situation and progress trends of the machines for low power-consuming harvesting of root crops and potatoes has been conducted. Moreover, a new system of cleaning root crops and potatoes from soil impurities and crop residues, which provides the decrease in the intensity of the effect of operating elements on root crops and potatoes as they move away from a digger, has been suggested. On the basis of this principle a potato harvesting machine and a root crop harvester have been designed and constructed and their field experiments have been conducted as well.

Having analyzed the performance indicators of the designed semi-trailing root crop harvester МКР-3, rational values of its design and kinematic parameters and of its operating elements have been determined: operating rate of a machine V_m = 1.3 m/s, running speed of an intake conveyor canvas V_c = 1.2 m/s, slope angle of an intake conveyor bottom section α = 15°, slope angle of an intake conveyor upper section β = 70°.

REFERENCES

[1] Bonchyk V.S., (2007), A screw digging and separating device of a potato harvester (Шнековий підкопувально-сепаруючий пристрій картоплезбиральної машини*)*. UA, Patent, No. 22342;

[2] Bonchyk V.S., (2005), Rotary potato digger (Ротаційний картоплекопач), *Inventor and Innovator (Винахідник і Раціоналізатор)*, Vol. 9, pp.28-29, Kyiv / Ukraine;

[3] Dumych V., Salo Ya. (2013), Analysis of structures of technical means for combine harvesting of potatoes (Аналіз конструкцій технічних засобів для комбайнового збирання картоплі), *Engineering and technology AIC (Техніка і технології АПК)*, vol. 41, no. 2, pp.19-22, Doslidnytske / Ukraine;

[4] Fedirko P.P., Bonchyk V.S., Zhuk Y.O., (2014), Potato digger (Картоплекопач). UA, Patent, No. 88722;

[5] Heruk S.M., Minenko S.V., Khomenko S.M., (2008), Potato digger (Картоплекопач). UA, Patent, No. 34451;

[6] Hevko R.B., Sinii S.V., Tkachenko I.G., (2015), Investigation of root crop and potato harvesting machines (Исследование машин для уборки корнеклубнеплодов), *New materials, equipment and technology in industry: thesis of International Belarusian and Russian Conference of Young Scientists. Belarusian and Russian University (Новые материалы, оборудование и технологии в промышленности: тезисы международной научно-технической конференции молодых ученых)*. pp.51-52, Mohilev;

[7] Hrushetskiy S.M., (2008), Ground of construction and parameters of ploughshare-turn poptato-harvesting with the drum separator of potato lots (Обгрунтування конструкції і параметрів лемішно-полицевого картоплекопача з барабанним сепаратором картопляного вороху), PhD dissertation, Winnitca state agrarian university, Winnitca / Ukraine;

[8] Kalverkamp Klemens, (2011), Potato-harvesting machine (Картоплезбиральна машина). UA, Patent, No. 93866;

[9] Klybanskyi O. P., (2010), Potato digger (Картоплекопач). UA, Patent, No. 47814;

[10] Kotsiuk V.V., Spirin A.V., Zhukov V.P., (2006), Potato digger (Картоплекопач). UA, Patent, No. 16693;

[11] Nalobina O.O.,Shymko A.V., (2015), Analysis of development industry of the potato cultivation and overview potato harvesting technic (Аналіз розвитку галузі картоплярства та огляд картоплезбиральної техніки), *Agricultural machinery (Сільськогосподарські машини)*, vol.31, Lutsk National Technical University, pp.106-113, Lutsk / Ukraine;

[12] Osukhovskyi V.M., Saputskyi V.M., (2010), *A potato combined harvester (Картоплезбиральний комбайн)*, UA, Patent, No. 51984.

DESIGN OF A NEW TYPE OF CONTINUOUS STACK-UP JUICE PRESS AND PROOF ON EXPERIMENTAL MACHINE
/
一种新型连续层叠式榨汁机设计与试验机验证

As. A.P. Dr. Songbai Ma [1), 2)], Prof. Shaoying Zhang*[1)] , FengchengLi[1)],WenjunWei[1)]
[1)] Engineering College, China Agricultural University, Beijing/China;[2)]School of Metearial and Mechanical Engineering, Beijing Technology andBusiness University, Beijing/China
Tel: +18800110891; E-mail: masongbai@126.com

Keywords: *continuous stack-up press, filter-press unit, experimental machine confirming*

ABSTRACT
The fruit-vegetable juice processing industry plays an increasingly important part in the agricultural commodities processing industry in many countries. Existing fruit-vegetable juice press machines in fruit-vegetable juice processing industry has difficulty meeting the need for high-nutrition and high-quality fruit-vegetable juice products. Thus, researching for a new type of juice press with low-energy, high-juice yield, and high-quality of juice products is significant to meet the demands of modern and high-efficient production of fruit-vegetable juice. A new type of continuous stack-up juice press was presented based on the analysis on demands of fruit-vegetable juice processing and on advantages and disadvantages of some typical industrial press machines. The mechanical structure and working principle of the juice press wereillustrated. Moreover, an experimental machine, in which the basic filter-press unit is the core, was created to prove this technological solution. Juice press experiments of Ralls apples were conducted using the experimental machine. Results show that, when the driving motor rotates around 600 rpm, the juice yield rate is 81.16%, and the average value of the pressure force in the entire filter-press passage is about 1200 kilopascal. The quality of pressed juice is good for preserving most nutrients of raw materials.

摘要
果蔬汁加工产业在各国农产品加工产业中所占比重越来越大，目前果蔬汁加工行业普遍采用的果蔬榨汁机已很难适应市场对果蔬汁产品的高营养、高品质的要求。因此，开展低能耗，高出汁率，高出汁品质榨汁机的研究以满足现代化的高效果蔬汁生产的要求意义重大。论文在分析果蔬汁加工要求及现有一些典型工业榨汁机优缺点的基础上，提出一种新型连续层叠式榨汁机技术方案，对榨汁机机械结构及工作原理进行了描述，建立了以基本压滤单元为核心的试验验证机并进行了苹果汁的压榨作业试验，试验结果表明，驱动电机在600r/min 转速下，在整个压滤通道内可获得平均 1.20Mpa 左右的推料压榨力，出汁率达 81.16%，榨出的果汁较好地保留了原料中的大部分营养成分，果汁品质良好，证明新型连续层叠式榨汁机方案切实可行，对推动农产品加工行业发展具有重要意义。

INTRODUCTION
In recent years, the market demands of fruit-vegetable juice and fruit-vegetable juice drink have increased, and the fruit-vegetable juice processing industry has become one of mainstay industries in the agricultural commodity processing field.The standard system and quality-control requirements of fruit-vegetable juice products are greater and stricter in many countries as consumers' needs of "safety, natural, fresh, and tasty" for fruit-vegetable juice products increase. These requirements lead to more advanced technology demands for fruit-vegetable juice processing devices, especially to juice press machines *(Amaki K. et al.,2011; De Paepe D. et al., 2013)*.There is high application value and realistic significance to developing a new type of fruit-vegetable juice press machine with high productivity and good quality of juice products.

Universal hydraulic-filter juice press and belt-type filter juice press have dominating positions and are widely used in fruit-vegetable juice processing industry owing to their high productivity and better universality The best-known universal hydraulic-filter juice press machines are the HPX-Series universal hydraulic-filter juice press machines of Swiss Bucher Unipektin and the 6TZ-Series universal hydraulic-filter juice presses that are jointly developed by China Agricultural University and other cooperators in 2003 *(Domien De Paepeet al., 2015; Zhang SH.Y. et al., 2008;Grimi N. et al., 2011; Le Bourvellec C. et al.,2004)*. The universal hydraulic-filter juice press has the following characteristics: good sealing performance during pressing process, sound hygienic conditions, high productivity, high automation level, high juice yield (82%–

85% for apple juice), and improved universality. However, this press has some defects, such as interrupted working mode, severe oxidative browning phenomenon of pressing post stage, complicated PLC controls and hydraulic driving system, and expensive acquisition and running cost. Another common juice press machine of the fruit-vegetable juice processing industry is the belt-type filter juice press, which is acceptable for large-scale juice production. This juice press has a continuous operating mode, high working efficiency, improved universality, and moderate cost. The most widely used models of belt-type filter juice press machines are produced by Germany FLOTTWEG company and Germany BELLMER company; the belt-type extracting juice press was then designed by Ensheng Guo (*Guo ESH. et al., 1997;Mollov P. et al., 2006;Nabila Labsi et al., 2013; Garcia-Torres R. et al., 2009*). However, the belt-type juice press has become obsolescent because of the drawbacks of open working environment, high browning levels, side leakage-prone of belt, high content of pulp, severe microbial contamination, and large consumption of wash water. Therefore, an excellent juice press machine should have high productivity, high juice yield, high quality of juice, and low energy consumption. Scholars and industry insiders have been carrying out a series of research and applications on main juice press machines. However, there is still no one type of machine with those characteristics.

A new type of continuous stack-up juice press is presented to realize the aims of continuous working mode, sealing filter-press environment without oxygen, large separating area, and short cycling time of press. The press machine consists of multiple sets of basic filter-press units with continuous filter-press passages and large separating area. They are concentrically stacked up and form a tandem sealing working environment, where the forward impetus of materials and press forces are from pumping pressure and push force of rotating push-wheel blades. The main structures and working process of the press are described.

The remainder of this paper is organized as follows. Section 2 describes the mechanical structure and the working principle of the new type of continuous stack-up juice press. Section 3 introduces the structure of an experimental machine and its passage pressures acquisition system. Section 4 presents the experiments to assess the performance of the new type of continuous stack-up juice press. Section 5 summarizes the conclusions.

MATERIAL AND METHOD

The Structure of New-Type Continuous Stack-up Juice Press

The structure of new-type continuous stack-up juice press is shown in Figure 1. This juice press consists of a pedestal, top lid, fixing guide-pillar, group of filter-press units, the top seal bearing, the bottom seal bearing, driving motor, coupling, and actuating shaft. Multiple large and laminar basic filter-press units made up the group of filter-press units, where all filter-press units were installed concentrically. The actuating shaft went through the center of the group of filter-press units and was connected with pushwheels of all filter-press units.

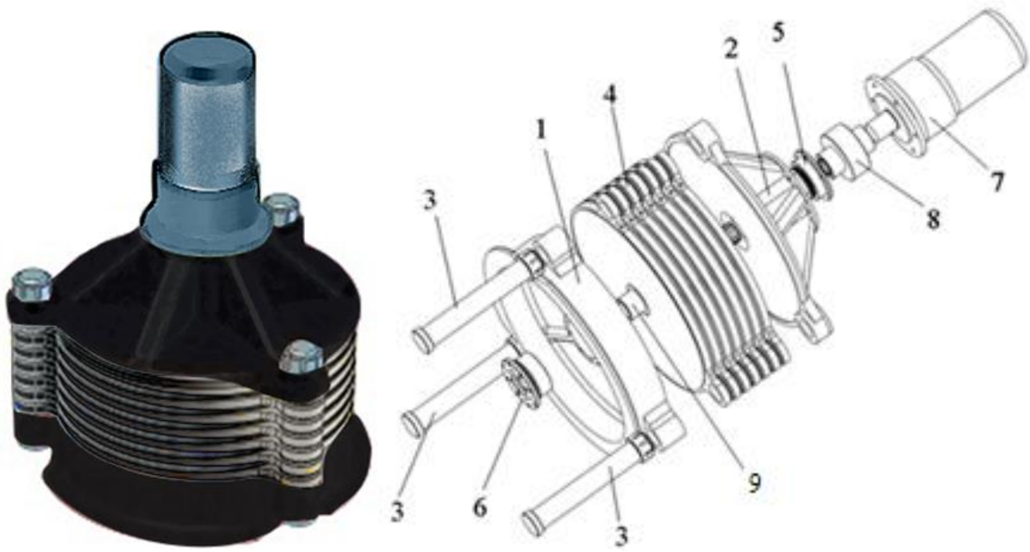

Fig.1- Structure diagram of new-type continuous stack-up juice press
1 - pedestal, 2 - top lid, 3 - fixing guide pillar, 4 - group of filter-press units, 5 - the top sealed bearing, 6 - the bottom sealed bearing, 7 - driving motor, 8 - coupling, 9 - actuating shaft

The right exploded view was created according to its left real object.

The Basic Filter-pressUnit

The basic filter-press unit is the core part of the continuous stack - up juice press, as shown in Figure 2. It consists of a pushwheel and the subassembly of juice collecting plate, where the pushwheel was arranged in the space of two subassemblies of the juice collecting plate.

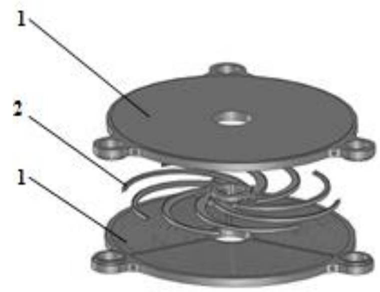

Fig.2 - The Structure diagram of filter-press unit
1 - subassembly of juice collecting plate, 2 - push-wheel

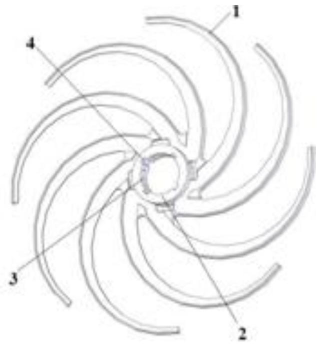

Fig.3 - The shape of push-wheel
1 - blade of push-wheel , 2 - wheel hub, 3 - feeding throat, 4 - keyway

The right view was created according to its real object of push wheel.

The shape of the push wheel is given in Figure 3. It is 20 mm thick. The radius of periphery is 600 mm, and the radius of the wheel hub is 100 mm. The push wheel has eight radial blades with caster angle, four axial direction keyways that connect with the keys of the actuating shaft, and four equispaced feeding throats along the circumferential direction. “The filter-press passage” is just formed by the gap between two adjacent blades and the other parts of basic filter-press unit. The caster angle structure for blade is chosen to facilitate the formation of high pressing forces that blades act on materials and uniform pressure distribution in the whole filter-press passage when push-wheel rotates.

The equations of blade curve be described as follows:

$$\begin{cases} \tau = -\dfrac{3(r-120)^2}{5120} + 60 & r \in [120{,}280] \\ \tau = \dfrac{3(r-600)^2}{10240} + 15 & r \in [280{,}600] \end{cases} \tag{1}$$

and

$$\tan\tau = \frac{dr}{r \times d\theta} \qquad r \in [120{,}600], \qquad \theta \in [0°{,}150°] \tag{2}$$

Define τ (in polar coordinates) as the caster angle, *r* as the radius, and *θ*as the radius angel.

The subassembly of juice collecting plates’ role is to collect juice. The subassembly has two types: the end and the center subassembly of the juice collecting plate. Figure 4 shows that both of them consist of the juice collecting plate and filter - nets, and the filter - nets are covered on the surface of the juice collecting plate. Moreover, the holes of filter - net were processed as long strips and laid along the perpendicular direction to the juice guide grooves to contribute in juice collection.

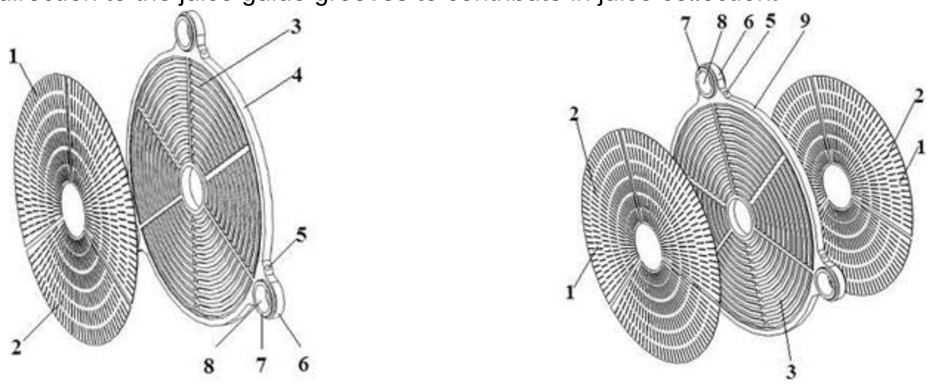

(a) End face juice collecting plate subassembly (b) Center juice collecting plate subassembly

Fig.4 - The constituting structures diagram of juice collecting plate subassemblies
1 - filter net, 2 - filter holes, 3 - juice guide grooves, 4 - end juice collecting plate, 5 - discharge holes of juice, 6 - chucking lug, 7 - location step, 8 - location hole, 9 - center juice collecting plate

All model graphs were created according to their real objects.

The end subassembly of juice collecting plate is arranged at the top and the bottom of the filter-press unit; thus, only one side of its juice collecting plate has juice - guide - grooves and is covered by filter - net. The center subassembly of the juice collecting plate is arranged at the middle of the filter-press unit. Thus, both sides of the center juice collecting plate have juice - guide - grooves and covered by filter - nets. All peripheries of all kinds of juice collecting plates have juice discharge holes that interconnect with the juice guide grooves. Moreover, each juice collecting plate has three chucking lugs that connect with the fixing guide pillar to locate with and compact all components of group of filter-press units to ensure the sealing and oxygen - free condition of inner press space. Furthermore, each juice collecting plate has an annular groove to place a hollow wear - resisting rubber ring to adjust the resistance of discharge residues and keep sufficient press force in the filter-press unit.

The Actuating Shaft

The actuating shaft feeds materials and drives the push wheel to rotate with it. Its shape is given in Figure 5. It is a special hollow pipe with a feeding throat of pulps (the entrance of pulps from feeding the screw pump), some equispaced outlets of pulps along the axial and circumferential directions (interconnecting with the feeding throats of the push wheel), four long keys (connecting with four keyways of the push wheel), spline - shape shaft end (connecting with the driving motor); and locating shaft shoulder (located with a group of filter-press units along axial direction). The actuating shaft goes through the center of a group of filter-press units and drives the push wheels of all filter-press units to rotate with it by the connections of keys.

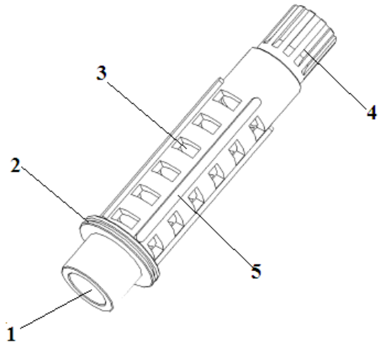

Fig.5 - The outside view of actuating shaft

1 - feeding throat of pulps, 2 - locating shaft shoulder, 3 - outlet of pulps, 4 - spline - shape shaft end, 5 - long - key

The model graph was created according to its real object.

The Structure of Experimental Machine

An experimental machine is set up to confirm the feasibility of the technical solution, as shown in Figure 6. The machine mainly comprises a base frame, feeding screw pump system, pre - filter system, hold - down mechanism (group of hold - down wheels), simplified filter-press unit, driving motor, damping adjustment device, and pressure measurement system of filter-press passages.

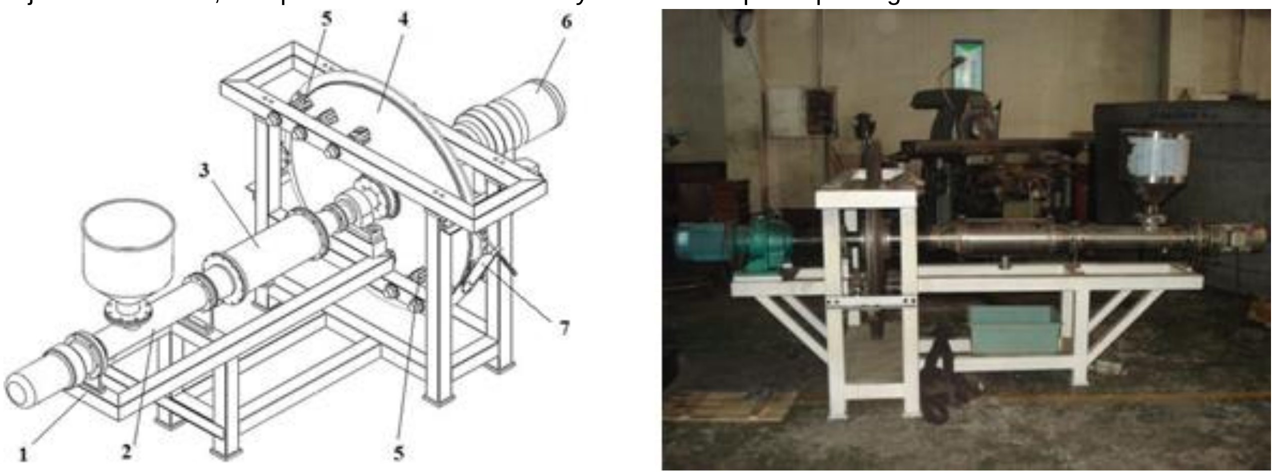

Fig.6 - The constituting structures diagram of experimental machine

1 - base frame, 2 - feeding screw pump, 3 - pre - filter system, 4 - simplified filter-press unit,
5 - group of tight compressing wheels, 6 - driving motor, 7 - damping adjustment device

The left model graph was created according to its right real object.

The push wheel in the experimental machine is simplified as the structure of two filter-press passages that belong to the same filter-press unit. The detailed structure is given in Figure 7. The structure mainly consists of two fins, a centering ring, and two sets of damping devices. The fin is made of alloy steel, and its thickness is 12 mm. The short cutting edge of the fin (I position) has the same curve shape as described in Equations (1) and (2). The long cutting edge of the fin (II position) is round and is 600 mm in radius. The centering ring has a central location hole (86 mm radius), some fixing thread holes, and two feeding throats (through - holes). Two fins are fixed on the centering ring by bolt connections, and the spaces between the short cutting edges of two fins are filter-press passages, which interconnect with two feeding throats of the centering ring. Moreover, two sets of damping devices are arranged at the outlets area of filter-press passages. The damping device consists of a damping pull rod, damping spring, nut, and damping block. Adequate pressure distribution is kept in filter-press passages, and overpressure protection around the outlet areas of filter-press passages is created by adjusting the damp spring to control the resistance of residue discharge.

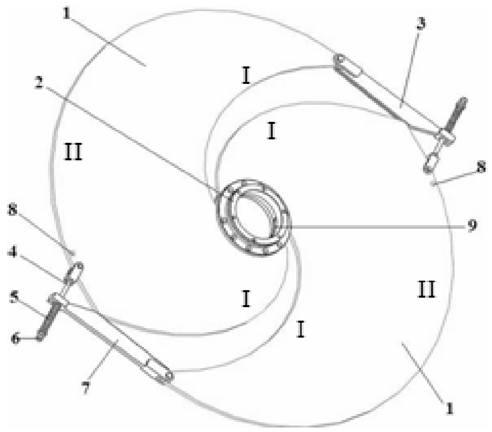

Fig.7 - The structure of the simplified push-wheel

1 - fin, 2 - centering ring, 3 - damping device, 4 - damping pullrod, 5 - damping spring, 6 - nut, 7 - damping block, 8 - mounting hole, 9 - feeding throat

The model graph was created according to its real object.

Two sets of end face juice collecting plate subassemblies are fixed on the flange of the actuating shaft by bolting connections, and the simplified push-wheel are installed between them. Two fins are attached on the base frame by bolt connections, as shown in Figure 8. The actuating shaft drives two sets of end face juice collecting plate subassemblies to rotate. Moreover, seals are installed between end face juice collecting plate subassemblies and actuating shaft to prevent juice leakage.

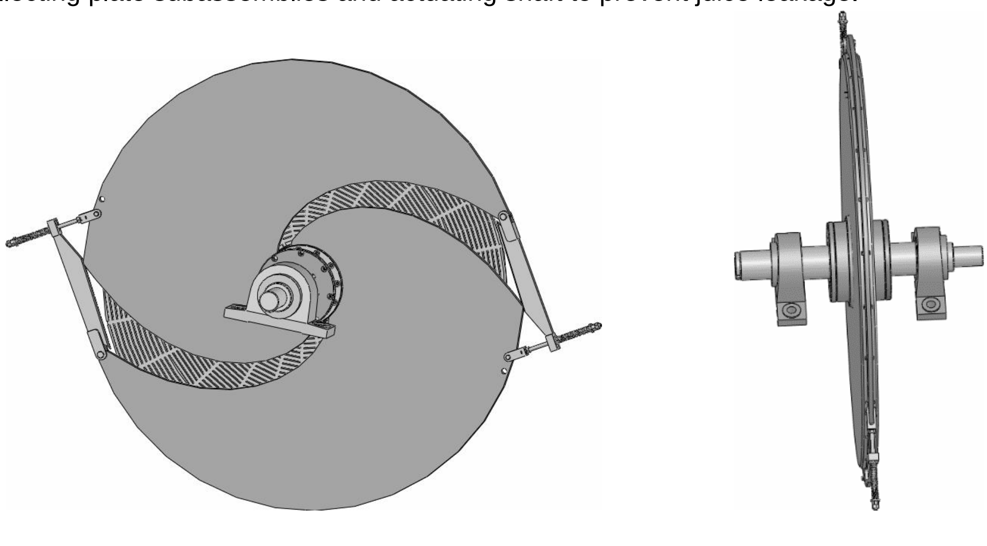

(a) One side of simplified filter-press unit (b) Whole structure of simplified filter-press unit

Fig.8 - Graph of simplified filter-press unit

All models graphs were created according to its real object.

The PassagesPressure Acquisition System

This study arranges a passage pressure acquisition system (Figure 9) to obtain the pressures values of different areas of filter-press passages during the juice pressing process. Eight equispaced pressure taps are on the short cutting edges of each fin. Each of pressure tap is connected with a minor pipe. The pipe goes through the measure tap, reaches the exterior of filter-press passages, and connects with a pressure sensor (FreescaleMPX5700DP). The pressure sensor has two connecting points. One is used to measure positive pressures, and the other is used to measure negative pressures. The positive connecting point connects with the other end of the minor pipe, and the negative connecting point is exposed in air. Thus, juices in filter-press passages are pressed into the minor pipes and act on the positive connecting points of sensors.

The pressure values of all pressure taps would be detected and converted to voltage values by sensors. All voltage values would be transmitted to a data acquisition card (DAQ, MPS - 010602), which could acquire and store 16 channels analogue signals simultaneously. DAQ is installed on a computer. The real time pressures of filter press passages could be recorded, stored, converted, and displayed by a record - display system based on LabView software.

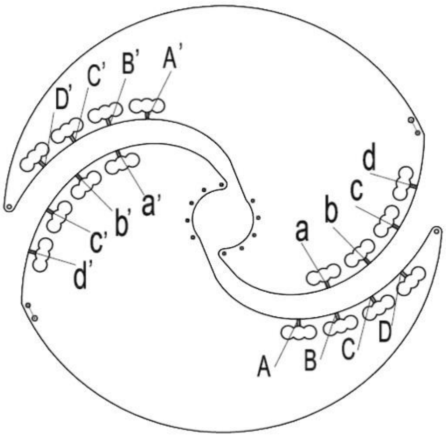

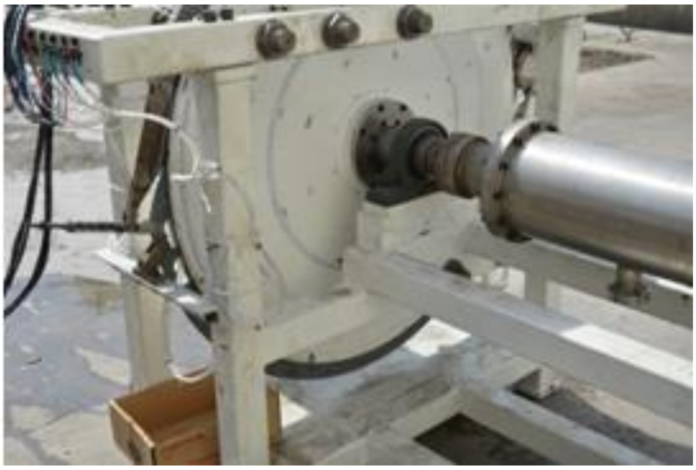

Fig.9 - Diagram of Pressure Taps Layout and Arrangement of Channel Pressure Acquisition System

The model graph was created according to its real object.

RESULTS

Instruments, Equipment, and Detection Methods

Instruments, equipment, and detection methods include Gary eclipse fluorescence spectrophotometer, T - 1000 electronic balance, Refrigerated cabinet TDL - A - 5 desk centrifuge, S10 high - speed homogenate machine, 722S visible spectrophotometer, PHS - 25 PH meter with digital display, MS300 hot plate magnetic stirrer, SPME manual sample injector, Water bath, H_2O_2, and Determination Kit for GSH. All reagents are of analytical grade *(Markowski J. et al., 2009)*.

Total ascorbic acid (TAA) was determined by fluorophotometry. Samples were homogenized at 8000 rpm in two percent oxalic acid protective solution (solid - to - liquid ratio was 1:1). About 3555 g of homogenates (particle size < 0.2 mm) were centrifuged in twenty minutes. The supernatant was extracted as further experimental samples. Reductive - form ascorbic acid (AA) was determined by 2 - 6 dichloro - indophenol titration method. Dehydroascorbic acid (DHA) is the difference between TAA and AA*(Yao G. et al., 2015)*. The samples were randomly selected. Three apples were in one sample, and three samples were in one group. Each group was determined for three times and took the average.

Soluble sugar was determined by the anthrone colorimetry method. Each sample was determined for three times, and the average was taken.

The content of malicacid was converted from the mass fraction of malicacid in titratable acid, and the conversion ratio is 6.7. The titratable acid was determined by NaOH potentiometric titration.

Sugar - acid ratio is the ratio of soluble sugar and malicacid. The contents of H_2O_2 and GSH in apples and apple juice were determined and calculated in terms of their different determination regulations and kits.

The on - sale, matured, free from contusion and putrefaction, free from live insects, and uniform size "Ralls" apples were chosen as the experimental materials. The Ralls apples were saved at 4 °C and washed by 200 mg/L of chlorine water before processing. Before pressing, each apple was cut into four pieces and broken up in the pounding crusher *(Yao G. et al., 2014)*.

The pounded apple mash was poured into the hopper of feeding screw pump. The mash was fed into the actuating shaft and filter-press passages to be pressed continuously. The average pressure of filter-press passages was obtained according to the output from passage pressure acquisition system. The whole working process of experimental machine is shown in Figure 10.

a) Starting experimental machine

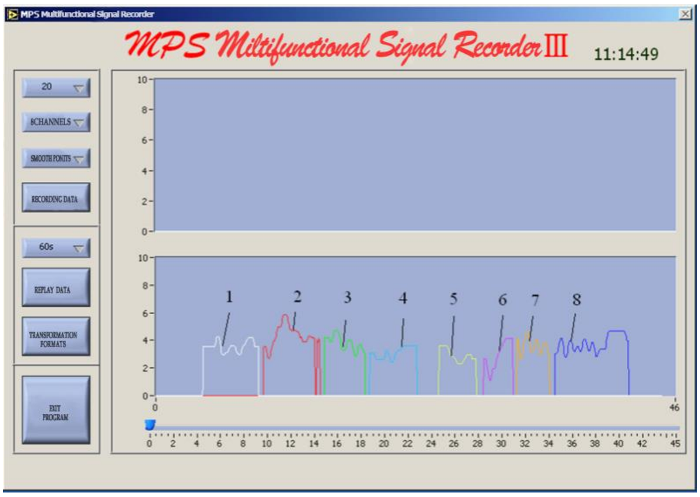

b) Recording pressures of filter-press passages

c) Collecting juice

d) Discharging residues

Fig.10 - The working process of experimental machine

In the fig.10, b, the horizontal axis of this graph is a timeline (second, s), and the vertical axis displays converted voltage (volt, V).

Figure 11 shows the relation curve of actuating shaft speed, average of passages pressures, and juice yield. When the actuating shaft rotates at 400 rpm, the average press force of whole filter-press passage is 1030 KPa, and the juice yield is 62.64 percent. The ideal speed range of the actuating shaft is from 600 rpm to 800 rpm. The average press force of the whole filter-press passage is above 1100 KPa within the speed range. When the actuating shaft rotates at 600 rpm, the average press force of the whole filter-press passage is 1200 KPa, and the juice yield is 81.16 percent. However, the performance of creating press force and juice yield is lessened when the actuating shaft speed is more than 800 rpm.

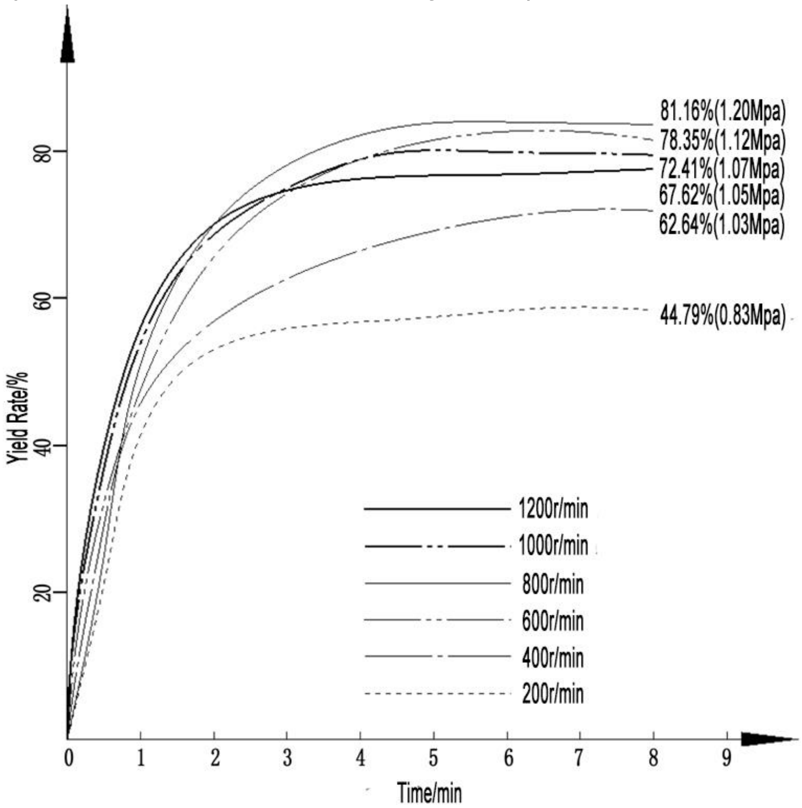

Fig.11 - The relation curve of driving motor speed, average channel pressure, and juice yield

Table 1 displays the comparison of primary nutrient content of apple before and after pressing. Squeezed apple juice keeps more nutrient content than a raw apple. The results demonstrate that the retention rates of TAA, AA, DHA, and soluble sugar were 71.29%, 63.96%, 82.27%, and 96.35%, respectively, which show almost no change in content of malicacid and sugar - acid ratio.

Table 1

Comparison of primary nutrient content of apple before and after pressed

Parameters	Raw apple	Apple juice
The mass ratio of TAA /(mg·(100g) - 1)	6.41	4.57
The mass ratio of AA /(mg·(100g) - 1)	5.05	3.23
The mass ratio of DHA /(mg·(100g) - 1)	1.41	1.16
The mass fraction of soluble sugar (percent)	12.61	12.15
The mass fraction of malic acid (percent)	0.56	0.54
The Sugar - acid ratio	22.85	22.84

CONCLUSIONS

A new type of juice press machine, continuous stack - up juice press, was presented; and an experimental machine was set up for confirmation. Ralls apple juice pressing experiments of Ralls apples were conducted on the experimental machine. The creativeness and aimability of this technological solution were proven according to the results of experiments. Design goals of high yield rate, high productivity, and good quality of juice were reached.

The conclusions are as follows:

(1) High productivity is achieved because of the creative design of the basic filter-press unit, which ensures that large quantities of materials could be processed in short periods for multiple inner smooth passages of material flow and juice collection and its large separated area. High productivity is also achieved because of its continuous working mode.

(2) High yield rate is mainly because of its high productivity and the special creating way of press - pressure,that is, the combination of pumping pressure and torque thrust of push-wheel blades.This combination could create high average press - pressure in filter-press unitswhen actuating shaft rotates at some rotating speed of (such as 600 rpm). Materials could be pressed well.

(3) Good quality of juice mainly is ascribed to its sealed working environment and the continuous removal of residues.

Developing highly - efficient fruit - vegetable juice processing technologies and equipment is significant to promote the development of the fruit - vegetable processing industry and the agricultural commodity processing industry. More experiments need to bedone to modifyand improve design parameters and mechanical structuresto contribute to improving overall design.

REFERENCES

[1] Amaki K., Saito E., Taniguchi K., Joshita K., & Murata M.,(2011), Role of Chlorogenic Acid Quinone And Interaction Of Chlorogenic Acid Quinone And Catechins In The Enzymatic Browning Of Apple, *Bioscience, Biotechnology and Biochemistry*, Vol.75, Issue.5, Japan Society for Bioscience, Biotechnology and Agrochemistry, pp.829–832, Tokyo/Japan;

[2] Domien De Paepe, Katleen Coudijzer, Bart Noten, Dirk Valkenborg, Kelly Servaes, Marc De Loose, Ludo Diels, Stefan Voorspoels, Bart Van Droogenbroeck, (2015),A Comparative Study Between Spiral - filter Press and Belt Press Implemented In ACloudy Apple Juice Production Process, *Food Chemistry*, Vol.173, pp.986–996, Elsevier B.V., Amsterdam/ Netherlands;

[3] De Paepe D., Noten B., De Loose M., Van Droogenbroeck B. & Voorspoels S.,(2013),An Improved Mass Spectrometric Method For Identification And Quantification Of Phenolic Compounds In Apple Fruits, *Food Chemistry*, Vol. 136, Issue.2,pp.368–375, Elsevier B.V., Amsterdam/ Netherlands;

[4] Guo ESH., Kan B.X., Zhao H., Ding S.M., Su Y.SH., Chen W.L.,(1997), *Belt Extraction Press Machine,* China, Patent, No.96219146.9;

[5] Garcia - Torres R., Ponagandla N.R., Rouseff R.L., Goodrich - Schneider R.M., Reyes - De - Corcuera J. I.,(2009), Effects Of Dissolved Oxygen In Fruit Juices And Methods Of Removal, *Comprehensive Reviews in Food Science and Food Safety*, Vol.8, Issue 4,The Institute of Food Technologists, pp.409–423, Chicago/ U.S.A.;

[6] Grimi N., Mamouni F., Lebovka N., Vorobiev E.& Vaxelaire J.,(2011),Impact Of Apple Processing Modes On Extracted Juice Quality: Pressing Assisted By Pulsed Electric fields, *Journal of Food Engineering*, Vol. 103, Issue.1, International Society of Food Engineering, pp.52–61, Chicago/ U.S.A.;

[7] Le Bourvellec C., Le Quéré J.M., Sanoner P., Drilleau J.F., & Guyot S.,(2004), Inhibition Of Apple Polyphenol Oxidase Activity By Procyanidins And Polyphenol Oxidation Products,*Journal of Agricultural and Food Chemistry*,vol. 52, Issue.1, American Chemical Society, pp.122–130, Washington, D.C./U.S.A.;

[8] Mollov P., Mihalev K., Buleva M., Petkanchin I., (2006), Cloud Stability Of Apple Juices In Relation To Their Particle Charge Properties Studied By Electro - Optics,*Food Research International*, Canadian Institute of Food Science And Technology, Vol.39, Issue.5, pp.519–524, Toronto, Ontario/Canada;

[9] Markowski J., Baron A., Mieszczakowska M., Płocharski W.,(2009), Chemical Composition Of French And Polish Cloudy Apple Juices,*Journal of Horticultural Science & Biotechnology*, Vol. 84, Issue.6,pp.68–74, Taylor & Francis, Oxford and London/UK.;

[10] Nabila Labsi,Youb Khaled Benkahla, Abdelkader Boutra, Abdellah Ammouri, (2013), Heat and Flow Properties of a Temperature Dependent Viscoplastic Fluid Including Viscous Dissipation, *Journal of Food Process Engineering*, vol.36, Issue.4,pp. 450–461, Texas A&M University, Texas/ U.S.A.;

[11] Yao G., Zhang SH.Y., Li Y.L., et al., (2014), *Effection Of Short Cold Stress On The Ascorbic Acid Of Apple Before Processing*（低温胁迫对加工前早熟苹果中抗坏血酸的影响）, Food Science and Technology, vol. 39 Issue.9,pp.60- 65, Beijing Institute Of Grain Science,Beijing/China;

[12] Yao G., Zhang SH.Y.,Li F.CH., (2015), Freshly Squeezed Effect On Low Temperature Stress For Apple(低温胁迫提升苹果鲜榨汁品质研究),*Transactions of The Chinese Society of Agricultural Machinery*, vol. 46, Issue.2, pp.229–230, Chinese Society for Agriculture Machinery, Beijing/China;

[13] Zhang SH.Y., Cao W.L.,Wei W.J.,(2008), Effect Of Pounding On Apple Press Process And Juice Yield(钝击破碎对苹果压榨效果的影响), *Transactions of the CSAE*, Vol. 24, no.2,pp.246–249, Chinese Society of Agricultural Engineering, Beijing/China.

DETERMINATION OF SOME MECHANICAL PROPERTIES FOR OILSEEDS USING UNIAXIAL COMPRESSION TESTS

/

DETERMINAREA UNOR CARACTERISTICI MECANICE ALE SEMINŢELOR OLEAGINOASE UTILIZÂND TESTELE DE COMPRESIUNE UNIAXIALĂ

Lect. Ph.D. Eng. Ionescu M.*[1)], Prof. Ph.D. Eng. Voicu Gh.[1)], Prof. Ph.D. Eng. Biriş S.Şt.[1)], Lect. Ph.D. Eng. Ştefan E.M.[1)], Lect. Ph.D. Eng. Ungureanu N.[1)], Lect. Ph.D. Eng. Dincă M.N.[1)]

[1)]Politehnica University of Bucharest, Faculty of Biotechnical Systems Engineering / Romania

Phone: +40734010193; E-mail: maneamaryana@yahoo.com

Keywords: *oilseeds, mechanical characteristics, compression test, force-deformation curve, rupture point, energy consumption*

ABSTRACT

Basic knowledge of the behavior of agricultural products to the mechanical forces application is essential for determination of necessary power for various work processes and for the design of machinery, equipment and agricultural installations. This paper presents the results obtained from uniaxial compression tests of sunflower seeds, rapeseeds and safflower seeds. Thus, data for the mechanical characteristics of the three types of oilseeds (force-deformation curve, forces, deformations and energy consumption at the point of shell rupture) were obtained.

REZUMAT

Cunoaşterea fundamentală a comportamentului produselor agricole la solicitările forţelor mecanice este esenţială pentru determinarea necesarului de putere pentru diferite procese de lucru, precum şi pentru proiectarea maşinilor, echipamentelor şi instalaţiilor agricole. Lucrarea de faţă prezintă rezultatele obţinute în urma testelor de compresiune uniaxială a seminţelor de floarea-soarelui, rapiţă şi şofrănel. Astfel, au fost obţinute date cu privire la caracteristicile mecanice ale celor trei tipuri de seminţe oleaginoase (curba forţă-deformaţie, forţele, deformaţiile şi consumul de energie în punctul de rupere a cojii).

INTRODUCTION

Oilseeds represent the main raw material for vegetable oils extraction. Among the most important oilseed grown in our country there are included sunflower seeds, rapeseeds and safflower seeds.

Oil raw materials are subjected to mechanical forces during the oil extraction process, those forces leading to the seeds deformation. Therefore, the mechanical behavior of oil seeds has an important role in the process of oil extraction, *(Ozumba I.C., Obiakor S.I., 2011).*

Compression test represents an objective method for determining the mechanical properties of cereal seed and one of the best techniques for determining the modulus of elasticity by studying their behavior to compression load using force-deformation curve, *(ASAE Standards 2000; Khodabakhshian R., Emadi B., 2011).*

Numerous works have been carried out by researchers in the field in order to highlight the physical and mechanical properties of oilseeds,*(Bagvand A., Lorestani A.N., 2013; Jafari S., Khazaei J. et al, 2011; Khodabakhshian R. et al, 2010).*

Thus, numerous works in the literature have been carried out on various oil seeds (sunflower, Moringa, safflower, jatropha, rapeseeds) in order to determine various physical properties (weight, size, average diameter, surface area, sphericity, coefficient of static friction, moisture content) *(Babić Lj., Radojčin M., Pavkov I., Babić M., 2012)* and mechanical properties (elasticity modulus, hardness, rupture force, deformation at the rupture point, consumed energy at rupture) thereof, *(Ajav E.A., Fakayode O.A., 2013; Gupta R.K., Das S.K., 2000; Herak D. et al, 2010; Herak D. et al, 2012; Jafari S., et al, 2011).*

Some researchers have studied the dependence of physical and mechanical properties of safflower seeds *(Feyzallahzadeh M., et al, 2013).* Thus, it was observed that there is a significant dependency between seed mass, mean diameter, sphericity and surface area and the mechanical properties of seeds. However, an insignificant dependence was observed between the mass, the sphericity and the average diameter with the safflower seeds deformation.

Other researchers*, (Gupta R.K., Das S.K., 2000),* studied the influence of the moisture content of sunflower seeds (and for the sunflower kernel) on the seeds behavior during compression tests and, also, the influence of seed position during compression. Thus, it was observed that the rupture force of the seeds and kernels decreased with increasing the moisture content and the force value was higher for the seed in vertical position compared to tests carried out with seeds in horizontal position. Another paper, *(Khodabakhshian R. et al, 2010),* studied the influence of moisture content on the physical and mechanical properties of sunflower seeds and kernels.

Knowing the importance of the mechanical properties of oilseeds, this paper presents the results obtained from uniaxial compression tests of sunflower seeds, rapeseeds and safflower seeds.

MATERIAL AND METHOD

For conducting the experiments were used sunflower, rape and safflower oilseeds. For the three types of seeds were carried out measurements on samples of 10 seeds in order to determine moisture content, oil content, the principal dimensions and mass of the seed. The moisture content of the seeds was determined by MAC 110 thermo-balance and had values from 4.65 to 4.77% for sunflower, 4.75 to 5.05% for rape or 5.19 to 5.49 % to safflower.

Using solvent extraction method was determined oil content of the seed and the following values were obtained: from 46.90 to 47.70% for sunflower, from 41.10 to 41.40 and from 34.23 to 37% for rapeseed, 0.1% for safflower. Measurement of the three main dimensions of seed (length, width and thickness), was performed using a digital caliper with precision of 0.01 mm, and then determined the individual seeds mass with Kern 572 electronic scales, having the accuracy of 10^{-3} g.

To determine the mechanical properties of oilseeds (sunflower, rapeseed and safflower) was used the Hounsfield/Tinius Olsen mechanical tests machine, model H1 KS, which enables the mechanical properties for a wide range of materials (wood, vegetable products, metal, plastic, textile, leather, ceramics, etc.). The main components of the machine are: support columns; a fixed flat plate to support material sample; pressing head with movable flat plate parallel to the base plate; display, adjustment and control panel; force cell; data acquisition system (computer) with QMAT software (fig. 1).

The seeds subjected to uniaxial compression are arranged between two parallel planes plate of the device, and on the movable plate is placed the 1 kN force cell that is fixed to the movable traverse for registering the displacement. Resistant force of the tested material sample is measured by a force cell, which can be changed easily and quickly by means of a special mechanism, depending on the material being tested. For the displacement measuring, the device has an accuracy of ± 0.0001 mm, and the movement speed can take values between 0.001 mm/min and 1000 mm/min. From the research in the studied field, it was concluded that for the compression test on oilseed the movement speed has to be constant at the value of 1 $mm \cdot min^{-1}$.

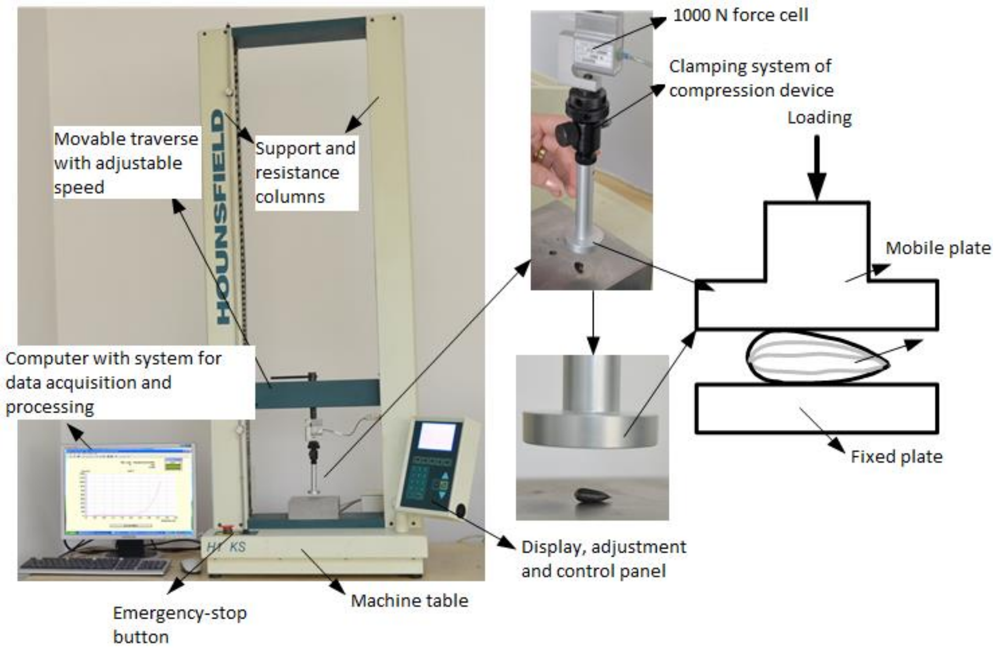

Fig.1 - Hounsfield/Tinius Olsen model H1 KS device for mechanical tests

After the compression tests on the 30 oilseeds (10 sunflower seeds, 10 rapeseeds and 10 safflower seeds) for which has been previously determined dimensional characteristics, the characteristic force-displacement curves were obtained, on which has been read the deformation values, force and energy consumed at different moments of compression and, also, the curve slope to shell rupture point (fig. 2).

The seeds were placed on the fixed plate of the machine in stable horizontal position and the speed of the mobile plate was set at 1 mm/min. The force and displacement values are obtained and saved by Qmat software of the mechanical testing device used in the compression test. Point "1" on the force-displacement curve (fig. 2) is the point where the oilseeds shell rupture occurred, here being observed a sharp drop of the force. Beyond that point, the seed kernel started to be compressed, this process taking place until the point "2" where the maximum force has been reached (about 1030 N), since the force cell was of 1 kN.

From the obtained graph the characteristic forces for the two points could be read, as well as the displacements and consumed energy at those moments. The energy consumption for each of the two points is determined by calculating the area under the curve, starting from the point where the force increases to the desired point. The curve slope up to the rupture force was traced starting from the point where the force begins to increase and to the point "1" when the shell rupture occurs.

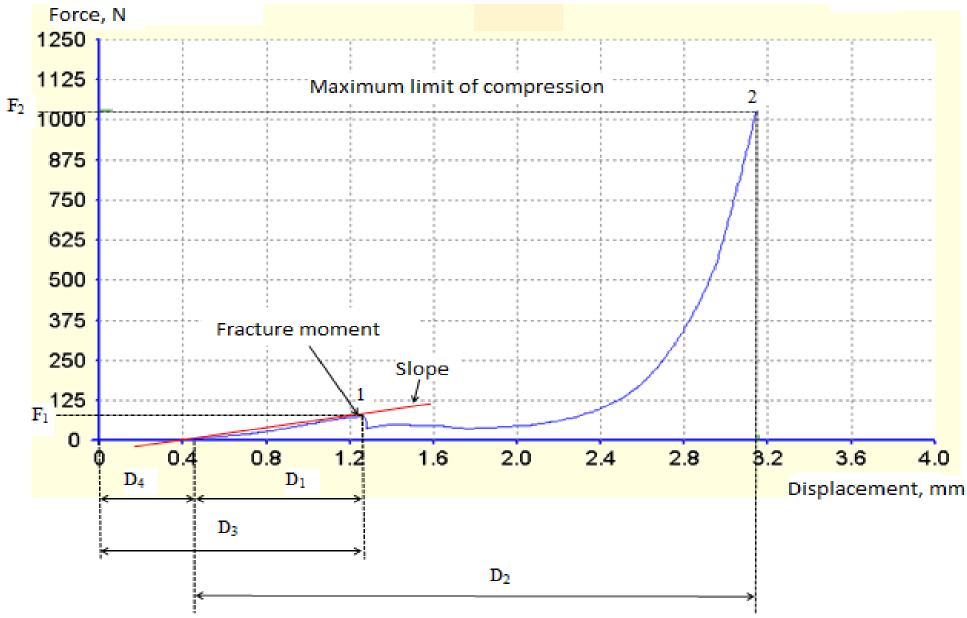

Fig. 2 – The force-strain curve and its characteristic points

RESULTS

In Tables 1, 2 and 3 are presented the values of force, deformation, consumed energy and slope read from the force-deformation curves for sunflower seeds, rapeseeds and safflower seeds.

Table 1

Measured and calculated values for sunflower seeds from the compression tests

Den. No.	F_1, (N)	F_2, (N)	Deformation, (mm)					Slope, (N/mm)	Energy, (J)	
			D_{max}	D_1	D_2	D_3	D_4		E_1	E_2
1	51.3	1030	3.272	1.121	2.909	1.484	0.363	43.18	0.0201	0.4610
2	47.5	1027	3.060	0.945	2.720	1.285	0.340	48.58	0.0155	0.4140
3	58.8	1030	3.420	0.856	3.156	1.120	0.264	66.60	0.0205	0.3374
4	75.0	1029	3.312	0.944	2.964	1.292	0.348	77.50	0.0269	0.5260
5	46.3	1026	3.780	0.996	3.416	1.360	0.364	43.84	0.0175	0.4930
6	53.8	1030	2.860	0.779	2.520	1.119	0.340	72.20	0.0203	0.4228
7	60.0	1028	3.352	0.960	2.980	1.332	0.372	60.10	0.0217	0.4927
8	45.0	1029	3.752	1.056	3.388	1.420	0.364	40.13	0.0144	0.5390
9	51.3	1026	3.240	0.956	2.924	1.272	0.316	52.00	0.0202	0.4774
10	57.5	1030	3.832	1.144	3.424	1.552	0.408	48.80	0.0219	0.5200

Table2

Measured and calculated values for rapeseeds from the compression tests

Den. No.	F_1. (N)	F_2. (N)	Deformation. (mm)					Slope. (N/mm)	Energy. (J)	
			D_{max}	D_1	D_2	D_3	D_4		E_1	E_2
1	11.25	1029	1.88	0.336	1.550	0.662	0.326	26.04	0.0031	0.3524
2	7.50	1028	1.98	0.340	1.624	0.696	0.356	14.71	0.0022	0.3467
3	10.00	1030	1.93	0.462	1.594	0.798	0.336	16.23	0.0027	0.3395
4	8.75	1028	2.11	0.365	1.785	0.690	0.325	17.12	0.0020	0.3450
5	16.25	1026	2.30	0.621	1.993	0.928	0.3075	22.16	0.0039	0.3407
6	12.50	1026	2.13	0.363	1.823	0.670	0.3075	27.59	0.0037	0.3368
7	7.50	1026	2.30	0.298	1.945	0.653	0.355	16.78	0.0023	0.3358
8	11.25	1029	2.26	0.408	1.925	0.743	0.335	21.45	0.0030	0.3341
9	16.25	1029	2.17	0.611	1.883	0.893	0.2825	24.57	0.0036	0.3358
10	11.25	1030	1.97	0.336	1.614	0.692	0.356	26.04	0.0032	0.3355

Table3

Measured and calculated values for safflower seeds from the compression tests

Den. No.	F_1. (N)	F_2. (N)	Deformation. (mm)					Slope. (N/mm)	Energy. (J)	
			D_{max}	D_1	D_2	D_3	D_4		E_1	E_2
1	42.5	1024	3.128	0.5	2.84	0.788	0.288	80	0.0168	0.3924
2	26.3	1029	2.86	0.332	2.572	0.62	0.288	71.5	0.0155	0.3303
3	45	1024	3.208	0.628	2.876	0.96	0.332	67.7	0.0159	0.4167
4	42	737	2.800	0.74	2.536	1.004	0.264	53.7	0.0145	0.2805
5	36.3	1027	3.472	0.788	3.072	1.188	0.4	60.5	0.0168	0.4044
6	53.8	1029	2.940	0.596	2.584	0.952	0.356	83.9	0.0197	0.397
7	78.8	1030	3.152	0.856	2.752	1.256	0.4	87.6	0.0212	0.3966
8	52.5	1025	3.120	0.764	2.788	1.096	0.332	63.8	0.0187	0.3626
9	61.3	1027	3.328	0.504	3.024	0.808	0.304	114.1	0.0218	0.4538
10	45	1027	3.088	0.58	2.792	0.876	0.296	71.1	0.0202	0.4465

After analyzing force-deformation curves obtained on the computer for the 30 oleaginous seeds, 10 from each seed type it was found that not all had the same point of origin for the displacement. In order to start from zero all the curves, both for horizontally and vertically positions the acquired data were processed in Excel and experimental curves were redrawn.

Further, there are presented the mean values force-deformation curves for the three types of seeds used in the experiments. Thus, in fig. 3 can be seen that the shell rupture for sunflower occurs between 1.112 and 1.504 mm for deformation and between 40.6 to 62 N for force, values which were read on the mean force-deformation curves.

As for the rapeseeds, the mean values of deformation and force at rupture point were between 0.271 and 0.561 mm. respectively 8.75 and 9.88 N. values that are much lower than those for the of sunflower seeds. It also notes that the mean deformation and force values at shell rupture for safflower seeds have higher values than those for rapeseeds i.e. 0.512 to 0.944 mm. respectively 34.65 to 39.28 N.

The slope of force-deformation curve till the rupture point of the shell represents the elasticity of the shell, but it must take into account that under the shell is the kernel (in contact with the shell) that also opposes resistance to crushing (or shell rupture). For this reason we cannot express a direct relation between the curve slope and the shell or kernel elasticity.

To establish a correlation between slope and rupture energy E_1 was performed in Microsoft Excel a regression analysis using linear variation law. Fig. 4 presents the variation of rupture energy depending on the slope for the three types of oilseeds. As a result of the regression analysis, it was found that the best correlation between slope and rupture energy is shown by rapeseeds (R^2=0.647) and the lowest correlation was obtained for sunflower seeds (R^2=0.528).

In fig. 4 is also shown another regression analysis using linear variation law in Microsoft Excel which has been made to establish a correlation between the force and the energy to the shell rupture point. F_1 and E_1. obtained from the compression tests on which the three types of oilseeds have been subject to. Analyzing the figure can be seen that the best correlation was obtained for sunflower seeds with R^2=0.873. while safflower seeds had the lowest correlation with R^2=0.605.

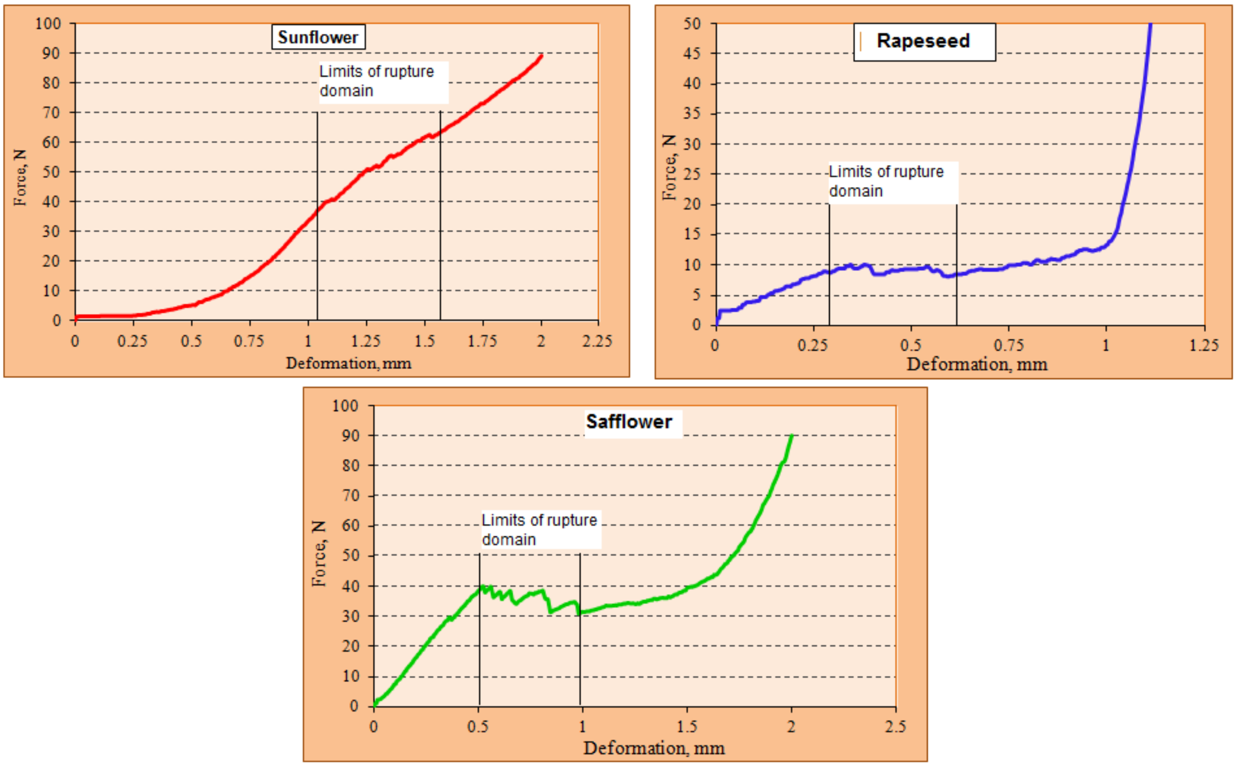

Fig. 3 - Average force-deformation curve for the three types of oilseeds

Relatively low values of correlation coefficients show the dispersion of experimental data points (curve slope-consumed energy) which are distributed in a very wide area. It is obvious.Therefore, not all culture seeds are developed the same and the different climatic conditions are affecting this phenomenon. It is further said that at the same plant the seeds are not developed equally, which is closely related to seeds position on stalk capitulum or on circular rows of the capitulum.

For this reason, the seeds do not have similar dimensions or mechanical characteristics in a narrow range of values.

A real image of these ranges of values could be obtained on a large number of experiments (on the same seeds culture) without a selection of them. However, the obtained values can be helpful for processors in order to achieve a proper adjustment of the machine, but also for designers and builders to optimally establish the actuators.

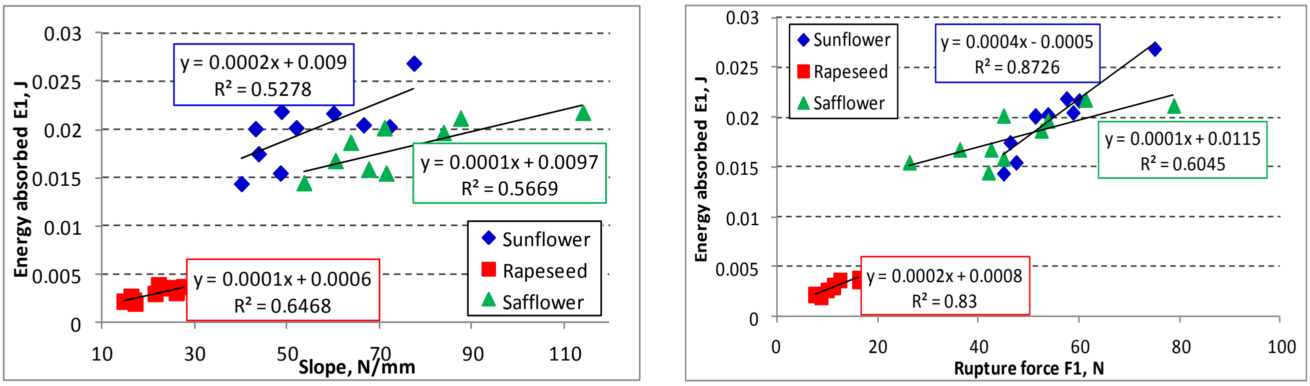

Fig.4 - Variations of the energy absorbed E1 with the slope/rupture force for the three types of oleaginous seeds

CONCLUSIONS

Using the force-deformation curves of the uniaxial compressive tests (performed on the thickness of the sunflower and safflower seeds) may be obtained precious information on the mechanical characteristics of seeds regarding the shell rupture force (taking into account the influence of kernel resistance), total deformation until rupture, the necessary energy (or consumed to deformation), seeds elasticity (in assembly), deformation limits and shell rupture forces for a mixture of seeds etc.

Thus, the necessary force for sunflower seeds shell rupture was within the limits of 45-75 N. while for safflower seed was in the range of 26.3-78.8 N and for rapeseed was from 7.5 to 6.3 N.

For these rupture forces registered by the device, total seeds deformation was 2.9-3.8 mm for sunflower, 2.8 to 3.5 mm for safflower and 1.9-2.3 mm in the case of rapeseeds.

Energy consumed for seeds rupture shows a linear correlation with the rupture force (with a high degree of correlation especially for rapeseed and sunflower) falls in the ranges $(1.4\text{-}2.7)\cdot10^{-2}$ J for sunflower. $(1.5\text{-}2.2)\cdot10^{-2}$ J for safflower and $(0.2\text{-}0.4)\cdot10^{-2}$ J for rapeseeds.

The elasticity of the seed as a whole, expressed by the value of the curve slope until the moment of breakage (rupture) of the shell shown also values in relatively wide limits. Thus, the sunflower seeds showed elasticity values within the limits of 40.1-77.5 N/mm. 53.7- 114.1 N/mm for safflower and between 14.7 and 27.6 N/mm for rapeseeds.

Knowing the values of the mechanical characteristics of oilseeds are really useful both for manufacturers but especially for operators of equipment used for oil extraction from oilseeds.

REFERENCES

[1] Ajav E.A., Fakayode O.A., (2013), Mechanical Properties of Moringa (Moringa oleifera) Seeds in relation to an Oil Expeller Design, *Agrosearch* 13, No.3, pp. 206–216;

[2] ASAE Standards 2000, (2008), Compression Test of Food Materials of Convex Shape, *American Society of Agricultural and Biological Engineers,* S368.4;

[3] Babić Lj.. Radojčin M.. Pavkov I.. Babić M. (2012), The physical and compressive load properties of sunflower (Helianthus annuus L.) fruit,*HELIA*35, No. 57, pp. 95-112;

[4] Bagvand A.. Lorestani A.N. (2013), Determination of Physical Properties and Mechanical Behavior of Sunflower seeds, *International Journal of Agriculture and Crop Sciences*, 5-11, pp.1255-1259, ISSN 2227-670X;

[5] Feyzallahzadeh M., Hosseinzadeh J., Nikbakht A.M., Modarres Motlagh A., (2013), Relation between physical and mechanical properties of safflower seed affected by irrigation treatments. *Technical Journal of Engineering and Applied Sciences*, 3-15, pp.1564-1571, ISSN 2051-0853;

[6] Gupta R.K., Das S.K. (2000), Fracture resistance of sunflower seed and kernel to compressive loading, *Journal of Food Engineering*, 46, pp.1-8;

[7] Herak D., Gurdil G., Sedlacek A., Dajbych O., Simanjuntak S., (2010), Energy demands for pressing Jatropha curcas L. Seeds, *Biosystems Engineering*, Vol. 106. pp. 527-534;

[8] Herak D., Kabutey A., Divisova M., Svatonova T., (2012), Comparison of the Mechanical Behaviour of Selected Oilseeds under Compression Loading, *Not Bot Horti Agrobo*, Vol. 40(2), pp.227-232, ISSN 0255-965X;

[9] Jafari S., Khazaei J., Arabhosseini A., Massah J., Khoshtaghaza M.H., (2011), Effects of some parameters on fracture resistance of sunflower seed,*Agronomics Research in Moldavia*, Vol. XLIV , No. 3 (147), pp.5-12;

[10] Jafari S., Khazaei J., Arabhosseini A., Massah J., Khoshtaghaza M.H. (2011), Study on mechanical properties of sunflower seeds, *Electronic Journal of Polish Agricultural Universities*, Vol.14, Issue 1, ISSN 1505-0297;

[11] Khodabakhshian R., Emadi B., Abbaspour Fard M.H., (2010), Some engineering properties of sunflower seed and its kernel, *Journal of Agricultural Science and Technology*, Vol.4, No.4 (Serial No.29), pp.37-46, ISSN 1939-1250, USA;

[12] Khodabakhshian R., Emadi B., (2011),Determination of the Modulus of Elasticity in Agricultural Seeds on the Basis of Elasticity Theory, *Middle-East Journal of Scientific Research* 7(3): 367-373, ISSN 1990-9233;

[13] Ozumba I.C., Obiakor S.I., (2011), Fracture resistance of palm kernel seed to compressive Loading, *Journal of Stored Products and Postharvest Research*, 2(13), pp.248-253.

RESEARCH THE FORCE PARAMETERS OF FORMING THE SCREW CLEANING ELEMENTS
/
ДОСЛІДЖЕННЯ СИЛОВИХ ПАРАМЕТРІВ ФОРМОУТВОРЕННЯ ГВИНТОВИХ ОЧИСНИХ ЕЛЕМЕНТІВ

Prof. Ph.D. Eng. Hevko Iv.B., Lect. Ph.D. Eng. Dychun A.Y., Prof. Ph.D. Eng.Lyashuk O.L., Ph.D. Eng.Martsenko, Eng. Gypka A.B.
Ternopil Ivan Pul'uj National Technical University, Ruska Str., 56, Ternopil, Ukraine
E-mail: gypkab@gmail.com

Keywords: *digger's disk, auger cleaner, Г-shaped, cleaning.*

ABSTRACT
In this article the results of theoretical research of power parameters while forming the deflected outer contour of acrew workpiece are analysed in this article. The design of disk digger for cleaning the disks' working surfaces isworked out. The advances of Г-shaped auger cleanersare substantiated. The power and kinematic computationof the suggested auger cleaners of disk digger of rootcrops is carried out.

РЕЗЮМЕ
У даній роботі викладенно результати теоретичних досліджень силових параметрів при формоутворенні відігнутого зовнішнього контура на гвинтовій заготовці. Розроблено конструкцію дискового копача із можливістю очищення робочих поверхонь дисків. Проаналізовано й обґрунтовано вибір Г–подібних шнекових очисників. Проведено силовий і кінематичний розрахунок запропонованих шнекових очисників дискових копачів коренеплодів.

INTRODUCTION
Г-shaped augers' spirals can be widely used in transport and technological systems in the future. Nowadays such spirals are used to supply dry, wet, sticky, lumpy, fibrous products in agriculture, and food, building, chemical and other industries, etc. However, they possess additional qualities that, depending on the inclination of the spiral, can manifest themselves as the functions of increasing the resistance of transporting the materials to the surface of displacement, or vice versa - reducing the friction of transported material to the surface of displacement. In the first case, this phenomenon can be widely used in wiping or shredding different materials, and in the second - in separating and pruning various materials from the surface displacement.

Grigoriev A.M. Preobrejenskiy P.A., 1967, Hevko B.M.,1986, Loveikin V., 2012, and others investigated the procces of creating and operating the screw mechanisms; their works are dedicated to the issue of efficiency of auger conveyors. *Pylypets M.I., 2002*, *Hevko R.B., 2013,* and others researched the process of separating the root chaff. *Rohatynskiy R.M., 1997* and other scientists researched the process of profiling screw spirals as well as the process of transportation by means of *Г*-shaped augers.

MATERIAL AND METHOD
The objective of this research is the designing of auger cleaner for efficient cleaning the disk diggers of root crops from contamination. The usage of such cleaner will reduce power consumption during the mechanism's operation and improve the quality of cleaning root crops.

The process of digging the roots is accompanied by significant soil and chaff sticking to the surfaces of disk diggers. The digging devices are equipped with Г-shaped spiral augers, which allow to clean them efficiently. The process of cleaning is accompanied by removing the chaff by the spiral from the working surface of the disk digger. Under such conditions the angle of inclination μ of screw spiral in its cross section influences much the force, which is necessary to overcome the resistance of material transportation (Fig. 1). Terefore, the usage of the spiral with inclined outer contour in direction of transportation is the most efficient one, because the vector of normal force between the coil and casing $\bar{N}_1$, acting on the product from the side of the coil, is directed from the tangent to the casing at an angle *γ1*.

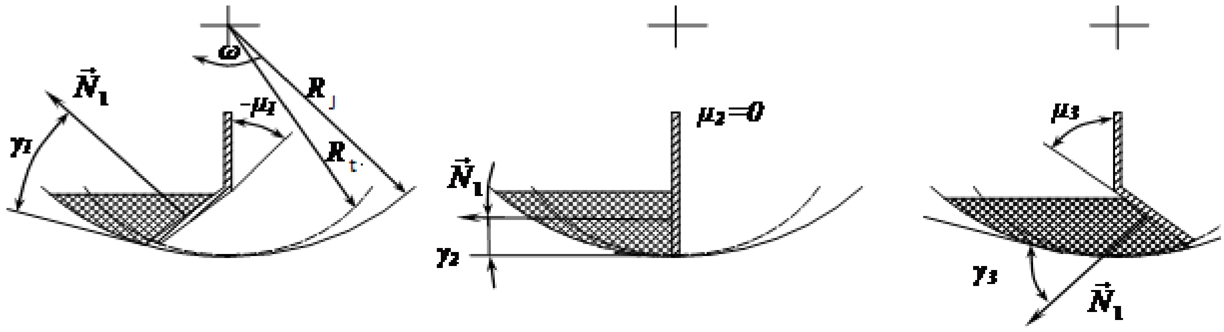

a) b) c)

Fig.1- Estimated circuit for determining the effect of slope angle helical tape in cross-section of the process jamming material

a) spiral slope in the direction of transportation; b) radial spiral;
c) the slope of the spiral in the opposite direction to the direction of transport

Investigating the force parameters of forming the screw purifying elements

The process of manufacturing the screw purifying elements is as follows:

1. Bending the shelf on a tape using the rollers.
2. Coiling the given tape with a shelf around a collet.

The process of coiling such a tape around the collet is shown in Fig.2.

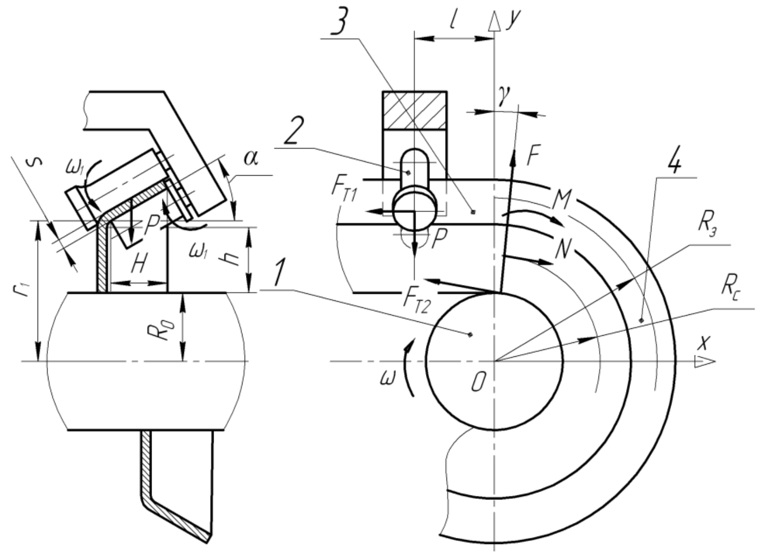

Fig.2 - Computational model of coiling the tape around the collet

1 – collet; 2 – clamp roller; 3 – tape; 4 – screw element

While coiling, the compression of tape fibers along the inner diameter occurs, as well as the tension of tape fibers along the outer diameter of the screw-purifying element (*Pylypets M.I., 2002*) . That is, in the shelf's zone, only the strain deformations occur, as well as in the workpiece's vertical part − the compressive deformations (*Hewko B. M., 1989, Rohatynskyi P.M., and others 2014).* Having considered the process of deformation in the hot state, the moment of tape bending in these zones can be defined.

As it is known, the radial stresses, occurring in the tape shelf, are determined by the formula *(Zubtsov M.E. 1980):*

$$\sigma_{\rho 1} = -\beta\sigma_s \cdot \ln\frac{R}{\rho} \quad (1)$$

Where:

β – the coefficient, which depends on the impact of the mean primary stress, equals 1.15;

σ_s – the liquid limit of screw clamping element material, MPa;

R – the outer bending radius, mm;

ρ – the polar coordinate of bending radius, mm.

Similarly, the radial stresses in the compression zone can be determined *(Rohatynskyi P.M., and others 2014, Aleksey Popov, 2010)*:

$$\sigma_{\rho 2} = -\beta\sigma_s \cdot \ln\frac{\rho}{r} \tag{2}$$

Where r – the inner bending radius, mm.

Tangential stresses in the tension zone:

$$\sigma_{\theta 1} = \beta\sigma_s \cdot \left(1 - \ln\frac{R}{\rho}\right) \tag{3}$$

Tangential stresses in the compression zone:

$$\sigma_{\theta 2} = -\beta\sigma_s \cdot \left(1 + \ln\frac{\rho}{r}\right) \tag{4}$$

According to the computational model in Fig.1, the radius of bending the workpiece's shelf changes from r_1 to $r(x)$, where

$$r(x) = r_1 + x \cdot \mathrm{tg}\alpha \tag{5}$$

where

r_1 – the smallest inner radius of bending the shelf, mm;

α - the inclination angle of the shelf, grade.

The outer radius of bending the workpiece:

$$R(x) = r_1 + \frac{s}{\cos\alpha} + x \cdot tg\alpha \tag{6}$$

Where s – the tape thickness, mm.

The value of bending moment while coiling with heating is considered as the integral sum from tangential stresses along the height of elementary elements' workpiece.

$$M = \int_0^H \int_{r(x)}^{R(x)} \sigma_{\theta 1}\rho d\rho dx + s\int_{R_0}^{R_0+h} \sigma_{\theta 2}\rho d\rho \tag{7}$$

where:

ρ_H - the radius of neutral surface of stresses, mm;

h – the height of the workpiece's vertical part, mm;

H – the height of the screw element's shelf, mm.

Using formulas (3) – (6) in the equation (7) we obtain:

$$M = \int_0^H \int_{r_1 + x\cdot tg\alpha}^{r_1 + \frac{s}{\cos\alpha} + x\cdot tg\alpha} \beta\sigma_s \cdot \left(1 - \ln\frac{r_1 + \frac{s}{\cos\alpha} + x\cdot tg\alpha}{\rho}\right) \cdot \rho d\rho dx + s\int_{R_0}^{R_0+h} -\beta\sigma_s \cdot \left(1 + \ln\frac{\rho}{R_0}\right)\rho d\rho \tag{8}$$

where R_0 - the collet radius, mm.

Having transformed the equation (8), we obtain:

$$M = \frac{1}{2}\cdot\beta\cdot\sigma_s([bH\left(r_1 + \frac{1}{2}b + Htg\alpha\right) + \frac{H}{3}(H\cdot tg\alpha\cdot\left(-r_1D + tg\alpha KH + \frac{1}{2}b + 3r_1K - Dtg\alpha H\right) + $$
$$+3r_1^2(K-D) - b(b+r_1)) + \frac{r_1^3(K-D-C+\ln r_1) + b^3(K-C) + r_1b^2}{tg\alpha}] + s(-\frac{1}{2}((R_0+h)^2 - R_0^2) - (R_0+h)^2\ln\left(\frac{R_0+h}{R_0}\right))), \tag{9}$$

where the following marks are used:

$$b = \frac{s}{\cos\alpha};\ K = \ln\left(r_1 + b + Htg\alpha\right);\ C = \ln(r_1 + b);\ D = \ln\left(r_1 + Htg\alpha\right)$$

According to the computational model in fig.1, the equilibrium equation of a tape part under deformation can be written as follows:

$$\left.\begin{array}{r}\text{axis x: } -F_{T1}-F_{T2}\cdot\cos\gamma+N\cdot\cos\gamma+F\cdot\sin\gamma=0\\ \text{axis y: } -P+F_{T2}\cdot\sin\gamma-N\cdot\sin\gamma+F\cdot\cos\gamma=0\\ \text{sum of points: } P\cdot l+F_{T1}\cdot R_з+F_{T2}\cdot R_0-N\cdot R_c-M=0\end{array}\right\} \qquad (10)$$

Where:

F_{T1}- friction force between the tape and the roller,

N; F_{T2} - friction force between the tape and the collet,

N; γ - collet's turning angle, grd.; N - direct force, N;

F- resultant force of the tape normal contact stresses, N;

P-the bending force by the clamp roller, N;

l -distance between the collet centre and the clamp roller centre, mm;

R_3- mean radius of screw element's interaction, mm;

R_c- mean radius of screw element, mm.

The friction forces can be developed from the dependences:

$$F_{T1}=\mu_1\cdot P \qquad (11)$$

$$F_{T2}=\mu_2\cdot F \qquad (12)$$

Where:

μ_1 - the coefficient of friction between the clamp roller and the tape;

μ_2 - the coefficient of friction between the collet and the crew element.

The resultant force of normal contact stresses is determined by the formula:

$$F=\sigma_r\cdot s\cdot L \qquad (13)$$

Where:

σ_r - the contact normal stresses along the screw workpiece's inner radius, MPa;

S - the tape thickness, mm; L - length of contact along the inner diameter, mm.

Provided the bending moment M is known, all forces, which occur while coiling, can be found after solving the equation system (7). In the given case:

$$F=\frac{-P\cdot\left(\mu_1\cdot tg\gamma-1\right)}{\mu_2\cdot\sin\gamma+tg\gamma\cdot\left(-\mu_2\cdot\cos\gamma+\sin\gamma\right)+\cos\gamma} \qquad (14)$$

$$N=\frac{\mu_1\cdot P+F\cdot\left(\mu_2\cdot\cos\gamma+\sin\gamma\right)}{\cos\gamma} \qquad (15)$$

According to the results of experimental research, the maximum bending force P by clamp roller occurs at the beginning stage of deformation, that is, when the angle γ equals zero. Therefore, to simplify calculations, the solution of equations system (10) will be as follows:

$$P=F \qquad (16)$$

$$N=\left(\mu_1+\mu_2\right)\cdot P \qquad (17)$$

$$P=\frac{M}{l+\mu_1\cdot(R_з-1)+\mu_2\cdot\left(R_0-1\right)} \qquad (18)$$

It should be noted that the friction coefficient μ_1 between the clamp roller and the profiled tape is the given value and does not correlate directly with the value of contacting materials' friction coefficient. The moment applied to coining the collet depends on collets' structural peculiarities, and is generally defined as it is shown in Fig. 1., accordingly to the dependences:

$$M_O=k_M\cdot P\cdot\left(l+\mu_1\cdot R_з\right) \qquad (19)$$

Where k_M – the coefficient, which depends on the structural manufacture of the collet.

Based on the proposed above formulas, the required technological equipment can be designed. Thus, to reduce the torque of collet, and consequently to reduce the required power of coiling the screw workpiece, it is necessary to minimize friction coefficient μ_1, for example, using the lubricants.

The coiling of a screw element being executed in the cold state, the workpiece material is being strengthened consequently, the bending moment increases, which can be determined by the formula:

$$M=\int_{0}^{H}\int_{r_1+x\cdot tg\alpha}^{r_1+\frac{s}{\cos\alpha}+x\cdot tg\alpha}\beta\left[\begin{array}{l}\sigma_{TO}\cdot\left(1-\ln\dfrac{r_1+\dfrac{s}{\cos\alpha}+x\cdot tg\alpha}{\rho}\right)+\\ +\dfrac{\Pi}{2}\cdot\left(2\ln\dfrac{\rho}{R_c}-\ln\dfrac{\rho\left(r_1+\dfrac{s}{\cos\alpha}+x\cdot tg\alpha\right)}{R_c^2}\ln\dfrac{\left(r_1+\dfrac{s}{\cos\alpha}+x\cdot tg\alpha\right)}{\rho}\right)\end{array}\right]\cdot\rho d\rho dx+s\beta\int_{R_0}^{R_0+h}\left[\sigma_{TO}\left(1+\ln\frac{\rho}{R_0}\right)+\frac{\Pi}{2}\left(2\ln\frac{R_0+h}{\rho}+\ln\frac{\left(R_0+h\right)^2}{\rho R_0}\ln\frac{\rho}{R_0}\right)\right]\rho d\rho,\quad(20)$$

where

$\sigma_{T.O}$ - extrapolated liquid limit, MPa;

Π - strengthening linear module, MPa.

RESULTS

The analytical method of solving the equation (20) is rather cumbersome, that is why the specific numerical value of bending moment should be defined by the numerical method, using appropriate software. Such method significantly reduces the calculation time.

An example of such calculation is shown in the graph in Fig. 3.

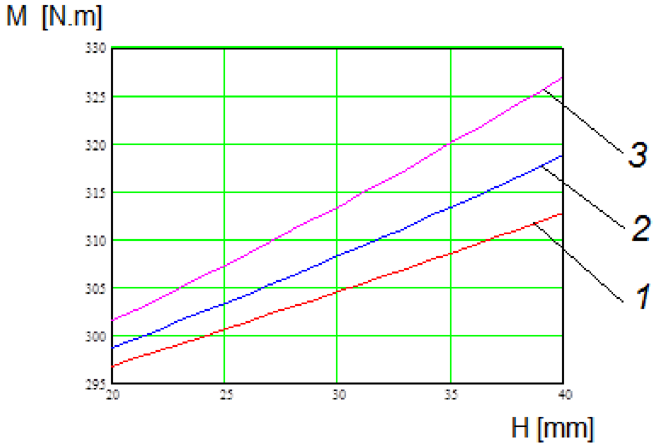

Fig.3- Graph of dependence of tape bending moment on height shelf (steel 08kP)

s=1,5 mm, R_0=30 mm: 1 - $\alpha=10^0$, 2 - $\alpha=20^0$; 3 - $\alpha=30^0$

Analyzing the graph in Fig.2 we conclude: the shelf height and its inclination angle increases, the moment of bending the screw element increases as well.

Based on the graph in Fig.3 and formula (18), the graphs of dependence of the tape bending force on the shelf height can be drawn (Fig.3).

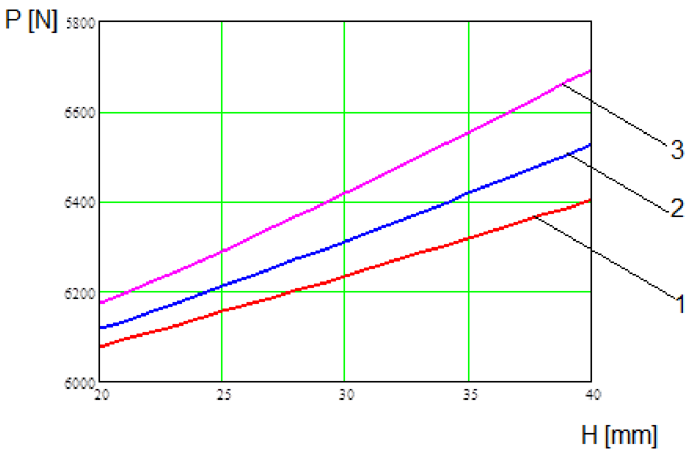

Fig.4 - Graph of dependence of the tape bending force on the shelf height (steel 08kp)

s=1,5 mm, R_0=30 mm: 1 - $\alpha=10^0$, 2 - $\alpha=20^0$; 3 - $\alpha=30^0$.

According to the results theoretical research and having analyzed the graphs in figures 2 and 3, we conclude that mainly the vertical part of the workpiece deforms; and while increasing the shelf height and the inclination angle of the screw element, the bending force increases as well. As the main working surface of a screw-purifying element is a shelf, the cuts on the vertical part of the tape must be performed to reduce the bending moment of such tape.

CONCLUSIONS

Based on the analysis of the patent search screw constructions and working bodies of the literature from the definition mode of operation of the proposed new design screw with curved outer contour

As a result of investigations proved the practical feasibility of the proposed mechanism for clearing L-shaped spirals screw drives root crop working surfaces

The proposed treatment technology manufacturing screw elements by bending the tape on shelves using clips and coiling the resulting tape with a shelf to be set.

The results can be used for designing different types of screw working bodies with curved working surfaces based on the rheological of properties of such screws when transporting bulk materials.

REFERENCES

[1] Aleksey Popov, (2010), The new theory of elastic contact strength of compressed bodies (Новая теория контактной прочности упруго сжатых тел), MOTROL, *Commission of Motorization and Power Industry in Agriculture Polish Academy of Sciences* Branch of Lublin Ropczyce School of Engineering and Management, Vol. 12A, pp. 223-232, Lublin;

[2] Grigoriev A.M., Preobrejenskiy P.A., (1967), *Complex mechanization and automation of cargo handling and transport operations in engineering and instrument (Комплексна механізація і автоматизація вантажорозвантажувальних і транспортних робіт в машинобудуванні і приладобудуванні)*, Naukova Dumka, p.116;Hevko B.M., (1986), *Manufacturing technology spiral auger (Технология изготовления спиралей шнеков)*, High school, p.128, Lviv;

[3] Hewko B. M., (1989), – Screw falling mechanisms of agricultural machinery (Винтовые подающие механизмы сельскохозяйственных машин), Higher school, p. 176, Lviv;

[4] Hevko R.B., Klendiy O.M. (2013), Methodology of investigation of a screw conveyer with a safety device (Методика проведення досліджень шнекового транспортера із запобіжним пристроєм.) *Agricultural Machinery: Scientific works*, No.24, Edition of Lutsk NTU, pp. 67-75., Lutsk;

[5] Loveikin V., Chovniuk Yu., Kulyk V. (2012), Optimizatsiia rezhimov kolebanii zernovykh smesei pri nalichii sukhogo treniia. Motrol – *Motoryzacja I energetyka rolnictva,* Vol. 14, v3, 140-149, Lublin;

[6] Pylypets M.I., (2002), *Scientifically and technological bases of production coiling machine parts billet*: Author. PhD.Thesis Engineering Sciences specials (Науково-технологічні основи виробництва навивних заготовок деталей машин : автореф. дис. на здобуття наук. ступеня доктора техн. наук), p.35, Lviv;

[7] Rohatynskyi P.M., and others (2014), *Scientific and applied backgrounds of creating the screw transport and technological mechanisms (Науково-прикладні основи створення гвинтових транспортно-технологічних механізмів)*, TNTU, p. 278, Ternopil;

[8] Rohatynskyi R. M., (1997), *Mechanical and technological backgrounds of interaction of screw working bodies with agricultural raw materials*, Thesis of Doctor of Sciences (Engineering)/ Rohatynskyi Roman Mykhailovych (Механіко-технологічні основи взаємодії шнекових робочих органів з сировиною сільськогосподарського виробництва : дис. докт. техн. наук), p. 502, Kyiv;

[9] Volkov R .A., Gnutov A. N., Diachkov V. K. and others, (1984), Conveyors (Конвейеры): Guide – under the editionship of Y.A. Perten, *Mechanical engineering,* p. 367, Leningrad;

[10] Zubtsov M.E., (1980), Sheet metal stamping (Листовая штамповка), *Machine building*, p.432. Leningrad;

[11] *** All Union State Standards Augers for agricultural machinery, (1973), AUSS 2705-73, Standards publisher, p.16, (National standards of Ukraine).

MATHEMATICAL MODELLING OF THE THRESHING PROCESS MADE BY THE THRESHING SYSTEMS WITH MULTIPLE ROTORS
/
MODELAREA MATEMATICĂ A PROCESULUI DE TREIER REALIZAT DE CĂTRE APARATELE DE TREIER CU ROTOARE MULTIPLE

Ph.D. Eng. Ivan Gh.
[2)]INMA Bucharest/ Romania
Tel: 0726190098; E-mail: geoivan2006@yahoo.com

Keywords: *combine harvester, tangential threshing system, threshing system with multiple rotors, threshing process, mathematical models*

ABSTRACT
The researches regarding the threshing process made by tangential threshing system of conventional harvester combines had as result the obtaining of mathematical models, based on experimental data, expressed through functions that partially define this process. Moreover, for the threshing systems with multiple rotors, the mathematical modelling of threshing process made by them is more difficult. This paper presents a mathematical model of the threshing process made by the threshing system with multiple rotors of the Romanian combine C110ATM. The mathematical model was based on the experimental data gathered by INMA Bucharest in 2001.

REZUMAT
Cercetările privind procesul de treier realizat de aparatul de treier tangenţial al combinelor convenţionale de recoltat cereale au avut ca rezultat obţinerea de modele matematice pe baza datelor experimentale, exprimate prin funcţii care definesc doar parţial acest proces. Cu atât mai mult, pentru aparatele de treier cu rotoare multiple modelarea matematică a procesului de treier realizat de acestea este şi mai dificilă. Lucrarea de faţă prezintă un model matematic al procesului de treier realizat de aparatul de treier cu mai multe rotoare al combinei româneşti C110ATM. Modelul matematic prezentat s-a bazat pe datele experimentale realizate de INMA Bucureşti în anul 2001..

INTRODUCTION
The threshing process of the conventional combine harvesters is made by the tangential threshing system and consists in breaking the link between the seeds and plant and separating them through a concave. (*Scripnic V., Babiciu P., 1979*)

The tangential threshing system is the main work part of a conventional combine harvester in terms of seeds separation and is positioned in the technological flow of this combine between the feeder house and the straw walkers (*Segărceanu M., 1981*). (Fig.1)

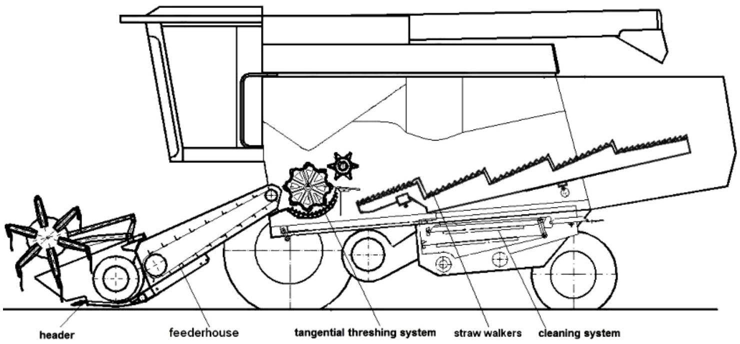

Fig. 1 – Tangential threshing system in the technological flow of a conventional combine harvester

In optimal conditions, the separation of seeds in tangential threshing system can be up to 85%, falling below 50-60% in the conditions of inadequate adjustments and a culture with high humidity. (*Miu P.1995*)

The tangential threshing system must ensure a threshing process with remained seeds in heads of grain under 1%, free seeds in straw under 14% and broken seeds under 2% of the harvested production. (*Segărceanu M., 1990*)

The main components of tangential threshing system are: threshing cylinder, concave, beater and concave extension (*Ivan Gh., Vlăduţ V., 2014*). (Fig. 2)

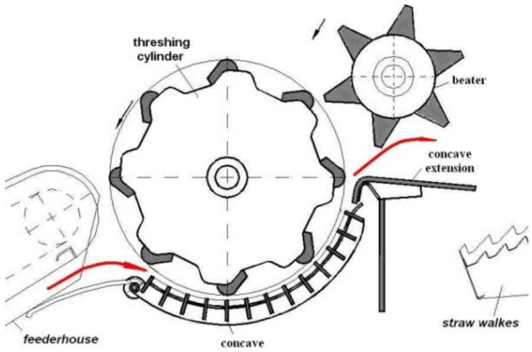

Fig. 2 – Main components of the tangential threshing system
(*Ivan Gh., Vlăduţ V., 2014*)

At the current combines equipped with tangential threshing system, in order to improve the threshing process, some firms use threshing systems with multiple rotors, that can be placed after the beater (*New Holland, Laverda*) or in front of the threshing cylinder (*Claas*), Fig. 3.

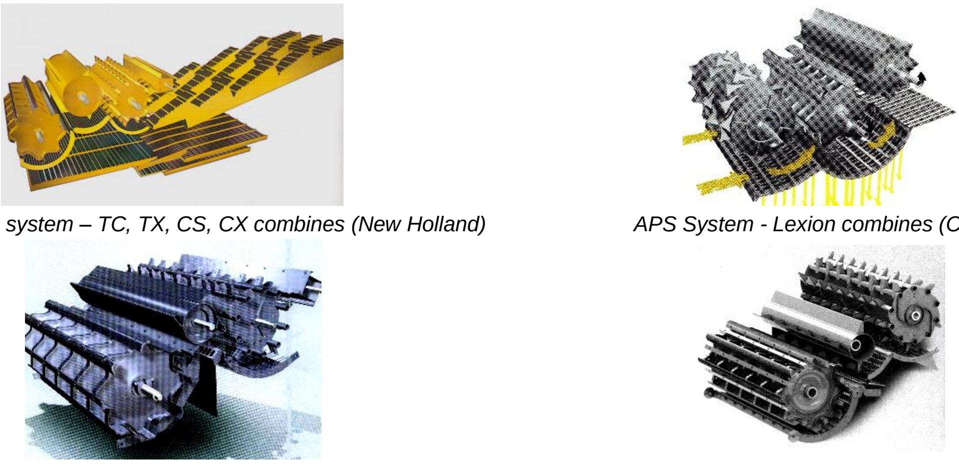

Multi-threshing system – TC, TX, CS, CX combines (New Holland) *APS System - Lexion combines (Claas)*

Multi-threshing system with Optithresh concave - CS combines (New Holland) *Multi Crop Separator - LXE, M300 combines (Laverda)*

Fig. 3 – Threshing systems with multiple rotors
(*Claas combine Prospects, Laverda combine Prospects, New Holland combine Prospects*)

At the threshing system with multiple rotors, the separation surface of seeds increases by 65-75%, the index of seeds separation being of 90-95%. (*Miu P.1995*)

The flow rate of a combine with threshing system with multiple rotors is higher by 14-20% than that of a conventional combine. (*Miu P.1995*)

Romanian combine C110ATM comprises a threshing system with multiple rotors, its location in the technological flow of the combine being shown in Fig. 4.

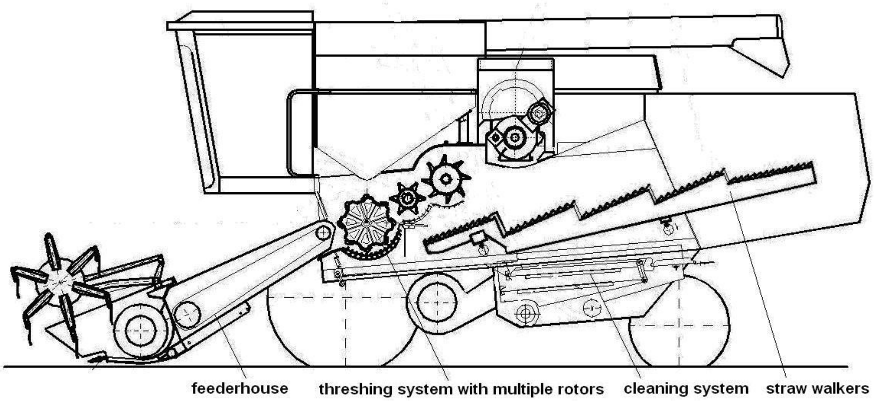

Fig. 4 – Location of the threshing system with multiple rotors at C110ATM combine (*Ivan Gh. ,2014*)

MATERIAL AND METHOD

The threshing process takes place in the threshing space, positioned between threshing cylinder and concave, the characteristic dimensions of this being the concave radius R_c, the concave winding angle α and the distances d_i and d_e between threshing cylinder and concave. (Fig. 5)

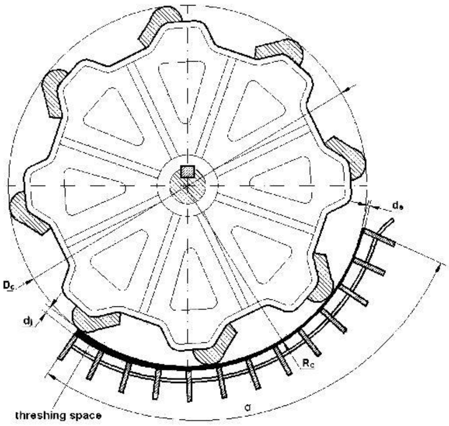

Fig. 5 – Threshing space of the tangential threshing system (*Ivan Gh., 2014*)

The threshing space length of the tangential threshing system can be calculated with relationship 1. (*Miu P.1995*)

$$s = \pi R_c \frac{\alpha}{180^0} \quad \text{[m]} \tag{1}$$

wheres is length of the threshing space; R_c– radius of the concave; α - winding angle of the concave.

The researches regarding the threshing process in the tangential threshing system had as a result the obtaining of mathematical models based on experimental data, expressed by functions that partially define the threshing process, the method used being the linear mathematical regression, nonlinear or multiple. (*Miu P., 1995*)

We present below the most important mathematical models concerning the percentage of seeds separated by concave depending on the length of threshing space at the conventional combines. (*Maertens K., De Baerdemaeker J. 2003, Rusanov A.I., 1974*)

Table 1

Mathematical models of the threshing process at the conventional combines

(*Maertens K., De Baerdemaeker J. 2003, Rusanov A.I., 1974*)

Model	Structure	Notations
Casper (1973)	$\xi_s(s) = 100\left(1 - e^{-\left(k_1 s + k_2 s^2 + k_3 s^3\right)}\right)\%$	where $\xi_s(s)$is the percentage of seeds separated by concave depending on the length of threshing space; s – length of the threshing space, in m; k_1, k_2, k_3 –threshing coefficients (experimental).
Rusanov A.J. (1976)	$\xi_s(s) = 100\left(1 - e^{-\mu s^{\alpha}}\right)\%$	α – winding angle of the concave, in radians; μ –threshing coefficient (experimental).
Trollope J.R. (1982)	$\xi_s(s) = 100\left[1 + \frac{c e^{-kP_0\psi} - kP_0 e^{-c\psi}}{kP_0 - c}\right]\%$	k, c – experimental coefficients; Ψ –geometric function on the winding angle.
Miu Petre (1995)	$\xi_s(s) = \frac{100}{a - b}\left[a\left(1 - e^{-bs}\right) - b\left(1 - e^{-as}\right)\right]\%$	s – length of the threshing space, in m; a, b – threshing coefficients (experimental).
Klenin N.I. and Lomakin S.G. (1972)	$\frac{d\xi_s(s)}{ds} = 100\left[1 - \frac{A}{k_2\mu}\left(k_2 e^{\mu s} - e^{k_2 s}\right) - (1 - A)e^{\mu s}\right]\%$	s – length of the threshing space , in m; A, k_2, μ –threshing coefficients (experimental).
Alferov S.A and Braginec V.S. (1972)	$\xi_s(s) = 100\left[1 - e^{-k_1 s} - A\frac{e^{-k_0 s} - e^{-k_1 s}}{k_1 - k_0}\right]\%$	s – length of the threshing space , in m; A, k_0, k_1–threshing coefficients (experimental).

Koen Maertens and Josse De Baerdemaeker have published in 2003 the results of experiments performed at stationary on the tangential threshing system of a New Holland combine harvester for feeding rates of 25-45 t/h (6.94-12.5 kg/s) 15.5-15.9% seeds humidity, 12-13% straw humidity, comparing with the 6 mathematical models shown in Table 1, the best results being achieved by mathematical models Rusanov, Caspers and Alferov-Braginec, in that order. (*Maertens K., De Baerdemaeker J. 2003*)

C110 combine harvester of the Romanian company "SEMĂNĂTOAREA", started to be manufactured in 1994. After year 2000, researches were made at INMA Bucharest, to increase the working capacity of this combine, by introducing a threshing system with multiple rotors (ATM), yielding an increase of the seeds separation surface at the level of threshing system with 84%.(*Prototype tests report for ATM, INMA Bucharest, 2002*)

The constructive scheme of the threshing system with multiple rotors at C110ATM combine is presented in Figure 5. (*Ivan Gh., 2014*)

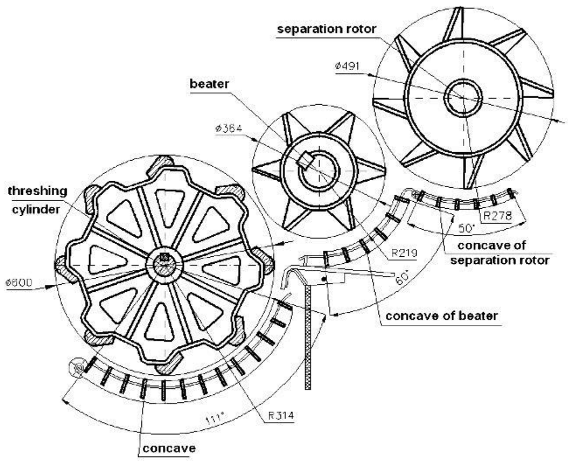

Fig. 6 - Constructive scheme of the threshing system with multiple rotors at C110ATM combine
(*Ivan Gh., 2014*)

Characteristic for ATM is possibility to rotate the last two concaves (hereinafter called separation concaves), their threshing function canceling, the rotor separation just having the role of transporting and directing the straw. The canceling of this function is made if the harvesting exceeds the optimum period, because in this case there is an excessive straw shredded with negative effects on shaking and cleaning processes. (*Prototype tests report for ATM, INMA Bucharest, 2002*)

Technical features of the threshing system with multiple rotors at C110ATM combine harvester are presented in Table 2. (*Prototype tests report for ATM, INMA Bucharest, 2002*)

Table 2

Technical features of the threshing system with multiple rotors at C110ATM combine harvester

Threshing cylinder	diameter [mm]	600
	length [mm]	1080
	number of bars	8
	RPM [rot/min]	460-1200
Concave	number of bars	13
	surface [m^2]	0.67
	winding angle	111°
Beater	diameter [mm]	360
	RPM [rot/min]	760
Separation rotor	diameter [mm]	491
	RPM [rot/min]	920
Beater concave	number of bars	7
	winding angle	60°
	surface [m^2]	0.303
	fixed distance between beater and concave [mm]	25
Separation rotor concave	number of bars	6
	winding angle	50°
	surface [m^2]	0.253
	fixed distance between rotor and concave [mm]	25

The mathematical model of the threshing process made by the threshing system with multiple rotors ATM, which we propose, is based on the mathematical model of Rusanov, considered by researchers Koen Maertens and Josse De Baerdemaeker as the mathematical model which best describes the separation seeds in the tangential threshing system. *(Ivan Gh., 2014)*

Thus, the percentage of seeds separated by the concaves ATM, depending on the length of threshing spaces and the winding angles size of the concaves, is given by relationship 2. (*Ivan Gh. ,2014*)

$$\xi_{sATM}(s)=100\left[1\text{-}e^{-\left(\mu_1 s_1^{\alpha_1}+\mu_2 s_2^{\alpha_2}+\mu_3 s_3^{\alpha_3}\right)}\right] \quad [\%] \qquad (2)$$

where $\xi_{sATM}(s)$ is the percentage of seeds separation in ATM; s_1 – the threshing space length of the concave; s_2 – the threshing space length of the beater concave; s_3 – the threshing space length of the separation rotor concave; α_1 – thewinding angle of the concave; α_2– the winding angle of the beater concave; α_3– the winding angle of the separation rotor concave; μ_1 – the threshing coefficient for seeds separation through concave; μ_2 – the threshing coefficient for seeds separation through beater concave; μ_3 – the threshing coefficient for seeds separation through separation rotor concave.

The threshing space length of ATM concave is calculated with the relationship 3.

$$s_1=\pi R_{c1}\frac{\alpha_1}{180^0} \quad [\text{m}] \qquad (3)$$

where$s_1$is the threshing space length of ATM concave; R_{c1}– radius of the concave; α_1**–** thewinding angle of the concave.

The threshing space length of beater concave is calculated with the relationship 4. (*Ivan Gh., 2014*)

$$s_2=\pi R_{c2}\frac{\alpha_2}{180^0} \quad [\text{m}] \qquad (4)$$

where$s_2$is the threshing space length of beater concave; R_{c2}– radius of the beater concave; α_2**–** thewinding angle of the beater concave.

The threshing space length of separation rotor concave is calculated with the relationship 5. (*Ivan Gh., 2014*)

$$s_3=\pi R_{c3}\frac{\alpha_3}{180^0} \quad [\text{m}] \qquad (5)$$

where$s_3$is the threshing space length of the separation rotor concave; R_{c3}– radius of the separation rotor concave; α_3**–** thewinding angle of separation rotor concave.

The sum consists of the percentage of free seeds remaining in straw and the percentage of seeds no threshing of the bale coming from the threshing cylinder of ATM (the separation concaves are out of the threshing flow) is given by relationship 6. (*Ivan Gh., 2014*)

$$\xi_l(s)+\xi_n(s)=100e^{-\mu_1 s_1^{\alpha_1}} \quad [\%] \qquad (6)$$

where $\xi_l(s)$ is the percentage of free seeds remaining in straw found at the exit from the threshing space located between threshing cylinder and concave; $\xi_n(s)$- the percentage of seeds non threshed at the exit from the threshing space located between threshing cylinder and concave; μ_1 - the threshing coefficient for seeds separation through concave; s_1 - the threshing space length of the concave; α_1- thewinding angle of concave.

The sum consists of the percentage of free seeds remaining in straw and the percentage of seeds non- threshed of the bale coming from all rotors of ATM is given by the relationship 6. (*Ivan Gh., 2014*)

$$\xi_{lATM}(s)+\xi_{nATM}(s)=100e^{-\left(\mu_1 s_1^{\alpha_1}+\mu_2 s_2^{\alpha_2}+\mu_3 s_3^{\alpha_3}\right)} \quad [\%] \qquad (7)$$

where $\xi_{lATM}(s)$is the percentage of free seeds remaining in straw found at the exit from ATM; $\xi_{nATM}(s)$- the percentage of non- threshed seeds at the exit from ATM; μ_1 - the threshing coefficient for seeds separation through concave; μ_2 - the threshing coefficient for seeds separation through beater concave; μ_3 - the threshing coefficient for seeds separation through separation rotor concave; s_1 - the threshing space length of concave; s_2 - the threshing space length of beater concave; s_3 - the threshing space length of separation rotor concave; α_1- thewinding angle of concave; α_2- thewinding angle of beater concave; α_3- thewinding angle of separation rotor concave.

The relations 6 and 7 represent the losses related to threshing processes made by ATM, to which the separation concaves were taken out of the flow of material (similarly the threshing system of conventional combine C110) and ATM at which the separation concaves were introduce in the threshing flow.

The report of the relations 7 and 6 represents the loss report of the two types of the threshing systems (of the combines C110ATM and C110), according to the relationship 8. *(Ivan Gh., 2014)*

$$\frac{\xi_{lATM}(s)+\xi_{nATM}(s)}{\xi_l(s)+\xi_n(s)}=e^{-\left(\mu_2 s_2^{\alpha_2}+\mu_3 s_3^{\alpha_3}\right)} \tag{8}$$

The losses report of the two types of threshing systems equals with the report of total losses to straw walkers of combine C110ATM.

The separation concaves, having the same configuration, μ_1 and μ_2 threshing coefficients can be considered equal and having μ_{ATM} value, resulting in the relationship 9. (*Ivan Gh., 2014*)

$$\frac{\xi_{lATM}(s)+\xi_{nATM}(s)}{\xi_l(s)+\xi_n(s)}=e^{-\mu_{ATM}\left(s_2^{\alpha_2}+s_3^{\alpha_3}\right)}=k \tag{9}$$

Where μ_{ATM} is the threshing coefficient of the separation concaves of ATM; k – the losses report value of the two types of threshing systems.

Knowing the losses report value of the two threshing systems types, it results the threshing coefficient value μATM of the separation concaves of ATM, according to the relationship 10. (*Ivan Gh., 2014*)

$$\mu_{ATM}=-\frac{\ln k}{s_2^{\alpha_2}+s_3^{\alpha}} \tag{10}$$

where $\mu_{ATM}$is the threshing coefficient of the separation concaves of ATM; k – the losses report value of the two types of threshing systems; s_2 - the threshing space length of beater concave; s_3 - the threshing space length of separation rotor concave; α_2- thewinding angle of beater concave; α_3- thewinding angle of separation rotor concave.

The intensification value of the threshing process made by the ATM threshing system with multiple rotors reported to the threshing process made by the threshing system of the conventional combine C110, is given by relationship 11. *(Ivan Gh., 2014)*

$$I_{ATM}=100\frac{\xi_l(s)+\xi_n(s)}{\xi_{lATM}(s)+\xi_{nATM}(s)}\ [\%] \tag{11}$$

where I_{ATM} is intensification of threshing process made by the threshing system with multiple rotors ATM, reported to the threshing process of the conventional combine C110; $\xi_l(s)$- the percentage of free seeds remaining in straw at the exit from the threshing system of C110 combine; $\xi_n(s)$- the percentage of non-threshed seeds at the exit from the threshing system of C110 combine; $\xi_{lATM}(s)$- the percentage of free seeds remaining in straw at the exit from ATM; $\xi_{nATM}(s)$- the percentage of non-threshed seeds at the exit from ATM.

RESULTS

The laboratory tests of the C110ATM combine harvester were conducted in June 2001 by DITRMA-INMA Bucharest Laboratory and field tests were conducted in July 2001 in Dor Mărunt locality, Calăraşi County. (*Prototype tests report for ATM, INMA Bucharest, 2002*)

In Table 3 are presented the values of the working regime and working quality indices for the tests with the separation concaves of ATM introduced into the material flow. (*Prototype tests report for ATM, INMA Bucharest, 2002*).

Table 3

The working regime and working quality indices for the tests with the separation concaves of ATM introduced into the vegetal mass flow

No.	Index	M.U.	Value determined	
WORKING REGIME				
1	Working speed	km/h	3,789	6,426
2	Flow rate combine	kg/s	**4,299**	**6,027**
3	Working width	m	4,1	
4	Cutting height	m	0,16	0,17

No.	Index	M.U.	Value determined	
WORKING QUALITY INDEXES				
1	Total losses per hectare at header: - seeds in uncut ears - seeds in cut ears - free seeds on the ground	%	0,2958 0,1472 0,1205 0,0281	0,3735 0,1872 0,1426 0,0437
2	Total losses at threshing machine: - total losses at straw walkers - seeds in non-threshed ears - free seeds in straw - total losses at cleaning system	%	1,2314 **0,0785** 0,0032 0,0753 1,1529	1,3124 **0,0839** 0,0027 0,0812 1,2285
3	Total losses at combine	%	1,5272	1,6859
4	Broken seeds	%	1,64	1,78
5	The purity of the material collected in bunker	%	99,59	99,41

In Table 3 are presented the values of the working regime and working quality indices for the tests with the separation concaves of ATM removed from the material flow. (*Prototype tests report for ATM, INMA Bucharest, 2002*).

Table 4

The working regime and working quality indices for the tests with the separation concaves of ATM removed from the material flow

No.	Index	M.U.	Value determined	
WORKING REGIME				
1	Working speed	km/h	3.747	6.286
2	Flow rate combine	kg/s	**4.186**	**5.988**
3	Working width	m	4.1	
4	Cutting height	m	0.15	0.19
WORKING QUALITY INDEXES				
1	Total losses per hectare at header: - seeds in uncut ears - seeds in cut ears - free seeds on the ground	%	0.3167 0.1272 0.1523 0.0372	0.3683 0.1659 0.1626 0.0398
2	Total losses at threshing machine: - total losses at straw walkers - seeds in no threshing ears - free seeds in straw - total losses at cleaning system	%	1.7594 **0.3501** 0.0663 0.2838 1.4093	2.0556 **0.4292** 0.0807 0.3485 1.6264
3	Total losses at combine	%	2.0761	2.4239
4	Broken seeds	%	1.69	1.73
5	The purity of the material collected in bunker	%	99.72	99.45

By entering the relationship 10 the test report data for the combine C110ATM for the total loss obtained at the straw walkers for the two positions of the separation concaves (similar to the two threshing system of C110 and C110ATM combines). the threshing coefficient values μ_{ATM} of the separation concaves and the intensification of threshing process I_{ATM} of ATM. are calculated according to Table 5.

Table 5

The threshing coefficient values of the separation concaves and the intensification of threshing process of ATM

(*Ivan Gh. .2014.Test results for approval of C110 self-propelled combine harvester cereal. INMA Bucharest. 1990*)

No.	Index	M.U.	Value determined			
			C110	**C110ATM**	**C110**	**C110ATM**
WORKING REGIM						
1	Flow rate of combine	kg/s	4.2*****		6.0*****	
2	Total losses at straw walkers	%	0.3501	0.0785	0.4292	0.0839
WORKING QUALITY INDICES						
1	Threshing coefficient μ_{ATM}	-	2.963		3.235	
2	Intensification of threshing process I_{ATM}	%	51.15		44.60	

***** The flow rate combines have been rounded to the first decimal

Analyzing the values presented in Table 5 it has resulted:

- The threshing coefficient. specific to ATM. has a variable value. increasing along with the flow rate value;

- ATM intensifies considerably the threshing process. the intensification value being variable. and decreasing according to the flow rate value;
- The small values of total losses of C110ATM combine harvester. it would require to test the combine at bigger flow rates .

CONCLUSIONS

1. The threshing systems with multiple rotors have the separation surface bigger by 65-75%. related to the separating surface of the tangential threshing system. which would allow the decreasing of straw walkers length;
2. The threshing systems with multiple rotors produces an intensification of the threshing process related to the tangential threshing system. but this does not mean that the flow rate must increase with equal percentage value. This explains why the flow rate of a combine with threshing system with multiple rotors is bigger only by 14-20% referring to the flow rate of a conventional combine harvester. (*Miu P.1995*)
3. The increase of threshing space length at the threshing system with multiple rotors has led to shredding the straw. being necessary changes of the straw walkers and the cleaning system. It also increases the specific energy consumption;
4. Combines with threshing system with multiple rotors are less universal. these being effective only for certain crops. the crops with large seeds (maize) or the crops with seeds more sensitive when harvesting with cereal combine harvester (sunflower. soybeans. beans . peas etc.). which can not be harvested with these combines;
5. The combines with threshing systems with multiple rotors are more complex. more expensive. harder to maintain and more susceptible to clog in case of crops with weeds and with high humidity;
6. The combines with threshing systems with multiple rotors are recommended for the cereals harvesting provided that the investment and modifications to the conventional combines be relatively low.

REFERENCES

[1] Ivan Gh. (2014), The threshing systems of combines harvester cereals. Terra Nostra Publisher. Iaşi;

[2] Ivan Gh.. Vlăduț V., (2014), Kinematic study of threshing process conducted by the tangential threshing system of conventional combine of cereal harvesting. *ISB-INMATEH 2014 Proceedings - International Symposium*; pp.65-74, Bucharest/Romania;

[3] Ivan Gh., Vlăduț V., (2015), Improving threshing system feeding with vegetal mass to conventional combine of cereal harvesting. *International Symposium XLIII,* pp.431,-440, Opatija/Croatia;

[4] Maertens K., De Baerdemaeker J., (2003), Flow rate based on prediction of threshing process in combine harvesters. *American Society of Agricultural Engineers,* Volume 19, pp.383–388, USA;

[5] Miu P., (1995), Modellingof the threshing process in cereal combine harvesters. *PhD.thesis,* University Politehnica of Bucharest;

[6] Rusanov A.I., (1974), Constructia triernih priborov razlicinih diametrov (Construction of the threshing systems with various diameters), *Magazine mechanization and electrification of agriculture,* No.6, Moscow/Rusia;

[7] Scripnic V., Babiciu P., (1979), Agricultural machines. Ceres Publisher House, pp.296-304 Bucharest/Romania;

[8] Segărceanu M., (1981), *Studies and researches on improving the quality parameters and computer modelling of the work process of the threshing system at combine harvesters cereal*, Polytechnic Institute of Bucharest;

[9] Segărceanu M., (1990), Calculation and construction of the agricultural machinery for harvesting. *Course* Polytechnic University of Bucharest;

[10] *** (1990), Test results for approval of C110 self-propelled combine harvester cereal, INMA Bucharest, Romania;

[11] *** (2002), Prototype tests report for ATM, INMA Bucharest, Romania;

[12] *** (1980…2008), CLAAS combine Prospectuses;

[13] *** (1980…2008), LAVERDA combine Prospectuses;

[14] *** (1980…2008), NEW HOLLAND combine Prospectuses.

A BIAS OPTIMIZATION METHOD FOR IMPROVING FARMING TRUCK TRANSMISSION RATIO BASED ON HOPE INTERVAL

/

基于希望区间的农用载货汽车传动比偏置优化方法的研究

Assoc. Professor XieB.[1], Assoc.Researcher Ph.D.Xu S.C.[2], Ph.D. Li P.Y.[3]
[1] Department of Mechanical Engineering, Anhui Vocational and Technical College, Hefei/China;
[2] State Key Laboratory of Automotive Safety and Energy, Tsinghua University, Beijing/China;
[3] Transportation Research Institute, University of Michigan, Ann Arbor/ United States
Tel:+86018949861834; E-mail:xiebaomail@126.com

Keywords: *farming truck; transmission ratio; hope interval; optimal design*

ABSTRACT

Farming truck engine operating conditions are typically far from the optimal economic region. In this study, we selected a 5-ton farming truck as the research subject and built a digital vehicle model by using Advanced Vehicle Simulator (ADVISOR) software. We set the operating condition as CYC-NYTRUCK and used transmission ratio as a variable. The objective function was set up based on the fuel consumption, which corresponded to the transmission ratio. By adopting the optimum method of hope interval, all levels of farming truck transmission ratios can be optimized. Then, we used a different gearbox ratio with a design based on different variables, and calculated fuel consumption. Results showed that the hope interval for the optimum transmission ratio fell within the range of 30% to 40%. Within the hope interval, we reduced the variable and resigned the transmission ratio. After calculation, the corresponding transmission ratio for the least fuel consumption was obtained. Keeping the transmission ratios for the 1st and 5th gears constant, the transmission ratios for the 2nd, 3rd, and 4th gears were adjusted to 4.97, 3.11, and 1.95 respectively. The fuel consumption of the transmission ratio after optimization was reduced by 1.2 L/100 km. Furthermore, the acceleration time within 0 km/h to 80 km/h was less than 0.1 s. Overall, the optimized transmission ratios greatly improved the fuel economy and power performance of the farming truck. The research results could provide reference to parameter optimization and application of the transmission system of the farming truck.

摘要

针对农用载货汽车发动机使用工况远离最佳经济区域的情况，本文以某 5 吨农用载货汽车为例，利用 ADVISOR 软件，构建了数字化的汽车模型，选取 CYC-NYTRUCK 工况，以传动比为变量，根据传动比对应的油耗量建立了目标函数，采用基于希望区间的优化方法对农用载货汽车变速箱的各级传动比进行了优化。结果表明：根据不同的偏置量设计汽车变速箱传动比，计算传动比对应的油耗量，找到了最优传动比的希望区间为偏置量在 30%到 40%之间的区域；在希望区间内，缩小偏置量对传动比重新设计，经计算得到油耗最小值对应的传动比为：保持Ⅰ、Ⅴ档传动比不变，Ⅱ、Ⅲ、Ⅳ档传动比分别调整为 4.97、3.11 和 1.95；优化后传动比工作的耗油量降低了 1.2 L/100km；0-80 km/h 加速时间减少了 0.1s。优化后的传动比明显改善了农用载货汽车的燃油经济性和动力性，研究结果可以为农用载货汽车动力传动系统的参数优化设计和匹配提供参考依据。

INTRODUCTION

The good or bad aspects of the fuel consumption and power performance of farming trucks lie in the performance of the truck engine and the application of the engine and gearbox. During the design and production phases, the one-sided pursuit of fuel consumption or power performance is more common owing to the excessive classification on labour *(Oberpriller et al., 2008)*. However, if the engine and chassis are not seen as a whole in improving the performance of any assembly, this oversight would not help improve overall performance because of improper matching with other assembly *(Lvand Yongchen et al., 2011)*. According to the literature, the current operating conditions of domestic farming trucks are usually far away from the optimal economic region*(Costagliola et al., 2012)*, and the best application within its transmission system is not yet realized. Hence a reasonable design and application to improve a farming truck's transmissionsystem could enhance transportation efficiency and reduce the fuel consumption of these farming trucks. Based on the above, this is a valuable research subject with practical significance.

Currently, there are two research methods used in terms of simulation and optimization on vehicle power transmission system: theoretical research and method research. Theoretical research includes the optimization method as well as the application and design for a power transmission system by integrating test and optimization algorithm, among others. Meanwhile, method research includes the development and application of the transmission system simulation software, the optimization of the design of transmission strategy *(Chih-Hsien et al., 2012)*, and so on. Simulation prediction research on vehicle power performance and fuel economy had been carried out in foreign countries in the earlier 1960s. From these, related simulation programs have been developed, such as GP-SIM program developed by General Motors, the TOFEP program developed by Fort Co., and the CSVFEP program developed by Nissan Co., to name a few *(Xiaomeng and Fuqiang et al., 2012)*. With the development of computer technology and numerical computation method, the relatively mature types of software in this field include AVL-Cruise from Austria, Advanced Vehicle Simulator (ADVISOR) from the USA, etc. *(Xiaohua et al., 2008; Thomasand Talon et al., 2012)*. In China, research on this field only began in the 1980s. The main studies were carried out on subjects, such as mathematical models for vehicle power transmission systems, application of simulation software, simulation research under given operating conditions, vehicle application design under fuzzy comprehensive evaluation theoretical guidance, reliability optimization research carried out by utilizing agent model technology, and so on *(Abdel-Halim, 2013; Zulkefli et al., 2011; Schwickart et al., 2014;Anile, 2013)*.

In terms of the optimization method, a number of feasible methods have been proposed by scholars both here and abroad, including Ratnaweera, who adopted fuzzy theory as guidance for designing a transmission system parameter and solving mathematical model by particle swarm method *(Karra, 2014)*; Lu Xi, who applied the genetic algorithm *(Shamekhi et al., 2014)*, and Zaman et al. *(Zaman et al., 2011; Dunweiet al., 2010)* who employed interval optimization methods in the study of parameter optimization of transmission system.

By analyzing several studies, the research on the simulation and optimization of vehicle power transmission system has, to a certain extent, provided theoretical basis for solving problems in designing transmission parameters and their optimization. However, the abovementioned simulation software designs and the optimization methods developed are all based on a common vehicle; less attention has been given to farming trucks.Many problems in the use of farming truck still exist, especially in terms of fuel economy and power performance. By considering the above problem, and using a 5-ton farming truck, in this article, we proposed a bias transmission ratio optimization method based on the hope interval, through which we optimized the design of each level of transmission ratio of the gearbox. The findings of this research could provide reference in improving the power transmission system of a farming truck and serve as reference in finding the best application between engine and power transmission system.

MATERIAL AND METHOD

Usually, the distribution of transmission ratios for farming trucks is based on a geometric series. However, the number of teeth in the gearbox of a farming truck is a discrete variable. In relation to this, all transmission ratio levels of the gearbox are usually biased with the optimal results, thereby affecting the vehicle power transmission system design *(Osornio et al., 2013)*. In this article, we take a 5-ton farming truck as an example. Similar to what is shown in Figure 1 below, by utilizing ADVISOR, we optimized the design on transmission ratio based on the hope interval optimization method. Our aim is to improve the fuel economy and power performance of the farming truck.

Fig.1 –The 5-ton farming truck used as the test vehicle

Constructing a digital vehicle using ADVISOR

ADVISOR is a vehicle performance simulation software developed by the US National Renewable Energy Laboratory (NREL) in MATLAB and SIMULINK software environments. ADVISOR uses a graphic user interface (GUI) that allows users to conveniently modify vehicle parameters *(Markel et al., 2002)*. A quick analysis of several factors, such as the fuel economy, power performance, and so on, of a traditional car, pure electric vehicle, or hybrid vehicles can be performed by utilizing this software.

Establishment of the engine sub module

The universal characteristic curve of a farming truck shows the fuel consumption under different RPMs and load conditions, which can be expressed as the relation (1):

$$g_e = \sum_{j-0}^{s}\sum_{i=0}^{j} A\left[\frac{1}{2e}\left(j+1\right)\left(j+2\right)-j-1+i\right]M^i n^{j-1} \tag{1}$$

Where g_e is the engine fuel consumption rate, g/kW•h; *M* is engine valid torque, N•m; and *n* represents rotate speed, r/min.

By adopting the method of surface fitting, the parameters could be solved in this model. The established regression model is given by the relation (2):

$$\begin{bmatrix} Z_1 \\ Z_2 \\ \cdots \\ Z_n \end{bmatrix} = \begin{bmatrix} 1 & x_1 & y_1 & x_1^2 & x_1y_1 & y_1^2 & x_1^s & x_1^{s-1}y_1 & \cdots & y_1^s \\ 1 & x_2 & y_2 & x_2^2 & x_2y_2 & y_2^2 & x_2^s & x_2^{s-1}y_2 & \cdots & y_2^s \\ \cdots & \cdots & \cdots & \cdots & \cdots & \cdots & \cdots & \cdots & \cdots & \cdots \\ 1 & x_n & y_n & x_n^2 & x_ny_n & y_n^2 & x_n^s & x_n^{s-1}y_n & \cdots & y_n^s \end{bmatrix} \times \begin{bmatrix} a_0 \\ a_1 \\ \cdots \\ a_{k-1} \end{bmatrix} + \begin{bmatrix} e_1 \\ e_2 \\ \cdots \\ e_n \end{bmatrix} \tag{2}$$

where n is the number of test points, $\{a_0, \ \cdots, \ a_{k-1}\}$ is the coefficient to be determined in the model, $\{e_1, \ \cdots \ e_n\}$ is the random error, and k is the series of polynomial $\left(k=(s+1)(s+2)/2\right)$.

Expressing this in matrix form yields by the relation (3):

$$Z = G \bullet A + E \tag{3}$$

where G is $N \times k$-matrix, Z and E are all $N \times 1$ column vectors, and A is the K order vector.

By using the least squares method, the coefficient vector of regression equation can be calculated, and the regression equation of test data is obtained, which is given by the relation (4):

$$Z = \left(1, \quad x, \quad y, \quad x^2, \quad xy, \quad y^2, \quad x^3, \quad x^2y, \quad xy^2, \quad y^3, \quad \cdots \quad y^n\right)\begin{bmatrix} a_0 \\ a_1 \\ \cdots \\ a_{k-1} \end{bmatrix} \tag{4}$$

By utilizing MATLAB and the function of three-dimension curve plotting, the universal characteristic curve of the farming truck engine is obtained, similar to what is shown in Figure 2 below.

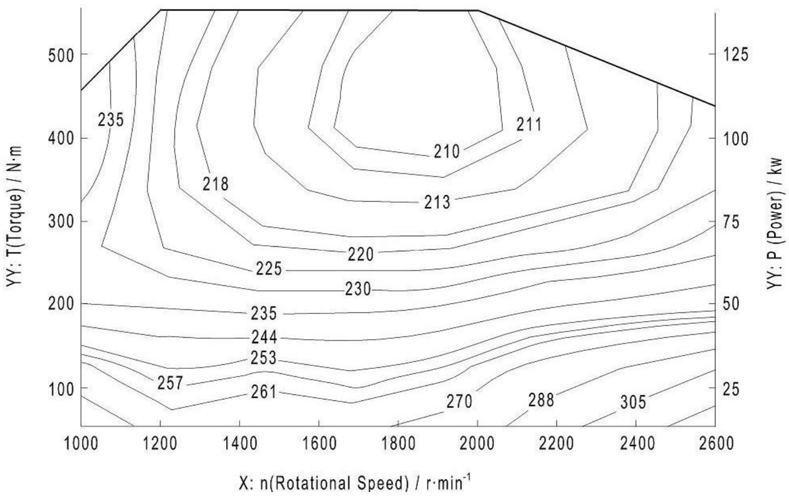

Fig.2 -The universal characteristic of the 5-ton farming truck engine

The program image2map.m in ADVISOR can scan and transfer the universal characteristic curve to the corresponding data file. A new engine model is constructed by scanning the farming truck engine's universal characteristic curve and embedding the data file into the engine database.

Establishment of the transmission system modules

According to the universal characteristic curve of the test vehicle, we can confirm that the transmission ratio of the main reducer is 5.3, the maximum transmission ratio of the gearbox is 6.515, and the minimum transmission ratio of the gearbox is 1.00. We employed a 5-speed gearbox and designed the transmission ratio of each gear according to geometric series. The transmission ratios from the 1st to 5th gears are 6.515, 4.096, 2.56, 1.6, and 1.00, respectively. We digitized the 5-speed gearbox of the farming truck and embedded it into the transmission sub module of ADVISOR. The main instructions are given by:

Gb-ratio=[6.515 4.096 2.56 1.6 1.00]*5.3,

where 5.3 is the transmission ratio of the main reducing gear, and the data in the bracket are the transmission ratios from the 1st to 5th gears, respectively.

Selection of driving cycles

As shown in Figure 3 below, the CYC-NYTRUCK operating condition in ADVISOR is selected to simulate the fuel consumption of the 5-ton farming truck.

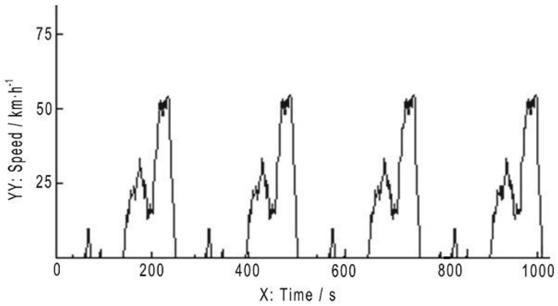

Fig.3 -CYC-NYTRUCK operating condition

Farming trucks usually run in a slow speed; hence, the economic fuel consumption under low speed is required. The condition of the CYC-NYTRUCK has the highest speed of 54.72 km/h and the average speed of 12.16 km/h. In designing the transmission ratios of all the gears for the original gearbox under geometric series, we assume that the probability of use of all gears is equal. However, when the farming truck is driving under CYC-NYTRUCK, it is obvious that the probability of use under the low speed block is higher. In order to adapt to the farming truck that operates under low speed block most of the time, we must reduce low-grade spacing by changing the design of the gear transmission ratios from the original geometric series to the bias geometric series. Here, we take the relation (5) as the applicable design.

$$\frac{i_{gk}}{i_{gk+1}} < \frac{i_{gk+1}}{i_{gk+2}} \tag{5}$$

where i_{gk} ,i_{gk+1}, and i_{gk+2} are the transmission ratios of the three adjacent gears, respectively.

Construction of the optimized objective function

Once the engine model of the farming truck is constructed, we can now utilize ADVISOR to optimize the transmission ratio of each gear in the farming truck gearbox via interval optimization method.

Objective function

For every set of vehicle transmission ratios, we can calculate the fuel consumption under the designated operating condition by using ADVISOR. The aim of optimization is to determine the best fuel economy. Selecting the cycle operating condition in Figure 3 to work out the fuel economy, we arrive at the relation (6):

$$\min\ f(X) = com\_FE \tag{6}$$

where com_FE refers to the fuel consumption calculated under CYC-NYTRUCK operating condition, L/h, where the relation (6) is the objective function.

Optimization variable

The original transmission ratio of the selected farming truck is designed under geometric series, and the resulting transmission ratios from the 1st to 5th gears are i_{g1}=6.515, i_{g2}=4.096, i_{g3}=2.56， i_{g4}=1.60, and i_{g5}=1.00, respectively. In order to ensure that the climbing performance and the maximum speed are unchanged, we use the bias optimization method to obtain the 2nd, 3rd, and 4th gear transmission ratios with the ig5=1.00 and ig1=6.515 unchanged. From this, the optimization variables can be obtained using,, which is given by the relation (7):

$$X = \left[i_2, \quad i_3, \quad i_4\right]^T = \left[x_{i2}, x_{i3}, x_{i4}\right]^T \tag{7}$$

where x_{i2}, x_{i3}, and x_{i4} are the bias amounts, respectively.

Constraint condition

The farming truck transmission system parameters that have been optimized should meet the requirements on fuel economy and power performance. Hence, fuel economy should be the target of optimization and accelerating time (an important evaluation index for vehicle power performance) is taken as the constraint condition, and its constraint function *(Jimin et al., 2012)* is given by the relation (8):

$$t \leqslant 12.2 \tag{8}$$

where t is the accelerating time from 0 km/h to 80 km/h.

RESULTS

Implementation of interval bias optimization method

After analyzing the parameters of farming truck and the application under the CYC-NYTRUCK operating condition, the transmission ratio of the gearbox is offset to the low speed direction, which is beneficial to the fuel economy. Owing to the difficulty of judging the optimized bias variable, the transmission ratio that is originally distributed based on geometric series must be redesigned. We calculated 10 sets of transmission ratios, whose bias amounts are within 5% to 50%; the bias increase amount corresponding to each set of transmission ratio is at 5%. Based on ADVISOR, we could simulate and calculate the fuel consumption corresponding to each set of transmission ratio after the bias is set. The results are shown in Table 1 below.

Table 1

Fuel consumption of the farming truck with the bias of transmission ratio

No.	Fuel Consumption (L/100 km)	Bias	x_{i2}	x_{i3}	x_{i4}
1	54.6	5%	4.217	2.637	1.648
2	54.1	10%	4.338	2.714	1.696
3	54.0	15%	4.459	2.791	1.744
4	54.1	20%	4.58	2.868	1.792
5	54.2	25%	4.701	2.945	1.84
6	54.0	30%	4.822	3.022	1.888
7	53.8	35%	4.943	3.099	1.936
8	53.9	40%	5.064	3.176	1.984
9	54.4	45%	5.185	3.253	2.032
10	54.5	50%	5.306	3.33	2.08

Using the second-order polynomial to fit the results, we achieved the diagram of fuel consumption in relation to bias transmission ratio, as shown in Figure 4 below.

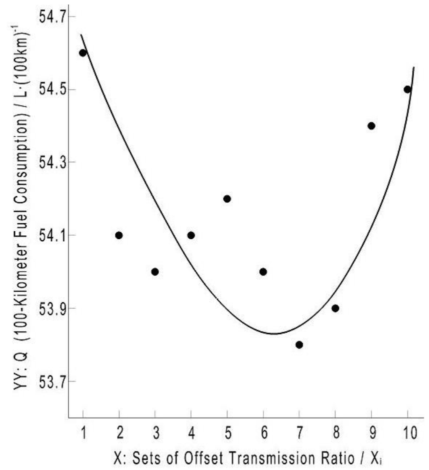

Fig.4 -Fuel consumption fitted by second-order polynomial

By analyzing Table 1 and Figure 4, we conclude that the fuel consumption between set 6 and set 8 has the minimum value, which is between 53.9 L/100 km to 54.0 L/100 km. Then, the bias amount for set 6 transmission ratio is 30%, whereas that for set 8 is 40%. We conclude that the bias amount range of 30% to 40% is a low fuel consumption range. Hence, this interval is the hope interval where we can locate the optimized transmission ratio. Given that the bias amount assigned must be recalculated, we thus calculated 10 sets of transmission ratios whose bias amounts are within 31% to 40%. Here, the bias increase amount corresponding to each set of transmission ratio is at 1%. Based on ADVISOR, we could simulate and calculate the fuel consumption corresponding to each set of transmission ratio after the reset bias. The results are shown in Table 2 below.

Table 2

Fuel consumption calculated under totally biased transmission ratio within the hope interval

No.	Fuel Consumption (L/100 km)	Bias	x_{i2}	x_{i3}	x_{i4}
1	54.0	31%	4.846	3.037	1.898
2	54.0	32%	4.870	3.053	1.907
3	53.95	33%	4.895	3.068	1.917
4	53.8	34%	4.919	3.084	1.926
5	53.75	35%	4.943	3.099	1.936
6	53.75	36%	4.967	3.114	1.946
7	53.7	37%	4.991	3.130	1.955
8	53.75	38%	5.016	3.145	1.965
9	53.75	39%	5.040	3.161	1.974
10	54.1	40%	5.064	3.176	1.948

Using the second-order polynomial to fit the results, we achieved the curve shown in Figure 5 below.

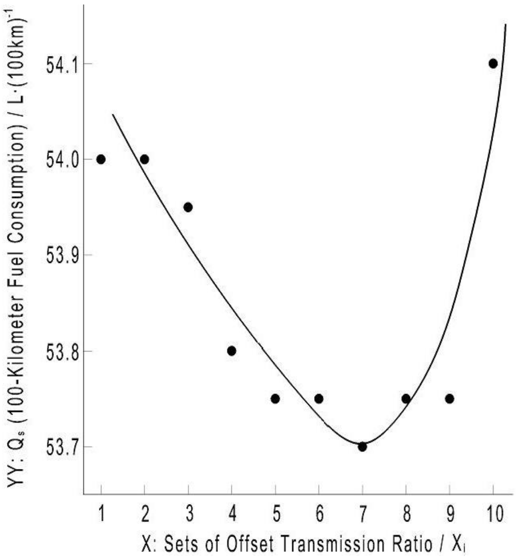

Fig.5 - Fuel Consumption fitted by second-order polynomial in hope interval

By analyzing Table 2 and Figure 5, we conclude that the fuel consumption between set 7 and set 8 is the minimum value, which is between 53.7 L/100 km to 53.75 L/100 km. The bias amount for set 7 transmission ratio is 35%, whereas that for set 8 is 40%. We further conclude that there exists a low fuel consumption range within the bias amount of 35% to 40%. Locating the minimum fuel consumption point in Figure 5, when the bias amount of transmission ratio is 36.5%, the farming truck consumes the minimum fuel. Then, we round-off the number for bias amount. When the bias amount of transmission ratio is at 36%, the transmission ratios calculated for the corresponding 5 gears are i_{g1}=6.515, i_{g2}=4.97, i_{g3}=3.11, i_{g4}=1.95, and i_{g5}=1.00, respectively. These are the transmission ratios of the gearbox at the minimum fuel consumption value.

Analysis of the optimization result

Once the optimal transmission ratios for all gears of the gearbox of the farming truck are obtained, we use ADVISOR to calculate the respective fuel consumption rates and power performances of the test farming truck before and after the optimization. The calculation results are shown in Table 3 below.

Table 3

Comparison of power performance, fuel consumption, and all transmission ratios of the farming truck before and after optimization

Item	Before Optimization	After Optimization	Rate of Change
i_{g1}	6.515	6.515	—
i_{g2}	3.976	4.97	—
i_{g3}	2.284	3.11	—
i_{g4}	1.428	1.95	—
i_{g5}	1.00	1.00	—
Fuel Consumption Qs （L/100 km）	55.1	53.9	-2.18%
0 km/h to 80 km/h Accelerating time (s)	12.2	12.1	-0.82%

By comparing the results shown in Table 3, we can see that there is a large discrepancy between the original scheme and the optimized scheme. After the optimization, the fuel consumption per 100 km is reduced from 55.1 L/100 km to 53.9 L/100 km; the accelerating time within 0 km/h to 80 km/h is also reduced from 12.2 s to 12.1 s. Transmission ratio is thus improved in the optimized scheme compared with the original scheme; furthermore, the fuel economy and power performance are also greatly improved.

CONCLUSIONS

For the reason that farming truck engine operating conditions are far from the optimal economic regions, in this article, we selected a 5-ton farming truck as research subject. We adopted the optimization method based on hope interval. We also performed optimization analysis of all the transmission ratios of the farming truck gearbox. The main conclusions are stated below.

(1) By analyzing the design method of traditional farming truck transmission and its operating conditions, we have concluded that distributing each gear's transmission ratios based on geometric series is unreasonable. We proposed an optimization method of bias transmission ratio based on hope interval and find that this method is reasonable and feasible in actual conditions.

(2) We chose the fuel consumption of farming truck under CYC-NYTRUCK as the objective function. Then, we took the transmission ratios of the 2nd, 3rd, and 4th gears as design variables and considered the accelerating time within 0 km/h to 80 km/h as constraint condition. We optimized the objective function based on ADVISOR. The transmission ratios corresponding to the minimum fuel consumption obtained are as follows: keeping the 1st and 5th gears constant, the transmission ratios of the 2nd, 3rd, and 4th gears are adjusted to 4.97, 3.11, and 1.95, respectively. From the optimization result, we observe the accuracy of the optimized model as well as the feasibility of the proposed optimization method.

(3) By comparing the fuel economy and power performance of the farming truck before and after optimization, we have found that the fuel consumption for 100 km is reduced by 2.18%, and accelerating time from 0 km/h to 80 km/h is reduced by 0.82%. Thus, the optimization method of bias transmission ratio based on hope interval has a significant effect on improving vehicle fuel economy and power performance. This finding can be used as a reference in improving the power transmission system of a farming truck and the reasonable application between the engine and power transmission system.

Combining the requirements on fuel economy and power performance, we studied the optimization of all the transmission ratios of a farming truck gearbox, through which some beneficial conclusions are obtained. Nevertheless, owing to the complexity of a vehicle power transmission system, several issues still need further research, including the simulation of real operating conditions by selecting more accurate mathematical modeling, the comprehensive evaluation of the power transmission system of farming truck with the combination of emission performance, and the establishment of an expert database on vehicle performance simulation, to name a few.

ACKNOWLEDGEMENT

The study was supported by the Excellent Young Talents Fund Key Projects of Colleges and Universities in AnhuiProvince (Grant No. 2013SQRL123ZD), and the Outstanding Young Talent Support Plan Projects of Colleges and Universities in AnhuiProvince (Grant No. 168).

REFERENCES

[1] Abdel-Halim N. A., (2013), Use of vehicle power-train simulation with AMT for fuel economy and performance,*Modern Mechanical Engineering*, Vol.3, Issue 3, Helwan University, pp.127-135, Cairo/ Egypt;

[2] AnileA. M., (2013), Stochastic response surface method and tolerance analysis in microelectronics,*Compel International Journal of Computations & Mathematics in Electrical*, Vol. 22, Issue 22, National Research Council, pp.314-327, Roma/ Italy;

[3] Chih-Hsien Y., Chyuan-Yow T., Chih-Ming C., (2012), Study on power train of two axles four wheel drive electric vehicle, *Energy Procedia*,Issue 14, Elsevier, pp.1528-1535, Pingtung/Taiwan;

[4] Costagliola M. A., Simio L. D., Iannaccone S., et al., (2012), Combustion efficiency and engine out emissions of a s.i. engine fuelled with alcohol/gasoline blends, *Applied Energy*,Vol. 111, Issue 11, Elsevier, pp.1162-1171, Roma/ Italy;

[5] Dunwei G. W., Yong Z., Chengliang Q., (2010), Environmental/economic power dispatch using a hybrid multi-objective optimization algorithm,*International Journal of Electrical Power & Energy Systems*, Vol. 32, Issue 6, Elsevier, pp.607-614, Suchow/ China;

[6] Jimin N., Xiangyang X., Xianyong W., et al., (2012), Research on matching and optimization of a manual transmission coach power train,*Chinese Journal of AutomotiveEngineering*, Vol. 2, Issue 5, pp.341-347, Tongji UniversityShanghai/ China;

[7] KarraP., (2014), Diesel engine performance improvement in a 1-d engine model using particle swarm optimization : nonlinear engineering, *Pigment & Resin Technology*, Vol. 8, Issue 4, pp.257-262, Trine University Angola/ U.S.A;

[8] Lv C., Yongchen L., (2011), Transmission ratio design of zl50 loader based on working condition,*Transactions of the Chinese Society of Agricultural Engineering*,Vol. 27, Issue 2, pp.141-145, Huaiyin Institute of Technology, Huaian/ China;

[9] Markel T., Brooker A., Hendricks T., et al., (2002), Advisor: a systems analysis tool for advanced vehicle modelling, *Journal of Power Sources*, Vol. 110, Issue 2, Elsevier, pp.255-266, Colorado/ U.S.A;

[10] OberprillerB., BurkhardtL., GriesbachB., (2008), Bench-mark 3 continuous press hardening, *Proceedings of the 7th International Conference and Workshop on Numerical Simulation of 3D Sheet Metal Forming Processes*,pp.115-129, Institute of Virtual Manufacturing, Interlaken/ Switzerland;

[11] Osornio C., Villarreal-Calva R.C., Molina-Cristobal A., et al., (2013), Optimization of Power Train and Control Strategy of a Hybrid Electric Vehicle for Maximum Energy Economy,*Advanced Chemical Engineering Research*, Vol. 14, Issue 1, pp.65-80, University of Sheffield, Sheffield/ England;

[12] Schwickart T., Voos H., Hadji-MinaglouJ. R., et al., (2014), Design and simulation of a real-time implementable energy-efficient model-predictive cruise controller for electric vehicles, *Journal of the Franklin Institute*, Vol. 352, Issue 2, pp.603-625, Elsevier, Luxembourg/ Luxembourg;

[13] ShamekhiA. H., Bidgoly A., Noureiny E. N., (2014), Optimization of the gear ratios in automatic transmission systems using an artificial neural network and a genetic algorithm, *Proceedings of the Institution of Mechanical Engineers Part D Journal of Automobile Engineering*, Vol. 228, Issue 11, pp.1338-1343, Toosi University, Tehran/ Iran;

[14] Thomas V., Talon V., (2012), Deployment of system simulation as a support tool for the control development, *Engine & Power train Control Simulation & Modelling*, Vol.45, Issue 30, pp.184-190, LMS International, Lyon/ France;

[15] Xiaohua Z., Qingnian W., Dafeng S., et al., (2008), System design and parameter matching for the new generation of hybrid electric city bus, *SAEInternational Journal of Fuels & Lubricants*, Vol. 1, Issue 1, pp.843-848, Jilin University, Changchun/ China;

[16] Xiaomeng Q., Fuqiang L., (2012), The study on optimal matching of light truck power train, *Applied Mechanics & Materials*, Vol. 271-272, pp.1168-1172 Jiangsu University, Nanjing/ China;

[17] Zaman K., Rangavajhala S., Mcdonald M. P., et al., (2011), A probabilistic approach for representation of interval uncertainty, *Reliability Engineering & System Safety*, Vol. 96, Issue 1, pp.117-130 Elsevier, Dhaka/ Bangladesh;

[18] ZulkefliM. A. M., Jianfeng Z., Zongxuan S., et al., (2011), Hybrid power train optimization with trajectory prediction based on inter-vehicle-communication and vehicle-infrastructure-integration, *European Conference on Antennas and Propagation*, Vol.45, pp.41-63, Elsevier, Minneapolis/ U.S.A.

ELEMENTARY AND COMPLEX SIMULATION OF A RIVER POLLUTION IN ORDER TO RAISE ENVIRONMENTAL TRAINING AND AWARENESS
/
SIMULAREA ELEMENTARĂ ŞI COMPLEXĂ A POLUĂRII UNUI RÂU PENTRU INSTRUIRE ŞI CONŞTIENTIZARE DE MEDIU

Math. Cardei P., Ph.D. Eng. Muraru V., Eng. Sfiru R., Ph.D. Eng. Muraru C., Tech.Ticu T.
INMA Bucharest / Romania
Tel: 0726142837; E-mail: petru_cardei@yahoo.com

Keywords: *simulation, modeling, environmental, awareness, teaching, practice, pollution*

ABSTRACT
This paper shows the role of numerical simulation of physical processes in the environmental awareness and education, emphasizing the right choice of its complexity depending on the level of depth at which should or can be done the exposure. The authors insist on the important role incumbent on incremental simulation (based on mathematical models as simple as possible) in environmental awareness and even in higher education field. The jump to complex simulators can be done only after knowing (which means to know a model and a simulator, that we will try to explain in the paper) the basic models, and the use of complex simulation is effective only within specialist teams including at least 2 -3 or more related fields. These views are supported in the paper with simulators and their use in practical case of pollution of a river simulation.

REZUMAT
Lucrarea prezintă rolul simulatoarelor proceselor fizice in procesul de conștientizare de mediu si in învățământ, accentuând asupra alegerii potrivite a complexității acestuia funcție de nivelul de profunzime la care trebuie sau poate fi făcută expunerea. Autorii insista asupra rolului mai important ce revine simulatoarelor elementare (bazate pe modele matematice cat mai simple), in procesele de conștientizare de mediu si chiar in învățământul superior de profil. Saltul către simulatoarele complexe se poate face numai după cunoașterea (ce înseamnă a cunoaște un model si un simulator, ne vom strădui sa explicam in lucrare) modelelor elementare, iar folosirea eficienta a simulatoarelor complexe este eficienta numai in echipe de lucru care include specialist in cel puțin 2-3 sau mai multe domenii conexe. Aceste opinii se susțin in lucrare cu exemple de simulatoare si utilizarea lor in cazul practic al simulării poluării unui râu.

INTRODUCTION
After *Bailey and Borwein, 2003* or *Merriam Webster, Learner' Dictionary,* the simulation is something that is made to look, feel, or behave like something else especially so that it can be studied or used to train people:

- a computer simulation of spaceflight
- simulations of body movements
- a simulation of the planet's surface
- computer simulation to predict weather conditions.

After *Pimpunchat et al., 2009* or *Oxford Dictionary*simulate means:

- to pretend that you have a particular feeling;
- to create particular conditions that exist in real life using computers, models, etc., usually for study or training purposes;
- to be made to look like something else;

After *Pimpunchat et al., 2009*, the origin of this word is located in time in the mid of 17th century from the Latin word, simulate that means copied or represented, from the verb simulare, from similis "like".

Very interesting are the definitions given by *Cambridge Dictionaries Online, 2015* for the notion of simulation. After *Cambridge Dictionaries Online,2015*, in British for the simulation are usual the next definitions:

- a model of a set of problems or events that can be used to teach someone how to do something, or the process of making such a model;

- in football, the act of pretending to have been fouled to try to win a penalty or free kick unfairly.

In American, the simulation is used after *Cambridge Dictionaries Online, 2015* preferential meaning: a model of a real activity, created for training purposes or to solve a problem.

Also *Cambridge Dictionaries Online,2015* proposes the usual meanings in business simulation:

- a situation or event that seems real but is not real, used especially in order to help people to deal with such situations or events;

In *http://www.webopedia.com/TERM/S/simulation.html*, the simulation suggests imitation: the process of imitating a real phenomenon with a set of mathematical formulas.

In fact, as with many other words, the simulation has several meanings, acquired a vague and relative sense to areas where it is used. It is certainly a feature of modern language, which as you want exactly, becomes inaccurate, the more are increasingly using many words.

Consequently, by *www.meriam-webster.com/dictionary/simulator,*, a device that enables the operator to reproduce or represent under test conditions phenomena likely to occur in actual performance, is called simulator. This device can be a physical (small-scale simulation model, its electronic one - analogue simulation, a computer) or theoretical (theoretical model with analytical solutions available).

A notion that can replace simulation that when this is done theoretically, is numerical experiments. In this case, the simulator is human mind or more generally, thinking, or computer. According to *Bailey and Borwein, 2003*, the numerical experiment is included in what is called the experimental mathematics. By (*Bailey and Borwein, 2003*), experimental mathematics, *(Weisstein, 2016)* is a type of mathematical investigation in which computation is used to investigate mathematical structures and identify their fundamental properties and patterns. As in experimental science, experimental mathematics can be used to make mathematical predictions which can then be verified or falsified based on additional computational experiments.

Borwein and Bailey (2003) use the term "experimental mathematics" to mean the methodology of doing mathematics that includes the use of computation for:

1. Gaining insight and intuition.
2. Discovering new patterns and relationships.
3. Using graphical displays to suggest underlying mathematical principles.
4. Testing and especially falsifying conjectures.
5. Exploring a possible result to see if it is worth formal proof.
6. Suggesting approaches for a formal proof.
7. Replacing lengthy hand derivations with computer-based derivations.
8. Confirming analytically derived results.

Whatever type of simulation and the simulator, it can be used with confidence only after validation. This means that between the physical quantities involved in the process must be examined, at least within certain limits, relations between same characteristic values of the real process. After validation, the simulator can be used to find new relationships, finding optimal working processes, or improvement in order to generalize.

There are many works written in this field in recent years, among which: *(Tyagi et al., 2012)*, *(Benedini and Tsakiris, 2013)*, *(Marusic, 2013)*, *(Nopparat et al., 2006), (Cakaj, 2010), (Shiffman, 2012)*.

I made a long introduction to define as precisely as possible the instruments whose use tries to comment on the work of environmental and pedagogical awareness.. We try to prioritize their work by the complexity of environmental and educational awareness and pedagogical. Below we give a few examples, and then we draw conclusions.

MATERIAL AND METHOD

We examine a particular case, a pollution of a river, but the most elementary possible, but coupled with interaction with oxygen in the river water. This will give greater scope conclusions.

The mathematical model underlying the simulation, consists of a system of two partial differential non-linear equations, though simple, as the number of equations and shape, boundary condition and initial pose difficult problems to solve. List of model parameters is given in Table 1.

Table 1

List of model parameters, notations, units of measurement and simulation values Neajlov River

Model parameters		Values in model
Notation	**Name (units SI)**	
L	polluted length of the river, m	>10000
D_P	pollutant dispersion coefficient on the variable direction x ($m^2 day^{-1}$)	34.56
D_X	dispersion coefficient of dissolved oxygen in the direction of the variable x ($m^2 day^{-1}$)	34.56
v	water speed in the direction of the x, m day^{-1}	21600
A	normal sectional area of the river, m^2	12.5
q	rate added pollutant along the river, kg m day^{-1}	0.06
K_1	coefficient of pollutant degradation rate at 20^o C	8.27
K_2	de-airing the rate coefficient for dissolved oxygen at 20^o C	44.10
k	halfsaturated concentration ratio of oxygen required to decompose the pollutant, kg m^{-3}	0.007
α	mass transfer of oxygen from air to water, $m^2 day^{-1}$	16.5
S	oxygen saturation concentration, kg m^{-3}	0.01

The equations of the mathematical model are:

$$\begin{aligned}\frac{\partial(AP)}{\partial t} &= D_P \frac{\partial^2(AP)}{\partial x^2} - \frac{\partial(vAP)}{\partial x} - K_1 \frac{X}{X+k} AP + qH(x),\ (x < L \le \infty, t > 0)\\ \frac{\partial(AX)}{\partial t} &= D_X \frac{\partial^2(AX)}{\partial x^2} - \frac{\partial(vAX)}{\partial x} - K_2 \frac{X}{X+k} AP + \alpha(S - X),\ (x < L \le \infty, t > 0)\end{aligned} \tag{1}$$

Where:

P is the pollutant, and *X* is the oxygen concentration in the river water, and:

$$H(x) = \begin{cases} 0, x \le 0 \\ 1, x > 0 \end{cases} \tag{2}$$

is Heaviside function.

Equations (1) add initial and boundary conditions that will result for a particular case. Nonlinearities make the system of equations to not be solved analytically on the initial form (system solutions are possible only in numerical form, at least currently). Basic analytical solutions can be obtained in individual cases which although possible, are generally rare in nature. However, these solutions are the first that can validate theoretical model, then opening the door to other analytical and numerical investigations.

Particular solution

According with the authors of *(Pimpunchat et al., 2009)*, is consider only the steady-state solution in the case when dispersion can be take negligible, D_p=0, D_x=0. For this case the system (1) became:

$$\begin{aligned}\frac{d(vAP_s(x))}{dx} &= -K_1 \frac{X_s(x)}{X_s(x)+k} AP_s(x) + q,\ (x > 0)\\ \frac{d(vAX_s(x))}{dx} &= -K_2 \frac{X_s(x)}{X_s(x)+k} AP_s(x) + \alpha(S - X_s(x)),\ (x > 0)\end{aligned} \tag{3}$$

with boundary conditions:

$$P_s(0) = 0, X_s(0) = S \tag{4}$$

In addition, to linearize equations is needed also the hypothesis that the half-saturated oxygen demand concentration for pollutant decay is negligible (k=0). In these circumstances, the solution is obtained:

$$P_s(x)=\frac{q}{K_1A}\left(1-e^{\frac{-K_1x}{v}}\right),\; X_s(x)=S-\frac{K_2q}{K_1}\left(\frac{1}{\alpha}-\frac{1}{\alpha-K_1A}e^{\frac{-K_1x}{v}}\right)-\frac{K_2qA}{\alpha(\alpha-K_1A)}e^{\frac{-\alpha x}{vA}} \tag{5}$$

As a consequence of assumptions, the solution (5) does not depend on time and is valid only for $x>0$ for $x<0$ with: $P_S(x)=0$ and $X_S(x)=S$. Asymptotic behaviour of the solution is given by:

$$\lim_{x\to\infty}P_s(x)=\frac{q}{K_1A},\lim_{x\to\infty}X_s(x)=S-\frac{qK_2}{\alpha K_1} \tag{6}$$

A graphical representation of the solution to facilitate awareness

For application, I have got Neajlov River, Giurgiu County. The spill occurs near the bridge over the Neajlov, the settlement Calugareni. The graphical representation of the solution is given in Fig.1. It was the first level of complexity of the pollutant transport on the river phenomenon simulator.

In *(Pimpunchat et al., 2009*), the authors make another application through analytical results, but with a broader hypothesis, however improbable characteristics of situations in reality. Next we preferred to generalize the result to situations more likely in reality to solve numerically the problem (1) - (4).

We constructed a simulation using Mathcad software facility (can use Matlab, Mathematica, FlexPDE, COMSOL, and many other well-known software programs).

The results of this simulator can be given in Fig.1 or in separate graphical representations.

This is the second level of complexity of the simulator phenomenon of pollutant transport on the river. The third level of complexity begins with complex software programs, specialized, such as WASP, ISIS, FLO-2D and 3D SoilVision, etc. This category of simulators includes, also, those created in programs that made complex simulation for a wide range of physical phenomena *(Cristea et al., 2010)*.

There are approaches earlier in this issue, with results which must be reconsidered *(Bouchard and Duplex, 1994; Shagalova, 1996)*.

In this article we shall merely list them and show the difficulties of use.

RESULTS

A first result obtained using the mathematical model (Eq.1-4) in the simplifying assumptions that allow analytical solution (Eq.5) is given in Figure 1. This result allows an awareness and education of good quality, fast and useful, but not technically accessible than only to university level.

Figure 1 shows overlapping plots of solution component variations over river aerial photograph of the area that aims phenomenon of pollution: pollutant concentrations and dissolved oxygen. On the aerial photo of the area are marked places for distance measurement reference to river axis.Marking labels appear on the horizontal axis of the graphs of variation in pollutant concentrations and dissolved oxygen.The map in Figure 1 can be used for delimitation of the river zone where certain species of animals or plants are in danger of losing their life, to determine the location where remediation might make optimal aeration for delimitation of any prohibited areas access to people and animals.

Map of Figure 1 represents an important public awareness on how the phenomenon takes place, especially around the affected area residents can identify their homes or workplaces.

Using experimental values, presented in table 2, were drawn charts of variation of the average values for the coefficient of static friction and the angle of natural slope for the six grist fractions analyzed, using MS Excel program version 12 (fig. 2).

Values of bulk density, specific surface, porosity and mean diameter of the grist fractions analyzed are presented in table 3.

Based on the data obtained and presented in Table 3, were drawn, as graphic, variations of bulk density, density, specific surface and porosity of grist intermediate products analyzed.

As can be seen from the analysis of data from table 3, and of charts in figure 3, bulk density of fractions resulted at sorting of grist in plansifter compartment C2 has a random variation, it depends such on the type of sieve frame fabric, and the size of apertures of the working sieve, but also on the initial granulation of grist or on shell content adhesive on the semolina particles subjected to grinding.
In Fig. 2-6 simulator results are given, namely pollutant transport phenomenon along a river, in the context of the phenomenon of aeration as a remedy.

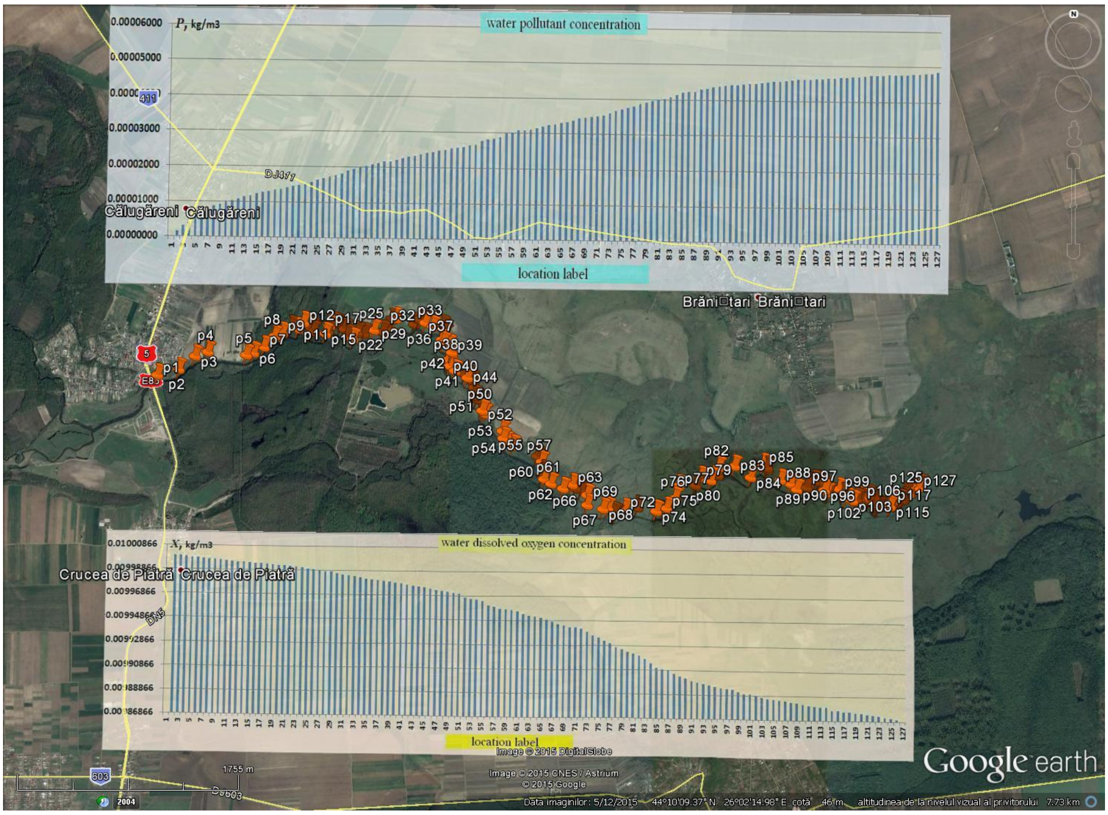

Fig.1 - Variation in pollutant and water dissolved oxygen concentrations along a section of river

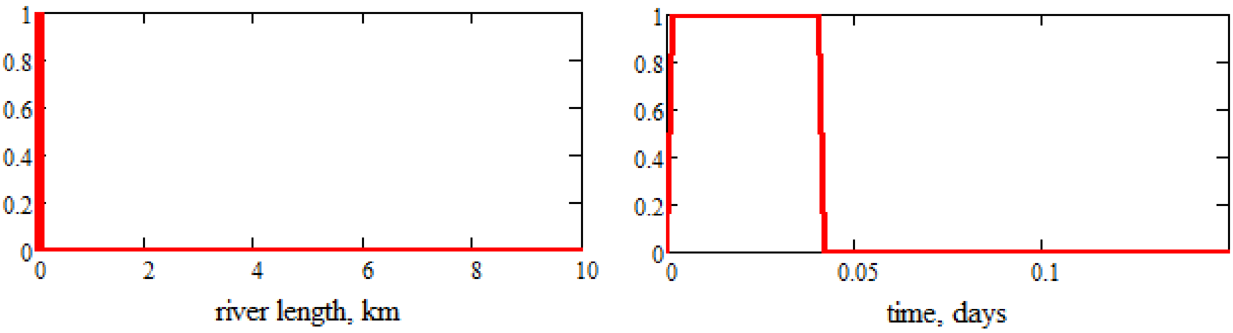

Fig.2 - Space (left) and time (right) history of the time and space factor control (discharge function)

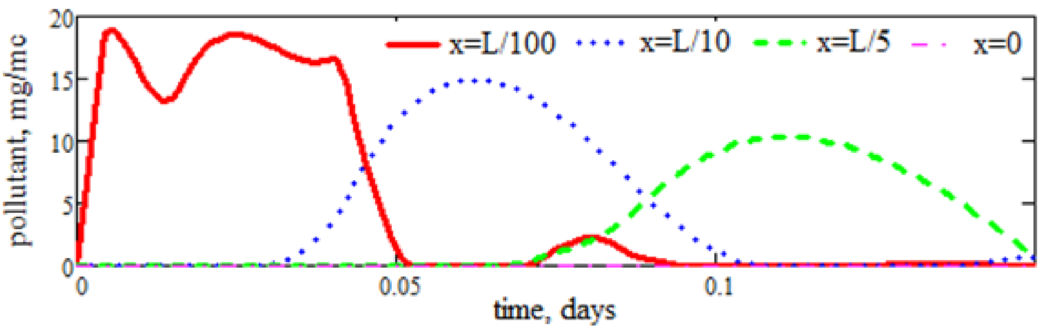

Fig.3 - Time history of the pollutant concentration in four locations along the river

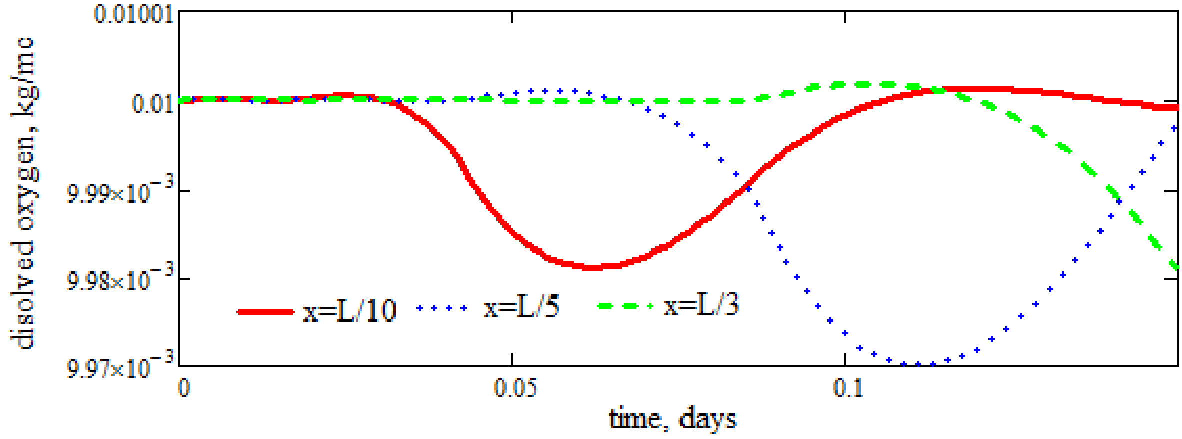

Fig.4 - Time history of the dissolved oxygen concentration in three locations along the river

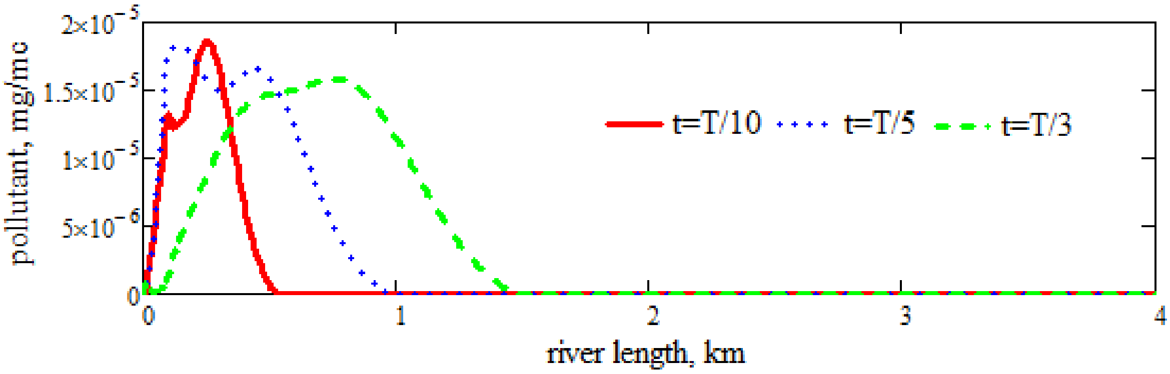

Fig.5 - Variation along the river of the pollutant concentrations at three time points

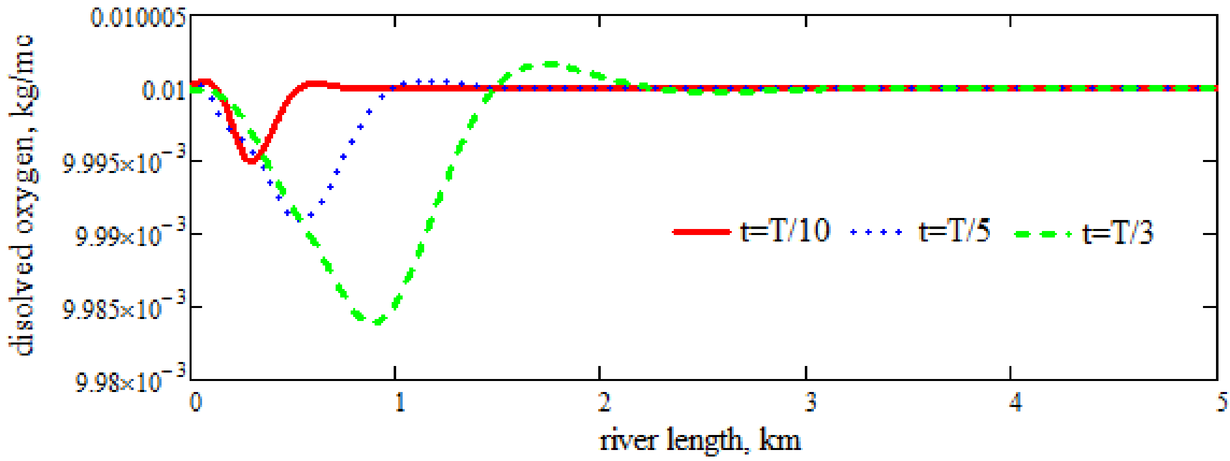

Fig.6 - Variation along the river of the dissolved oxygen concentrations at three time points

The function of discharge shall form a constant multiplied by factors trapezoidal in time and space, factors that delimit the range of temporal and spatial discharge occurs. Temporal and spatial variation of the discharge function are given in fig. 2. Spill (pollutant discharge) occurs on a portion of length 99 m starting from 1 m elevation (center area under the bridge at Calugareni over Neajlov) for one hour at a rate q = 0.06 kg m^{-1} day^{-1}.

History of the pollutant concentration of 3.6 hours in four locations in the river (100 m, 1000 m, 2000 m and 0 m) is given in Fig.3. History of the water dissolved oxygen concentration of 3.6 hours in four locations in the river (100 m, 1000 m, 2000 m and 0 m) is given in Fig.4.

Changes in concentrations of pollutants over the first four kilometers of river measured from the central area under the bridge at three time points, is given in Fig.5. Varying the concentration of dissolved oxygen in the water during the first four kilometers of the river measured from the central area under the bridge at three time points, it is given in Fig.6.

To achieve these results was considered a maximum length of riverbed observable L= 10 km (until the first tributary whose appearance made inoperative model). Model characteristic parameters were fixed at values in Table 1.

Calculation program has run a total of 100 temporal steps and 1500 steps in space.

There are some fine points of the solutions (right solution must be positive and after cancel remain zero until the end if other leaks do not occur) that must meet to obtain the correct solution.

CONCLUSIONS

Several conclusions can be drawn even if a description of the same level computing very complex models cannot be included in this article.

First, it is clear that at the level of awareness or learning, mathematical models and simulators based on them are more useful than the complex software programs which include among other facilities the contaminant transport simulation.

1D mathematical model is simple and easily verified by our intuition about the phenomena of dispersion and propagation of attenuated wave. The results of these models allow the assessment of the time before a dangerous pollutant concentration reaches a certain distance from the spill site. This is the time available for intervention. Some of the results are readily accepted and even obtained an audience that is not technical background. The operation of the simulator is not recommended however, without further instructions. In contrast, students in technical and specialized audience, we recommend using these simulators and the confrontation of the results with the intuition and reality. Doing so can see advantages and disadvantages of these models and simulators. The use of elementary models and simulators facilitates the understanding of the logic of complex programs that solve such problems. Even the simple model presented in this work is not the easiest, because it includes parameters that characterize the flow of water, oxygen and pollutant dispersion and their interaction. Therefore, to ensure the accuracy of results are required qualifications for modeling dispersion and hydraulic phenomena in the transport of substances, and (in the least) in numerical calculation. A basic model of the 1D cannot play a series of important aspects of pollutant concentrations difference between the central area of the riverbed and banks, concave geometric concentration in certain areas (ports, piers, river basins in communication with) etc. Other issues on which model they contain are not exposed to the influence of thermal field, the influence of atmospheric pressure, influence the quality of river fluid (density, viscosity, speed side) interaction with river tributaries, normal variation riverbed section, additional flows from rainfall etc. To account for these phenomena, enter third level of models and simulators, namely complex software programs. These problems coupled fluid flow problem with the transport of substances and energy problem, the problem of heat transfer and biomass and contain empirical relationships between certain parameters of the model. To give a brief idea on how these programs can address demands an example of the WASP program is offered for free.

Inputs include: geometry riverbed, the necessary data integration (start time and end time, minimum step, the method of integration, etc.), system polluted with their main properties, constants parts to the surface and pores data about fluid flow and how it is done downloading pollutant, boundary conditions, Time for loading and border conditions, the output. Therefore the use of this program required knowledge in different domains, consequently a number of specialists in various fields. For this reason it is not recommended to use such simulators in awareness activities and training specialist's formation. These programs are recommended by specialist teams already trained in the necessary fields.

ACKNOWLEDGEMENT

This work has been done within the project “Network and web platform to improve the public awareness on environmental management and protection in the cross - border area Giurgiu - Rousse and adjacent cross - border areas" funded by “Romania – Bulgaria Cross-Border Cooperation Programme 2007 – 2013” *(www.envirobg.eu)*.

REFERENCES

[1] Bailey, D. H. and Borwein, J. M., (2003), *Sample Problems of Experimental Mathematics*, http://crd.lbl.gov/~dhbailey/expmath/expmath-probs.pdf;

[2] Benedini, Marcello, Tsakiris, George, (2013), Water Quality Modeling for Rivers and Streams, Springer;

[3] Bouchard J. P., Duplex J., (1994), Simulation of Pollutant contamination of rivers after an atmospheric release, *Proceedings of the Rostov-on-Don Symposium*, IAHS Publ. no.219;

[4] Busayamas Pimpunchat, Winston L. Sweatman, Graeme C. Wake, Wannapong Triampo, Aroon Parshotam, (2009), A mathematical model for pollution in a river and its remediation by aeration, *Applied Mathematics Letters* 22, pp.304-308;

[5] Cakaj Shkelzen, (2010), Modelling Simulation and Optimization: Focus on Applications, *InTech;*

[6] Cristea V.M., Bagiu E.D., Agachi P.S., (2010), *Simulation and Control of Pollutant Propagation in Somes River Using COMSOL Multiphysisc*, 20th European Symposium on Computer Aided Process Engineering;

[7] Marusic Galina, (2013), A study on the mathematical modelling of water quality in “river-type” aquatic systems, *WSEAS Transactions on Fluid Mechanics*, pp.80-89;

[8] Merriam Webster, Learner' Dictionary, http://www.learnersdictionary.com/definition/simulation;

[9] Oxford Dictionary, http://www.oxforddictionaries.com/definition/learner/simulate;

[10] Pochai Nopparat, Tangmanee Suwon, Miller J.J, (2006), A Mathematical Model of Water Pollution Control Using the Finite Element Method, *PAMM, Proc. Appl. Math. Mech*. 6, pp.755–756;

[11] Shagalova Natalia N., (1996), Accidental pollution simulated system and pollutant trans boundary transport problems for the River Tura, *Proceedings of the Conference held at Anheim*, California, IAHS Publ. no.239;

[12] Shiffman Daniel, (2012), The Nature of Code: Simulating Natural Systems with Processing, *The Nature Code;*

[13] TyagiBabita, Kapoor Ritu, Sinha Deepa, Bhargava D.S., (2012), Mathematical Modelling and Simulation for Predicting DO Condition in Rivers, *International Journal of Environmental Protection*, vol.2, pp. 29-34;

[14] Weisstein Eric W., (2016), Experimental Mathematics, MathWorld ;

[15] *** Cambridge Dictionaries Online, Cambridge Advanced Learner’s Dictionary & Thesaurus © Cambridge University Press (2015);

[16] *** http://www.webopedia.com/TERM/S/simulation.html;

[17] *** www.meriam-webster.com/dictionary/simulator

DETERMINATION OF MOVEMENT STABILITY OF ESPECIALLY LARGE CLASS HYBRID BUS WITH ACTIVE TRAILER
/
ДО ВИЗНАЧЕННЯ СТІЙКОСТІ РУХУ ГІБРИДНОГО АВТОБУСА ОСОБЛИВО ВЕЛИКОГО КЛАСУ З АКТИВНИМ ПРИЧЕПОМ

Prof.Ph.D.Sakhno V.P.[*1)], Prof.Ph.D.Polyakov V.M.[1)], Prof. Ph.D. Murowanyi I.S.[2)], Prof. Ph.D. Stelmashchuk V.V.[2)]
[1)] National Transport University / Ukraine, [2)]Lutsk National Technical University / Ukraine
Phone. +380442804252, fax: +380442804252, e-mail: sakhno@ntu.edu.ua

Keywords: *bus, power, hybrid auto train, stability, critical speed*

ABSTRACT
The paper aims to achieve the normalized maneuverability indicators for buses of especially large class (hinge-jointed) possible by appropriate layout schemes and use of controlled (self-installed) wheels of trailer's section (trailer) which drive can be carried by an electric motor located in the trailing section. Furthermore, the electric motor may be pulling for the bus during movement in urban "traffic jams" when movement speed does not exceed 5 m/s.
In view of the lateral wheel's abduction of SHZA was determined total resistance power for rolling wheels. In addition there was defined electric motor power that is set in the trailing section of the bus, based on the need to perform the following modes of movement as starting out from place, rectilinear bus motion, motion along a circle and turn the wheels of trailer's section to improve the maneuverability of an articulated bus.
Analysis of static stability conditions SHZA at the implementation of tractive force on the axle of the trailer showed that the coefficient of aerodynamic resistance will not affect the value of the critical velocity (not included in the expression of critical speed), and the coefficients of rolling resistance on the first and second axes slightly affect the value of the critical velocity and a critical value of parameter alpha, which determines the amount of tractive effort. However, even under by optimum selected stiffness and selected layout parameters critical speed of the hinge-articulated buses does not exceed 12.5 m/s, those buses requiring special system against assembly.

РЕЗЮМЕ
Досягнення нормованих показників маневреності автобусів особливо великого класу (шарнірно-зчленованих) можливе як за рахунок відповідних компонувальних схем, так і застосуванням керованих (самоустановлювальних) коліс причіпної секції (причепа), привід яких може здійснюватися від електродвигуна, розташованого у причіпній секції. Крім того, цей електродвигун може бути тяговим для автобуса при русі у міських «пробках», коли швидкість руху не перевищує 5 м/с. З урахуванням бічного відведення коліс ШЗА визначена сумарна сила опору коченню коліс. Крім того, визначена потужність електродвигуна, встановленого у причіпній секції автобуса, виходячи з необхідності виконання таких режимів руху як рушання з місця, прямолінійний рух автобуса, рух по колу, а також поворот коліс причіпної секції для поліпшення маневреності зчленованого автобуса.
Аналіз умов статичної стійкості ШЗА при реалізації сили тяги на осі причепа показав, що значення коефіцієнта аеродинамічного опору не впливає на величину критичної швидкості (не входить у вираз критичної швидкості), а значення коефіцієнтів опору кочення на першій і другій осях незначно впливає на величину критичної швидкості і критичне значення параметра alpha, що визначає величину тягового зусилля. При цьому навіть за оптимально обраних жорсткісних і компонувальних параметрів критична швидкість руху шарнірно-зчленованих автобусів не перевищує 12,5 м/с, тобто такі автобуси потребують спеціальної системи проти складання.

INTRODUCTION
Transportation is one of branched industries that provide movement of people. The social importance of transport is reduced to increase efficiency and labor productivity of citizens due to reductions in the transport fatigue of daily trips (productivity drops to 10-15% if the time of trip exceeds 40 minutes, and even more if the waiting time of transport is more than 15 minutes). The development of transport speeds population displacement, improve cultural level and the public mood (*Smorodintseva E.E., 2013*).

Recently, on the streets of cities it has observed a deterioration in passenger traffic, intensive motorization leading to a sharp decrease in the speed of public transport. Public transport, on average, is moving at a speed less than 30 km/h *(Sakhno V.P., 2011).* The reason - traffic jams.

According to the information of International Union of Public Transport, urban public transport requires at the same carrying capacity in 20 times smaller the area of the road network compared with individual cars. Modern bus in 5 times less polluting the atmosphere and requires 3 times less energy costs per one transported passenger compared with individual passenger car *(Balabaeva I., 2008).*

According to recommended (based on national studies) norms the ratio between the number of buses of various classes, which are used in big cities, three-quarters of the entire bus fleet of city with population over 1 million residents should be buses of large and especially large class (45% and 30% respectively). The feasibility of such a ratio is confirmed by foreign practices: at the disposal of Autonomous Management of Paris Public transport (RATP) to 21% of buses especially large class *(Belevtsova N.L., 2014).*

Uncontrolled replacement of buses of large and especially large classes to minibuses resulted in worsening traffic situation in the city streets; bus congestion landing sites; increasing the probability of traffic accidents; increase emissions of toxic substances into the environment.

For any vehicle, including for the bus, the main purpose parameters (indicators of its ability to perform its functions) are dimensions, mass settings, speed and dynamic characteristics of the performed transport work and others. Depending on the service conditions (traffic and transport) to the fore go various settings. For all urban buses, these settings are passenger capacity, rate of passenger exchange, acceleration dynamics, stability, manageability, and for especially large urban, besides maneuverability. In most countries the overall length of single buses is limited to 12 meters, although there are structures up to 15 meters and articulated ones of 18 m. This is explained by the need to meet the requirements of the prescriptions of UNECE №36 and GOST 27 815 - 88, particularly p.p.5.9.1. «... when in motion on the turn on right as on left, bus should be completely placed on the outermost point for body or bumper in circle radius of 12.5 m»; and 5.9.2. «... when in motion on the turn on right as on left, when most protruding body points or bumper describe a circle with a radius of 12.5 m, bus should be placed in a corridor 7.2 m» *(Regulations ISO UN ECE R 36-03:2002)*.

Achieving standardized indicators of buses maneuverability especially large class (hinge-jointed) may be possible by appropriate layout schemes and application managed (bearing) wheels towed section (trailer), which drive can be carried by an electric motor located in the trailing section. Furthermore, this electric motor may be pulling for the bus when driving in urban "traffic jams", when speed is no less than 5 m/s. Therefore, the work's purpose is determination the parameters of sustainability of the bus when the driving element is a trailer section.

MATERIAL AND METHOD

In the article *(Sakhno V.P., 2015)* is proposed to determine the power of electrical motor of hybrid auto train based on the condition to provide movement of road train with a minimum speed in conditions of road train maneuvering and opportunities for movement in urban areas with "creeping" speed.

Road train's maneuvering is connected with its movement along the trajectory of the great curvature. The decisive here is the dimensional road train lane that is defined by its inner and outer dimensional radiuses. These radiuses can be determined or experimentally, or by means of calculations with the help of mathematical model.

In the article *(Sakhno V.P., 2011)* presented a system of equations, describing motion of road train by circle:

$$
\begin{aligned}
&(m+m_1)\dot{U}-[cm_1+m_1d_1)\cos\varphi_1+m_1d_1\times\cos\varphi_1]\ddot{\varphi}_1+(m+m_1)\omega V-m_1d_1\omega_1^2\sin\varphi_1-\\
&=Y_1\cos\theta_1-X_1\sin\theta_1+Y_1^{'}\cos\theta_1^{'}-X_1^{'}\sin\theta_1^{'}+\sum(Y_{1i}+Y_{1i}^{'})+\sum(Y_{2j}+Y_{2j}^{'});\\
&-cm_1\dot{U}+\{I+c^2m_1+cm_1d_1\cos\varphi_1\ddot{\varphi}_1-cm_1\omega V+cm_1d_1\omega_1^2\sin\varphi_1=\\
&=(X_1\sin\theta_1-Y_1\cos\theta_1)(\varepsilon\sin\theta_1+a)+(Y_1^{'}\cos\theta_1^{'}-X_1^{'}\sin\theta_1^{'}(a+\varepsilon\sin\theta_1^{'})+(Y_1\sin\theta_1+X_1\cos\theta_1)\times\\
&\times(H+\varepsilon\cos\theta_1)-(Y_1^{'}\sin\theta_1^{'}+X_1^{'}\cos\theta_1^{'})(H+\varepsilon\cos\theta_1^{'})-c\sum[(Y_{2j}+Y_{2j}^{'})b_{2j}-M_1;\\
&m_1d_1\cos\varphi_1\dot{U}-[I_1+m_1d_1(c\cos\varphi_1+d_1)\dot{\omega}+(I_1+m_1d_1^2)\ddot{\varphi}_1+[V\cos\varphi_1-(U-\omega c)\sin\varphi_1]m_1d_1\\
&=\sum l_1(Y_{2j}+Y_{2j}^{'})+M_1;
\end{aligned}
\tag{1}
$$

In the above described system of equations the following notations were made:

m, m$_1$*, I, I*$_1$ – respectively the mass and moment of inertia of car-tractor and semitrailer;

v, u, ω - longitudinal, lateral and angular speed of the tractor;

a, b,c, d$_1$*, l*$_1$*,* ε - auto train layout parameters;

X_1, $У_1$, $X_1^{/}$, $Y_1^{/}$, $X_{1i}^{/}$, $Y_{1i}^{/}$, X_{2j}, $У_{2j}$, $X_{2j}^{/}$, $Y_{2j}^{/}$ - respectively longitudinal and lateral forces on the wheels of front axle of the tractor, rear axles of tractor and axles of the semitrailer (i=2, j=3);

θ_1, φ_1 – rotation angle of the tractor's steering wheels and assembly of auto train.

Expressions for the longitudinal and lateral velocity of mass center for semitrailer are written in the form:

$$\begin{aligned} v_2 &= v_1\cos\varphi_1 - \left(u_1 - \omega_1\left(b_1 - c_1\right)\right)\sin\varphi_1, \\ u_2 &= v_1\sin\varphi_1 + \left(u_1 - \omega_1\left(b_1 - c_1\right)\right)\cos\varphi_1 - \omega_1 a_2. \end{aligned} \tag{2}$$

Angular velocity of semitrailer will be equal to angular velocity of road tractor:

$$\omega_2 = \omega_1 = const.$$

Considering the fact that abduction angles of trailer's axes do not exceed 10°, tangents of these angles can be considered equal values to angles with an error that does not exceed 1%. Therefore, the expressions for defining angles of abduction are written in the form:

$$\begin{aligned} &\delta_1 = \theta_1 - \frac{u_1 + \omega_1 a_1}{v_1}; \quad \delta_2 = \frac{-u_1 + \omega_1 b_1}{v}; \\ &\delta_3 = \frac{-u_2 + \omega_2 b_3}{v_2}; \quad \delta_4 = \frac{-u_2 + \omega_2 b_4}{v_2}; \quad \delta_5 = \frac{-u_2 + \omega_2 b_5}{v_2}; \end{aligned} \tag{3}$$

After determining the longitudinal and lateral velocity of bus and trailers, section angles abduction follows: δ_1= 0.051 rad., δ_2= 0.048 rad., δ_3= 0.044 rad., δ_4= 0.045 rad., δ_5= 0.045 rad.

Considering the lateral abduction of wheels SHZA, the total power of resistance for bus's wheels rolling is defined as:

$$P_f = \sum G_i \times g \times f_{сум} \,, \tag{4}$$

where $f_{сум}$ - coefficient of rolling resistance caused by the interaction of wheels with a support surface and lateral diverting wheel;

G_i – weight that accounted on the axis of the bus and trailer's section, $\sum G_i$ =28000 kg.

At rolling wheel with abduction, except of radial deformation of tire it also deforms in the lateral direction that increases losses on rolling. The coefficient value of rolling resistance by extraction can be determined by empirical formulas. Formula of Professor V.A. Illarionov is as follows:

$$f_{ув} = f_0 + \frac{k_{ув}\,\delta_{ув}^2}{F_Z} \tag{5}$$

where $f_{ув}$, f_0 – coefficient of rolling resistance wheels with and without taking into account the abduction of wheels, f_0 =0,015;

$\delta_{ув}$ – abduction angle of wheels axes of auto train, rad.;

$k_{ув}$ – resistance coefficient of lateral abduction of wheels axes of auto train,

F_Z – load on the wheel of auto train.

Due to the fact that the angle of auto train lateral axis's abduction is different, like as the resistance coefficient of lateral abduction of wheel's axes of SHZA, then the total coefficient of rolling resistance and rolling resistance force are determined for each individual axis of SHZA. In view of this fact, rolling resistance force of auto train was P_f= 6311 N at an average coefficient of rolling resistance $f_{ув}$=0.023.

The power of electric motor based on the need to perform the following modes of motion was defined.

1) Starting from the point. In this mode, the aim is to overcome rolling resistance of bus's wheels and bus force of inertia that is counted as additional rolling resistance.

Then:

$$P_f = G_{ап} \times g \times f = 28000 \times 9.8 \times 0.03 = 8232 \text{ N},$$

where $G_{ап}$ – gross bus's weight, $G_{ап}$ = 28000 kg;

f – coefficient of rolling resistance at bus starting, *f* = 0.03.

g – acceleration of free falling, *g*=9.8 m/s^2.

The force of bus inertia:

$$P_j = \delta \times G_{an} \times j = 3.5 \times 28000 \times 0.3 = 9800 \text{ N},$$

where

δ – coefficient that takes into account growth of inertia forces translational mass of bus by rotating masses, δ=3.5 Ns^2/m^4 *(Smorodintseva E.E., (2013)*;

j – acceleration at bus start, *j* = 0.1 m/s^2.

Thus, resistance force of movement at bus start will be:

$$P_{on} = P_f + P_j = 18032 \text{ N}$$

The traction force that is possible for implementation on axis of the trailers section:

$$P_{PT} = G_3 \cdot \varphi = 10000 \times 9.8 \times 0.6 = 58860 \text{ N}$$

Since the the traction force that is possible for implementation on wheels of trailers section SHZA, is more than the sum of resistance forces of motion, it will provide it with the starting out from the place.

Power required for bus starting out at speed v = 1 m/s will be:

$$N = \frac{P_{on} \times v}{1000 \times \eta} = 18.98 \text{ kW}$$

where

η - coefficient of transmission efficiency in the transmission of power from electric motor to the driving wheels.

Power required for straight-line motion of bus at speed *v*=1...2 m/s will be:

$$N = \frac{P_f \times v}{1000 \times \eta} = 4.34...8.68 \text{ kW}$$

Power required for auto train's motion around the circle at speeds 1...2 m/s will be:

$$N_p = \frac{P_f \times v}{1000 \times \eta} = 6.64....13.28 \text{ kW}$$

Therefore, required power of electric motor for the bus rectilinear movement at a speed of 1.0....2.0 m/s, generally does not exceed 9 kW, while at starting from the point is - 19 kW. According to motor power 19 kW bus can move along rectilinear area with a maximum speed of 4.4 m/s (16 km/h).

If the electric motor that is located on the trailing section is used for turning the wheels, it is necessary to identify the electric motor power to rotate the steering wheels of the axle.

In the basis of selection and justification of drive management over the wheels of the semitrailer should put reliance of moment resistance turning his steering wheels from constructive and operating factors.

The most complete method of determining the points of resistance at turning the steering wheels of the car-tractor and semitrailer when driving auto train was developed by A.P. Soltusom in his work *(Sakhno V.P., 2015)*. According to this method in the work *(Sakhno V.P., 2015)* was determined resistance turning point of trailer driven axles for its load within 80 kN. For SHZA load on axle of trailer section is typically 100 kN. Therefore, we define the moment of resistance rotation wheels of axis according to the method *(Sakhno V.P., 2015)*. According to this work, force interaction of driven wheels with supporting surface in motion should be considered for three cases:

- rectilinear motion (in practice rectilinear motion of the vehicle, and therefore of controlled wheel carried out by coupling curves of large radius);
- move on a curved trajectory of constant curvature;
- move on a curved trajectory of variable curvature.

Special interest represents motion dynamics of elastic controlled wheel on a curved trajectory of variable curvature, as the first two of them can be viewed (in terms of force interaction of elastic wheel to the supporting surface) as partial cases.

At the motion of controlled elastic wheel on a curved trajectory of variable curvature are affected the force of gravity, inertial and side forces; forces due to uncontrollable car wheels that moving curvilinear trajectory; the resistance movement and rotation about the axis of kingpin. In general, the reaction motion in the tire footprint with the supporting surface is reduced to three resultants, applied at the center of a print, and points in respect of each axis of coordinates. And this is correct in the absence of rotation of controlled wheel and for the axis of kingpin. In the presence of the angular velocity of rotation, pins of driven wheels on axle kingpin have additional resistance turning point, due to the angular velocity of rotation pins.

Due to the structural parameters of controlled bridge, points of the resultant reactions bearing surface that brought to the center of a print tires, are shifted as for the axis of the kingpin.

As the result of this shift, each of resultant creates relatively the axis pivot point. It is obvious that for a turn of managed the wheel concerning kingpin axis, it is necessary to overcome these moments. Consider each of them.

The moment of resistance to rotation of the controlled wheels of the car-tractor and semitrailer at the motion of auto train (with sufficient accuracy for practical calculations) can be represented as such *(Sakhno V.P., 2015)*:

$$\sum M_к(\theta)=\sum M_\omega(\theta)+M_ш(\theta)+\sum M_{Rz}(\theta)+M_{Ry}(\theta)+\sum M_{Rx}(\theta)+M_{TPш}(\theta)+\sum M_{Rду}(\theta)+\sum M_{Rдх}(\theta) \qquad (6)$$

where $\sum M_к(\theta)$ - moment of resistance to rotation of the steering wheels relative to the axis kingpin;
$\sum M_\omega(\theta)$, $M_ш(\theta)$, $\sum M_{Rz}(\theta)$, $M_{Ry}(\theta)$, $\sum M_{Rx}(\theta)$, $M_{TPш}(\theta)$, $M_{R\partial y}\sum M_{R\partial x}$- components of resistance rotation moment, which caused in accordance with angular velocity of rotation pins, stabilizing tire's moment that arises in the result of rolling of steering wheels with abduction; weighted stabilizing factor; moments caused by resultant lateral and longitudinal reactions of supporting surface on the steered wheels, and friction in node.

Calculation of points resistance of rotation of the steering wheels of trailer section performs on condition the mass that falls on its wheels is 9,000 kg.

Weighing stabilizing moment at the combined inclination pivot axis defined by the following dependencies *(Sakhno V.P., 2015)*:

- for left steering wheel:

$$M_{Rz1} = M_{Rz\alpha ш1} + M_{Rz\beta ш1}$$

- for right steering wheel:

$$M_{Rz2} = M_{Rz\alpha ш2} + M_{Rz\beta ш2} \qquad (7)$$

where $M_{Rz\alpha ш1,2}$, $M_{Rz\beta ш1,2}$ - weight stabilizing moments caused in accordance longitudinal and transverse inclination of axis pivot $\alpha_{шо}$, $\beta_ш$.

At the mass on steering axle of trailer's sections 9000 kg, weighting stabilizing point on the left wheel amounted in 776,84 Nm, on the right – 779,58 Nm, when calculating weighting stabilizing moment can be limited to just one wheel and double the result.

The resulting moment due to resultant lateral reactions at combined inclination of kingpin is determined by dependence:

- for left steering wheel:

$$M_{Rx\Sigma 1} = R_x l_ц \sin\varphi[-\cos\varphi\cos\theta_л\sin(\theta_{о1}+\theta_{л1}) - \sin\alpha_{Шо}\cos\beta_Ш\sin\theta_л\sin(\theta_{о1}+\theta_{л1}) + \cos\beta_Ш\sin\theta_л\cos(\theta_{о1}+\theta_{л1}) + R_x r_д \cos\gamma_Ш(\sin\beta_Ш\cos\alpha_{Шо} + \sin\alpha_{Шо}\sin\theta_л); \qquad (8)$$

- for right steering wheel:

$$M_{Rx\Sigma 2} = R_x l_ц \sin\varphi[\cos\alpha_{Шо}\cos\theta_п\sin(\theta_{о1}+\theta_{п2}) - \sin\theta_п\cos\beta_Ш\cos(\theta_{о1}+\theta_{п2})] + R_x r_д \cos\gamma_Ш(\sin\alpha_{Шо}\sin\theta_п - \cos\alpha_{Шо}\sin\beta_Ш\cos\theta_п), \qquad (9)$$

where $\theta_{л,п}$ – rotation angle of left and right steering wheel;

$\theta_{о1}$ – no. of rotation angle of the steering wheels;

$\alpha_ш$, $\beta_ш$ – longitudinal and transverse axis of the angles kingpin

$\alpha_{шо}$, $\beta_{шо}$ $\gamma_{шо}$ – the angles of inclination of kingpin axis and the collapse of the wheels in neutral position;

$\gamma_ш = \gamma_{шо}+\beta_ш(1-\cos\theta_о)$– current angle of collapse.

In contrast to the weighted stabilizing moment, the moment caused by resultant lateral reactions at combined kingpin inclination for left and right wheels significantly differs both in sign and in magnitude. The maximum value of this point is independent of weight that falls on controlled bridge, reaching a peak in the minimum and maximum value of angle between the axis of the kingpin and pins:

- for left steering wheel – 374,1 і 533,5 Nm;

- for right steering wheel – (330,2 i 251,3) Nm,

then, these points should be calculated separately for each wheel.

However, state of this moment in the overall moment of rotation resistance is insignificant and this aspect at engineering calculations can be neglected.

The resulting moment caused by resultant longitudinal reactions at combined inclination of kingpin axis is determined by relationship:

- for left steering wheel:

$$M_{Ry\Sigma1} = R_y l_ц \sin\varphi[-\cos\alpha_{Шо}\sin\theta_п) + \sin\alpha_{Шо}\sin\beta_Ш\cos\theta_п)\sin(\theta_{o1}+\theta_{п1}) - \cos\beta_Ш\cos\theta_п\cos(\theta_{o1}+\theta_{п1})] + R_x r_д \cos\varphi \quad (10)$$

- for right steering wheel:

$$M_{Ry\Sigma2} = R_y l_ц \sin\varphi[\cos\alpha_{Шо}\sin\theta_п+\sin\alpha_{Шо}\sin\beta_Ш\cos\theta_п)\sin(\theta_{o1}+\theta_{п2})+ \cos\beta_Ш\cos\theta_п\cos(\theta_{o1}+\theta_{п2})] + R_y r_д \cos\varphi \quad (11)$$

Where $\varphi=0,5\pi - \alpha_{Шо}-\gamma_{Ш0}$ – angle between the axis of pins and pivot.

By calculation's results, moment of rotation resistance caused by resultant longitudinal reactions from the maximum value of the angle between the axis of kingpin and pin φ=0.292 rad. amounted to 175 Nm, which must be considered when determining the total moment of rotation resistance.

Gyroscopic moment caused by the angular velocity rotation steering wheel around kingpin axis $\omega_ц$ during movement, operates in a plane passing through the axis of the pin and kingpin, causing a redistribution of reaction between the steered wheels of automobiles and is determined by dependence:

$$M_{г1} = I_k \omega_k \omega_ц \sin\varphi \quad (12)$$

where I_k – moment of inertia of the wheel concerning an axis of its rotation,

$\omega к$ – angular velocity of the wheel.

Gyroscopic moment, due to fluctuations in the controlled bridge relatively to the longitudinal axis of the vehicle, which may be caused by irregularities of the supporting surface, kinematics of rotation of the steering wheels in the presence of inclination angles of pins. The value of this moment does not exceed 8 Nm and this moment can be neglected when determining the total moment of rotation's resistance.

The moment caused by the angular velocity of pin's rotation if we consider dependence of the resistance moment of the rotation tires $M\omega$ of the rotation angle Q, than conditionally function $M\omega =f(Q)$ may be divided into three areas *(Soltus A.P., 2006)* :

1. where dependence $M\omega =f(Q)$ is linear;
2. where dependence $M_\omega =f(Q)$ is nonlinear;
3. where $M_\omega =f(Q)$ is limited traction of tires to the supporting surface and does not depend on the angle of rotation Q .

This conditional division of dependence $M_\omega=f(Q)$ in three typical areas can significantly simplify, on the one hand, the research of the physical nature of the phenomena, that take place at the interaction of elastic wheels to the supporting surface, and the other - to get comfortable, for practical calculations, dependence determination of the moment $M\omega$.

The moment caused by the angular velocity of turnover pin, is defined as:

$$M_\omega = \begin{cases} c_\omega \times Q_z, if(Q_z < Q_A) \\ M_{\psi\,max} - (M_{\psi\,max} - c_\omega \times Q_z)\dfrac{(Q_z - Q_A)^2}{(Q_z - Q_B)^2}, if(Q_z < Q_B) \\ M_{\psi\,max}, if(Q_z > Q_B), \end{cases} \quad (13)$$

where $M\psi$ - limited by the clutch of resistance of moment for rotation;

$c\omega$ - angular stiffness of the wheel with tire;

Qz, QA, QB – corresponding angles at which dependency $M\omega =f(Q)$ is linear, nonlinear and limited by tire's clutch to the supporting surface and does not depend on the value angle of rotation *Q.*

Considering the fact that the jointed bus works on the road with solid advanced surface, then the moment caused by the angular velocity of pin's rotation should be determined for the linear dependence $M_\omega=f(Q)$. The value of this moment does not exceed 12 Nm and this moment can be neglected.

Besides the moment of resistance to rotation, caused by work of CCM during movement, while turning vehicle in pins connection, appears a moment of friction.

Calculation of friction moment in pins node $M_{Тш}$ brought in general to determine the reactions that act on each bearings of pins, and then - to the direct calculation for known analytical dependencies.

Thus, the magnitude of friction moment in the sleeve is defined by the formula *(Sakhno V.P., 2015)*:

$$M_{вт} = (2/\pi)\, P_{вт}\, f_c\, d_в \qquad (14)$$

where $P_{вт}$ - the force that act on the sleeve, f_c - coefficient of sliding friction that depends on the material of coupled surfaces of kingpin and bushings, as well as lubricants between them; $d_в$ - diameter of the sleeve.

The friction moment of heel is defined as:

$$M_п = (1/3)\, P_п\, f_c\, [(d^3{}_2 - d^3{}_1)/(d^2{}_2 - d^2{}_1)], \qquad (15)$$

where $P_п$ - the force that acts on the heel; f_c - coefficient of sliding friction in the heel; d_2, d_1- respectively outer and inner diameter of the heel.

In the persistent bearing, friction moment is defined as:

$$M_{под} = P_н\, D\, f_k, \qquad (16)$$

where $P_н$ - the force that acts on the bearing; D - diameter of the circle passing through the centers of the balls; f_k - given friction coefficient of rolling, f_k= 0.001....0.003.

The moment of friction in conical bearings of rolling in general form determined by the dependence:

$$M_{кон} = R^N d_1 [(f_k / d_2) + f_c \sin(\beta/2)] \qquad (17)$$

where R^N - normal to the surface of rolling ball reaction in conical bearing;

d_1 - the average diameter of the track rolling inner ring of bearing;

f_k - friction coefficient of rolling in conical bearing, f_k = 0.001;

d_2 - average diameter of conical surface of roller;

f_c - coefficient of sliding friction in a pair of friction 'roller - guide clamp of inner ring of conical bearing, f_c = 0.03...0.06;

β - the angle between the extreme forming rollers.

For the selected output data moments of friction in the sleeve, the heel, conical rolling bearings and kingpin node $M_{шв1}$ made up:

$M_{вт}$ = 21.66 Nm; $M_п$=13.68 Nm; $M_{кон}$ =22.58 Nm; $M_{шв1}$= 57.92 Nm.

For the control wheel module $M_{Тш}=2M_{Тш1}$=115.84 Nm.

Depending on the angle of rotation of the steering wheels, the angular velocity of pin rotation and speed of bus movement in total moment of resistance rotation of wheels varies from 1957 to 1954 Nm.

The moment of viscous friction in steering control hook section is proportional to angular velocity rotation of wheels *(Sakhno V.P., 2015)*:

$$M_i = h_i \times \dot{\theta}_i, \qquad (18)$$

where h_i - coefficients of viscous friction in the details of steering control, h_i= 15 Nms/rad;

$\dot{\Theta}_i$ — the angular velocity of rotation of steering wheels.

The angular velocity of rotation of steering wheels determined by regime coefficient of rotation $K_п$, was proposed by Ya.H.Zakinym. This coefficient is determined by the dependence:

$$K_n = \frac{\dot{\theta}}{v},$$

where v – the bus speed, m/s.

Regime coefficient of rotation $K_п$ for real mode of the bus rotation is within 0.1 $м^{-1}$ for the velocity of the auto-train v=5 m/s. Then, $\dot{\theta}_i =$0.5 rad./s and M_i=7.5 Nm.

The moment of elasticity in steering control of semitrailer is proportional to angle of rotation of the wheels and stiffness of steering gear *(Sakhno V.P., 2015)*:

$$M_{pi} = \chi_i \times \dot{\theta}_i \qquad (19)$$

where χ_i – stiffness coefficient of the steering gear, χ_i = 170 Nm/rad, M_{pi} = 85 Nm.

Thus, the total resistance moment of rotation for the angular velocity of rotation of steering wheels $\dot{\Theta}_i$ = 0.5 rad./s made up $\sum M_к(\theta)$ =1967 …2050 Nm. Thus the maximum power of the electric motor to rotate steering wheels of axles of semitrailer does not exceed 1.1 kW, e.g. engine with 20 kW will provide as bus movement with "creeping" speed and the turn of wheels of trailers section.

RESULTS

Model SHZA in the implementation of traction effort on the axis of the trailer gets a range of dynamic properties, specific to the system of "inverted" pendulums. First, note the unfavorable tendency for taking SHZA (case of static stability loss).

Determination of SHZA configurations and other settings of steady state after stability loss of rectilinear motion and the conditions of its stability take the second phase of the study of nonlinear dynamic system. In this formulation of the problem in the model must be enter the equation of longitudinal movement, parameter *v* - velocity of longitudinal movement becomes additional variable phase (defined expanded equations and parameter *alpha,* which characterizes the tractive force and *theta0* – rotation of angle of control wheel module (CCM).

Numerical modeling of system will allow to evaluate the impact of controlled parameters on the dynamic qualities SHZA as a system and to determine corresponding steady state and properties of stability.

When implementing of traction effort on the axis of trailers section SHZA in the equation of planar parallel movement is introduced such a system of parameters (active controlled parameters): *alpha*, *theta*0 define the entire set of stationary states of the system: v - velocity of longitudinal movement, $u1$, ω - lateral and angular velocity of the center of mass of the tractor, f – angle of compilation, ω_1 - angular velocity of trailer's links; *X1, X2, X3* - longitudinal force on the first, second and third axes:

$$X1=-kf\,Z1;\; X2=-kf\,Z2-Kas\cdot v^2;\; X3=alpha\cdot Z3 \quad (20)$$

where *kf* – coefficient of rolling resistance of wheels of the bus axis; *Z1, Z2, Z3* – normal reaction of the bearing surface on the wheels of the bus axis; *Kas* – factor of streamlining of the bus; *alpha* – factor that determines what portion of the normal reactions of bearing surface is realized in the form of traction force on the driving wheels of trailers links.

The system of differential equations of motion on the phase variables (*v, u,* ω, θ, Θ, ϕ, Φ) should be supplemented by a new phase variable - speed of longitudinal movement of mass center of the first level.

Abduction angle of wheels of trailer's link in expanded form:

$$\delta_3=-\theta_1-arctan\left(\frac{v\sin\varphi+(u-\omega c)\cos\varphi-(\omega-\dot{\varphi})d_1-(\omega-\varphi)b_1}{v_1}\right);$$

$$v_1=v\cos\varphi-(u-\omega c)\sin\varphi.$$

Characteristic linear dimensions of the first and second level of SHZA:

$$l=a+b-\lambda, \qquad L_1=b_1+d_1$$

Vertical load on the axis of SHZA and lateral forces of abduction of wheels axis (The last defined as monotonic function of the abduction angles):

$$Z_1=m_1g+\frac{mgb-\dfrac{m_2gb_1(c-b)}{L_1}}{l};\quad Z_2=\frac{mga+\dfrac{m_2gb_1(a+c)}{L_1}}{l};\quad Z_3=\frac{m_2gd_1}{L_1};\quad Y_i\,\frac{k_i\delta_i}{\sqrt{1+\dfrac{k_i^2\delta_i^2}{k_i^2Z_i^2}}}.$$

In implementing rectilinear motion speed of SHZA undisturbed movement is defined as the ratio:

$$v=\sqrt{\frac{\alpha\ Z3-kf(Z1+Z2)}{Kas}}, \quad (21)$$

where K_{as} – factor of streamlining of SHZA.

In the case of stable circular regime, value of longitudinal speed of movement of first link is determined by solution of the final equation with other equilibrium phase variables:

$$m\omega u - k_f Z_2 - Kasv^2 - \sin\theta Y_1 - \cos\theta k_f Z_1 + m_1\omega u + m_1 a\omega^2 - m_1\cos\theta\lambda\omega^2 + \alpha\cos\varphi Z_3 +$$
$$+ \sin\varphi Y_3 - m_2\cos\varphi d_1\omega^2 + m_2 u\omega - m_2 c\omega^2 = 0$$
$$m\omega v - k_f Z_1\sin\theta + \cos\theta Y_1 - \sin(\varphi+\theta_1)\alpha Z_3 + +\cos(\varphi+\theta_1)Y_3 - m_1\sin\theta\lambda\omega^2 +$$
$$+ m_2\sin\varphi d_1\omega^2 + Y_2 - m_1\omega v - m_2\omega v = 0;$$
$$cm_2 v\omega - am_1\omega v - a\sin\theta k_f Z_1 + c\sin(\varphi+\theta_1)\alpha Z_3 + a\cos\theta Y_1 - c\cos(\varphi+\theta_1)Y_3 - bY_2 +$$
$$+ kk_1(\theta-\theta_0) + kk_2(\varphi-\varphi_0) - am_1\sin\theta\lambda\omega^2 - cm_2\sin\varphi d_1\omega^2 = 0;$$
$$\lambda(Y_1 - \sin\theta m_1\omega u - \sin\theta m_1 a\omega^2 - \cos\theta m_1\omega v) - kk_1(\theta-\theta_0) = 0;$$
$$-L_1Y_3\cos\theta_1 + L_1\alpha Z_3\sin\theta_1 + d_1\cos\varphi m_2\omega v - d_1\sin\varphi m_2\omega v + cm_2\sin\varphi d_1\omega^2 - kk_2(\varphi-\varphi_0) = 0 \quad (22)$$

(in the system that determines the equilibrium value, the phase velocity (Θ , Φ) is equal to zero).

Rectilinear motion of SHZA corresponds to zero value of parameter *theta*0, at $\theta_0 \to 0$ to trivial decision strive the circular steady state of sufficiently large radius. It enables to apply graph-analytical method for the extension for parameter by moving on branch of equilibrium states.

Below are values of phase variables corresponding to the equilibrium state of the system that can serve as a starting point in the implementation of the method of continuation by parameter (along with trivial mode).

Integrating the system of equations (22) carried on the same data source typical for SHZA.

The values of the phase variables that correspond to stationary states of SHZA and sets the corresponding values to it: theta0=0.1; X3=0.1Z3.

{u = -.1454343890e-1, v = 5.629191511, omega = .1451613858, phi = .1958011278, theta = .1019656310};

eigenvalues of matrix coefficients of equations (22) indicate that the circular stationary regime is stable.

$$eigv := -6.986921098, -3.969798706 - .5108965081\,I, -3.969798706 + .5108965081\,I,$$
$$-1.057375428, -.9785077698 - 13.90994274\,I, -.9785077698 + 13.90994274\,I,$$
$$-.3554712212\text{e-}1$$

With an increase of traction effort in two times we have the next stationary mode:

theta0=0.1; X3=0.2 Z3;

{omega =.3597611916, phi = .4113165810, theta = .1054213101, u = -.8090095905, v = 7.435758605};

eigenvalues of matrix coefficients of equations (22) indicate that the circular stationary regime is stable.

$$eigv := -5.373724168, -2.185804771 - 1.873731709\,I, -2.185804771 + 1.873731709\,I,$$
$$-1.052815285 - 13.90091946\,I, -1.052815285 + 13.90091946\,I,$$
$$-.9928401012\text{e-}1 - .4632056434\,I, -.9928401012\text{e-}1 + .4632056434\,I$$

At further increase of traction force, circular stationary regime loses stability:

theta0=0.1 ; X3=0.3 Z3;

{phi =.6220454182, u = -1.136704740, omega =.4735732903, v = 6.455904321, theta = .1024505047};

eigenvalues of matrix coefficients of equations (22).

$$eigv := -6.146575049, -2.136688971 - 1.662291704\,I, -2.136688971 + 1.662291704\,I,$$
$$-1.009804871 - 13.87431469\,I, -1.009804871 + 13.87431469\,I,$$
$$.1033177514 - .5562877329\,I, .1033177514 + .5562877329\,I.$$

A set of eigenvalues indicates flatten instability corresponding to steady state, the system allowing the existence of another one more not stable circular mode, for which along with flatten instability takes place divergent imbalance:

{u =4.774121575, phi=-.5680849951, omega=2.469381759, theta=.6912609845e-1, v = .1568547332};

$$eigv := -2.441157656 - 2.744480930\,I, -2.441157656 + 2.744480930\,I,$$
$$-1.226538298 - 14.66281452\,I, -1.226538298 + 14.66281452\,I,$$
$$.2033799634 - 3.715976489\,I, .2033799634 + 3.715976489\,I, .2456426373$$

.

In Fig.1, Fig.2 are shown the trajectory of the center of mass of the tractor SHZA in the plane of the road, phase trajectory angle of drafting and angle of rotation of CCM at different values of traction force that developing on the axis of the trailer.

Analysis of Fig.1, Fig.2 shows a loss of stability of circular stationary modes implemented at parameter values 0.5<*alpha*<0.75, and loss of stability of rectilinear motion at *alpha* = 0.245. The critical speed in this case is v_{kp}= 12.38 m/s.

Critical speed of steady circular motion essentially depends on the values of parameter *theta0.* Loss of stability occurs with the emergence of multiple equilibrium (due to a bifurcation or merge of birthed multiple stationary modes). According to the results of applied catastrophe's theory many critical in some small neighborhood of rectilinear motion should be implemented in the form of semi cubic parabola.

Analysis of cumbersome conditions of static stability of SHZA at the implementation traction force on the axle of the trailer showed that value of coefficient of aerodynamic resistance will not affect the value of the critical velocity (not included in the expression of critical speed), and the coefficients values of resistance movement in the first and second axes slightly affect the value of critical speed and critical parameter *alpha*, which determines the amount of traction.

Analysis of Fig. 3 shows the significant dependence of the critical speed of SHZA movement of the coefficient value, which shows what part of vertical load on the axle of the trailer is realized in the form of traction.

In accordance with the accepted assumptions in this paper, each value of parameter *alpha* > *alpha** corresponds to a certain value of sustainable longitudinal speed of movement $v=\sqrt{\dfrac{\alpha\ Z3-kf(Z1+Z2)}{Kas}}$.

Thus, the point of intersection of two dependencies (received before and this) determines the value of critical velocity and critical of parameter *alpha*, Fig.3 (c).

Analysis of the relationship, Fig.3 (c) shows that even for optimum selected stiffness and layout parameters critical speed of SHZA is not more than 12.5 m/s, thus, such buses require special system versus compilation; however at movement with speed lower than values of critical speed of movement, SHZA stability is provided without additional versus compilation measures.

theta0=0.1 ; X3=0.75 Z3

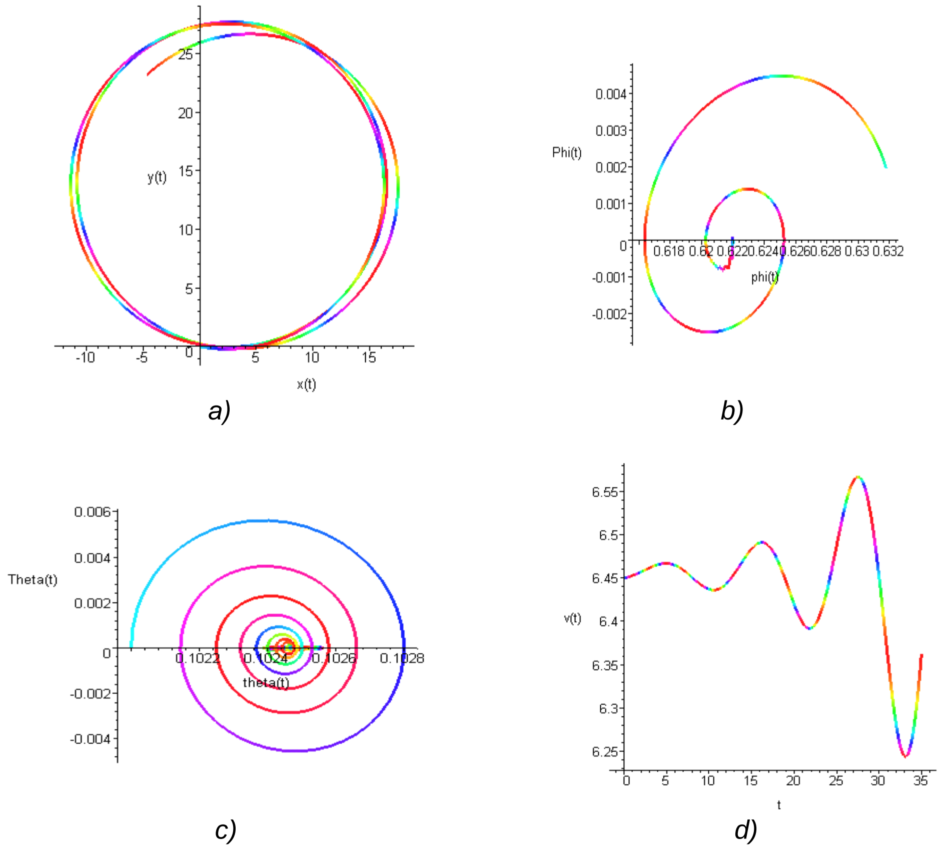

Fig.1 - Parameters of SHZA's stationary movement at the value of pushing force *X3=0.75Z3*

theta0=0.1 ; X3=0.2 Z3

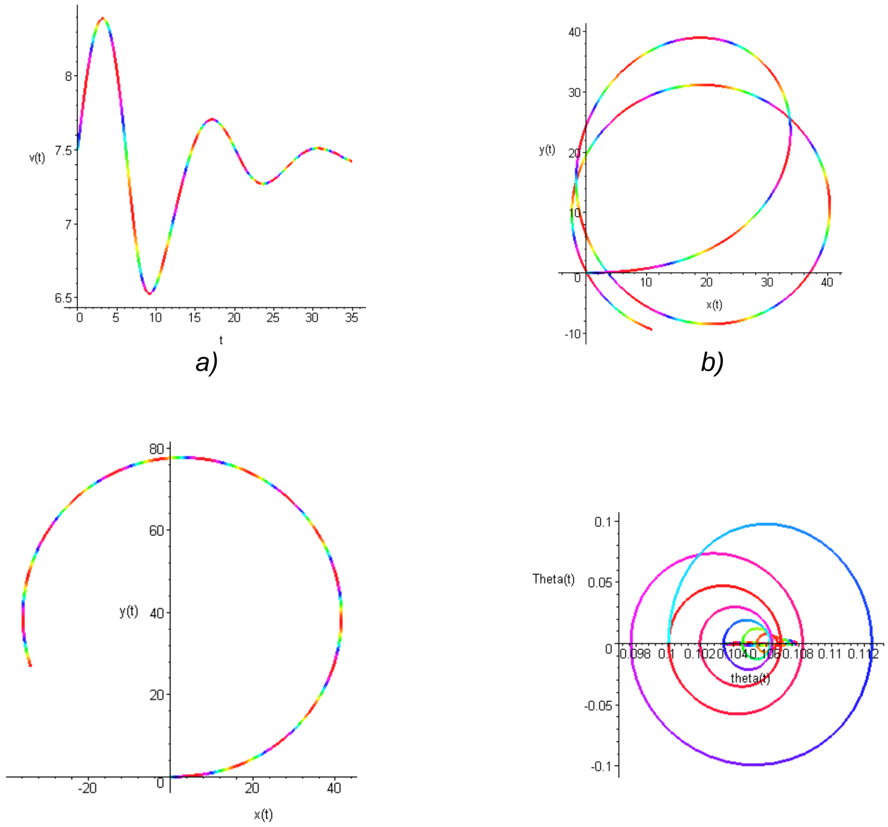

a) *b)*

c) *d)*

Fig.2 - Parameters of SHZA's stationary movement at the value of pushing force X3=0.2Z3

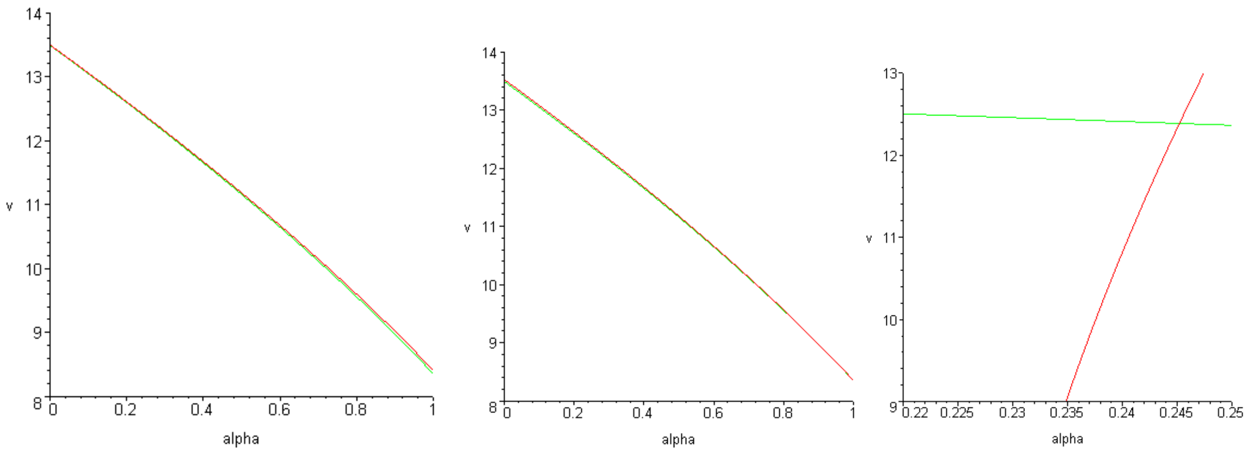

(*kk1*=4000 N/rad) (*a*) (*b*) (*c*)

Fig. 3 - Critical velocity of SHZA: the stiffness coefficient of control wheeled module of trailers section:
*kk*1=4000 N/rad *(a)*, the value of traction effort on the axis of trailers link at *kf* =0.025 (*b*), parameter alpha (*c*)

CONCLUSIONS

In the article is determined the necessary power of electrical motor that was established on trailing section of the bus, taking into account the pick-up from the place, rectilinear motion and circular motion. In the work is shown that at power of electrical motor of 19 kW, bus can move at maximum speed of 4.4 m/s, which is less than the critical speed, therefore stability of the bus movement in this case, will be provided. However, even under optimum selected parameters of stiffness and layout, critical movement speed of the hinge-articulated buses in the implementation of traction on the axle of trailer's section does not exceed 12.5 m/s, that is why such buses require special system of versus compilation.

REFERENCES

[1] Balabaeva I., (2008), Prospects for the development of passenger transportation in megapolis (Перспективы развития пассажирских перевозок в мегаполисе), *Automobile transport (Автомобильный транспорт),* Vol.4, pp.28–29, Ukraine;

[2] Belevtsova N.L., Verbitsky V.G., Efimenko A.M., (2014), Stability analysis of high-speed specialized car on cylindrical rubberized wheels (Аналіз стійкості швидкісного спеціалізованого вагона на циліндричних прогумованих колесах), *Bulletin of HNADU (Вісник ХНАДУ),* Vol. 67, pp.19–24, Charkiv/Ukraine;

[3] Common technical prescriptions concerning formal approval of passenger transport vehicles of large capacity in relation to the overall design (Єдині технічні приписи щодо офіційного затвердження пасажирських транспортних засобів великої місткості стосовно загальної конструкції), Regulations UN ECE №36-03: 1993, IDT, ISO UN ECE R 36-03:2002, Kyiv/Ukraine;

[4] Sakhno V.P., Polyakov V.M., Timkov O.M., Lysenko O.O. (2015), The scientific basis for the creation of hybrid auto trains with improved power characteristics, maneuverability, agility and resistance movement (Наукові основи створення гібридних автопоїздів з покращеними енергетичними характеристиками, прохідністю, маневреністю і стійкістю руху), *Proceedings of the 8 International Scientific conference "Modern technologies and prospects of development of road transport",* pp.219-220, Vinnytsia/Ukraine.

[5] Sakhno V.P., Kuznetsov R.M., Marchuk R.M., Onischuk V.P., (2011) Determination of sustainability indicators of the auto-train-container in rectilinear motion (До визначення показників стійкості автопоїзда-контейнеровоза у прямолінійному русі), *Bulletin SevNT, Series Machine instrument engineering and transport (Вісник СевНТУ. Збірник наукових праць. Серія Машиноприладобудування та транспорт)*, Vol. 121/2011, pp.3-6, Sevastopol/Ukraine;

[6] Sahno V.P., Kostenko A.P., Zahorodnov M.I., (2014), *Dynamics and fuel efficiency of vehicles (Динамічність та паливна економічність автотранспортних засобів)*, p.444, Donetsk/Ukraine;

[7] Sahno V.P., Polyakov V.M., Timkov O.M., Sharay S.M., Lysenko O.O., (2015), The creation of hybrid auto trains with improved power characteristics, performance, maneuverability and resistance movement (До створення гібридних автопоїздів з покращеними енергетичними характеристиками, прохідністю, маневреністю і стійкістю руху), Modern Technologies engineering and transport (Сучасні технології в машинобудуванні та транспорті), *Scientific Journal of Lutsk* National Technical University, Vol.2 (4), pp.128-134, Lutsk/Ukraine;

[8] Sahno V.P., Polyakov V.M., Kostenko A.P., (2015), Operational properties of vehicles (Експлуатаційні властивості автотранспортних засобів), p.400, Donetsk/Ukraine;

[9] Soltus A.P., (2006), *The theory of operation of the car properties (Теория эксплуатационных свойств автомобиля),* p.188, Ukraine;

[10] Smorodintseva E.E., (2013), Integrated transport system: a series of lectures (Единая транспортная система: курс лекций), *USURT*, p.207, Ekaterinburg/Russia.

OPTIMIZATION OF ENERGY CONSUMPTION BY MIXING LIQUIDS USED IN THE FOOD INDUSTRY
/
OPTIMIZAREA CONSUMULUI ENERGETIC LA MALAXAREA UNOR LICHIDE UTILIZATE IN INDUSTRIA ALIMENTARĂ

Prof. PhD. Eng. Csatlos C.
TransilvaniaUniversity of Brasov, Facultyof Food and Tourism/Romania;
Tel: 0745766336; E-mail: csk@unitbv.ro

Keywords: *mixing liquids, food industry, homogenization, isotropic turbulence, non-isotropic turbulence*

ABSTRACT
The paper-work presents a series of theoretical and practical aspects connected to the method of approaching the energetic study of mechanical blenders with applications in food industry. The mathematical shaping and the development of studied cases were accomplished for Newtonian food liquids. The presented method can be applied for the projection and for the accomplishment of blenders for Newtonian liquids in food industry, with or without the observance of similitude conditions.

REZUMAT
Lucrarea prezinta o serie de aspect teoretice si practice legate de metoda de abordare a studiului energetic al malaxoarelor mecanice cu aplicare in industria alimentara. Punerea sub forma matematica si dezvoltarea cazurilor studiate a fost facuta pentru lichidele alimentare Newtoniene. Aceasta metoda poate fi aplicata pentru proiectarea si realizarea de malaxoare pentru lichidele Newtoniene in industria alimentara, cu sau fara respectarea unor conditii similare.The paper-work presents a series of theoretical and practical aspects connected to the method of boarding the energetic study of mechanical blenders with applications in food industry. The mathematical shaping and the development of studied cases were accomplished for Newtonian food liquids. The presented method can be applied for the projection and for the accomplishment of blenders for Newtonian liquids in food industry, with or without the observance of similitude conditions.

INTRODUCTION
Mixing of is one of the most well known procedures in food industry, because it influences the expected result of different stages of processing.

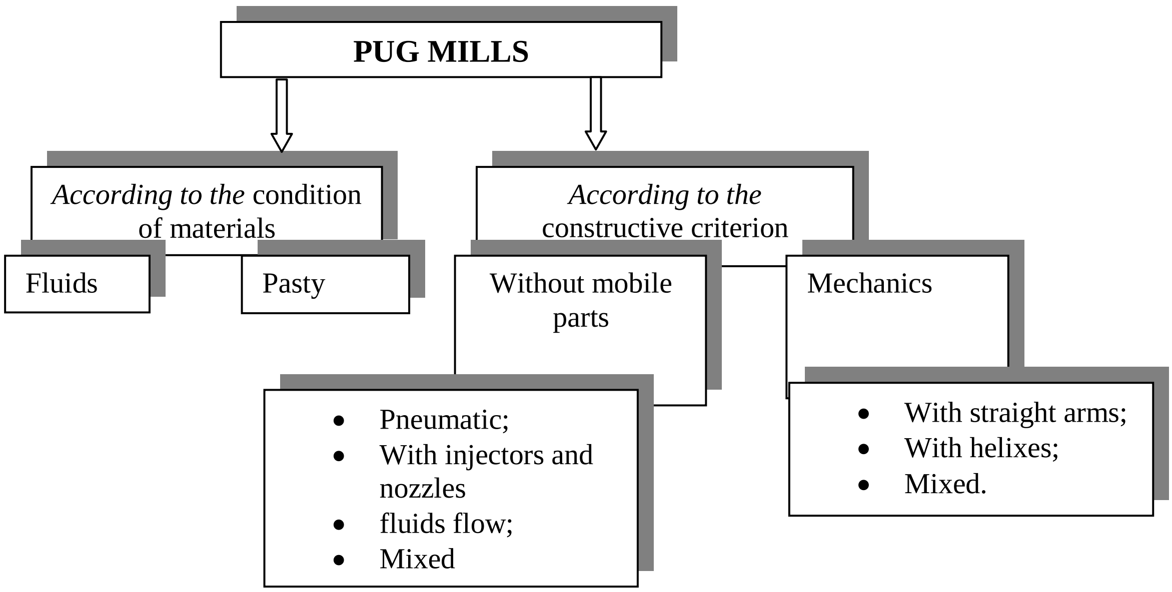

Fig. 1 -Mixers classification
(Banu, C. et al, 1998; Luca G., 1978)

The main purpose of mixing is homogenization. This takes place by submitting all the components of an assembly of motions, finally resulting in the transformation of particles' disposal and their dispersal in the blending mass.

Homogenization also manifests by reducing both concentration gradients and of temperature.

We distinguish mixings in liquid phase, with liquid-gas phase, gas-solid, liquid-solid etc.

The variety of used stirrers in food industry is considerable. In figure 1 is shown a classification of stirrers according to the state of materials subjected to mixing and respectively with their structure and driving.

MATERIAL AND METHOD

The influenced factors of mixing process

The knowledge of influenced factors upon the mixing process is important to the optimization of power consumption.

The most important factors which influence the mixing process and also its efficiency are:

- the nature of introduced materials and of resulted products as a result of mixing operation;
- the way of performing the mixing operation.

Taking into consideration that the main subject of the present paper are fluids, we can classify them in two major groups as follows: Newtonian and non Newtonian fluids. In the first category we can classify gases and Newtonian liquids, and in the second one the liquids and the non Newtonian pasture. The main properties which influence Newtonian fluids are: density, viscosity, diffusion and reciprocal solubility. The non Newtonian ones are influenced by: density, viscosity displayed most of the time through consistency and cohesion. Generally, the pasty materials have an increased consistency and cohesion and thus they significantly influenced the mixing process.

From a hydrodynamic point of view, mixing consists in realization of a turbulent motion as a rule. In the case of Newtonian food fluids, the turbulence results from a forced convection which is obtained through an efficient motion of fluid.

In the mixing process the type of flowing and the geometrical configuration where takes place the flowing can be considered important factors. It is very important the existence of the conditions created by the turbulence when the fluid slips with different momentary velocities.

It is known the fact that the nature of flowing in a mixer is determined on the basis of modified Reynolds criterion in which the fluid velocity (in the case of mechanical mixers) is estimated as a marginal velocity at the exterior end of the machine which is in a motion of rotation and the diameter of the rotary machine is adopted as a distinctive length. In the case of mixing, the limit of laminated flowing experimentally determined is Re = 10...20.

The velocity fluctuation can be considered as being momentary value of rotational motion. Thus, it results two types of turbulence: isotropic and non isotropic.

In the case of isotropic turbulence, the velocity fluctuations have an equal probability in all the directions. Each of one of these velocities has, at any moment, the same number of positive and negative values.

The non isotropic turbulence is a state in which the velocity fluctuations are neither equal nor probable and they don't have an equal size in all directions.

Prandtl has introduced as a measure of turbulence a size named mixing length. It represents the measure of the distance which a swirl covers in the surrounding fluid from a layer in motion until its velocity becomes equal with the environment, and loses its personality. The mixing length is as much bigger as the turbulence is more intense. It is not constant n the in the whole mass of fluid.

The mixing length, l_a is obtained from Prandtl equation and has the expression: *(Banu, C. et al, 1998; Bratu, E. et al., 1984)*

$$l_a = \sqrt{\frac{\sigma_t}{\rho}}\,\frac{1}{\frac{dv}{dy}} \qquad (1)$$

where:

σ_t - tangential tension of turbulence;

ρ - fluid density;

dv/dy - the velocity gradient in the considered point.

The equipment where the mixing is produced influences the process through the connection elements with the shape and the size of the pot, the mixing device and its position towards the pot.

The mixing device must work out in the pot a shearing force big enough so that to result limit layers as thin as possible, essential to turbulence. At the same time the mixing device must attract the new product in the area of high velocities.

Another factor which influences the process of mixing is the size of the pot or the quantity of processed material. The most striking results are observed in case of mixers with desultory operation. It is recommended that in such situations to be used stirring devices with low capacities.

RESULTS

Elements of dynamics specific to mechanical mixers, with arms

These types of mixers realize the homogenization of raw material with the help of some mobile elements named: arms, blades, propellers, anchors, etc.

In the case of liquids, the mechanical mixers produce a certain working conditions of flowing.

According to the way in which device stirring conveys the liquid motion, it has developed two categories of machines:

- machines which convey the quantity of motion by stress shearing, so that this transmission to be made to a right angle towards direction of motion stirring device.
- machines which convey the quantity of motion through the pressure of blades upon the liquid, that is in the direction of motion of stirring device.

The latter type is the most frequently used. All the stirring devices with blades are part of this category. The rotary blades exert a pressure upon the liquid bulling a part of it in the environment, starting at the same time a rotating motion in the liquid. Also, behind the blades is created a diminishing of pressure allowing to attract an important part of the liquid involved in the mixing process. The liquid brought creates some vortex flows. Due to the increase of speed rotation, the liquid between the blades is submitted to some centrifugal forces, which create in the end its radial jumping-up. This liquid penetrates in the surrounding layers through a transfer quantity of motion. Then it follows an increase of section cross of liquid current and slow loss of velocity at the same time with the increase of the distance towards the blade.

Regarding the main directions of current lines we notice three types of flowing *(Foucault S. et al, 2005; Rayner M., Dejmek P., 2015):*

- tangential flowing where the liquid flows in parallel with the paddle direction;
- radial flowing where the liquid is removed through centrifugal forces in a radial direction towards the rotary axis;
- axial flowing in which the liquid penetrates the stirring device and removes itself from it according to parallel direction with the rotary axis.

In the case of stirring devices with perpendicular arms on the rotary axis, the stirring devices are located central towards the pot in general.

As a consequence of some series of experimental tests, for a stirring device which scheme is presented in figure 2, we observed that for a proper working we must respect the followings rapports of basis dimensions:

- d/D = 0.5…0.9;
- h/d=0.08…0.12;
- H/D=0.8…1.3
- H1/d=0.05…0.3

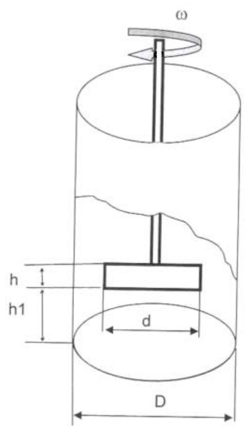

Fig.2 - The mixer scheme with assured similarity

It is recommended a diversity of peripheral velocities of 1.25…2.5 m/s in function of the product *(Maa Y.F., Hsu C., 1996; Verma A. K, 2014)*.

In order to find out the consumption of power used for mixing up Newtonian fluids in food industry, we start from Newton equation written for the elementary force exerted by the surface element dA upon the liquid in the regime period:

$$dF = \xi \cdot \frac{v^2 \cdot \rho \cdot dA}{2} \tag{2}$$

where:

ξ is the dimensionless resistance coefficient;

v – motion velocity of a certain point of the arm surface;

ρ - specific mass of liquid;

dA - elementary projection of area of the motion blade on straight-down plane on direction of motion.

If we consider the blade from figure 3 we can write:

$$\begin{aligned} dA &= h \cdot dx; \\ v &= 2.\pi.n.x; \end{aligned} \tag{3}$$

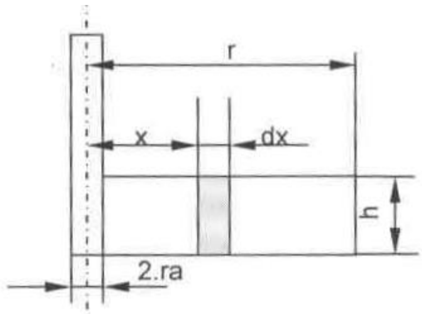

Fig. 3 - The scheme for the differential calculation of straight paddle

On the whole arm of the blade equation (2) becomes:

$$F = \xi \cdot \frac{(2 \cdot \pi \cdot n)^2}{2} \cdot \rho \cdot h \cdot \int_{ra}^{r} x^2 \cdot dx \tag{4}$$

If we consider that the starting point of application of resulted forces is at half of arm's width and the distance x_0 from ax, it results:

$$x_0 = \frac{\int x \cdot dF}{F} \tag{5}$$

Power can be written in a first stage:

$$P_1 = F \cdot v_0 \tag{6}$$

Where v_o is the velocity point of application of resulted forces:

$$v_0 = 2 \cdot \pi \cdot n \cdot \frac{\int x \cdot dF}{F} \tag{7}$$

Expression of theoretical consumed power becomes:

$$P_1 = \xi \cdot \rho \cdot h \cdot \pi^3 \cdot n^3 \cdot (r^4 - r_a^4) \tag{8}$$

Because r_a is incomparable less than *r*, it can be neglected towards this one. Also if we consider *2.r=d* and *h/d =a*, with a unique constant ξ' we obtain:

$$P_1 = \xi' \cdot \rho \cdot n^3 \cdot d^5 \tag{9}$$

The experimental unique constant ξ' depends on Reynolds modified criterion:

$$\xi' = \frac{c}{Re_M^m} = \frac{c}{\left(\frac{n \cdot d^2}{\nu}\right)^m} \tag{10}$$

Introducing this expression in the power equation given by the relation (9) it results:

$$P_1 = c \cdot \rho \cdot \nu^m \cdot n^{3-m} \cdot d^{5-2\cdot m} \tag{11}$$

Because of the fact that in many situations is more likely to use the equation in function of dynamic coefficient of viscosity η, we write: *(Banu, C. et al, 1998; Bratu, E. et al., 1984; Loncin M., 1979).*

$$P_1 = c \cdot \eta^m \cdot \rho^{1-m} \cdot n^{3-m} \cdot d^{5-2\cdot m} \tag{12}$$

The last two expressions of the consumed power used for mixing are used for the classical model presented in figure 2 and 3, meaning in the case of satisfied similarity.

The constants c and m are experimental and they can be found in tables from literature of specialty.

In the situations in which the stirring device doesn't correspond to geometrical features of similarity given by the results of experimental essays, we correct them by applying multiplication factors of power expression.

We observe two cases for which the multiplication factors are *(Banu, C. et al, 1998; Loncin M., 1979)*:

a. Stirring device with paddles and non satisfied similarity:

$$K = \left(\frac{D}{3 \cdot d}\right)^{1,1} \cdot \left(\frac{H}{D}\right)^{0,6} \cdot \left(\frac{4 \cdot h}{d}\right)^{0,33} \tag{13}$$

b. Stirring device with propeller or turbine and non satisfied similarity:

$$K = \left(\frac{D}{3 \cdot d}\right)^{0,93} \cdot \left(\frac{H}{D}\right)^{0,6} \tag{14}$$

These relations can be applied in the conditions: D/d=2.5…4, H/D=0.6…1.6, h/d=0.2…0.67 and h1/D=0.2…0.5.

The programme demonstration and the presentation of results

Based upon the mathematical model presented above there were analyzed the power consumption at mixing for milk and for saccharose solution.

For milk we used the following constants: ρ=1032,6 kg/m^3, η=0.001804 Pa.s and for the saccharose solution of 30%: ρ=1448.5 kg/m^3, η= 3.187 Pa.s la 20^{0}C.

The other constants and geometrical dimensions of stirring device were chosen in this way: c=6.8, m=0.2, d=0,3 respectively 0.4 m, D=3.8.d, H=3.5.D, h=0.4.d and n=1.25…2.5m/s. *(Banu, C. et al, 1998; Loncin M., 1979; Maa Y.F., Hsu C., 1996; Terada K. et al, 1998).*

In order to achieve a comparative analyze we initiate the following working program shown in figure 4.

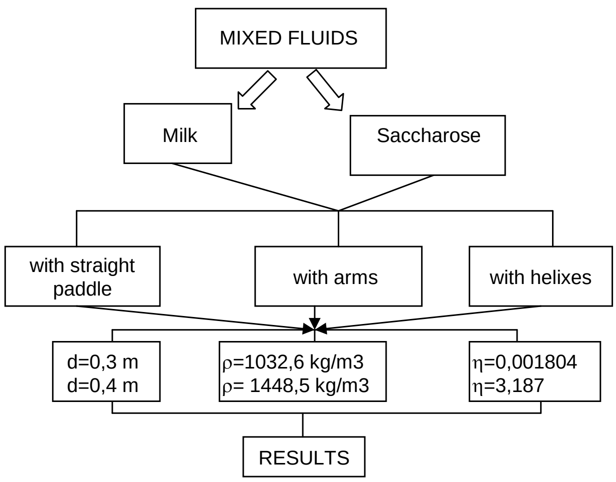

Fig. 4 - The working programme for the comparative analysis

From the point of view of types of constructive stirring devices were analyzed three specific cases:

- classic mixer with straight paddles and respected the similarity conditions;
- mixer with straight paddles which doesn't correspond to imposed similarity conditions;
- mixer with propeller which doesn't correspond to imposed similarity conditions.

For each case it was traced the power variation of mixing depending on revolution, according to model presented in figure 5. , where index 1 corresponds to milk mixing with rotor of 0.3 m diameter, index 2 for saccharose solution with a concentration of 30% and a rotor with the same diameter , index 3 for milk and a rotor of 0.4 m diameter, and index 4 for saccharose solution and a rotor with the same diameter.

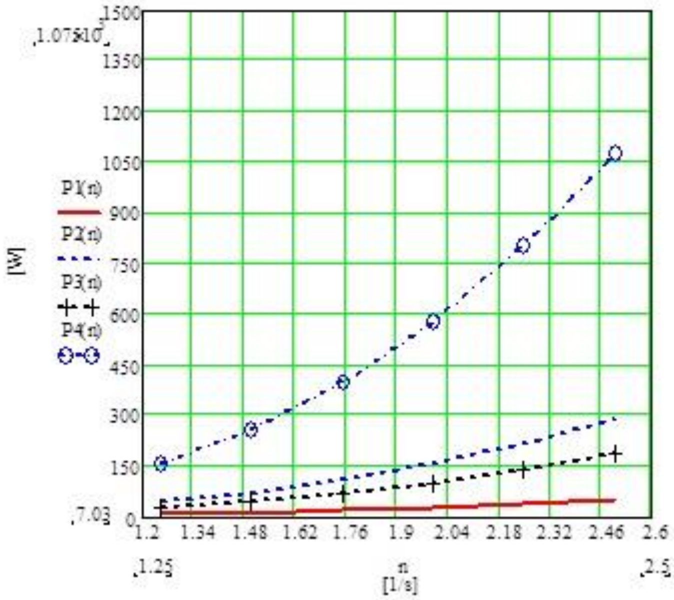

Fig. 5 - The variations of consumed powers depending on turning round

We can observe an important increase of consumed power in case 4, also at a minimal revolution and also to the maximum one taken in consideration.

In order to be able to compare the evolutions of consumed powers at proper mixing, we draw the diagrams from figures 6 and 7.

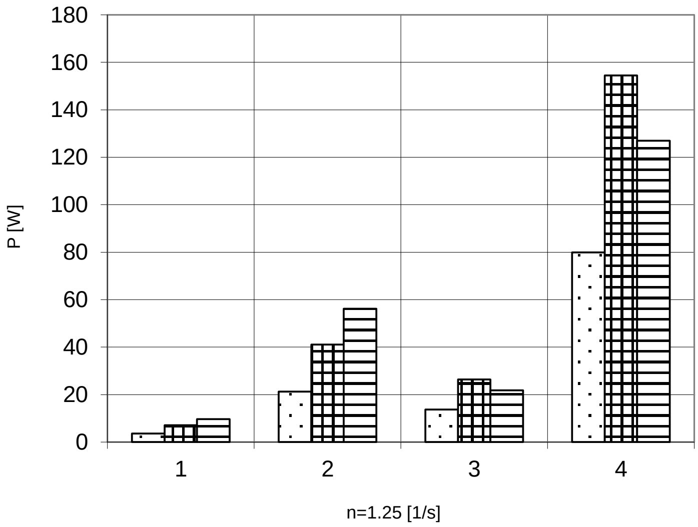

Fig. 6 - The variations of power consumption at minimum turning round

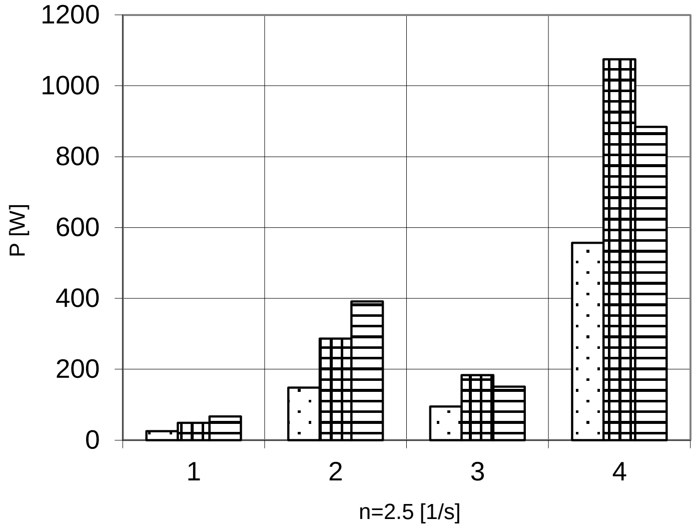

Fig. 7 - The variations of power consumption at maximum turning round

In figure 6 we observe the evolution of consumed powers at a revolution of 1.1 rot/s and in figure 7, at a revolution of 2.5 rot/s.

CONCLUSIONS

The four power variations were grouped in three certain variants: one variant for mixer with straight paddles and were respected the similarity conditions, one for the mixer with arms and conditions of similarity were unconsidered finally one for the mixer with propeller and conditions of similarity were also unconsidered. It can be observed that the minimal power is consumed (irrespective of revolution) at the mixer with straight paddles (case a). For case b, the mixer with arms and unconsidered similarity the power consumptions are much more increased to the maximum recommended values of revolution, going beyond over the values for the mixer with propeller .

To these consumed powers we add about 10…20% for the pots with rugged walls, about. 10% for the hydraulic resistance created in laggings, up to 100% for the existence of thermic treating coil and the consumed power in transmission depending on the type and its complexity.

For other types of mixers than the ones analyzed above, the geometrical features and the recommended constants are presented in table 1.

Table 1

The geometrical features and the recommended constants

Den. no.	Mixer type	Constants		Observations
		c	m	
1.	With two paddles in vertical position	111 14.35 6.8	1 0.51 0.20	Re<20; h/d=0.885; D/d=2; H/d=2; h1/d=0.36 10^2<Re<5.10^4; h/d=0.885; D/d=2; H/d=2; h1/d=0.36 Re>5.10^4; h/d=0.25; D/d=3; H/d=3; h1/d=0.33
2	With two arms inclined down to 45^0	4.05	0.20	h/d=0.25; D/d=3; H/d=3; h1/d=0.33
3	With four arms in vertical position	8.52	0.20	h/d=0.25; D/d=3; H/d=3; h1/d=0.33
4	With four arms inclined down to 45^0	5.05	0.20	h/d=0.25; D/d=3; H/d=3; h1/d=0.33
5	With four arms inclined up to 45^0	4.42	0.20	h/d=0.25; D/d=3; H/d=3; h1/d=0.33
6	With six arms in vertical position	12.50	0.25	h/d=0.066; D/d=1.11; H/d=1.11; h1/d=0.11
7	Anchor with two arms	6.2	0.25	h/d=0.066; D/d=1.11; H/d=1.11; h1/d=0.11

REFERENCES

[1] Banu C., Nicolau A., Barascu E., Stoica A., (2002), *Engineer's Manual of food industry (Manualul inginerului de industrie alimentară)*, Technical Publishing House, Bucharest, ISBN 937-31-2071-5;

[2] Bratu E. et al., (1984), *Unitary operations in chemical industry*, vol.II, (*Operații unitare în industria chimică*), Technical Publishing House, Bucharest;

[3] Foucault S., Ascanio G., Tanguy P.A. (2005), Mixing Times in Coaxial Mixers with Newtonian and Non-Newtonian Fluids, *Industrial & Engineering*, ACS Publications;

[4] Sahu J.K., (2014), *Introduction to Advanced Food Process Engineering,* CRC Press, Taylor & Francis Group 6000 Broken Sound Parkway New York;

[5] Loncin M., (1979), *Food Engineering,* Acad. Press, N.Y., London;

[6] Luca G. (1978), *Problems of operations and machines in food industry* (*Probleme de operații și mașini în industria alimentară*), Technical Publishing House, Bucharest;

[7] Maa Y.F., Hsu C., (1996), Liquid-liquid emulsification by rotor/stator homogenization, *Journal of Controlled Release*, Volume 38, Issues 2–3, pp.219-238;

[8] Rayner M., Dejmek P., (2015), *Engineering Aspects of Food Emulsification and Homogenization,* CRC Press, London/U.K.;

[9] Terada K. et al, (1998), Characterization of the Mechanical behaviors of Solid Fluid Mixture by the Homogenization Method, *Computer Methods in applied Mechanics and Engineering*, Volume 153, Issues 3-4, pages 223–257;

[10] Verma A., K, (2014), *Process Modelling and Simulation in Chemical, Biochemical and Environmental Engineering*, CRC Press, Taylor & Francis Group. U. New.

WRITING NORMS

Article Types

Three types of manuscripts may be submitted:

1. **Regular articles:** These should describe new and carefully confirmed findings, and experimental procedures should be given in sufficient detail for others to verify the work. The length of a full paper should be the minimum required to describe and interpret the work clearly (max.10 pages, even number);
2. **Short Communications:** A Short Communication is suitable for recording the results of complete small investigations or giving details of new models or hypotheses, innovative methods, techniques or apparatus. The style of main sections has not necessarily to be in accordance with that of full-length papers (max. 6 pages, even number);
3. **Reviews:** Submissions of reviews and perspectives covering topics of current interest are welcome and encouraged (max.10 pages, even number).

Manuscripts should be written in English (American or British usage is accepted, but not a mixture of these) and submitted **electronically** at the following e-mail addresses: ***inmatehjournal@gmail.com***
Please be sure to include your full affiliation and e-mail address (see Sample manuscript)
The authors are responsible for the accuracy of the whole paper and references.
There are allowed 2 papers by each first author.
The text layout should be in single-column format. To avoid unnecessary errors it is strongly advised to use the "spell-check" and "grammar check" functions of your word processor.

Review Process

All manuscripts are reviewed by 2 members of the Scientifically Review Office. Decisions will be made as rapidly as possible and the journal strives to return reviewers' comments to authors in approx.3 weeks.
The editorial board will re-review manuscripts that are accepted pending revision.

NOTE:

Submission of a manuscript implies: that the work described has not been published before (excepting as an abstract or as part of a published lecture or thesis) that it is not under consideration for publication elsewhere.

1. REGULAR ARTICLES

- Manuscripts should be concise, in ***1.15 line spacing***, and should have 2 cm all over margins. The font should be ***Arial 10 pt.*** Ensure that each new paragraph is clearly indicated, using **TAB at 1 cm**.
- Title will be ***Arial 12 pt***. and explicit figures will be ***Arial 9 pt***.
- Text will be written in English.
- Chapters' titles are written by ***Arial 10 pt, Bold, Uppercase*** (e.g INTRODUCTION, MATERIAL AND METHODS), between chapters is left a space for 10 pt. At the beginning of each paragraph, leave a tab of 1 cm.
- The paper body will be written in ***Arial 10 pt., Justify alignment***.

TITLE ***Arial 12 pt., Uppercase, Bold, Center*** *(in English language)* and ***Bold Italic*** *(in native language)*.
Should be a brief phrase describing the contents of the paper. Avoid long titles; a running title of no more than 100 characters is encouraged (without spaces).

AUTHORS ***ARIAL 9, Bold, Centre alignment***
Under the paper's title, after a space (enter) 9 pt., write ***authors' names*** and ***affiliations (Arial 8 pt.-Regular)***
When the paper has more than one author, their name will be followed by a mark (Arabic numeral) as superscript if their affiliation is different.
Corresponding author's name (next row), ***(Arial 8 pt.)***. Should be added also: phone, fax and e-mail information, for the paper corresponding author (***font: 8 pt., Italic***).

KEYWORDS ***(In English)*** about 4 to 7 words that will provide indexing references should be listed (title: ***Arial 10pt, bold italic,*** text ***Arial 10 pt., italic***).

A list of non-standard *Abbreviations* should be added. In general, non-standard abbreviations should be used only when the full term is very long and used often. Each abbreviation should be spelled out and introduced in parentheses the first time it is used in the text. Standard abbreviations (such as ATP and DNA) need not to be defined.

ABSTRACT ***(in English and Native language, Arial 10 pt.)***, the title *bold*; the text of abstract: *italic*) should be informative and completely self-explanatory, briefly present the topic, state the scope of the experiments, indicate significant data, and point out major findings and conclusions. The Abstract should be max.250 words. Complete sentences, active verbs, and the third person should be used, and the abstract should be written in the past tense. Standard nomenclature should be used and abbreviations should be avoided. No literature should be cited.

INTRODUCTION (*Arial 10 pt.)* should provide a clear statement of the problem, the relevant literature on the subject, and the proposed approach or solution. It should be understandable to colleagues from a broad range of scientific subjects. We should refer to the current stage of researches performed in the field of the paper to be published, by quoting up-to-date specialty studies, preferably published after 2006, excepting certain referential specialty books/studies, especially papers issued in magazines/journals/conferences/ISI quoted symposia or in other international data bases, which are well known and available.

MATERIALS AND METHODS (*Arial 10 pt.)* should be complete enough to allow experiments to be reproduced. However, only truly new procedures should be described in detail; previously published procedures should be cited, and important modifications of published procedures should be mentioned briefly. Methods in general use need not be described in detail.

RESULTS (*Arial 10 pt.)* should be clarity presented. The results should be written in the past tense when describing findings in the authors' experiments. Results should be explained, but largely, without referring to the literature. Discussion, speculation and detailed interpretation of data should not be included in the Results, but should be put into the Conclusions section.

CONCLUSIONS (*Arial 10 pt.)* The main conclusions drawn from results should be presented in a short Conclusions section. Do not include citations in this section.

Formulae, symbols and abbreviations: Formulae will be typeset in Italics (preferable with the Equation Editor of Microsoft Office 2003) and should be written or marked as such in the manuscript, unless they require a different styling. They should be referred to in the text as Equation (4) or e.g. (4). The formulae should be numbered on the right side, between brackets *(Arial 10 pt.)*:

$$P = F \cdot v \tag{1}$$

Terms of the equation and the unit measure should be explained, e.g.

P is the power, [W];
F – force, [N];
v – speed, [m/s]

SI units must be used throughout.

Tables should be self-explanatory without reference to the text. The details of the methods used in the experiments should preferably be described in the legend instead of in the text. The same data should not be presented both in table and graph form or repeated in the text.

Table's title will be typed ***Arial 9 pt, Bold, Centered***

In the table, each row will be written Arial 9 pt, single-spaced throughout, including headings and footnotes.

The table should be numbered on the right side, between brackets *(Arial 10 pt)*:

Figure (Arial 9 pt., Bold, Center) should be typed in numerical order (Arabic numerals). Graphics should be high resolution (e.g.JPEG). Figure number is followed by what represent the figure or graph e.g.:

Fig.1 – Test stand

Legend:* *Arial 8 pt, Italic, Center, e.g.

1 - plansifter compartments; 2- break rolls; 3 – semolina machines; 4 – reduction rolls; 5 – flour

ACKNOWLEDGMENTS (*Arial 10 pt.)* of people, grants, funds etc should be brief (*if necessarily*).

REFERENCES (*Arial 10 pt.)*

(In alphabetical order, in English and in the original publication language).

Minimum 10 references, last 10 years, minimum 3 references from the last 2 years

It can be used "References" tool from the Word Editor.

References should be cited in the text in brackets as in the following examples:

(Babiciu P., Scripnic V., 2000)

All references must be provided in English with a specification of original language in round brackets.

Authors are fully responsible for the accuracy of the references.

References should be alphabetically, with complete details, as follows:

Examples:

Books: Names and initials of authors, year (between brackets), title of the book (Italic), volume number, publisher, place, pages number or chapter, ISSN/ISBN:

[1] Vlădut V., (2009), *Study of threshing process in axial flow apparatus (Studiul procesului de treier la aparatele cu flux axial),* vol.1, ISSN/ISBN …………., "Terra Nostra" Publishing House, Iaşi/Romania;

Journal Article: Names and initials of authors, year (between brackets), full title of the paper, full name of the journal (Italic), volume number, publisher, place, ISSN, page numbers:

[1] Lizhi Wu, Yan Di., (2005), Demonstrational study on the land consolidation and rehabilitation (LCR) project of saline-alkali soil in arid areas: a case study of Lubotan LCR project in Pucheng County, Shaanxi Province（干旱区盐碱化土地整理工程实证研究-以陕西蒲城县卤泊滩土地整理项目为例）, *Transactions of the Chinese Society of Agricultural Engineering*, vol.21, no.1, ISSN ………, pp.179-182, Madison/Wisconsin;

[2] Leonov I.P., (1973), Basic machine theory for tobacco stringing. Post-harvest care of tobacco and rustic tobacco (Основы теории машин для закрепления табака на шнуры. Послеуборочная обработка табака и махорки), *Collection of scientific articles (сборник научно-исследовательских работ)*, pp.37-45;

Conference or Symposium: Names and initials of authors, year (between brackets), full title of the paper (Regular), full name of the conference/symposium (Italic), volume number, publisher, place, ISSN, page numbers

[1] Bungescu S., Stahli W., Biriş S., Vlăduţ V., Imbrea F., Petroman C., (2009), Cosmos program used for the strength calculus of the nozzles from the sprayers (Program Cosmos folosit pentru calculul de rezistenţ ă la zgomot al aparatelor de distribuţ ie)*, Proceedings of the 35 International Symposium on Agricultural Engineering "Actual Tasks on Agricultural Engineering",* pp.177-184, Opatija / Croatia;

Dissertation / Thesis: Names and initials of authors, year (between brackets), full name of the thesis (Italic), specification (PhD Thesis, MSc Thesis), institution, place;

[1] Popa L., (2004), *Research on the influence of structural and functional parameters of the braking system on the braking performance of agricultural trailers (Cercetări privind influenţa caracteristicilor constructive şi funcţionale ale sistemelor de frânare asupra performanţelor de frânare ale remorcilor agricole)*, PhD dissertation, Transylvania University of Braşov, Braşov / Romania.

Patents: Names and initials of authors, year (between brackets), patent title (Italic), patent number, country:

[1] Grant P., (1989), *Device for Elementary Analyses*. Patent, No.123456, USA.

Legal regulations and laws, organizations: Abbreviated name, year (between brackets), full name of the referred text, document title/type (Italic), author, place:

[1] *** EC Directive, (2000), Directive 2000/76/EC of the European Parliament and of the Council of 4 December 2000, on the incineration of waste, Annex V, *Official Journal of the European Communities*, L332/91, 28.12.2000, Brussels.

Web references: The full URL should be given in text as a citation, if no other data are known. If the authors, year, and title of the documents are known and the reference is taken from a website, the URL address has to be mentioned after these data:

The title of the book, journal and conference must be written in Italic, the title of the article, chapter of the book, must be written Regular.

Citation in text

Please ensure that every reference cited in the text is also present in the reference list (and vice versa). Do not cite references in the abstract and conclusions. Unpublished results, personal communications as well as URL addresses are not recommended in the references list.

Making personal quotations (one, at most) should not be allowed, unless the paper proposed to be published is a sequel of the cited paper. Articles in preparation or articles submitted for publication, unpublished, personal communications etc. should not be included in the references list.

Citations style

Text*:* All citations in the text may be made directly (or parenthetically) and should refer to:

- ***single author****:* the author's name (without initials, unless there is ambiguity) and the year of publication:
 "as previously demonstrated *(Brown, 2010)*".
- ***two authors****:* both authors' names and the year of publication: *(Adam and Brown, 2008; Smith and Hansel, 2006; Stern and Lars, 2009)*
- ***three or more authors****:* first author's name followed by "et al." and the year of publication: "As has recently been shown *(Werner et al., 2005; Kramer et al., 2000)* have recently shown ...."

Citations of groups of references should be listed first alphabetically, then chronologically.

Units, Abbreviations, Acronyms

- Units should be metric, generally SI, and expressed in standard abbreviated form.
- Acronyms may be acceptable, but must be defined at first usage.

Edited by: INMA Bucharest
6 Ion Ionescu de la Brad Blvd., sect. 1, Bucharest, ROMANIA
Tel: +4021.269.32.60; Fax: +4021.269.32.73
http://www.inmateh.eu
e-mail: ***inmatehjournal@gmail.com***